Novel iridium(III) complexes for electrogenerated chemiluminescence labelling and detection

AUTHOR(S)

L Chen

PUBLICATION DATE

16-07-2019

HANDLE

10536/DRO/DU:30137194

Novel iridium(III) complexes for electrogenerated chemiluminescence labelling and detection

By

Lifen Chen

Submitted in fulfilment of the requirements for the degree of
Doctor of Philosophy

Deakin University
March 2019

DEAKIN UNIVERSITY

ACCESS TO THESIS - A

I am the author of the thesis entitled

Novel Iridium(III) Complexes for Electrogenerated Chemiluminescence Labelling and Detection

submitted for the degree of

DOCTOR OF PHILOSOPHY

This thesis may be made available for consultation, loan and limited copying in accordance with the Copyright Act 1968.

'I certify that I am the student named below and that the information provided in the form is correct'

Full Name: Lifen Chen

Signed: Signature Redacted by Library

Date: 21/3/2019

DEAKIN UNIVERSITY

CANDIDATE DECLARATION

I certify the following about the thesis entitled

Novel Iridium(III) Complexes for Electrogenerated Chemiluminescence Labelling and Detection

submitted for the degree of

DOCTOR OF PHILOSOPHY

a. I am the creator of all or part of the whole work(s) (including content and layout) and that where reference is made to the work of others, due acknowledgment is given.

b. The work(s) are not in any way a violation or infringement of any copyright, trademark, patent, or other rights whatsoever of any person.

c. That if the work(s) have been commissioned, sponsored or supported by any organisation, I have fulfilled all of the obligations required by such contract or agreement.

d. That any material in the thesis which has been accepted for a degree or diploma by any university or institution is identified in the text.

e. All research integrity requirements have been complied with.

'I certify that I am the student named below and that the information provided in the form is correct'

Full Name: Lifen Chen

Signed: Signature Redacted by Library

Date: 21/3/2019

Table of contents

Abstract

Electrogenerated chemiluminescence (ECL) is the process whereby electrochemically generated species undergo electron-transfer reactions in solution and emit light. ECL has been widely used as a mode of detection due to advantages such as high sensitivity, selectivity and wide dynamic range. Tris(2,2′-bipyridine)ruthenium(II) ([Ru(bpy)$_3$]$^{2+}$) and various derivatives are the most commonly employed ECL luminophore, but the low luminescence quantum yield of [Ru(bpy)$_3$]$^{2+}$ (3.9% in water) limits the sensitivity of its ECL system. Therefore, considerable effort has been devoted to developing new ECL luminophores such as cyclometalated iridium(III) complexes, which exhibit much higher quantum yields (some nearly 99% in acetonitrile). Additionally, iridium(III) complexes enable the ECL emission to be tuned to different wavelengths throughout the visible region, creating opportunities for 'mixed-ECL' from solutions containing multiple different-coloured luminophores.

The research described herein explored the ECL of iridium(III) complexes, from several perspectives, including (i) a re-evaluation of complexes previously reported as highly promising candidates for ECL, (ii) the development of novel water-soluble iridium(III) complexes for ECL detection, (iii) elucidation of the key reaction pathways of ECL with iridium(III) complexes, and (iv) the development of new ECL labels containing iridium(III) complex luminophores.

Firstly, the ECL of iridium(III) complexes containing an acetylacetonate (acac) ligand with tri-*n*-propylamine (TPrA) co-reactant in acetonitrile was examined under a range of chemical and instrumental conditions. This demonstrated that the ECL intensities of iridium(III) complexes are highly dependent on experimental conditions. In some cases, exceptional intensities previously reported for iridium(III) complexes may have been

derived using instrumental or chemical conditions that unintentionally disadvantaged the $[Ru(bpy)_3]^{2+}$ reference electrochemiluminophore.

Secondly, a series of new water-soluble iridium(III) complexes containing a 2,2′-bipyridine (bpy) ligand with one or two tetraethylene glycol (TEG) groups were synthesised and their ECL behaviours were studied. The novel $[Ir(C^\wedge N)_2(Me\text{-}bpy\text{-}TEG)]Cl$ and $[Ir(C^\wedge N)_2(TEG\text{-}bpy\text{-}TEG)]Cl$ complexes (where $C^\wedge N$ represents a ligand with carbon and nitrogen atoms involved in the coordination of the ligand to the metal centre) in aqueous solution largely retained the redox potentials and emission spectra of the parent $[Ir(C^\wedge N)_2(Me\text{-}bpy\text{-}Me)]PF_6$ (where Me-bpy-Me = 4,4′-methyl-2,2′-bipyridine) luminophores in acetonitrile, and exhibited ECL intensities similar to those of $[Ru(bpy)_3]^{2+}$ and the analogous $[Ir(C^\wedge N)_2(pt\text{-}TEG]Cl$ complexes (where pt-TEG = 1-(TEG)-4-(2-pyridyl)-1,2,3-triazole). The distinct spectral distributions of $[Ir(ppy)_2(Me\text{-}bpy\text{-}TEG)]^+$ and $[Ir(ppy)_2(pt\text{-}TEG)]^+$, which can both be readily adapted for bioconjugation, reveals a viable strategy to create ECL-labels with different emission colours from the same commercial $[Ir(ppy)_2(\mu\text{-}Cl)]_2$ precursor.

Lastly, a series of new ECL labels with iridium(III) complex luminophores were created by adding a suitable functional group to a phenyltriazole ligand, and the potential of these labels was examined using two different commonly binding assays. The novel $[Ir(C^\wedge N)_2(pt\text{-}TEG\text{-}Sq)]^+$ labels were obtained through a more convenient and versatile synthetic approach and provided superior ECL responses to the commercial $[Ir(C^\wedge N)_2(mbpy\text{-}COOH)]^+$ analogues in both assays. Comparison of ECL intensities from various labels under different assay conditions provided new insight into the reaction mechanism of ECL with iridium(III) complexes.

Acknowledgements

I would like to start by thanking my primary supervisor, Professor Paul Francis. I could not have finished my PhD study without your help: thanks for being amazing; thanks for giving me the opportunity to start my PhD work; thanks for always encouraging me when I had trouble and teaching me the ability to solve problems during the experimental work; and thanks for always making time to have meetings and discuss experimental details during the three years. I feel very lucky that I would have a nice supervisor in my life. Thanks also to my co-supervisor Dr Egan Doeven, who guided my experiments through my whole PhD study. Thanks for always answering my many questions with patience and helping me to develop my whole systematic knowledge of chemistry. I would also like to thank my co-supervisor Dr Wenrong Yang, who helped me throughout my PhD studies with a lot of advice.

Finally, I sincerely appreciate all my co-workers in the lab: Dr Zoe Smith, Dr Richard Alexander, Dr David Hayne, Ms Tien Pham and Mr Ben Newman, and my collaborators: Assoc. Prof. Luke Henderson, Dr Emily Kerr, Assoc. Prof. Conor Hogan, Dr Serena Carrara, , Dr Timothy Connell, Dr Yi Heng Nai, Mr Richard Alexander, Mr Johnny Agugiaro, Assoc. Prof. David Wilson and Assoc. Prof. Paul Donnelly for their specific contributions to various projects, as outlined in each section.

List of Publications

The following publications are included in this thesis:

(1) **L. Chen**, E.H. Doeven, D.J.D. Wilson, E. Kerr, D.J. Hayne, C.F. Hogan, W. Yang, T.T. Pham, P.S. Francis; Co-reactant electrogenerated chemiluminescence of iridium(III) complexes containing an acetylacetonate ligand, *ChemElectroChem*, 2017, 4, 1797-1808.

(2) **L. Chen**, D.J. Hayne, E.H. Doeven, J. Agugiaro, D.J.D. Wilson, L.C. Henderson, T. U. Connell, R. Nai, R. Alexander, S. Carrara, C.F. Hogan, P.S. Donnelly, P.S. Francis; A conceptual framework for the development of iridium (III) complex electrogenerated chemiluminescence labels. Submitted for publication.

(3) **L. Chen**, B. Newman, L.C. Henderson, E.H. Doeven, P.S. Francis, D.J. Hayne; Water-soluble iridium(III) complexes containing tetraethylene glycol derivatised bipyridine ligands for electrogenerated chemiluminescence detection. In preparation

Significant contributions to other projects during my PhD candidature also resulted in the following publications:

(4) L.C. Soulsby, D.J. Hayne, E.H. Doeven, **L. Chen**, C.F. Hogan, E. Kerr, J.L. Adcock and P.S. Francis, Electrochemically, spectrally and spatially resolved annihilation electrogenerated chemiluminescence of mixed metal complexes at the working and counter electrodes, *ChemElectroChem*, 2018, 5, 1543-1547.

(5) N.K. Burns, T.D. Ashton, P.G. Stevenson, J.R. Pearson, I.L. Fox, P.S. Francis, Z.M. Smith, N.W. Barnett, **L. Chen,** J.M. White and X.A. Conlan; Extraction, identification and detection of synthetic cannabinoids found pre-ban in Victoria, Australia, *Forensic Chemistry*, 2018, 7, 19-25.

(6) L.C. Soulsby, D.J. Hayne, E.H. Doeven, D.J.D. Wilson, J. Agugiaro, T.U. Connell, **L. Chen**, C.F. Hogan, E. Kerr, J.L. Adcock, P.S. Donnelly, J.M. White and P.S. Francis,

Mixed annihilation electrogenerated chemiluminescence of iridium(III) complexes

Phys. Chem. Chem. Phys., 2018, 20, 18995-19006.

Chapter 1: Introduction

1.1 Electrogenerated chemiluminescence

Electrogenerated chemiluminescence (ECL) is the phenomenon resulting from electrogenerated species undergoing an electron-transfer reaction at the electrode surface, resulting in the emission of light.[1] Compared with chemiluminescence, ECL shows several advantages: (1) some luminescence reagents can be regenerated at the electrode surface and as a result take part in the reaction more than once.[2] (2) Due to advantages offered by spatial and temporal control, ECL can readily be combined with multiple other technologies such as flow injection analysis (FIA),[3] high-performance liquid chromatography (HPLC)[4] and capillary electrophoresis (CE),[5] making it possible to detect the specific targets in complicated samples, without the need of adding a chemical oxidant or other chemiluminescence reagent. (3) Due to the reaction taking place at the electrode, ECL emission can be controlled through the electrochemical potential to improve the sensitivity and selectivity of the method.[6] The details of the current comprehensive understanding of ECL processes have been summarized in many reviews in the past few years.[7-11] Since the first detailed ECL studies were reported on the 1960s by Hercules and Bard,[12, 13] the number of publications per year increased to a plateau around 2014 (Figure 1.1). ECL has become a major focus of research, encompassing fundamental studies, reagent development, and analytical applications. In recent years, ECL biosensors have become an area of intense interest (Figure 1.2).[8] After decades, ECL has evolved as a powerful technique that is widely applied in areas such as environmental monitoring,[14] medical diagnosis,[15] and forensic science.[16]
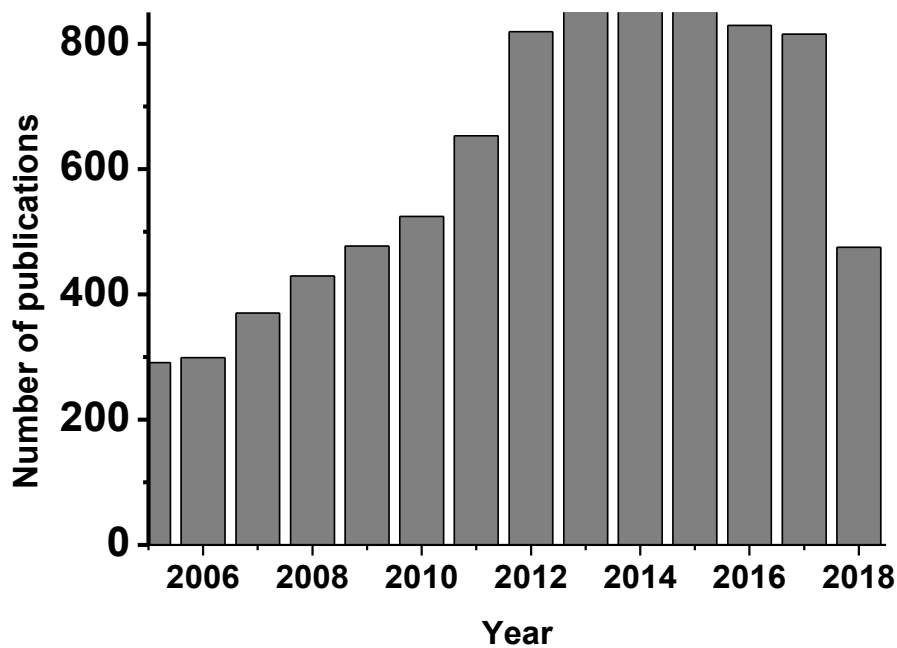
Figure 1.1. Number of publications related to ECL as a function of year published on the research topic of ECL according to SciFinder Scholar. The search was conducted in May, 2018.
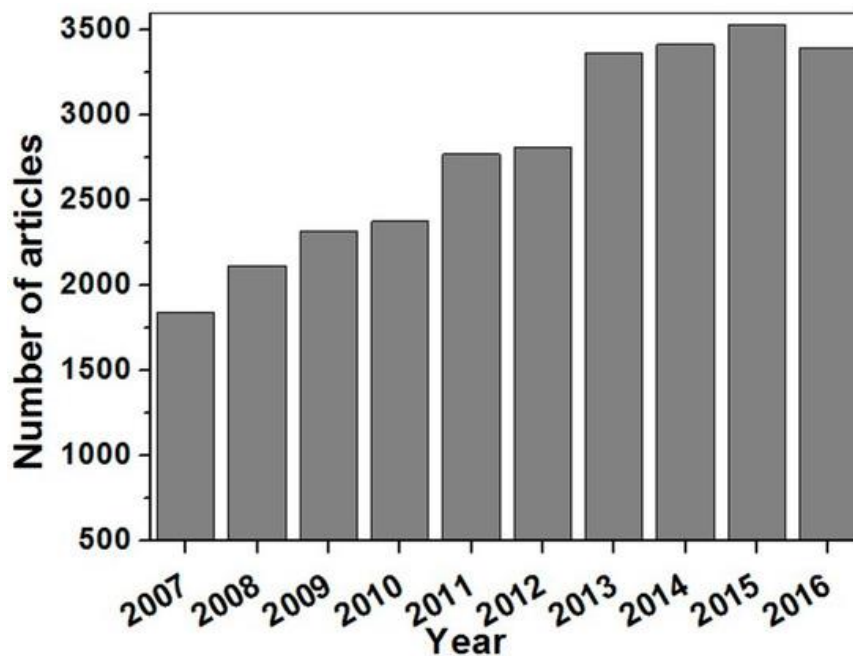

Figure 1.2. Number of articles punished on ECL biosensors in the last 10 years. Graph adapted from reference 8.

1.1.1 Annihilation ECL

Light emission triggered by electrochemical reactions can be produced *via* a number of different mechanisms, among which the 'annihilation' route was the first explored.[17, 18] When the potential applied is alternated between positive and negative, electrochemically oxidized and reduced species are both generated at electrode. The excited state product is generated through electron transfer from the reduced to the oxidized species. The reactions in the annihilation ECL route are shown below in Scheme 1.1.

$$(1) \quad A - e^- \rightarrow A^{\bullet+} \qquad \text{(oxidation at the electrode)}$$

$$(2) \quad A + e^- \rightarrow A^{\bullet-} \qquad \text{(reduction at the electrode)}$$

$$(3) \quad A^{\bullet-} + A^{\bullet+} \rightarrow A^* + A \quad \text{(excited state formation)}$$

$$(4) \quad A^* \rightarrow A + h\nu \qquad \text{(light emission)}$$
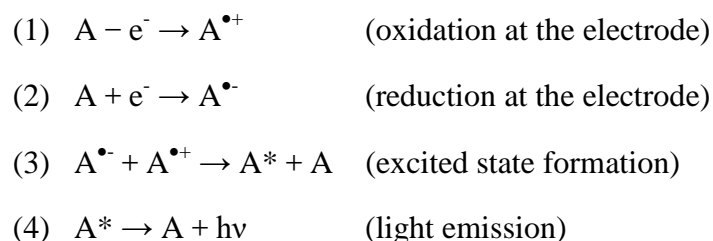
Scheme 1.1. Mechanism of annihilation ECL reaction.

Annihilation ECL is simple, but is limited to reactions in organic solvents, because the potential window of aqueous solutions is generally not large enough to both oxidize and reduce the luminophore.[19] Furthermore, not all the oxidized or reduced ECL luminophores are stable enough to undergo annihilation ECL, which limits emission intensity.[20] Finally, the annihilation route is more sensitive to quenching by oxygen. Therefore, most ECL applications are based on the 'co-reactant route', as described below.

1.1.2 Co-reactant ECL

Although the first detailed ECL studies involve annihilation ECL, 'co-reactant' ECL has become the dominant approach for analytical applications, including all commercial ECL instruments.[21] There are two pathways for co-reactant ECL systems: 'oxidative-reduction' or 'reductive-oxidation'. Scheme 1.2 shows the general mechanism for oxidative-reduction ECL, where the co-reactant forms a highly reducing species after being electrochemically oxidized by luminescent species 'A' or at the electrode, which then reacts with $A^{\bullet+}$,

followed by light emission. Alternatively, the reduced co-reactant can reduce A, allowing the annihilation generation of the excited state species. ECL can be generated as result of pulsing the electrode in a single direction in the presence of a co-reactant.[22] Most co-reactants are either strong reducing agents or strong oxidizing agents which can be easily oxidized or reduced with the luminophore species and undergo a rapid chemical reaction to form an intermediate, which then reacts with the ECL luminophore to produce ECL emission. For example, a series of co-reactant systems, such as oxalate,[23] pyruvate,[24] peroxydisulfate,[25] and tri-n-propylamine (TPrA)[26] have been explored to serve as co-reactants for ECL emission. TPrA is the most commonly used co-reactant, which is believed to produce a strong reduced species.

(1a) $A - e^- \rightarrow A^{\bullet+}$ (oxidation at electrode)

(1b) $C - e^- \rightarrow C^{\bullet+}$ (oxidation at electrode)

(2) $A^{\bullet+} + C \rightarrow A + C^{\bullet+}$ (homogeneous electron transfer)

(3) $C^{\bullet+} \rightarrow C_{red}$ (co-reactant degradation)

(4) $C_{red} + A \rightarrow A^{\bullet-} + Products$ (reduction of luminophore)

(5a) $C_{red} + A^{\bullet+} \rightarrow A^* + Products$ (excited state formation)

(5b) $A^{\bullet+} + A^{\bullet-} \rightarrow A^* + A$ (excited state formation)

(5c) $A^{\bullet+} + C_{red} \rightarrow A^* + Products$ (excited state formation)

(6) $A^* \rightarrow A + h\nu$ (light emission)
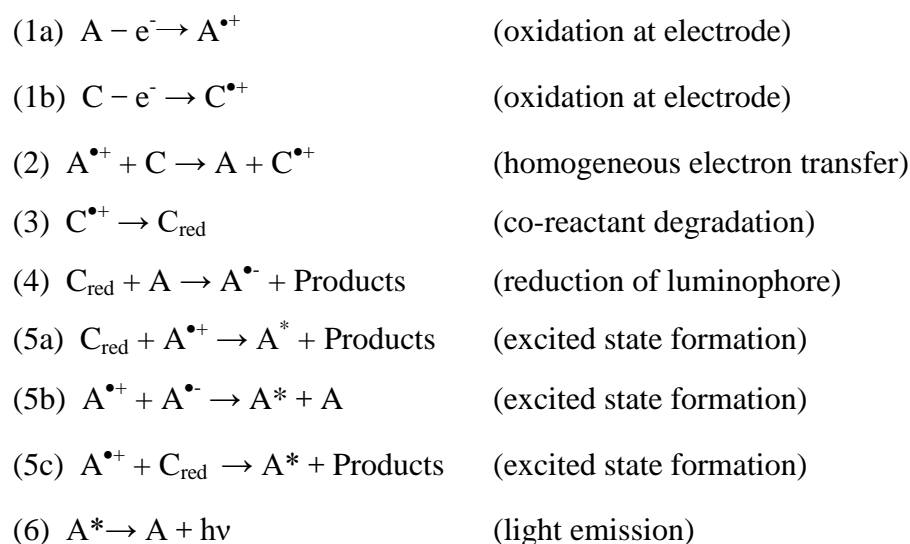
Scheme 1.2. General mechanisms of oxidative-reduction ECL.

1.2 Main ECL systems

1.2.1 ECL inorganic luminophores

The ECL luminophore is the main component of an ECL system and developing and testing of efficient and new ECL luminophores is the long-term aim for researchers. According to the chemical properties of the luminophores, ECL systems can be simply classified into three types, namely inorganic,[27] organic[28] and nanomaterials.[29] The inorganic systems,

which mainly use organometallic complexes as the luminophore, have been extensively studied because they possess unique optical properties, electrochemistry, and excellent ECL. So far, many metal complexes comprising europium,[30] ruthenium,[31] iridium[27] and copper[32] have been synthesized and their ECL properties have been investigated.

1.2.2 ECL from Ru(bpy)$_3^{2+}$ and its derivatives

The first report on ECL of Ru(bpy)$_3^{2+}$ was published in 1972 by Bard's group, where annihilation ECL was generated from ruthenium complexes *via* electron-transfer reactions between oxidized and reduced species.[20] This was followed by many further studies of the ECL behaviour of Ru(bpy)$_3^{2+}$ and its derivatives. A considerable number of studies have examined the mechanism of Ru(bpy)$_3^{2+}$.[7, 9, 11, 33] Taking the Ru(bpy)$_3^{2+}$-TPrA system as an example, ECL emission can occur through various routes (Schemes 1.3-1.6), and the dominant pathway is dependent on the ratio of the concentration of Ru(bpy)$_3^{2+}$ and TPrA. When Ru(bpy)$_3^{2+}$ is at a high concentration, the excited state is generated by reaction of the oxidized Ru(bpy)$_3^{3+}$ with either TPrA$^{\bullet}$ (Scheme 1.3) or Ru(bpy)$_3^{+}$ (Scheme 1.4). Under these conditions, the oxidation of TPrA by Ru(bpy)$_3^{3+}$ (Scheme 1.5) is also an important pathway. On the contrary, if the co-reactant TPrA is in large excess, then the TPrA oxidation reaction at the electrode plays the dominant role, and the excited state product is mainly generated by the reaction of Ru(bpy)$_3^{+}$ and TPrA$^{\bullet+}$ (Scheme 1.6). The clear understanding of the mechanism of Ru(bpy)$_3^{2+}$/TPrA ECL is useful to design highly efficient ECL systems and enhance reproducibility of the Ru(bpy)$_3^{2+}$ based immunoassay and other binding assays.
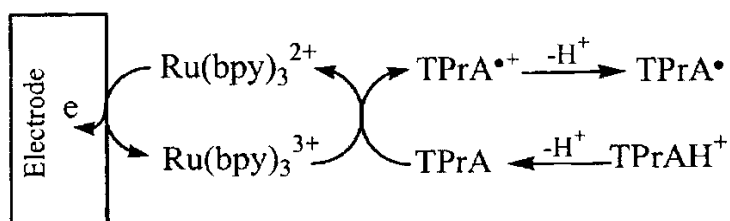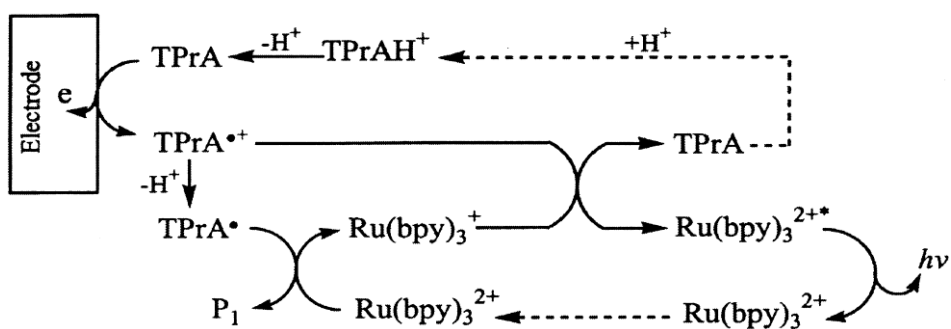
Scheme 1.3
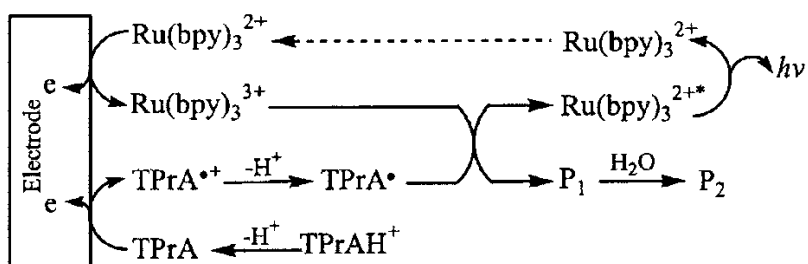
Scheme 1. 4
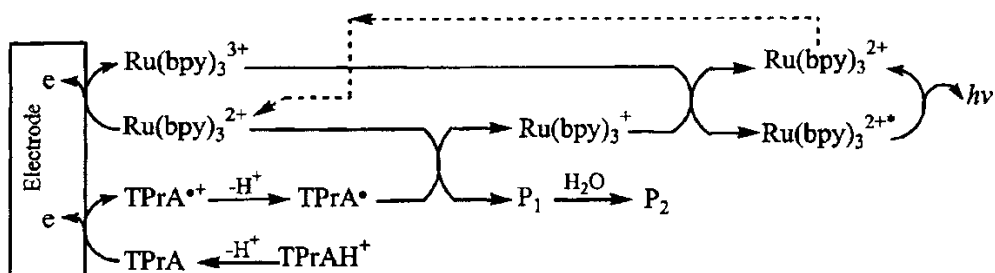
Scheme 1.5

Scheme 1.6

Scheme 1.3-1.6. General reaction mechanism of TPrA with Ru(bpy)$_3^{2+}$ under different conditions. Adapted from reference 33.

The photoluminescence quantum yield of $Ru(bpy)_3^{2+}$ in aqueous solutions is only 2.8%,[34] and thus limits the sensitivity of $Ru(bpy)_3^{2+}$-based analytical methods. Therefore, many attempts have been made to explore ruthenium complexes with higher efficiency than that of $Ru(bpy)_3^{2+}$. For example, Ciana $et\ al.$[35] investigated a family of Ru(II) complexes bearing mixed 2,2'-bipyridine (bpy) and bathophenanthroline disulfonate (BPS) ligands ($[Ru(BPS)_n(bpy)_{3-n}]^{(2n-2)-}$), where n decreases from 3 to 1. The electrochemistry of these species in acetonitrile showed reversible or partially reversible oxidation processes and fully reversible reductions, indicating that these species could generate ECL through cation-anion annihilation. As shown in Figure 1.3a, in the case of $[Ru(BPS)_2(bpy)]_2$, the electrochemical behaviour is very similar to that of $Ru(bpy)_3^{2+}$ with three reduction peaks and a single oxidation. The oxidation peak was a reversible one-electron processes, which was attributed to the Ru(II) metallic centre. Therefore, the ECL spectra of the complexes could be produced by ion annihilation reactions or co-reactant pathways. As the net charge changed from -4 to 0, the ECL intensity dramatically increased, with the neutral complex $[Ru(BPS)(bpy)_2]$ approximately 26 times greater than $Ru(bpy)_3^{2+}$. This was ascribed to the highly negative charge that promoted the formation of a filming product at the electrode during oxidation, resulting in the increased ECL intensity.

Besides improving luminescence yield of ECL luminophores to amplify the sensitivity of ECL assays, in recent years, several researchers have focused on making self-enhanced ECL reagents by linking co-reactants to a ruthenium complex. The efficiency can be improved significantly by introducing a co-reactant into the ligand structure of complexes due to more efficient intramolecular electron transfer between complexes and co-reactants than when in solution individually. A series of self-enhancing ECL co-reactant based on the complex $Ru(bpy)_3^{2+}$ have been developed and successfully used in amplified assays.[36, 37]
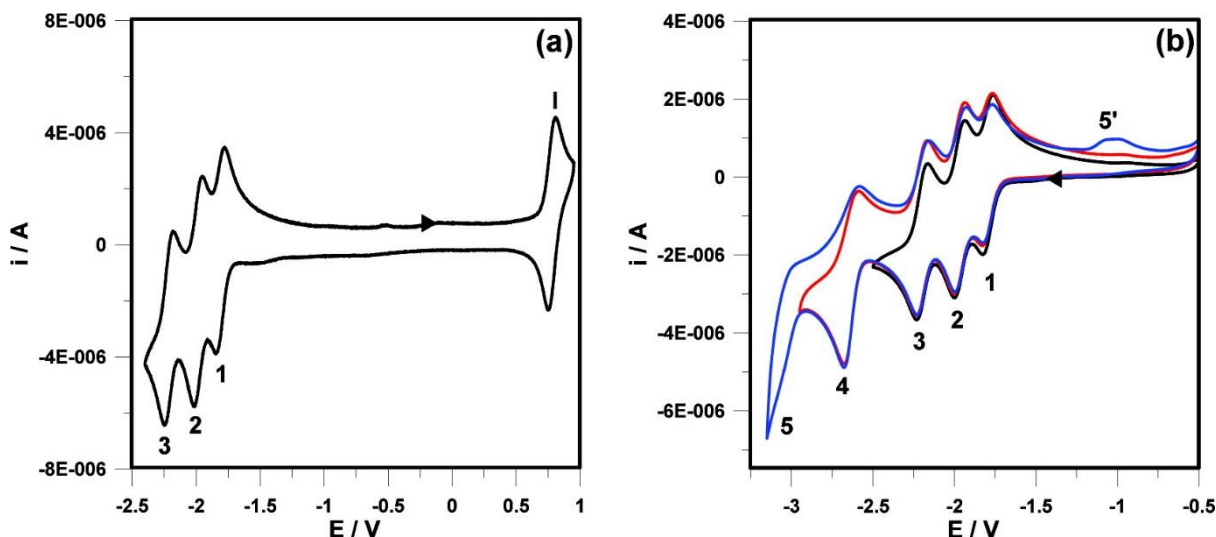
Figure 1.3. Cyclic voltammetric curves of 0.5 mM [Ru(BPS)(bpy)$_2$] in solution. Working electrode: Pt disk (diameter 3 mm).Scan rate: (a) 0.5 and (b) 0.2 V/s. Cyclic voltammogram under the same experimental conditions including the third (black line), fourth (red line), and fifth (blue line) reduction process occurring at the edge of the solvent window. Figure from reference 35.

Most of the ruthenium complexes are limited to emission wavelengths of around 600-650 nm, due to the highest occupied molecular orbital (HOMO) energy level based on the ruthenium metal centre being reasonably constant, thus reducing the possibility of developing multicolour ECL analytical techniques. Therefore, a family of ruthenium complex derivatives were designed and synthesized to broaden the emission wavelength range. Puodziukynaite and co-workers[38] successfully tuned the emission wavelength from 640 to 700 nm by introducing acrylate on the bipyridine ligand (Figure 1.4). Electrochemiluminescent devices based on the complexes exhibited colours from red-orange to deep red. The main reason for the color change is that their ligand-based lowest unoccupied molecular orbital (LUMO) value decreased and this resulted in lower energy triplet metal-to-ligand charge-transfer excited state transitions. The complexes were utilized as cross-linked electrochromic films and electrochemiluminescent layers in light-emitting electrochemical cell devices (Figure 1.4).
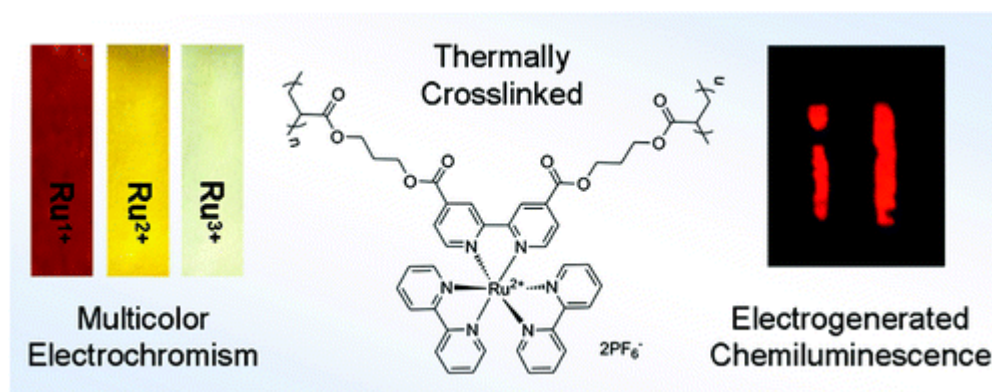
Figure 1.4. Acrylate-containing Ru(bpy)$_3^{2+}$-based coordination complexes. Figure from reference 38.

1.3 Iridium complexes

Over the last decade, iridium complexes have emerged as promising alternative ECL luminophores for ECL due to their versatile synthesis and excellent spectroscopic and electrochemical properties. Unlike ruthenium complexes, which are limited to the ligand-field splitting energies of ruthenium, iridium complexes could be easily tuned to desirable emission wavelengths (even near-infrared) through the introduction of substituents on the ligands, enabling manipulation of both HOMO and LUMO levels. Moreover, iridium complexes have high luminescence quantum yields, some approaching 100%, which facilitates the development of more sensitive and multiplexed ECL assays.[39, 40] In this regard, many groups have been focusing on the development of ECL active iridium luminophores with highly efficient luminescence and large emission wavelength ranges. Kim and co-workers[41] have reported that (pq)$_2$Ir(acac) and (pq)$_2$Ir(tmd) (pq = 2-phenylquinoline anion, acac = acetylacetonate anion, tmd = 2,2′,6,6′-tetramethylhepta-3,5-dione anion; see structures in Figure 1.5) with the co-reactant TPrA gave higher ECL intensities than the [Ru(bpy)$_3$]$^{2+}$-TPrA system. Particularly Ir(pq)$_2$acac, which has a low enough oxidation potential (expected to accelerate generation of the radical ion TPrA$^{\bullet}$) and well-matched reduction potential to accept electron efficiently from TPrA$^{\bullet}$, which means that the complexes more efficiently form excited states and emit light. The results demonstrated that

the ECL efficiency of luminescent metal complex molecules could be tuned through controlling energetics between the electron donor-acceptor pair (HOMO and LUMO levels) based on the electrochemical properties of complexes and available co-reactants. The significantly improved ECL efficiencies showcased the potential of iridium complexes becoming an alternative to ruthenium complexes for ECL sensing applications. However, this type of iridium complex with pq ligand has a similar emission wavelength to ruthenium complexes.
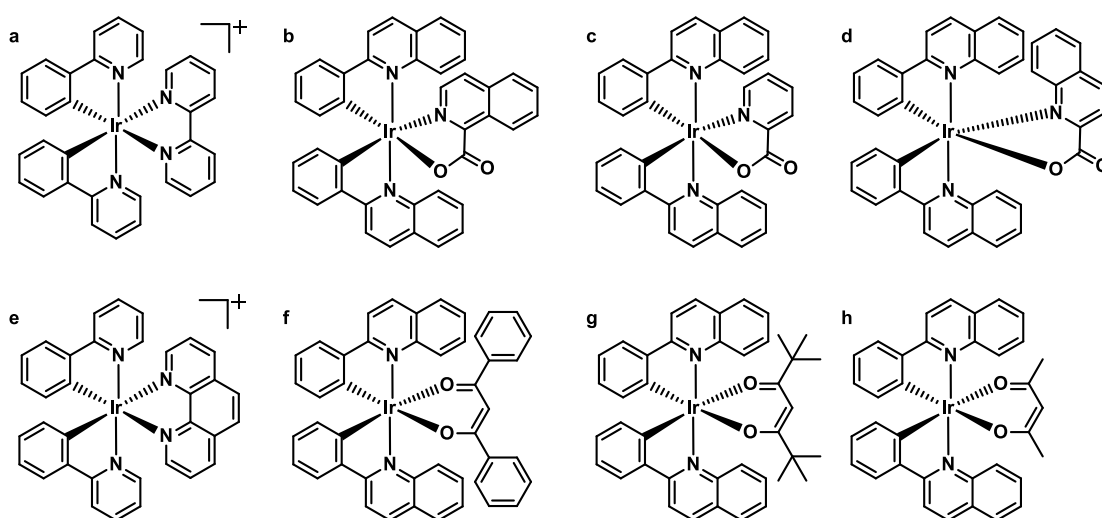
Figure 1.5. Intense ECL-emitting iridium complexes with 2-phenylpyridine or 2-phenylquinoline cyclometallating ligands and a variety of ancillary ligands reported by Kim *et al.*, (a) [Ir(ppy)$_2$(bpy)]$^+$, (b) Ir(pq)$_2$(3-iq), (c) Ir(pq)$_2$(pic), (d) Ir(pq)$_2$(quin), (e) [Ir(ppy)$_2$(phen)]$^+$, (f) Ir(pq)$_2$(dbm), (g) Ir(pq)$_2$(tmd), (h) Ir(pq)$_2$(acac). Figure from reference 41.

Recently, many iridium(III) complexes exhibiting blue/green luminescence have been reported. The common strategy to tune their emission colour is by controlling the energetic gap between HOMO and LUMO levels by attaching electron-withdrawing or electron-donating groups to different ligands. Swanick *et al.*[42] reported four bright electrochemiluminescent iridium(III) complexes containing aryltriazole cyclometallating ligands, with emissions down to the blue-cyan region at 503 nm.[42] This was achieved by adding fluorine substituents on the phenyltriazole ligands, which greatly increased the

HOMO–LUMO energy gap and resulted in a large hypsochromic shift in the emission. Inspired by the study, Ladouceur *et al.*[43] explored two strongly blue luminescent cationic heteroleptic iridium complexes containing an 4,4′-bis(dimethylamino)-2,2′-bipyridine (dmabpy) ancillary ligand and either 1-benzyl-4-(2,4-difluorophenyl)-1H-1,2,3-triazole (dFphtl) or 2-(2,4-di-fluorophenyl)-5-methylpyridine (dFMeppyH) cyclometalated ligands (Figure 1.6). These complexes showed efficient blue-shifted ECL emission, which further demonstrated that the feasibility of hypsochromically shifting the emission could be accomplished by anchoring the fluorine groups to the phenyl moiety of the ligands to stabilise the HOMO. After comparison of the electrochemical and ECL properties of these complexes which had the same fluorine group but with minor changes on the neutral ancillary ligand, we can understand the idea that the LUMO could be destabilised by attaching electron-donating groups to the bipyridine groups of the ligands while ensuring favourable energetic conditions for the ECL reaction. Other electron-withdrawing groups on the cyclometalating ligand (C^N) that result in a blue-shift of the phosphorescence of Ir(III) complexes are trifluoromethyl, sulfonyl,[44] and cyclometalated heterocycles.[45]

Green-emitting complexes have also received attention. Ir(ppy)$_3$$^{2+}$ was the first complex that showed green emission in 2002, explored by Bruce and Richter.[46] However, the ECL efficiency was only 0.33 compared with the standard ruthenium complex. Shavaleev *et al.*[47] used stronger electron-withdrawing sulfur pentafluoride groups (SF5) to modify 1-phenylpyrazole and 2-phenylpyridine cyclometalating (C^N) ligands, the resulting complexes exhibited green to yellow-green ECL emission with wavelength maxima ranging from 501 nm to 520 nm. Besides modifying the ligand of metal complexes, multi-color ECL systems can also be achieved by tuning the applied potential to the system, which will be illustrated in the following section.
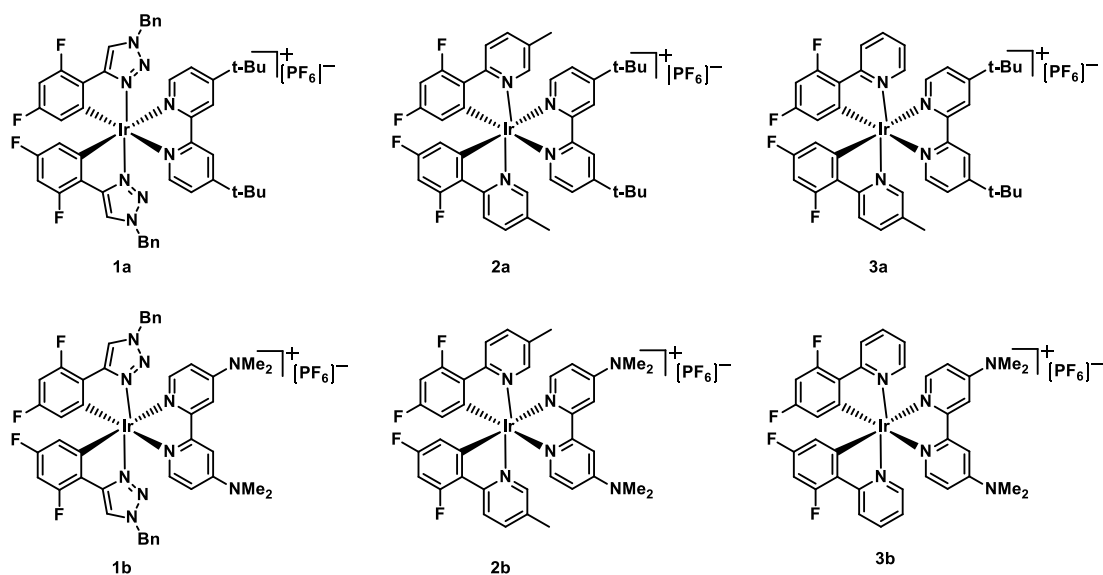
Figure 1.6. Complexes from the literature. Image from reference 43.

1.4 Synthesis of water-soluble iridium complex

Iridium complexes have many advantages such as high ECL efficiency and the ability to be easily tuned over a wider color range. However, the hydrophobic properties of iridium complexes limit their analytical applications, so it is still a significant challenge to develop practical approaches to make them more water soluble and biocompatible. Various strategies have been reported to overcome this problem. The basic protocol is that the ligands of iridium complexes can be modified with more hydrophilic groups, such as saccharide,[48] sulfonate[49] or polyethylene glycol chains (Figure 1.7).[50] For example, Li's group[48] made a water-soluble iridium complex with a hydrophilic appended sugar, and the ECL intensity of the complex was higher than the conventional ruthenium complex under certain conditions, the iridium complex was successfully applied to test antibiotics with a detection limit of 3 nM.[48]

Kiran *et al.*[51] reported an intense chemiluminescence of bis(2-phenylpyridine-C^2,N")(bathophenanthrolinedisulfonate) iridium(III), Ir(p-py)$_2$DSBPNa, and bis(2,4-difluorophenylpyridine-C2,N)(bathophenanthrolinedisulfonate) iridium(III)

(Ir(fppy)$_2$DSBPNa) which had a hydrophilic diimine ligand, DSBP^{2-}. These complexes normally showed red shifted emission after addition of the hydrophilic ligand. To obtain water-soluble green or blue emitting iridium complexes, Kerr *et al.*[52] made a series of complexes with an ancillary 1,2,3-triazol-4-ylpyridine ligand containing sulfonate substituents or tetraethylene glycol (TEG) groups which allowed for higher aqueous solubility, as shown in Figure 1.7, the results showed that Ir(df-ppy)$_2$(pt-TEG)]$^+$ (df-ppy = 2-(2,4-difluorophenyl)pyridine, pt-TEG = 1-(2-(2-(2-(2-hydroxyethoxy)ethoxy)ethoxy)-ethyl)-4-(2-pyridyl)-1,2,3-triazole) produced higher ECL intensity over the orange-red emitter [Ru(bpy)$_3$]$^{2+}$, making it a highly effective blue emitter .
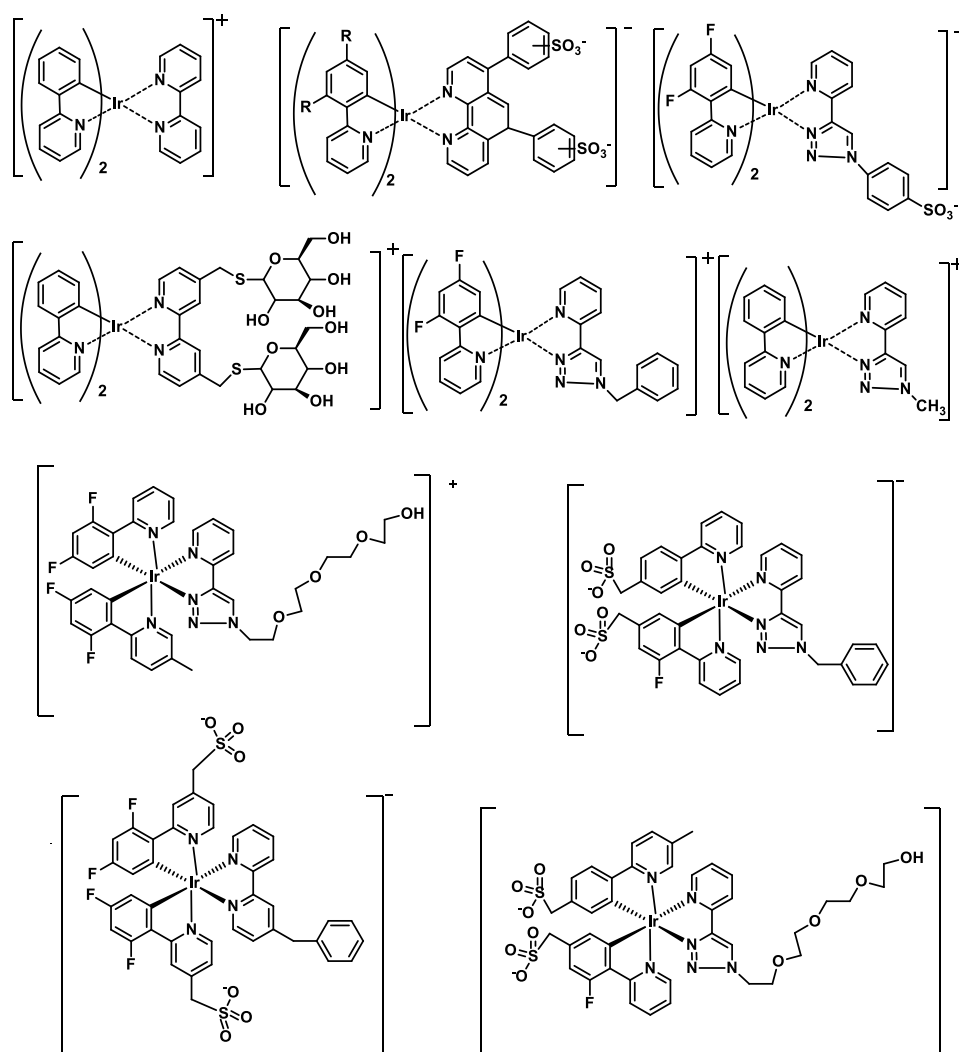

Figure 1.7. Various water-soluble Ir(III) complexes previously examined for photoluminescence, chemiluminescence, and/or ECL detection. Figure adapted from reference 52.

The second method to improve the water-solubility or aqueous applicability is the practice of doping the complex into nanoparticles, which can then be dispersed in water. The nanoparticle can not only can dissolve in water but also avoid quenching from oxygen. Moreover, the nanoparticles exhibit low toxicity, and are cheap and simple to prepare. Xue and co-workers[53] developed an iridium-complex loaded polypyrrole nanoparticle for photodynamic therapy. However, this kind of nanoparticle could not be used as an ECL reagent, due to the polymer most likely blocking and quenching the ECL properties of the iridium complex. To overcome this problem, silica nanoparticles have been the most commonly used nano-size material to encapsulate the metal complex. The hydrophobic iridium complex $Ir(pq)_2(acac)$ (acac = acetylacetonato; pq = 2-phenylquinolinato), $Ir(iqbt)_2(dpm)$ or fac-$Ir(iqbt)_3$ (dpm = 2,2,6,6-tetramethyl-3,5-heptanedione; iqbt = 1-(benzo[b]thiophen-2-yl)-isoquinoline), which showed intense ECL emission, was doped into silica nanoparticles with a hydrophilic polyethylene glycol outer shell in aqueous media (Figure 1.8).[54] The ECL characterization and photoluminescence experiments confirmed that even though the complexes are defined in a silica insulating matrix, electron-transfer still occurred and resulted in ECL emission. Additionally, after the $Ir(pq)_2acac$ was doped into silica nanoparticles (SiNPs), the resulting nanoparticle was used to develop a nanoparticle-based sensor for the sensitive and selective detection of cyanide anions.[55]
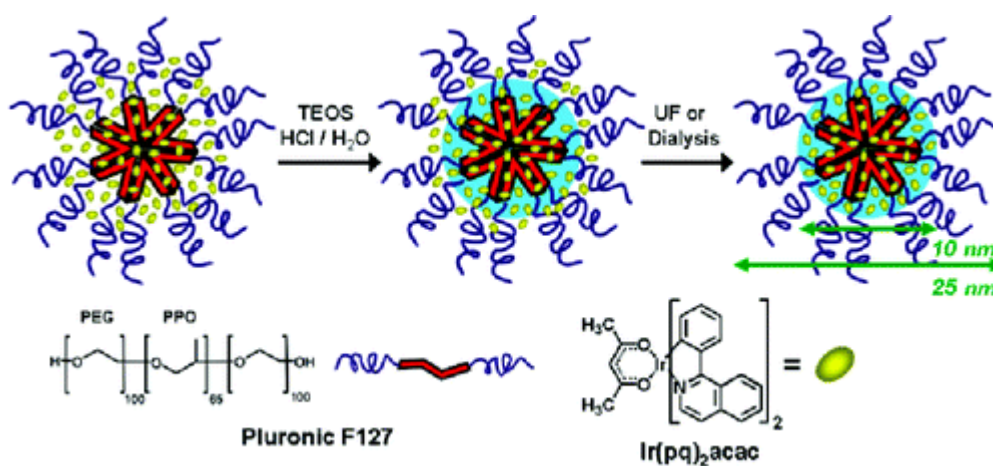

Figure 1.8. Schematic structure and preparative steps. Figure from reference 54.

1.5 Factors contributing to ECL comparison for metal complexes

In recent decades, efforts have been made to explore alternative metal complexes to replace $Ru(bpy)_3^{2+}$. Therefore, the comparison between other metal complexes and the standard $Ru(bpy)_3^{2+}$ complex plays a very important role when evaluating relative ECL intensity. Kim *et al.*[41] reported that for $Ir(pq)_2(acac)$ and $Ir(pq)_2(tmd)$ ECL intensities were 77-fold and 49-fold greater than that of $[Ru(bpy)_3]^{2+}$ in the presence of the co-reactant TPrA in acetonitrile solution. But for $Ir(pq)_2(acac)$, Zhou *et al.*[56] recorded a much lower value of 10 (*vs* $[Ru(bpy)_3]^{2+} = 1$) under the experimental conditions.

There are many factors that may contribute to the variation in the ECL efficiency for the same metal complex. The first factor is the method: several types of electrochemical methods are used for ECL initiation and investigation, most commonly involving cyclic voltammetry[57] and chronoamperometry.[58] Depending on which species are oxidized and reduced, the methods can involve different reaction pathways for the complexes and could result in the difference in ECL intensities often reported.

The second factor is the choice of light detector. Currently, the photomultiplier tube (PMT)[59] and charged coupled device (CCD) spectrometer[11] and are two of the most commonly used optical detectors for ECL. PMT's with different peak spectral responses can be used to optimize the response from different luminophores. CCD spectrometers provide significant advantages over PMTs due to the ability to provide spectral information but are considerably less sensitive. An alternative photodetector, which can also provide discrimination between different coloured emitters is a digital camera. Doeven *et al.*[60] successfully captured ECL at an electrode surface from three different emitters using a digital camera, the RGB colour channels of the photographs could be separated and analysed using ImageJ software, which allowing sensitive detection of the red, green and blue luminophores at concentrations as low as 0.07, 0.4 and 0.2 µM respectively. The

concept of using cameras as photodetectors opens a now door for developing low cost, portable and sensitive multiplexed ECL detection systems.

The third factor is the concentration of co-reactant, as mentioned previously, different ratios of concentrations between TPrA and $Ru(bpy)_3^{2+}$ can lead to different ECL generation pathways, and further affect the ECL intensity. Additionally, the factors such as solvent, electrolyte, and reaction time all could contribute to changes in ECL intensity. These will be discussed in Chapter 2.

1.6 Multi-colour ECL from metal chelates

Iridium complexes can be tuned in to a wide range of emission wavelengths, (i.e. from blue to red), which makes them important ECL reagents, as it opens the possibility of developing multicolor ECL systems for multiplex analysis. The first demonstration of multi-colour ECL was reported by Bruce and Richter,[61] where $Ru(bpy)_3^{2+}$ was combined with green emissive $Ir(ppy)_3$ (ppy = 2-phenylpyridine). As shown in Figure 1.9, the wavelength of peak emission for $Ir(ppy)_3$ was distinguishable from $Ru(bpy)_3^{2+}$, which made it possible to get separate signals in a solution with both complexes present with the co-reactant TPrA.

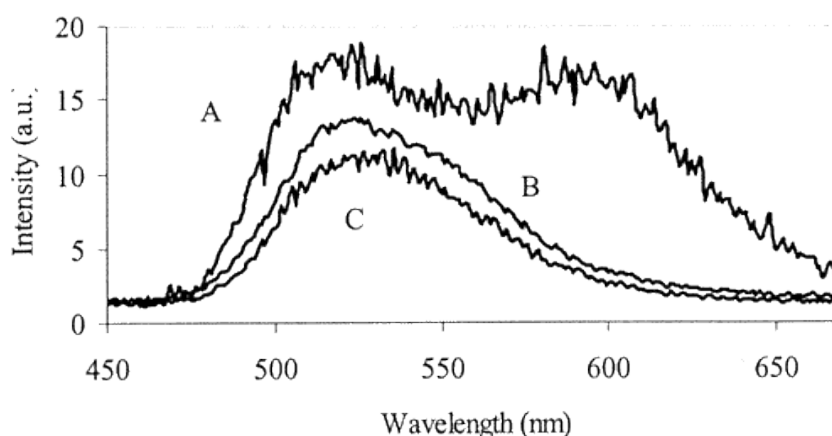**Figure 1.9**. ECL spectra of (A) a 10 uM $Ir(ppy)_3$ and 10 uM $Ru(bpy)_3^{2+}$ solution in CH_3CN containing 0.05 M TPrA (0.1 M Bu_4NPF_6 as electrolyte, (B) 10 uM $Ir(ppy)_2$ (0.05 M TPrA) in CH_3CN (0.1 M Bu_4NPF_6) , and (c) 10 uM $Ir(ppy)_3$ (0.05 M TPrA) in CH_3CN/H_2O (50:50 (v/v), 0.1 M KH_2PO_4). Figure from reference 61.

After that, many attempts had been made to develop efficient spectrally resolved ECL systems by combining metal chelates with different emission colours.[60, 62] However, only a small number of iridium complexes with high ECL efficiency were suitable for this approach, and the mixture can result in considerable overlap of the emission maxima. Doeven *et al*.[62] proposed that ECL of metal complex could be selectively detected from the mixed metal chelate system by the modulation of the applied potential. Solutions of $[Ru(bpy)_2(L)]^{2+}]$ (ppy = 2-phenylpyridine; L is a derivative of 2,2'-bipyridine) and either $Ir(df-ppy)_2(BPS)]^-$ (df-ppy = 2-(2,4-difluorophenyl)pyridine) or Ir(ppy) were selected to test the concept. The emission of ECL intensity *vs* electrode potential and emission wavelength could be simplified by automated acquisition of ECL spectra using a CCD or camera synchronised with the cyclic voltammetry or chronoamperometry experiments. This provided new avenues for multianalyte ECL detection. Following this work, they extended the concept to three-component ECL systems.[60] For the mixture of $[Ru(bpy)_2(dm-bpy-dc)]^{2+}$ (dm-bpy-dc = dimethyl 2,2'-bipyridine-4,4'-dicarboxylate), $Ir(ppy)_3$ and $Ir(df-ppy)_3$, the colour of the system could be switched between green, blue and red using the applied potential. However, the mechanism of the multi-component system was more complicated than single emitter systems because the multi-colour phenomenon was also related to the concentration of co-reactant and electrochemiluminophores. More recently, the ability to modulate the colour of annihilation ECL emission in mixtures of luminophores was also demonstrated.[63, 64]
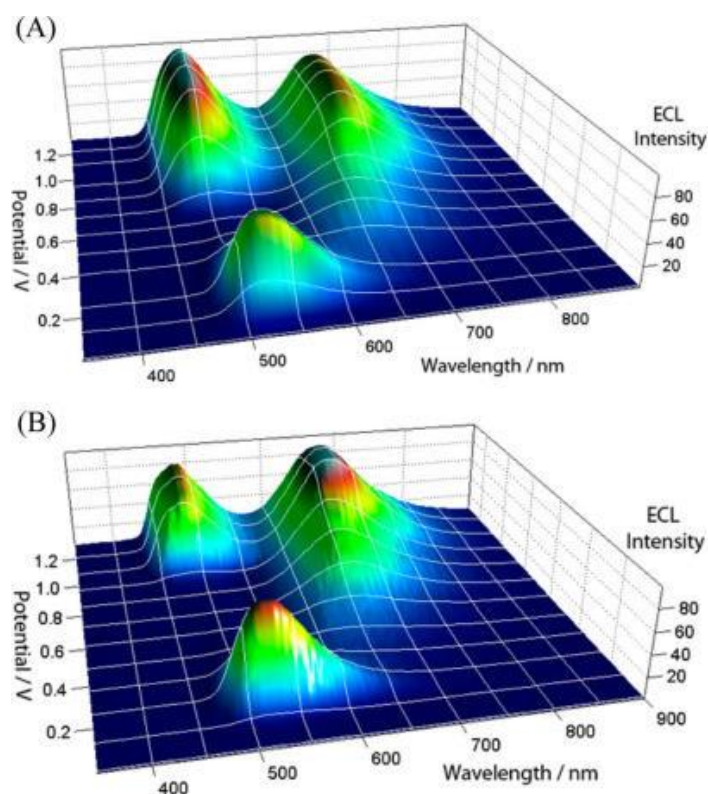
Figure 1.10. 3D-ECL excitation−emission matrices for red−green−blue electrogenerated chemiluminescence (RGB-ECL) system. Figure from reference 60.

1.7 Metal chelate-based ECL labels

A number of metal chelate-based ECL luminophores possess excellent ECL emission, and some of them have been found to emit more intensive ECL than $Ru(bpy)_3^{2+}$ in organic solvents.[42, 65, 66] Among these metal chelates, ruthenium and iridium complexes have become the most commonly used ECL labels for the development of various assays for DNA (deoxyribonucleic acid), proteins, small molecules and so on. However, the practical applications have been limited due to their poor solubility in aqueous solution and the lack of straight forward bioconjugation. For use as labels in immunoassay or other binding assays, a bioconjugation group such as carboxylic acid, *N*-succimidyloxycarbonylpropyl, biotin or amino are required to link the metal complex to the biologically active species. Additionally, the electrochemical reaction occurs within the diffusion layer close to the surface of the working electrode, if metal complexes are labelled with a high molecular

weight or long strand nucleic acid molecule, this could keep the metal complex far away from working electrode surface, reducing or inhibiting the direct oxidation of the metal complex and reducing the ECL emission due to the different ECL reaction pathway which occurs.[67] Based on the above consideration, only a small amount of metal complex would be used for ECL detection. The ECL labels in commercial ECL systems are limited to derivatives of the classic $[Ru(bpy)_3]^{2+}$ luminophore. Therefore, it is important to explore new metal-complex based ECL labels for possible application in the immunoassay market. Yu *et al*.[68] synthesized two new ECL labels based on ruthenium complexes shown in Figure 1.11 (Label 1 and Label 2)[68] with carboxylic acid as the bioconjugation group, which were compared with one used in commercial systems (Label 3). In this study, mouse IgG was used as the analyte (antigen), while goat anti-mouse IgG(H+L) and biotinylated rabbit anti-Mouse IgG(H+L) were labelled with metal complexes and used as capture antibodies, respectively. The results demonstrated that ECL immunoassay performance could be improved by taking advantage of the more intense emission of new ruthenium complexes for the development of ECL-based clinical immunoassays. Besides ruthenium labels, five novel cationic iridium labels and one control ruthenium label, each bearing a carboxylic group, were prepared,[69] and the BSA-labelled iridium complex displayed an ECL signal that was 1.9 times higher than the same amount labelled by the traditional ruthenium-based label in Procell buffer solution. These novel iridium labels, exhibiting various emission colors, shed light on the further development of ECL-based analytical technology.

In addition to ruthenium and iridium complexes, several other transition metal chelates (La, Os, Cr, Re) have been reported as potential labels. For example, osmium polypyridine complexes[70] showed better photostability and lower oxidation potentials than their ruthenium analogues, and therefore they could be useful in the design of DNA-labelling agents. However, no immunoassay utilizing these labels has yet been described.
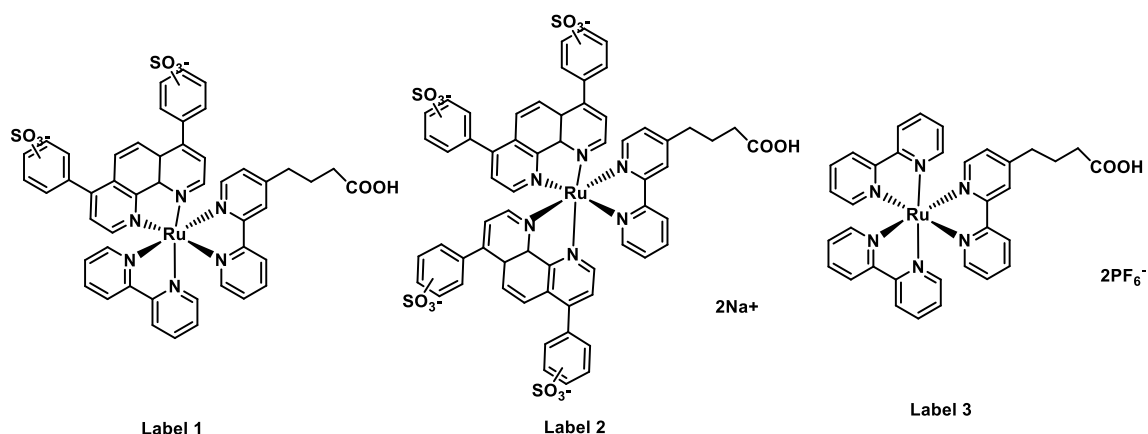
Figure 1.11. Molecular structures of ruthenium(II) diimine labels. Figure adapted from reference 68.

1.8 Iridium complex-based ECL for bio-application

During the last few decades, iridium complex-based ECL systems have been successfully used to detect different analytes, including protein,[71] nucleic acid[72] and various other small molecules.[73] For example, analytes such as ammonia,[73] NH_4^+,[74] hydroxide and ethoxide ions,[75] have been detected as alternative co-reactants to TPrA. Based on the study by Qi *et al.* that showed the iridium complex (pq)$_2$Ir(N-phMA) (pq is 2-phenylquinoline anion, N-phMA is *N*-phenylmethacrylamide) could be immobilized onto a glassy carbon electrode and respond sensitively to TPrA,[74] Song *et al.*[40] developed a solid-state ECL sensor for the detection of NH_4^+ using a (pq)$_2$Ir(N-phMA) modified electrode. In order to more clearly understand the electrochemical process and the ligand effect on ECL efficiency, they studied the ECL response to ammonia using four iridium complexes (ppy)$_2$Ir(acetylaniline), (ppy)$_2$Ir(N-phMA), Ir(ppy)$_3$ and (pq)$_2$Ir(acac)[72] with minor changes to the ligand with each complex. It was found that (pq)$_2$Ir(acac) showed greater ECL efficiency than the other complexes when ammonia was employed as co-reactant. This is because the lowest LUMO energy level made the complex more easily accept the electron from the radical NH_2 species which was produced from the dehydrogenation of NH_3. The concentration of analyte could

be detected at concentrations as low as 4×10^{-8} M, and the sensor was applied to quickly determine NH_3 in the atmosphere with recovery of 92.5–101.9%.

Based on the intercalation of the metal complex and DNA, another kind of ECL sensor has been fabricated for the determination of DNA. It was reported that certain iridium complexes could be employed as efficient binders for G-quadruplex, including telomeric DNA.[76, 77] This group of iridium complexes normally must have an ancillary ligand that can be specifically interacted into G-quadruplex DNA but has no response to double-stranded or single-stranded DNA. Based on these studies, a number of luminescent iridium complexes have been employed as probes for the development of G-quadruplex assay for the detection of a wide range of analytes including interferon-gamma,[78] adenosine,[79] and Siglec-5.[80] To extend the concept for ECL application, a new class of cyclometalated iridium(III) complexes bearing π-extended phenylimidazole phenanthroline ligands (shown in Figure 1.12) were described by Sleiman's group.[71] Complex 2 and 5 showed a "switch-on" effect in the presence of G-guadruplex DNA and the ECL signal was greatly enhanced. These promising results demonstrated that iridium complexes could be used as ECL reagents to construct label-free sensor for the detection of low levels of DNA.
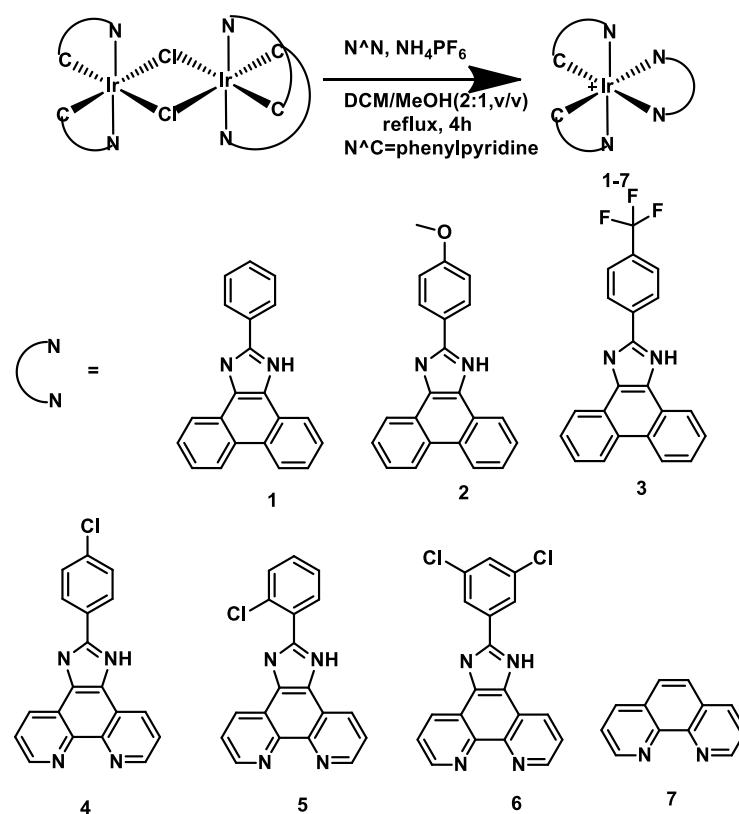
Figure 1.12. Synthesis of Complexes 1−7. Figure adapted from reference 71.

Iridium complexes are also used as ECL labels to detect a variety of biomolecules. Iridium complexes with functional groups (e.g. amino, carboxyl) can also be loaded onto a nanoparticle surface to serve as a nanoprobe. For example, a simple gold nanoparticle (AuNP) driven ECL aptasensor was fabricated by Zhao's group (Figure 1.13).[81] Using AuNPs decorated with iridium complexes as an ECL label, Fumonisin B1 was successfully detected with limit of detection as low as 0.27 ng/mL.
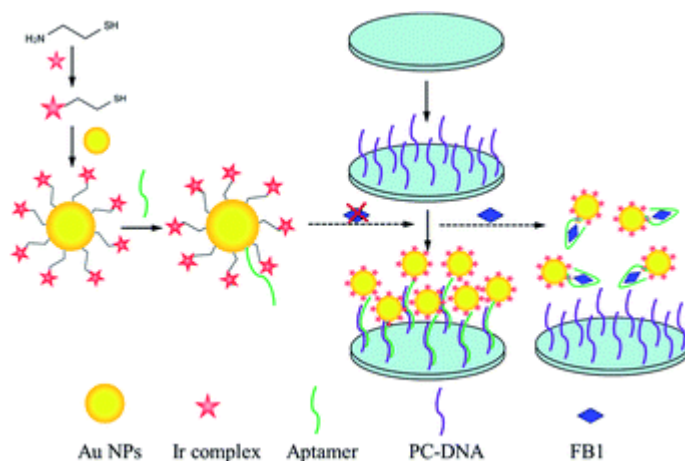
Figure 1.13. Illustration of AuNPs driven ECL aptasensors for FB1 detection. Figure from reference 81.

Magnetic bead technology is another potential amplification method employed in the construction of ECL bioassays, which allows the metal-complex based ECL label to be separated from unbound labels without a complex separation step. Commercial instruments based on magnetic bead technology have been available for the detection of a wide range of biomolecules. For example, in the operation of the commercial ECL instrument, BioVerris M-Series analyzers, the $Ru(bpy)_3^{2+}$-tagged species are immobilized on magnetic beads that are brought to an electrode surface magnetically for analysis. This provides much more sensitive ECL detection than the immunoassay without beads. Many other magnetic beads based ECL assays have been explored due to the success of these instruments. As shown in Figure 1.14,[82] sequences of ssDNA or antibody can be loaded on the surface of magnetic beads, the ECL-label tagged species are attached by hybridizing with the probe ssDNA or forming sandwich immunoassay, the beads are then brought to the electrode surface by the application of a magnetic field. This approach can result in improvement in sensitivity of almost 100 times compared to a previously reported surface-immobilized ECL method. The high sensitivity showed that most of the $Ru(bpy)_3^{2+}$ attached to the bead *via* the attached recognition element was involved in the ECL reaction and contributed to the ECL intensity. However, only small amount of $Ru(bpy)_3^{2+}$ close to the electrode can be directly oxidized

on the electrode due to the beads blocking on the surface. This concept is also suitable for developing bioassays based on iridium complexes.

Figure 1.14. Schematic diagrams of (a) DNA hybridization and (b) sandwich type immunoassay using a polystyrene bead as the ECL label carrier and a magnetic bead for the separation of analyte-containing ECL label/polystyrene beads. Adapted from reference 82.
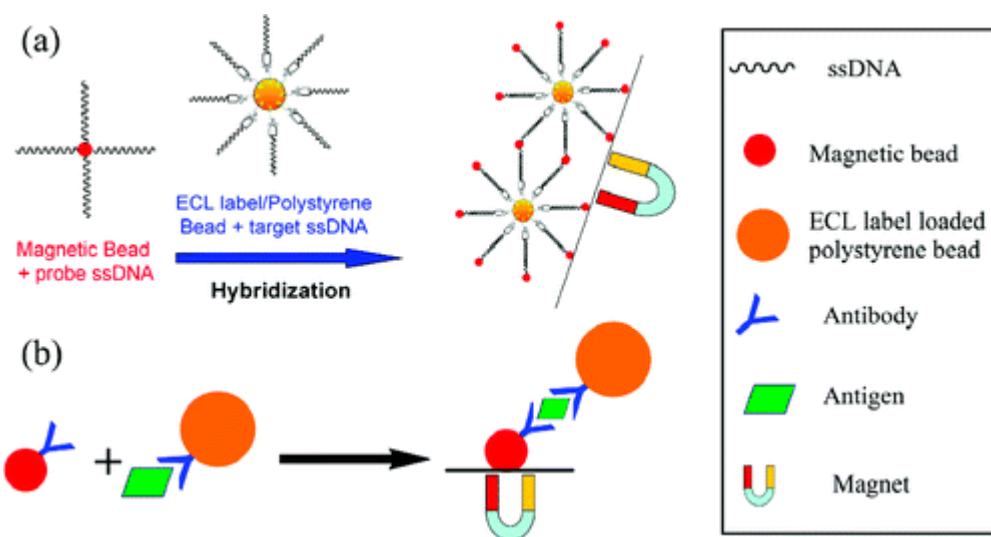
1.9 Linking Statement

The papers presented in this thesis focus on a series of novel iridium complexes and the study of their ECL properties, encompassing detailed electrochemical, structural and photophysical investigations. This includes exploration of the effects of reaction conditions and electrochemical methods used to initiate ECL, the design and evaluation of new water-soluble iridium complexes for ECL detection, examination of the influence of ligand structure on ECL intensity and reaction mechanism, and the application of novel ECL labels in real-world assays for the detection of ssRNA and protein targets.

Chapter 2 is a re-evaluation of a set of heteroleptic iridium(III) complexes containing an acetylacetonate ligand (acac) that were previously reported to exhibit high ECL intensities, to understand the influence of instrumental and chemical conditions on relative ECL intensities, and elucidate source of some conflicting prior findings.

Chapter 3 describes the synthesis and evaluation of new water-soluble iridium(III) complexes containing a 2,2′-bipyridine (bpy) ligand with one or two tetraethylene glycol (TEG) groups, as potential ECL luminophores with different emission colours and a convenient point of attachment for bioconjugation.

Chapter 4 examines the limitations of contemporary iridium(III) complex ECL labels, and introduces a convenient and versatile synthetic approach to prepare iridium(III) labels incorporating a phenyltriazole derivative designed for bioconjugation. The ECL intensities from the labels under two different assay conditions is exploited to derive a new understanding of the mechanisms of ECL reactions with iridium(III) complexes.

As outlined in the Conclusions and Future Work (Chapter 5), this research makes significant contribution to the understanding and application of iridium complexes in ECL detection systems, and reveals several important new strategies for the development of highly sensitive ECL detection systems.

1.10 References

1.   A. W. Knight, TrAC Trends in Analytical Chemistry, 1999, 18, 47-62.

2.   M. Su and S. Liu, Analytical Biochemistry, 2010, 402, 1-12.

3.   M. M. P. S. Neves, M. B. González-García, D. Hernández-Santos and P. Fanjul-Bolado, ChemElectroChem, 2017, 4, 1686-1689.

4.   S. P. Forry and R. M. Wightman, Analytical Chemistry, 2002, 74, 528-532.

5.   S. Sun, Y. Wei, H. Wang, Y. Cao and B. Deng, Talanta, 2018, 179, 213-220.

6.   H. Peng, M. Jian, H. Deng, W. Wang, Z. Huang, K. Huang, A. Liu and W. Chen, ACS Applied Materials & Interfaces, 2017, 9, 14929-14934.

7.   W.-Y. Lee, Microchimica Acta, 1997, 127, 19-39.

8.   M. Rizwan, N. F. Mohd-Naim and M. U. Ahmed, Sensors, 2018, 18, 166.

9.   K. A. Fähnrich, M. Pravda and G. G. Guilbault, Talanta, 2001, 54, 531-559.

10.   Z. Liu, W. Qi and G. Xu, Chemical Society Reviews, 2015, 44, 3117-3142.

11.   L. Hai-Juan, H. Shuang, H. Lian-Zhe and X. Guo-Bao, Chinese Journal of Analytical Chemistry, 2009, 37, 1557-1565.

12.   D. M. Hercules, Science, 1964, 145, 808-809.

13.   K. Santhanam and A. J. Bard, Journal of the American Chemical Society, 1965, 87, 139-140.

14.   S. S. Miao, M. S. Wu, L. Y. Ma, X. J. He and H. Yang, Talanta, 2016, 158, 142-151.

15.   X. Fu, X. Tan, R. Yuan and S. Chen, Biosensors and Bioelectronics, 2017, 90, 61-68.

16.   W. Gao, C. Wang, K. Muzyka, S. A. Kitte, J. Li, W. Zhang and G. Xu, Analytical Chemistry, 2017, 89, 6160-6165.

17.   H. Li, S. Voci, A. Wallabregue, C. Adam, G. M. Labrador, R. Duwald, I. Hernández Delgado, S. Pascal, J. Bosson, J. Lacour, L. Bouffier and N. Sojic, ChemElectroChem, 2017, 4, 1750-1756.

18. R. Dai, F. Wu, H. Xu and Y. Chi, ACS Applied Materials & Interfaces, 2015, 7, 15160-15167.

19. P. Bertoncello and R. J. Forster, Biosensors & Bioelectronics, 2009, 24, 3191-3200.

20. N. E. Tokel and A. J. Bard, Journal of the American Chemical Society, 1972, 94, 2862-2863.

21. H. Wei and E. Wang, Luminescence, 2011, 26, 77-85.

22. Y. Hu, L. Li, A. P. Shaw, J. R. Norton, W.Sattler, Y. Rong Organometallics, 2012, 31, 5058−5064.

23. F. Kanoufi and A. J. Bard, Journal of Physical Chemistry B, 1999, 103, 10469-10480.

24. A. W. Knight and G. M. Greenway, Analyst, 1995, 120, 2543-2547.

25. H. Wang, R. Yuan, Y. Chai, Y. Cao, X. Gan, Y. Chen and Y. Wang, Biosensors & Bioelectronics, 2013, 43, 63-68.

26. W. Miao, J.-P. Choi and A. J. Bard, Journal of the American Chemical Society, 2002, 124, 14478-14485.

27. A. Fiorani, G. Valenti, M. Iurlo, M. Marcaccio and F.Paolucci, Current Opinion in Electrochemistry 2018, 8, 31-38.

28. C. A. Marquette and L. c. J. Blum, Analytica Chimica Acta, 1999, 381, 1-10.

29. M. Liu, Y. Xu, Y. Wang, X. Chen, X. Ji, F. Niu, Z. Song and J. Liu, Advanced Optical Materials, 2017, 5, 1600661.

30. S. Lis, K. Staninski and T. Grzyb, International Journal of Photoenergy, 2008, 2008.

31. Y. Yu, C. Lu and M. Zhang, Analytical Chemistry, 2015, 87, 8026-8032.

32. J. McCall, D. Bruce, S. Workman, C. Cole and M. M. Richter, Analytical Chemistry, 2001, 73, 4617-4620.

33. B. A. Gorman, P. S. Francis and N. W. Barnett, Analyst, 2006, 131, 616-639.

34. M. Zhou, G. P. Robertson and J. Roovers, Inorganic Chemistry, 2005, 44, 8317-8325.

35. L. Della Ciana, S. Zanarini, R. Perciaccante, E. Marzocchi and G. Valenti, Journal of Physical Chemistry C, 2010, 114, 3653-3658.

36. Y. Yuan, L. Zhang, H. Wang, Y. Chai and R. Yuan, Analytica Chimica Acta, 2017.

37. Y. Liao, X. Zhou, Y. Fu and D. Xing, Analytical Chemistry, 2017, 89, 13016-13023.

38. E. Puodziukynaite, J. L. Oberst, A. L. Dyer and J. R. Reynolds, Journal of the American Chemical Society, 2011, 134, 968-978.

39. N. M. Shavaleev, G. Xie, S. Varghese, D. B. Cordes, A. M. Slawin, C. Momblona, E. Orti, H. J. Bolink, I. D. Samuel and E. Zysman-Colman, Inorganic Chemistry, 2015, 54, 5907-5914.

40. S. Q. Sun, Q. J. Song, H. F. Yuan and Y. Q. Ding, Chinese Chemical Letters, 2008, 19, 1509-1512.

41. J. I. Kim, I.-S. Shin, H. Kim and J.-K. Lee, Journal of the American Chemical Society, 2005, 127, 1614-1615.

42. K. N. Swanick, S. Ladouceur, E. Zysman-Colman and Z. Ding, Chemical Communications, 2012, 48, 3179-3181.

43. S. Ladouceur, K. N. Swanick, S. Gallagher‐Duval, Z. Ding and E. Zysman‐Colman, European Journal of Inorganic Chemistry, 2013, 2013, 5329-5343.

44. E. C. Constable, C. D. Ertl, C. E. Housecroft and J. A. Zampese, Dalton Transactions, 2014, 43, 5343-5356.

45. S.-C. Lo, C. P. Shipley, R. N. Bera, R. E. Harding, A. R. Cowley, P. L. Burn and I. D. Samuel, Chemistry of Materials, 2006, 18, 5119-5129.

46 D. Bruce and M. M. Richter, Analytical Chemistry, 2002, 74, 1340-1342

47.   N. M. Shavaleev, G. Xie, S. Varghese, D. B. Cordes, A. M. Slawin, C. Momblona, E. Ort í H. J. Bolink, I. D. Samuel and E. Zysman-Colman, Inorganic Chemistry, 2015, 54, 5907-5914.

48.   M.-J. Li, P. Jiao, M. Lin, W. He, G.-N. Chen and X. Chen, Analyst, 2011, 136, 205-210.

49.   L. Yu, Z. Huang, Y. Liu and M. Zhou, Journal of Organometallic Chemistry, 2012, 718, 14-21.

50.   Z. M. Smith, E. Kerr, E. H. Doeven, T. U. Connell, N. W. Barnett, P. S. Donnelly, S. J. Haswell and P. S. Francis, Analyst, 2016, 141, 2140-2144.

51.   R. V. Kiran, E. M. Zammit, C. F. Hogan, B. D. James, N. W. Barnett and P. S. Francis, Analyst, 2009, 134, 1297-1298.

52.   E. Kerr, E. H. Doeven, G. J. Barbante, T. U. Connell, P. S. Donnelly, D. J. Wilson, T. D. Ashton, F. M. Pfeffer and P. S. Francis, Chemistry-A European Journal, 2015, 21, 14987-14995.

53.   F. Xue, M. Shi, Y. Yan, H. Yang, Z. Zhou and S. Yang, RSC Advances, 2016, 6, 15509-15512.

54.   S. Zanarini, E. Rampazzo, S. Bonacchi, R. Juris, M. Marcaccio, M. Montalti, F. Paolucci and L. Prodi, Journal of the American Chemical Society, 2009, 131, 14208-14209.

55.   J. Mu, Q. Feng, X. Chen, J. Li, H. Wang and M.-J. Li, Microchimica Acta, 2015, 182, 2561-2566.

56   Y. Zhou, W. Li, L. Yu, Y. Liu, X. Wang, M. Zhou, Dalton Transactions, 2015, 44, 1858-1865.

57.   D. Aikens, Electrochemical methods, fundamentals and applications. ACS Publications, 1983.

58.   G. J. Barbante, E. H. Doeven, E. Kerr, T. U. Connell, P. S. Donnelly, J. M. White, T. Lopes, S. Laird, D. J. Wilson and P. J. Barnard, Chemistry-A European Journal, 2014, 20, 3322-3332.

59   H. Yang, J. K. Leland, D. Yost and R. J. Massey, Nature Biotechnology, 1994, 12, 193.

60   E. H. Doeven, G. J. Barbante, E. Kerr, C. F. Hogan, J. A. Endler and P. S. Francis, Analytical Chemistry, 2014, 86, 2727-2732.

61.   B. D. Muegge and M. M. Richter, Analytical Chemistry, 2004, 76, 73-77.

62.   E. H. Doeven, E. M. Zammit, G. J. Barbante, C. F. Hogan, N. W. Barnett and P. S. Francis, Angewandte Chemie, 2012, 124, 4430-4433.

63.   E. Kerr, E. H. Doeven, G. J. Barbante, C. F. Hogan, D. J. Bower, P. S. Donnelly, T. U. Connell and P. S. Francis, Chemical Science, 2015, 6, 472-479.

64.   E. Kerr, E. H. Doeven, G. J. Barbante, C. F. Hogan, D. J. Hayne, P. S. Donnelly and P. S. Francis, Chemical Science, 2016, 7, 5271-5279.

65.   A. Kapturkiewicz and G. Angulo, Dalton Transactions, 2003, 3907-3913.

66.   A. Kapturkiewicz, J. Nowacki and P. Borowicz, Electrochimica Acta, 2005, 50, 3395-3400.

67.   K. Komori, K. Takada, O. Hatozaki and N. Oyama, Langmuir, 2007, 23, 6446-6452.

68.   L. Yu, Y. Liu and M. Zhou, Analytical and Bioanalytical Chemistry, 2016, 408, 7095-7103.

69.   Y. Zhou, K. Xie, R. Leng, L. Kong, C. Liu, Q. Zhang and X. Wang, Dalton Transactions, 2017, 46, 355-363.

70   D. Bruce, M. M.Richter and K. J. Brewer. Anal. Chem. 2002, 74, 3157-3159.

71.   K. J. Castor, K. L. Metera, U. M. Tefashe, C. J. Serpell, J. Mauzeroll and H. F. Sleiman, Inorganic Chemistry, 2015, 54, 6958-6967.

72. H. J. Kim, K.-S. Lee, Y.-J. Jeon, I.-S. Shin and J.-I. Hong, Biosensors & Bioelectronics, 2017, 91, 497-503.

73. C. Li, S. Zhu, Y. Ding and Q. Song, Journal of Electroanalytical Chemistry, 2012, 682, 136-140.

74. W. Qi, H. Yuan, Q. Song, Y. Liu, G. Ran and Y. Ding, Analytical Letters, 2011, 44, 2503-2512.

75. X. Ni, T. Li and Q. Song, Journal of Electroanalytical Chemistry, 2014, 719, 30-34.

76. W. Wang, T.-S. Kang, P. W. H. Chan, J.-J. Lu, X.-P. Chen, C.-H. Leung and D.-L. Ma, Science and Technology of Advanced Materials, 2015, 16, 065004.

77. K.-H. Leung, H.-Z. He, W. Wang, H.-J. Zhong, D. S.-H. Chan, C.-H. Leung and D.-L. Ma, ACS Applied Materials & Interfaces, 2013, 5, 12249-12253.

78. S. Lin, B. He, C. Yang, C.-H. Leung, J.-L. Mergny and D.-L. Ma, Chemical Communications, 2015, 51, 16033-16036.

79. L. Lu, H.-J. Zhong, B. He, C.-H. Leung and D.-L. Ma, Scientific Reports, 2016, 6, 19368.

80. S. Lin, L. Lu, T.-S. Kang, J.-L. Mergny, C.-H. Leung and D.-L. Ma, Analytical Chemistry, 2016, 88, 10290-10295.

81. Y. Zhao, Y. Luo, T. Li and Q. Song, RSC Advances, 2014, 4, 57709-57714.

82. W. Miao, Chemical Reviews, 2008, 108, 2506-2553.

Chapter 2: Co-reactant electrogenerated chemiluminescence of iridium(III) complexes containing an acetylacetonate ligand

Lifen Chen,[a] Egan H. Doeven,[b,]* David J. D. Wilson,[c] Emily Kerr,[a] David J. Hayne,[a] Conor F. Hogan,[c] Wenrong Yang,[a] Tien T. Pham[a] and Paul S. Francis[a,]*

[a]*Centre for Chemistry and Biotechnology, School of Life and Environmental Sciences; Faculty of Science, Engineering and Built Environment, Deakin University, Waurn Ponds, Victoria 3216, Australia.*

[b]*Centre for Regional and Rural Futures (CeRRF), Faculty of Science, Engineering and Built Environment, Deakin University, Waurn Ponds, Victoria 3216, Australia.*

[c]*Department of Chemistry and Physics, La Trobe Institute for Molecular Science, La Trobe University, Melbourne, Victoria 3086, Australia.*

AUTHORSHIP STATEMENT

1. Details of publication and executive author

Title of Publication	Publication details
Co-reactant Electrogenerated Chemiluminescence of Iridium(III) Complexes Containing an Acetylacetonate Ligand	ChemElectroChem, 2017, 4, 1797–1808; DOI: 10.1002/celc.201700222

Name of executive author	School/Institute/Division if based at Deakin; Organisation and address if non-Deakin	Email or phone
Professor Paul S. Francis	School of Life and Environmental Sciences	psf@deakin.edu.au

2. Inclusion of publication in a thesis

Is it intended to include this publication in a higher degree by research (HDR) thesis?	Yes	If Yes, please complete Section 3 If No, go straight to Section 4.

3. HDR thesis author's declaration

Name of HDR thesis author if different from above. (If the same, write "as above")	School/Institute/Division if based at Deakin	Thesis title
Lifen Chen	School of Life and Environmental Sciences	Novel iridium(III) complexes for electrogenerated chemiluminescence labeling and detection

If there are multiple authors, give a full description of HDR thesis author's contribution to the publication (for example, how much did you contribute to the conception of the project, the design of methodology or experimental protocol, data collection, analysis, drafting the manuscript, revising it critically for important intellectual content, etc.)		
Major contribution to conception of project and experimental design, primary responsibility for the laboratory experimentation, data analysis and interpretation, and preparation of manuscript draft under the guidance of PhD supervisors, acknowledged by my position as the first author of the manuscript.		
I declare that the above is an accurate description of my contribution to this paper, and the contributions of other authors are as described below.	Signature and date	Signature Redacted by Library 14th March 2019

4. Description of all author contributions

Name and affiliation of author	Contribution(s) (for example, conception of the project, design of methodology or experimental protocol, data collection, analysis, drafting the manuscript, revising it critically for important intellectual content, etc.)
Egan H. Doeven; Centre for Regional and Rural Futures, Deakin University	Co-supervision of PhD student Lifen Chen. Contributed to the design of experiments (through discussion with Lifen Chen) and provided training in instrumental techniques. Assisted in editing the manuscript.
David J. D. Wilson; La Trobe Institute for Molecular Science, La Trobe University	Implementation of computational methods and interpretation of computational data.
Emily Kerr; School of Life and Environmental Sciences, Deakin University	Preliminary experiments to examine feasibility of project, and assistance in editing the manuscript.
David J. Hayne; School of Life and Environmental Sciences, Deakin	Construction of instrumentation. Provided training and advice on the cryostat system for collection of low temperature spectra. Assisted in

University	editing the manuscript. Co-supervision of undergraduate research project student Tien Pham
Conor F. Hogan; La Trobe Institute for Molecular Science, La Trobe University	Provided expertise in interpretation of electrochemical data and the design of certain ECL experiments within the project, and advice on specific technical aspects of the manuscript.
Wenrong Yang; School of Life and Environmental Sciences, Deakin University	Co-supervision of PhD student Lifen Chen. Assisted in editing the manuscript.
Tien T. Pham; School of Life and Environmental Sciences, Deakin University	Assisted Lifen Chen in selected experiments such as the collection of low-temperature emission spectra.
Paul S. Francis; School of Life and Environmental Sciences, Deakin University	Principal supervision of PhD student Lifen Chen and undergraduate research project student Tien Pham. Contribution to conception of project and experimental design (through discussion with Lifen Chen and Egan Doeven). Assisted in editing the manuscript.

5. Author Declarations

I agree to be named as one of the authors of this work, and confirm:

i.   *that I have met the authorship criteria set out in the Deakin University Research Conduct Policy,*

ii.   *that there are no other authors according to these criteria,*

iii.   *that the description in Section 4 of my contribution(s) to this publication is accurate,*

iv.   *that the data on which these findings are based are stored as set out in Section 7 below.*

If this work is to form part of an HDR thesis as described in Sections 2 and 3, I further

v.   *consent to the incorporation of the publication into the candidate's HDR thesis submitted to Deakin University and, if the higher degree is awarded, the subsequent publication of the thesis by the university (subject to relevant Copyright provisions).*

Name of author	Signature*	Date
Egan H. Doeven		15/03/2019
David J. D. Wilson		15/03/2019
Emily Kerr		18/03/2019
David J. Hayne		15/03/2019
Conor F. Hogan		15/03/2019
Wenrong Yang		16/03/2019

Tien T. Pham		14/03/2019
Paul S. Francis		14/03/2019

6. Other contributor declarations

I agree to be named as a non-author contributor to this work.

Name and affiliation of contributor	Contribution	Signature* and date

* If an author or contributor is unavailable or otherwise unable to sign the statement of authorship, the Head of Academic Unit may sign on their behalf, noting the reason for their unavailability, provided there is no evidence to suggest that the person would object to being named as author

7. Data storage

The original data for this project are stored in the following locations. (The locations must be within an appropriate institutional setting. If the executive author is a Deakin staff member and data are stored outside Deakin University, permission for this must be given by the Head of Academic Unit within which the executive author is based.)

Data format	Storage Location	Date lodged	Name of custodian if other than the executive author
Electronic data	Ka5.127 and backed up using Dropbox software	Throughout PhD	

This form must be retained by the executive author, within the school or institute in which they are based.

If the publication is to be included as part of an HDR thesis, a copy of this form must be included in the thesis with the publication.

2.1 Abstract

We examine the electrogenerated chemiluminescence (ECL) of three Ir(C^N)$_2$(acac) complexes, where acac = acetylacetonate anion and C^N = 2-phenylpyridine (ppy), 2-phenylbenzothiazole (bt) or 2-phenylquinoline (pq) anions, with tri-*n*-propylamine co-reactant in acetonitrile, under a range of chemical and instrumental conditions, following somewhat conflicting recent claims of the ECL intensities from complexes of this type. Relevant electrochemical, spectroscopic and ECL properties are evaluated in direct comparison with those of Ir(ppy)$_3$ and [Ru(bpy)$_3$](PF$_6$)$_2$, and data from previous publications. DFT calculations on the Ir(C^N)$_2$(acac) complexes show the HOMOs to be composed of both the metal and C^N ligand, and LUMOs almost exclusively on the C^N ligand. The ECL intensities of the Ir(C^N)$_2$(acac) complexes (relative to [Ru(bpy)$_3$](PF$_6$)$_2$) were dependent on experimental conditions, and in some cases, the ECL intensities reported for iridium complexes may have been derived using conditions that unintentionally disadvantaged the reference electrochemiluminophore.

2.2 introduction

After the success of ruthenium(II) bipyridine complexes as electrogenerated chemiluminescence (ECL) reagents,[1] researchers began to examine a range of cyclometalated iridium(III) complexes exhibiting high photoluminescence efficiencies and a wide range of emission wavelengths, seeking advances in detection sensitivity[2] and multi-colour (multiplexed) detection systems.[3]

Initial demonstrations of ECL reactions involving homoleptic Ir(ppy)$_3$ (ppy = 2-phenylpyridine anion) were promising.[3a, 4] Kapturkiewicz and co-workers then examined a series of heteroleptic iridium(III) complexes containing an acetylacetonate anion (acac) ligand, such as Ir(ppy)$_2$(acac) and Ir(bt)$_2$(acac), where bt = 2-phenylbenzothiazole anion (Figure 2.1).[5] Like Ir(ppy)$_3$, these complexes exhibited high photoluminescence

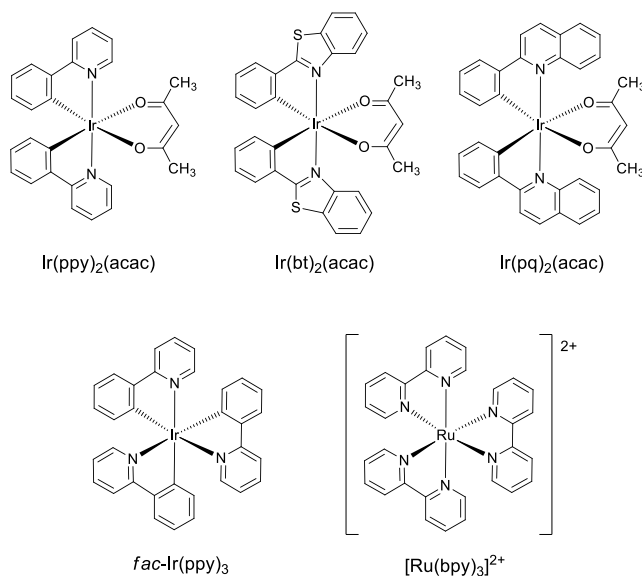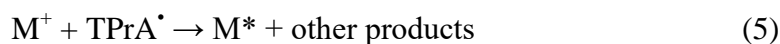efficiencies and had previously been employed as electroluminescence phosphors in organic light emitting devices.[6]

Figure 2.1. Ir(ppy)$_2$(acac): bis(2-phenylpyridine)(acetylacetonato)iridium(III); Ir(bt)$_2$(acac): bis(2-phenylbenzo[d]thiazole)(acetylacetonato)iridium(III); Ir(pq)$_2$(acac): bis(2-phenylquinoline)(acetylacetonato)-iridium(III); *fac*-Ir(ppy)$_3$: *fac*-tris(2-phenylpyridine)iridium(III); [Ru(bpy)$_3$]$^{2+}$: tris(2,2'-bipyridine)-ruthenium(II).

Kapturkiewicz *et al*. observed impressive ECL efficiencies (ϕ_{ECL} up to 0.55) when using the triple-potential-step technique to generate the oxidised [Ir(C^N)$_2$(acac)]$^+$ complex and the reduced radical anions of aromatic nitriles in 1:1 acetonitrile-dioxane,[5] compared to the self-annihilation of tris(2,2'-bipyridine)ruthenium(II) ([Ru(bpy)$_3$]$^{2+}$) in acetonitrile (ϕ_{ECL} = 0.05).[7] Around the same time, Kim *et al*.[2a] identified Ir(pq)$_2$(acac) and Ir(pq)$_2$(tmd) (pq = 2-phenylquinoline anion, tmd = 2,2',6,6'-tetramethylhepta-3,5-dione anion) as fulfilling two parameters essential for efficient co-reactant ECL with tri-*n*-propylamine (TPrA), considering the detailed ECL mechanism for [Ru(bpy)$_3$]$^{2+}$ and TPrA outlined by Bard and co-workers (Eqn 1-9),[8] where TPrA$^{+\bullet}$ is the corresponding aminium radical cation (Pr$_3$N$^{\bullet+}$) of TPrA, and TPrA$^{\bullet}$ is an α-amino alkyl radical (Pr$_2$NCH$^{\bullet}$CH$_2$CH$_3$).

$$M - e^- \rightarrow M^+ \qquad\qquad (1)$$

$$TPrA - e^- \rightarrow TPrA^{+\bullet} \qquad\qquad (2)$$

$$M^+ + TPrA \rightarrow M + TPrA^{+\bullet} \qquad\qquad (3)$$

$$TPrA^{+\bullet} \rightarrow TPrA^{\bullet} + H^+ \qquad\qquad (4)$$

$$M^+ + TPrA^{\bullet} \rightarrow M* + \text{other products} \qquad\qquad (5)$$

$$M + TPrA^{\bullet} \rightarrow M^- + \text{other products} \qquad\qquad (6)$$

$$M^- + M^+ \rightarrow M* + M \qquad\qquad (7)$$

$$M^- + TPrA^{+\bullet} \rightarrow M* + TPrA \qquad\qquad (8)$$

$$M* \rightarrow M + h\nu \qquad\qquad (9)$$

Kim *et al.*[2a] recorded relative co-reactant ECL efficiencies§ for Ir(pq)$_2$(acac) and Ir(pq)$_2$(tmd) (with TPrA in acetonitrile) that were 77-fold and 49-fold greater than that of [Ru(bpy)$_3$]$^{2+}$, respectively. They attributed the enhancement to the suitability of their respective redox potentials for fast generation of TPrA$^{+\bullet}$ *via* Eqn 3, and the efficient acceptance of electrons from TPrA$^{\bullet}$ in Eqn 6. In a closely related subsequent investigation, Zhou *et al.*[9] reported that the ECL signals for Ir(pq)$_2$(acac) and Ir(pq)$_2$(dm-acac) with TPrA co-reactant in acetonitrile were 10-fold and 38-fold greater than that of [Ru(bpy)$_3$]$^{2+}$, under identical conditions.† An even greater relative co-reactant ECL intensity (214-fold of that of [Ru(bpy)$_3$]$^{2+}$) was observed for Ir(bt)$_2$(acac) with TPrA in dichloromethane,[10] but unlike the previous studies,[2a, 9] their relative ECL intensities in acetonitrile were not reported.

These extraordinary ECL intensities with TPrA as co-reactant (relative to the conventional ruthenium(II) complex luminophore that is employed in commercial ECL-based immunodiagnostics systems) promise superior detection sensitivity and multi-colour detection techniques. However, Kapturkiewicz[2f] has questioned the validity of the prior, somewhat conflicting evaluations of the relative ECL intensities of these iridium complexes.

Moreover, Fernandez-Hernandez *et al.*[11] recently reported a much lower relative co-reactant ECL for Ir(pq)$_2$(acac) of 0.11 (*vs* [Ru(bpy)$_3$]$^{2+}$ = 1) under aqueous conditions.

With these considerations in mind, we have re-examined several promising electrochemiluminophores (Ir(ppy)$_2$(acac), Ir(bt)$_2$(acac) and Ir(pq)$_2$(acac)),[5, 9-10] in direct comparison with the archetypal [Ru(bpy)$_3$]$^{2+}$ and Ir(ppy)$_3$ complexes. We evaluate the relative ECL intensities of these complexes with TPrA co-reactant in acetonitrile across a range of complex and co-reactant concentrations, and instrument configurations. These experiments not only reconcile some wide discrepancies between previously reported data, but also reveal several major shortcomings of conventional approaches to evaluate ECL luminophore candidates.

2.3 Results and Discussion

2.3.1 Spectroscopic properties

The UV-visible absorption spectra of the Ir(C^N)$_2$(acac) complexes (Figure 2.2a) were in good agreement with previous reports,[10, 12] in which the intense absorption bands between 250 nm and 350 nm were assigned to spin-allowed singlet intra-ligand (^{1}LC) transitions ($\pi \rightarrow \pi^*$, ppy/bt/pq) and the weaker bands above 400 nm to mixed singlet and triplet metal-to-ligand charge-transfer (MLCT) transitions (dπ(Ir) $\rightarrow \pi^*$(ppy/bt/pq)) and intra-ligand transitions.[12a, 12b]

The photoluminescence emission spectra of the Ir(C^N)$_2$(acac) complexes in acetonitrile each exhibited a broad band (Figure 2.3a) with a maximum intensity at 525, 565 and 611 nm for Ir(ppy)$_2$(acac), Ir(bt)$_2$(acac) and Ir(pq)$_2$(acac), respectively. The luminescence of these complexes has previously been attributed to mixed ^{3}LC ($\pi \rightarrow \pi^*$) and ^{3}MLCT (dπ(Ir) $\rightarrow \pi^*$(ppy/bt/pq)) transitions.[12a] The vibronic fine structure of Ir(bt)$_2$(acac),

with a pronounced shoulder at ~600 nm, suggests a significant ligand $^3(\pi \rightarrow \pi^*)$ contribution in that case.
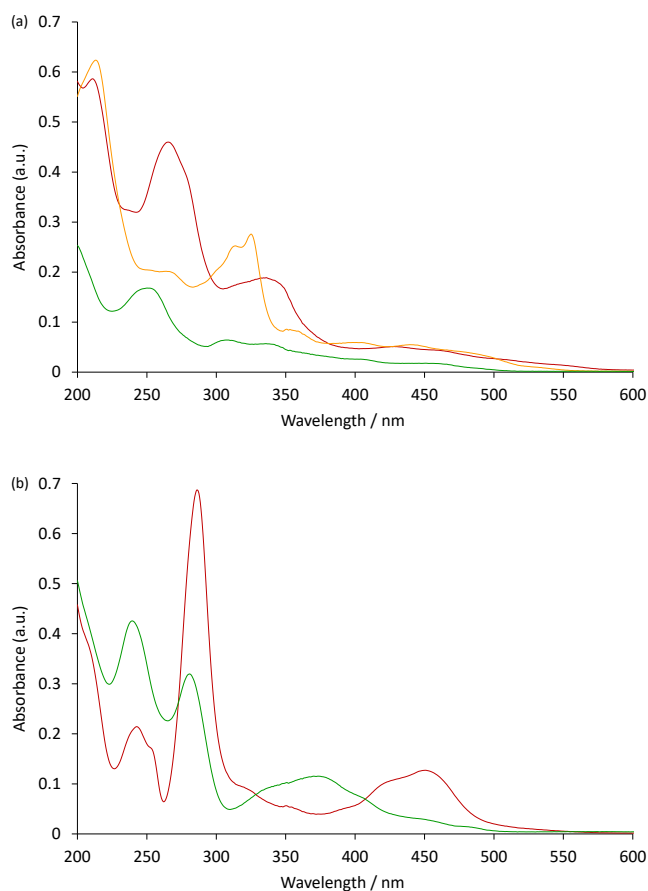

Figure 2.2. Absorption spectra of (a) Ir(ppy)$_2$(acac) (green line), Ir(bt)$_2$(acac) (yellow line), Ir(pq)$_2$(acac) (red line), and (b) Ir(ppy)$_3$ (green line), and [Ru(bpy)$_3$]$^{2+}$ (red line), at 10 μM in acetonitrile.

As shown in Table 2.1, the luminescence properties of Ir(bt)$_2$(acac) are somewhat intermediate to those of Ir(ppy)$_2$(acac) and Ir(pq)$_2$(acac), and also to those of Ir(ppy)$_3$ and [Ru(bpy)$_3$]$^{2+}$. The maximum emission wavelengths of these complexes increase in the order: Ir(ppy)$_3$ < Ir(ppy)$_2$(acac) << Ir(bt)$_2$(acac) << Ir(pq)$_2$(acac) < [Ru(bpy)$_3$]$^{2+}$, which is seen in their application as luminophores in green (Ir(ppy)$_3$ and Ir(ppy)$_2$(acac)), yellow (Ir(bt)$_2$(acac)) and orange-red (Ir(pq)$_2$(acac) and [Ru(bpy)$_3$]$^{2+}$) light-emitting devices.[6, 13] There is considerable variation in the wavelengths of maximum photoluminescence intensity (λ_{max}) reported in the literature (Table 2.1). The emission bands are broad,

exhibiting widths at half peak height (W$_{\frac{1}{2}}$) of 77-119 nm, and thus the maxima are vulnerable to error from small changes arising from solvent effects[3a, 14] and instrumental noise and intensity fluctuations. Moreover, significant error is introduced by the difference in the sensitivity of the instrument across the wavelength range (Figures S2.1-S2.5 in ESI), which is commonly left uncorrected. As the sensitivity of typical photomultiplier tubes decreases sharply into near-infrared region, this effect is most pronounced on luminophores with intensity maxima at the red end of the visible region, such as Ir(pq)$_2$(acac) and [Ru(bpy)$_3$]$^{2+}$. With our spectrometer, correction for this artefact resulted in changes in λ_{max} of up to 11 nm, and our corrected values were in good agreement with previously reported corrected values in the same solvent.[11, 14-15]
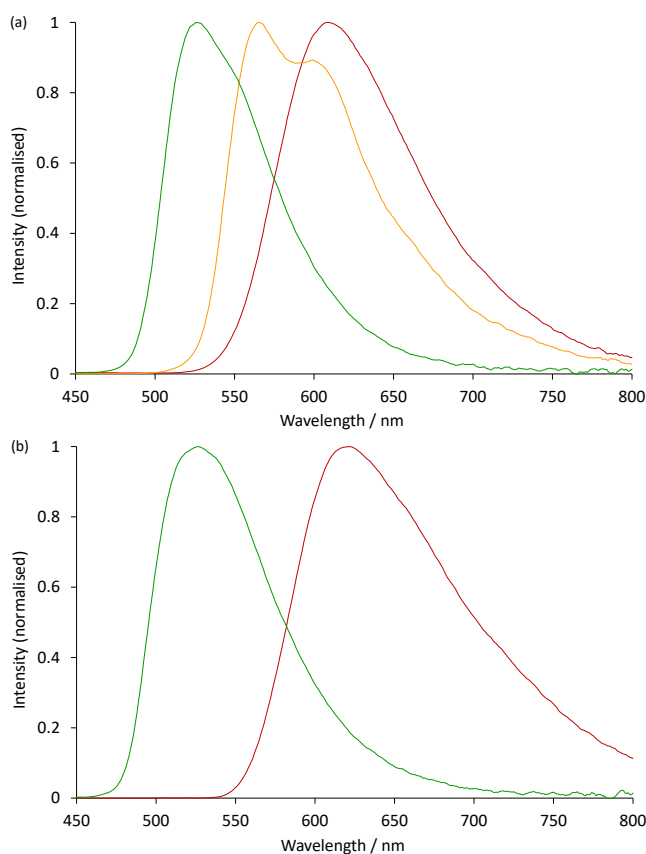

Figure 2.3. Corrected room-temperature photoluminescence emission spectra of (a) Ir(ppy)$_2$(acac) (green line), Ir(bt)$_2$(acac) (yellow line), Ir(pq)$_2$(acac) (red line), and (b) Ir(ppy)$_3$ (green line), and [Ru(bpy)$_3$]$^{2+}$ (red line), at

10 μM in acetonitrile. An excitation wavelength of 350 nm was used for all complexes except [Ru(bpy)$_3$]$^{2+}$, for which 450 nm was used. See also: Figures S2.1-S2.5.

Correction of spectra obtained at 77 K in 4:1 (v/v) ethanol:methanol had a much smaller effect on their λ_{max}, because the emission bands were narrower, although the intensity ratio of the multiple bands within each spectrum was significantly altered (Figure 2.4 and S2.1-S2.5). Our measurements of λ_{max} for Ir(ppy)$_3$ were within 2 nm of those previously reported by Dedeian et al.,[16] Nakamaru et al.,[17] and Djurovich et al.[18] (Table 2.1), despite differences in solvent and/or counter ion, with the exception of Ir(pq)$_2$(acac), for which we obtained 581 nm in 4:1 (v/v) ethanol:methanol, whereas Djurovich et al. reported 575 nm in 2-methyltetrahydrofuran (2-MeTHF). Frey et al.[12c] recently observed the λ_{max} of Ir(ppy)$_2$(acac) in 2-MeTHF at 77 K as 506 nm, but our result (501 nm) was in better agreement with that of Djurovich et al.[18] (500 nm) in the same solvent.

The reported photoluminescence quantum efficiencies (ϕ_{PL}) of the Ir(C^N)$_2$(acac) complexes in deaerated solutions vary widely (Table 2.1), but when compared under the same conditions within a single study,[12a] they decrease in the order Ir(ppy)$_2$(acac) > Ir(bt)$_2$(acac) > Ir(pq)$_2$(acac). In general, the ϕ_{PL} of the Ir(C^N)$_2$(acac) complexes are lower than that of Ir(ppy)$_3$, but much higher than that of [Ru(bpy)$_3$]$^{2+}$. However, in air-equilibrated solutions, the difference is off-set by the greater susceptibility of the electronically excited iridium complexes to oxygen quenching.[18] The ϕ_{PL} of Ir(bt)$_2$(acac) in aerated acetonitrile at room temperature (0.016),[12b] for example, is similar to that of [Ru(bpy)$_3$]$^{2+}$ (0.018).[14]
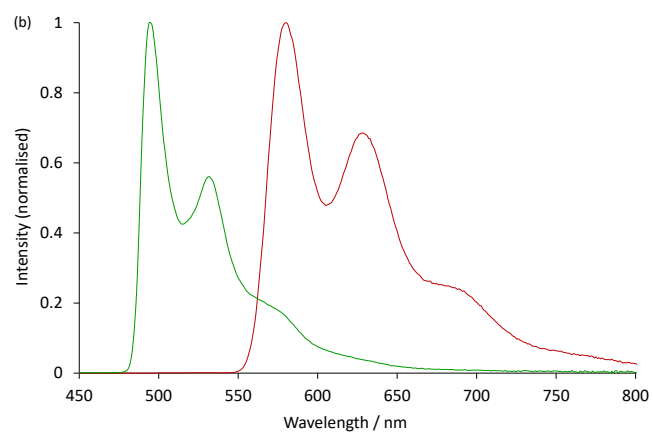
Figure 2.4. Corrected low-temperature (77 K) photoluminescence emission spectra of (a) Ir(ppy)$_2$(acac) (green line), Ir(bt)$_2$(acac) (yellow line), Ir(pq)$_2$(acac) (red line), and (b) Ir(ppy)$_3$ (green line), and [Ru(bpy)$_3$]$^{2+}$ (red line), at 5 μM in 4:1 (v/v) ethanol:methanol. See also: Figures S2.1-S2.5.

Table 2.1. Selected spectroscopic and electrochemical data for the Ir(C^N)$_2$(acac) complexes in comparison with those of *fac*-Ir(ppy)$_3$ and [Ru(bpy)$_3$](PF$_6$)$_2$

	Ir(ppy)$_3$	Ir(ppy)$_2$(acac)	Ir(bt)$_2$(acac)	Ir(pq)$_2$(acac)	[Ru(bpy)$_3$]$^{2+}$
Photoluminescence					
Emission colour	Green	Green	Yellow	Orange-Red	Orange-Red
λ$_{max}$/nm (298 K)	510 [2a]	516 (2-MeTHF) [12a]	557 (2-MeTHF) [12a]	589 [2a]	608 [2a]
	514 (toluene) [19]	517 (DCM) [20]	557, 590 sh (DCM) [12b]	597 (2-MeTHF) [12a]	615 (ACN) [22]
	517 (ACN) [3a]	526 (ACN-DX) [5b]	563, 603 sh (ACN) [12b]	600 (DCM) [21]	621 (ACN) [14]
	520 (ACN) [15]	528 (ACN) [12c]	566 (ACN-DX) [5b]	604 (ACN) [9]	625 (H$_2$O) [14]
				612 (ACN) [11]	
φ$_{PL}$ (298 K, deaerated)	0.40 (DCM) [2a]	0.11 (DCM) [9]	0.22 (DCM) [10]	0.10 (2-MeTHF) [12a]	0.063 (H$_2$O) [14]
	0.70 (ACN) [4c]	0.34 (2-MeTHF) [12a]	0.26 (2-MeTHF) [12a]	0.10 (DCM) [2a]	0.095 (ACN) [14]
	0.89 (DCE) [23]	0.53 (DCM) [20]	0.44 (ACN-DX) [5a]	0.59 (ACN) [11]	
	0.90 (DCM) [24]	0.72 (ACN-DX) [5b]		0.60 (ACN) [9]	
	0.97 (2-MeTHF) [25]			0.70 (DCE) [23]	
τ /μsec (298 K, deaerated)	1.6 (DCM) [24]	1.43 (toluene) [18]	1.41 (toluene) [18]	1.50 (toluene) [18]	0.65 (H$_2$O) [17]
	1.9 (ACN) [16]	1.6 (2-MeTHF) [12a]	1.8 (2-MeTHF) [12a]	2.0 (2-MeTHF) [12a]	0.89 (ACN) [17]
	2.0 (toluene) [19]	2.4 (DCM) [9]	2.0 (DCM) [10]	1.8 (ACN) [11]	1.10 (ACN) [22]
λ$_{max}$/nm (77 K)	494 (EtOH-MeOH) [16]	500 (2-MeTHF) [18]	544 (2-MeTHF) [18]	575 (2-MeTHF) [18]	582, 629 (EtOH-MeOH) [17]
		506 (2-MeTHF) [12c]			582 (EtOH-MeOH) [22]
τ /μsec (77 K)	5.0 (EtOH-MeOH) [26]	3.2 (DCM) [12a]	4.4 (2-MeTHF) [12a]		5.1 (EtOH-MeOH) [17]
E_{0-0}/eV	2.49 [19]	2.48 [18]	2.28 [18]	2.16 [18]	2.12 [8], 2.13 [22]
Electrochemistry					
E^o_{ox} /V vs Fc$^{0/+}$	0.31 (ACN-DX) [4c]	0.34 (DCM) [10]	0.50 (DCM) [10]	0.47 (ACN) [11]	0.89 (ACN) [29]
	0.32 [27]	0.40 (ACN-DX) [5b]	0.56 (ACN) [12b]	0.53 (ACN) [9]	0.93 (ACN) [2a]
	0.33 (ACN) [2e]	0.41 (DMF) [12c]	0.57 (ACN-DX) [5b]	0.56 (ACN) [2a]	0.97 (ACN) [30]
	0.36 (ACN) [16]			0.57 (ACN) [28]	
	0.44 (ACN) [2a]			0.64 (DCM) [21]	
E^o_{red}/V vs Fc$^{0/+}$	-2.62 (ACN) [2a]	-2.60 (DMF) [12c]	-2.29 [27]	-2.05 (ACN) [2a, 28]	-1.71, -1.90, -2.14 (ACN) [30]
	-2.67 (ACN) [2e]	-2.61 [27]	-2.63 (THF) [10]	-2.11 (ACN) [11]	-1.75, -1.93, -2.18 (ACN) [29]
	-2.69 [27]			-2.24 (ACN) [9]	-1.75 (ACN) [2a]
	-2.70, -2.95 (ACN-DX) [4c]			-2.52 (THF) [21]	
ΔE/V	3.00 [2e]	3.01 [12c, 27]	2.85 [27]	2.58 [11]	2.65 [29]
	3.01 [27]		3.13 [10]	2.62 [28]	2.68 [2a, 30]
				2.77 [9]	
Electrochemiluminescence					
φ$_{ECL}$ (annihilation)	0.14 (ACN) [4b]	-	-	0.16 (ACN) [28]	0.050 (ACN) [7]
	0.16 (ACN-DX) [4c]				
φ$_{ECL}$ (organic radical anions)	0.67 (with 2-cyanofluorene in ACN-DX) [4c]	0.55 (with 4,4′-dicyano-p-biphenyl in ACN-DX) [5b]	0.32 (with 1,4-dicyanobenzene in ACN-DX) [5a]	0.20 for closely related structural isomer Ir(piq)$_2$(acac) (with 1,4-dicyanobenzene in ACN-DX) [5b]	0.021 (with 9,10-anthraquinone in ACN) [31]
Relative intensity with TPrA as co-reactant§ (I_s/I_{ref})	0.0044 (ACN-H$_2$O 1:1) [3a]	0.96 (DCM) [10]	214 (DCM) [10]	0.1 (H$_2$O) [11]	1 (by definition§)
	0.014 (ACN) [2e]			10 (ACN) [9]	
	0.33 (ACN) [3a]			77 (ACN) [2a]	

The ϕ_{PL} is an important consideration in the exploration of new ECL luminophores. The ϕ_{ECL} is the product of the efficiencies of excitation to the excited state (ϕ_{ex}) and the subsequent luminescence (ϕ_{em}), the latter being equivalent to the ϕ_{PL}. Thus, in an ECL system where the excitation efficiency is very high, the ϕ_{ECL} will approach the ϕ_{PL} limit. This can be seen in the ϕ_{ECL} of systems in which these complexes are oxidised in conjunction with the reduction of certain aromatic nitriles and ketones (see Table 2.1, second last row).[4c, 5b, 31] Considering that the upper estimate of the ϕ_{PL} of Ir(bt)$_2$(acac) [5a] is less than 5-fold the ϕ_{PL} of [Ru(bpy)$_3$]$^{2+}$,[14] and if we assume that under identical conditions, the relative ECL intensity is approximately equal to the co-reactant ECL efficiency,[§] then the claimed relative ECL of 214 for Ir(bt)$_2$(acac) with TPrA ([Ru(bpy)$_3$]$^{2+}$ = 1)[10] would require more than 40-fold greater efficiency in the co-reactant excitation process (ϕ_{ex}) for the Ir(bt)$_2$(acac) complex compared to [Ru(bpy)$_3$]$^{2+}$.

2.3.2 Electrochemistry

In their examination of the co-reactant ECL of Ir(bt)$_2$(acac), Zhou et al.[10] initially attempted to characterise the electrochemical potentials of the complexes in dichloromethane with 0.1 M TBAPF$_6$ as the supporting electrolyte. Under these conditions, a reversible oxidation (0.50 V vs Fc$^{0/+}$) was observed, but an alternative solvent (tetrahydrofuran) with a more negative working potential range was required to detect the reduction peak (-2.63 vs Fc$^{0/+}$). However, this potential gap ($\Delta E = 3.13$ V) is much larger than that reported for related iridium(III) complexes exhibiting higher energy emissions, such as Ir(ppy)$_3$[2e, 27] and Ir(ppy)$_2$(acac)[12c, 27] (Table 2.1). Using acetonitrile as a solvent (with 0.1 M TBAPF$_6$ as the supporting electrolyte), we observed reversible oxidation and reduction peaks at 0.58 V and -2.24 V vs Fc$^{0/+}$ (Figure 2.5). These values are similar those reported by Chen et al.[27] and provide a more reasonable ΔE of 2.82 V. The oxidation peaks were attributed to metal-centered oxidation processes, and the reduction peaks can be

45

attributed to ligand-centered reduction processes. In our study, all of the complexes are under diffusional controlled conditions, as they are dissolved species in solution. The complexes had varying degrees of reversibility. Ruthenium-based complexes were highly reversible in aqueous and organic solutions, while the iridium complexes studied showed good reversibility in organic solutions, and generally poor reversibility in aqueous media. According to the Figure 2.5 and Table 2.2, the ratios of oxidation peak current ipa/ipc (ox) and reduction peak current ipa/ipc (red) for all the complexes were equal to 1, which further demonstrated that these specific CV's show a high degree of reversibility under these particular conditions. Potentials quoted in text are formal potentials for reversible redox couples, or peak potentials for irreversible reactions. The reversibility of processes was not studied in detail.
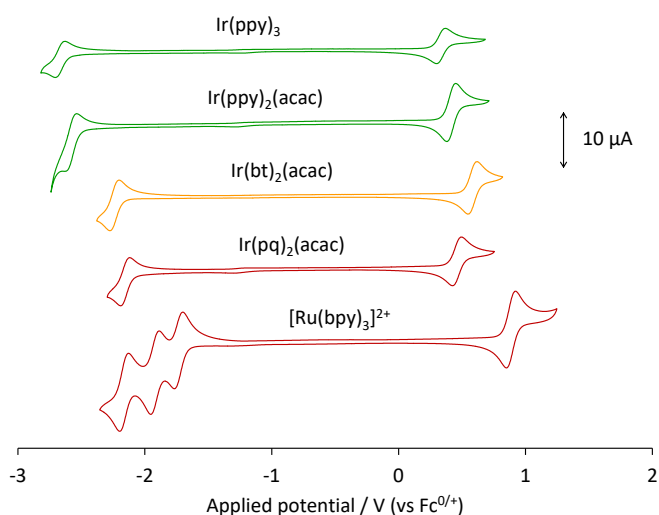
Figure 2.5. Cyclic voltammetry of the five complexes at 0.25 mM in acetonitrile with 0.1 M TBAPF$_6$, using a scan rate of 0.1 V s^{-1}. The voltammograms have been off-set on the y-axis for clarity only.

Our potentials for Ir(ppy)$_3$ and Ir(ppy)$_2$(acac) were also in good agreement with those reported.[27] Our data for Ir(pq)$_2$(acac) and [Ru(bpy)$_3$]$^{2+}$ (Table 2.2) were within the range of previously reported values, with the exception of the E°_{ox} for Ir(pq)$_2$(acac) of 0.46 V *vs* Fc$^{0/+}$, although this value was similar to the report of Fernandez-Hernandez *et al.* (0.47 V *vs*

Fc$^{0/+}$)[11] (Table 2.1). The difference in their first reduction and oxidation potentials (ΔE) increased in the order: Ir(ppy)$_3$ ≈ Ir(ppy)$_2$(acac) << Ir(bt)$_2$(acac) << Ir(pq)$_2$(acac) ≈ [Ru(bpy)$_3$]$^{2+}$ (Tables 2. 1 and 2. 2).

2.3.3 Theoretical Calculations

The electronic structure and nature of each complex was investigated with DFT calculations. A range of density functionals were considered, including pure and hybrid functionals; in each case the characteristics of the calculated MOs were qualitatively similar and calculated trends were consistent, but the orbital energies (and HOMO-LUMO gaps) were found to be strongly dependent on the proportion of Hartree-Fock exchange in the functional. As a result, only BP86 results (pure exchange-correlation functional without Hartree-Fock exchange) are presented. Having no Hartree-Fock exchange, the calculated HOMO-LUMO gaps represent a lower bound of DFT calculated values. The BP86 results also yield the smallest degree of spin contamination in the oxidized and reduced forms of the complexes (see below).

For the complexes considered here, plots of the frontier MOs are given in Figure 2.6 and S2.6. The MOs of [Ru(bpy)$_3$]$^{2+}$ are already well characterised, with a metal-centred HOMO and ligand-based LUMO.[2e, 29, 32] The triplet-state spin density (Figure 2.7 and 2.S7) shares the same spatial extent as the singlet HOMO and LUMO, for which the lowest singlet-triplet transition may be described as metal-to-ligand charge-transfer (MLCT).[32] For each of the iridium complexes, there is very little spatial overlap between the singlet-state HOMO and LUMO (*i.e.,* they are largely orthogonal), which indicates that the HOMO and LUMO energies might be independently 'tuned' by appropriate substitution of donor/acceptor groups on the ligands.
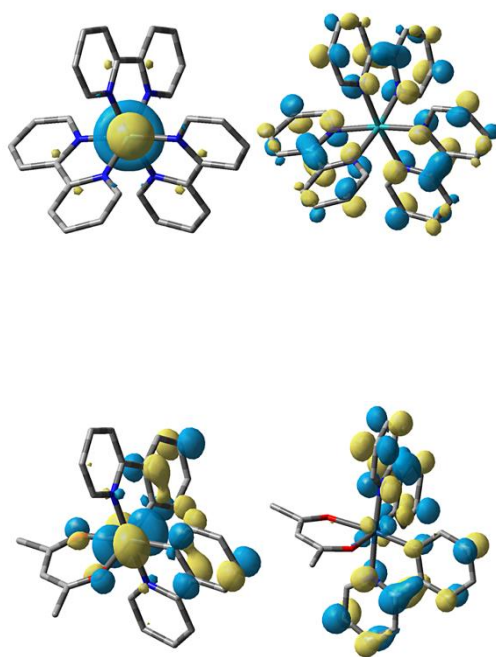
Figure 2.6. BP86/def2-TZVP ground-state singlet MO surfaces of [Ru(bpy)$_3$]$^{2+}$ (top) and Ir(ppy)$_2$(acac) (bottom). The MO plots of all complexes investigated in this study are shown in the ESI (Figure S2.1).

Table 2.2. Selected spectroscopic, electrochemical and ECL data (obtained in acetonitrile unless otherwise stated).

	Ir(ppy)$_3$	Ir(ppy)$_2$(acac)	Ir(bt)$_2$(acac)	Ir(pq)$_2$(acac)	[Ru(bpy)$_3$]$^{2+}$
Luminescence					
PL (r.t.), λ_{max}/nm[a]	520 (516)[b]	525 (523)	565, 605 (564, 600)	611 (602)	621 (610)
PL (77 K) λ_{max}/nm[a],[c]	494, 532	501, 537	546, 592, 645	581, 624	580, 628
E_{0-0}/eV[d]	2.51	2.47	2.27	2.13	2.14
ECL, λ_{max}/nm[a]	520	530	567, 602	613	620
Electrochemistry					
E^o_{ox} /V (*vs* Fc$^{0/+}$)	0.33	0.42	0.58	0.46	0.89
E^o_{red}/V (*vs* Fc$^{0/+}$)	-2.67	-2.59	-2.24	-2.15	-1.73, -1.92, -2.16
ΔE/V	3.00	3.01	2.82	2.61	2.62
ip_a/ip_c (ox)	1.05	1.06	1.02	1.01	1.02
ip_a/ip_c (red)	1.06	1.04	1.04	0.98	1.07
$E(M^*/M^+)$/V (*vs* Fc$^{0/+}$)[e]	-2.18	-2.05	-1.69	-1.67	-1.25
$E(M^-/M^*)$/V (*vs* Fc$^{0/+}$)[f]	-0.16	-0.12	0.03	-0.02	0.41
Relative ECL Intensity with TPrA co-reactant (I_s/I_{ref})					
Conditions A	0.016 (0.018)[b],[i]	0.033 (0.036)	1.15 (1.19)	3.08 (3.09)	1[h]
Conditions B	<0.001 (0.001)	0.011 (0.012)	0.51 (0.52)	1.13 (1.13)	1
Conditions C	<0.01	2.63 (2.95)	25.1 (26.1)	79.1 (79.5)	1
Conditions D[i]	(0.190)	(51.8)	(243.1)	(80.4)	1

[a]Luminescence spectra were corrected for the change in instrument sensitivity across the examined wavelength range. The correction factor was established using a light source with standard spectral irradiance. [b]Values in parentheses were obtained prior to correction. [c]Obtained in 4:1 ethanol:methanol. [d]Calculated from PL λ_{max} at 77 K. [e]Calculated: E^o_{ox} - E_{0-0}. [f]Calculated: E^o_{red} + E_{0-0}. [g]For *Conditions A-C*, the detection response was fairly uniform across the wavelengths of emission and therefore correction had very little influence on the relative ECL intensities. For *Conditions D*, the detector response was much poorer towards the red end of the visible spectrum and the ECL intensities were artificially raised (relative to [Ru(bpy)$_3$]$^{2+}$), which is more pronounced for the metal complexes with lower wavelengths of emission. [h]By definition, the ECL intensity of [Ru(bpy)$_3$]$^{2+}$ = 1 under each set of conditions. [i]Obtained using a PMT as the photodetector instead of the CCD spectrometer.
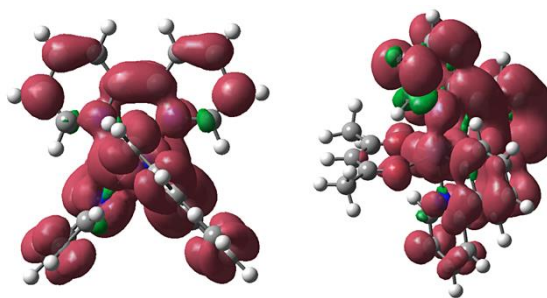
Figure 2.7. BP86/def2-TZVP calculated triplet spin density surfaces of $[Ru(bpy)_3]^{2+}$ (left) and $Ir(ppy)_2(acac)$ (right). The triplet spin density surfaces of all complexes investigated in this study are shown in ESI (Figure S2.2).

Löwdin population analysis of fragment contributions to the HOMO and LUMO is plotted in Figure 2.8 and S2.8. Iridium octahedral complexes differ from $[Ru(bpy)_3]^{2+}$ in that the HOMO has a reduced metal d-orbital contribution (typically 50% or less) compared to that of $[Ru(bpy)_3]^{2+}$ (~80%). The frontier MO characteristics of $Ir(ppy)_3$ lie between those of the $Ir(C^\wedge N)_2(acac)$ complexes and $[Ru(bpy)_3]^{2+}$, with a greater HOMO metal contribution (58%) than the $Ir(C^\wedge N)_2(acac)$ complexes. There are noticeable similarities in the $Ir(C^\wedge N)_2(acac)$ compounds: Ir contributes 43-47% of the HOMO while the $C^\wedge N$ ligand contributes 46-51%. The LUMO is almost exclusively composed of the $C^\wedge N$ ligand (95%). It is important to note that the LUMO has little density on the acac ligand, which results in the LUMO energies being dependent on the nature of the $C^\wedge N$ ligand. This observation suggests a simpler strategy of tuning photophysical properties of acac-containing iridium complexes via a straight-forward variation of the $C^\wedge N$ ligand. For example, the energies of the $C^\wedge N$ centred LUMOs of $Ir(ppy)_3$ and $Ir(ppy)_2(acac)$ are very similar (-1.60 and -1.64 eV), but differ from the $Ir(pq)_2(acac)$ and $Ir(bt)_2(acac)$ LUMO energies of -2.12 and -1.99 eV, respectively. In contrast, the HOMO energies of each of the Ir(III) complexes are similar (-5.21 to -5.43 eV). The net effect is that the HOMO-LUMO gap is greatest for the $Ir(ppy)_3$ and $Ir(ppy)_2(acac)$ complexes, which possess the least stable LUMOs.

For the Ir complexes, the triplet spin density surface (Figure 2.7 and S2.7) shares the same spatial extent as the singlet HOMO and LUMO, which in this case leads to a description of the lowest energy excited state as having a mixed MLCT and metal–ligand-to-ligand charge-transfer (MLLCT) character. The trends in HOMO and LUMO energies are in good agreement with the electrochemical results (Figure 2.9), and the trends in the HOMO-LUMO gaps are consistent with the spectroscopic results (Figure S2.9), where the energies increase in the order: $[Ru(bpy)_3]^{2+}$ < $Ir(pq)_2(acac)$ << $Ir(bt)_2(acac)$ << $Ir(ppy)_2(acac) \leq Ir(ppy)_3$.
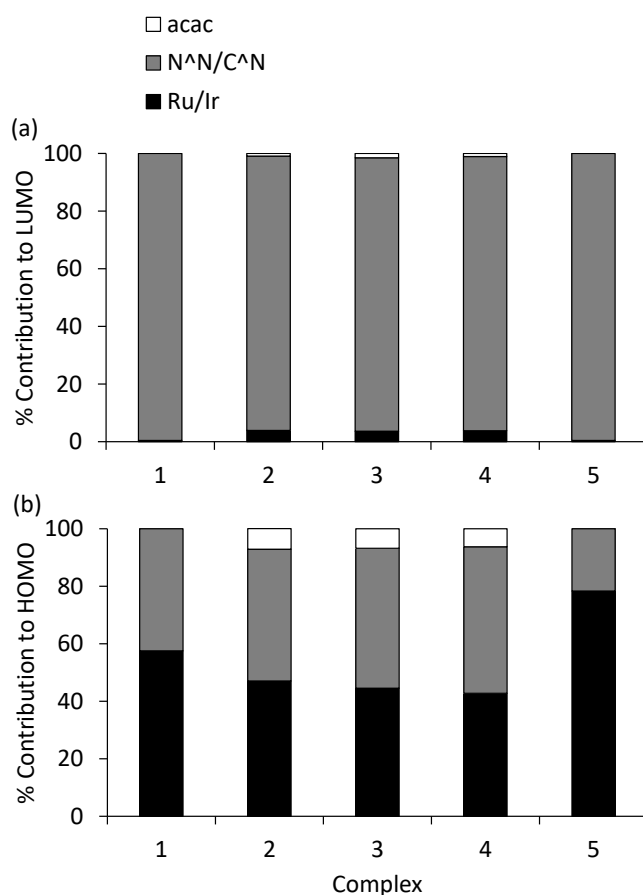
Figure 2.8. Contribution to (a) LUMO and (b) HOMO of metal centre and ligands in: (1) $Ir(ppy)_3$; (2) $Ir(ppy)_2(acac)$; (3) $Ir(bt)_2(acac)$; (4) $Ir(pq)_2(acac)$; and (5) $[Ru(bpy)_3]^{2+}$. A comparison of the contribution of the Ru/Ir centre to LUMO is shown in ESI (Figure S2.3).

2.3.4 Electrogenerated chemiluminescence

We sought to compare the relative ECL intensities of the complexes under oxidative potential with TPrA as co-reactant. Initially, we employed chemical and instrumental conditions (hereafter referred to as '*Conditions A*') that were similar to that of our previous comparisons of ECL intensities of various ruthenium and iridium complexes with TPrA co-reactant in acetonitrile.[2e, 33] In these previous studies, the electrochemiluminophores were typically compared at a concentration of 0.1 mM with a large excess of the TPrA co-reactant, applying an oxidative overpotential with a glassy carbon working electrode. The ECL intensities were measured by integrating emission spectra obtained with a spectrometer with a CCD detector. One of the most promising iridium complexes identified in these studies[2e] was [Ir(df-ppy)$_2$(ptb)](PF$_6$) (where df-ppy = 2-(2,4-difluorophenyl)pyridine anion, ptb = 1-benzyl-1,2,3-triazol-4-ylpyridine) (PL λ_{max} = 454, 484 nm; ϕ_{PL} = 0.21), which exhibited a co-reactant ECL intensity that was much greater than a range of other iridium complexes, but still only 0.24 compared to the [Ru(bpy)$_3$](PF$_6$)$_2$ reference intensity of 1.
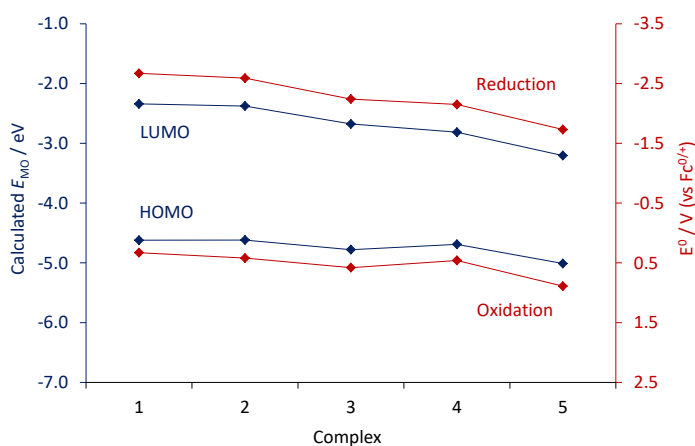
Figure 2.9. Comparison of MO energies (left axis) and electrochemical properties (right axis) of: (1) Ir(ppy)$_3$; (2) Ir(ppy)$_2$(acac); (3) Ir(bt)$_2$(acac); (4) Ir(pq)$_2$(acac); and (5) [Ru(bpy)$_3$]$^{2+}$.

Under *Conditions A*, the co-reactant ECL intensities of Ir(bt)$_2$(acac) and Ir(pq)$_2$(acac) were 1.19 and 3.09 relative to the [Ru(bpy)$_3$](PF$_6$)$_2$ reference, which exceeded that of the

previously reported [Ir(df-ppy)$_2$(ptb)](PF$_6$) complex (nb: the additional I_s/I_{ref} values shown in parentheses in Table 2.2 were obtained without correction for the sensitivity of the instrumentation across the wavelength range; the similarity with those obtained after correction show the reasonable consistency of the CCD spectrometer response across the investigated range). However, these values were well below the reported 214 for Ir(bt)$_2$(acac),[10] and either 10[9] or 77[2a] for Ir(pq)$_2$(acac) (Table 2.1). The relative ECL intensity for Ir(ppy)$_2$(acac) (0.036) was also more than an order of magnitude lower than that previously reported (0.96).[10] In an attempt to understand the large discrepancies between the observed and reported values, we considered numerous factors that could influence these ratios:

(1) *Decomposition*. The Ir(C^N)$_2$(acac) complexes can decompose by exchange of the acac ligand with solvent molecules.[34] However, the presence of acid is required for this to occur at an appreciable rate, and none of the characteristic changes in the absorption or emission spectra associated with this decomposition[34] were observed under the chemical conditions used in this study.

(2) *Solvent*. Bruce and Richter reported co-reactant ECL efficiencies for Ir(ppy)$_3$ of 0.33 in ACN, 0.0044 in mixed ACN and aqueous solution (1:1 v/v) and 0.00092 in aqueous solution (relative to [Ru(bpy)$_3$]$^{2+}$ = 1).[3a] It is therefore likely that even traces of water in the solvent will affect the relative ECL intensity for Ir(ppy)$_3$ and possibly also for the Ir(C^N)$_2$(acac) complexes. In our study, the ACN was freshly distilled over calcium hydride under nitrogen and we are confident that it would be at least as dry as that used in the previous reports of relative ECL intensities. In one of the previous studies,[10] Zhou *et al.* compared the ECL intensities of the Ir(ppy)$_2$(acac) and Ir(bt)$_2$(acac) complexes in dichloromethane (DCM) rather than ACN. Although both are organic, aprotic solvents, they provide a different electrochemical potential window, and Zhou *et al.* could not measure the reduction peaks of the complexes in DCM.[10] The potential window can affect the stability

53

of certain reactive intermediates of the multiple possible ECL reaction pathways.[8] This is elaborated in item 5 below.

(3) *Deaeration*. The longer excited-state lifetimes of the iridium(III) complexes than $[Ru(bpy)_3]^{2+}$ (Table 2.1) make them more susceptible to quenching by dissolved molecular oxygen, thus reducing their relative ECL intensity in its presence. With our experimental approach, which includes purging each solution in the electrochemical cell with argon for 15 min, we do not believe that the presence of any remaining oxygen was responsible for the much lower relative ECL intensities found under these conditions that those previously reported.[2a, 3a, 9-10] Moreover, the presence of oxygen is easily seen by cyclic voltammetry, and was not observed in our experiments.

(4) *Electrode materials and applied potentials*. The instrumental conditions for the evaluation of relative co-reactant ECL intensities are not standardised, and a survey of the literature shows a variety of different electrode materials and applied potentials that include the use of a single voltage for a set of complexes (e.g., 1.2 V[9] or 1.4 V *vs* $Fc^{0/+}$[2e, 33b]) and various voltages beyond the E_{ox} of each complex under investigation (e.g., 0.08 V,[10] 0.1 V,[35] or 0.5 V[2a]). In their study in which they reported a relative co-reactant ECL intensity of 77 for $Ir(pq)_2(acac)$, Kim *et al.*[2a] used the same reactant and electrolyte concentrations as our *Conditions A*, but they used a platinum disk working electrode and a higher overpotential (E_{ox} + 0.5 V), which was applied at 10 Hz for 10 s (total of 100 pulses). We attempted to replicate these experimental parameters (*Conditions B*), but observed a further decrease in the relative co-reactant ECL intensities of the iridium complexes compared to $[Ru(bpy)_3]^{2+}$ (Table 2.2). However, during these experiments it became evident that the decrease in ECL intensity with each subsequent applied potential pulse (of a single experiment) was less prominent for the $Ir(C^\wedge N)_2(acac)$ complexes than for $[Ru(bpy)_3]^{2+}$. Therefore, an increase in the number of pulses produced an increase in the ECL intensities

of the Ir(C^N)$_2$(acac) complexes relative to that of [Ru(bpy)$_3$]$^{2+}$, because the ECL intensity is integrated over the time period of the experiment (all pulses).

(5) *Reactant concentration*. The mechanism of co-reactant ECL with TPrA comprises several reaction pathways to the electronically excited state species that is responsible for the emission of light.[8] TPrA can be oxidised at the electrode (Eqn 2) or by the oxidised metal complex (Eqn 3) to form the corresponding aminium radical cation, denoted TPrA$^{\bullet+}$, which rapidly deprotonates to generate a highly reductive neutral α-amino alkyl radical, denoted TPrA$^{\bullet}$ (Eqn 4). The emitting species can then be generated by direct reaction between the oxidised metal complex and TPrA$^{\bullet}$ (Eqn 5), or via reduction of the metal complex by TPrA$^{\bullet}$ (Eqn 6), followed by annihilation of the oxidised and reduced metal complex (Eqn 7), or reaction of the reduced metal complex with TPrA$^{\bullet+}$ (Eqn 8). When comparing the potentials of the Ir complexes under investigation with those of TPrA (for which a peak potential was obtained at 0.43 V *vs* Fc$^{0/+}$ using square wave voltammetry[15]) and TPrA$^{\bullet}$ (estimated at -2.1 V *vs* Fc$^{0/+}$[36]), we find that Eqn 1-9 are not all energetically feasible for the Ir(III) complexes. Kim *et al.* attributed the intense ECL for Ir(pq)$_2$(acac) with TPrA in acetonitrile in part to an efficient transfer of electrons in Eqn 3 and 6,[2a] but Eqn 3 is not feasible for Ir(ppy)$_2$(acac) and Ir(ppy)$_3$, and Eqn 6 (and therefore also Eqn 7 and 8) is not feasible for Ir(bt)$_2$(acac), Ir(ppy)$_2$(acac) and Ir(ppy)$_3$. This, however, does not rule out the generation of ECL for these complexes, which can still occur *via* Eqns 1, 2, 4, 5 and 9.

For each feasible reaction pathway, the intensity of the ECL at any particular moment will be dependent on the rate that the emitting species is generated, which is dependent in part on the concentration of the reactants required for each step. The initial concentration of the metal complex and the co-reactant, and any experimental condition that influences the formation or stability of the intermediates, will influence the rate and relative contribution of the reaction pathways. This may include the electrode materials and geometry, the cell

configuration and dimensions, the solvent and electrolyte, and the magnitude and sequence of the applied potentials. For example, Zhou *et al.*[9] found that the co-reactant ECL intensity of Ir(pq)$_2$(acac) (relative to [Ru(bpy)$_3$]$^{2+}$ = 1) was 10.3 when the applied potential was stepped to 1.2 V (*vs* Fc$^{0/+}$), but increased to 42.5 when the potential was instead scanned at 0.1 V s^{-1} from 0.4 V to 1.2 V, which would have generated different concentrations of the key intermediates of the reaction pathways. Although many of the above parameters are difficult to examine, we can manipulate the rate and contribution of the distinct reaction pathways by changing the concentrations of the two starting reactants (the metal complex and the co-reactant), which achieves similar outcomes in terms of the relative ECL intensities.

Decreasing the concentration of the metal complex by two orders of magnitude (whilst also increasing the number of applied potential pulses to compensate for the reduced intensity) produced an increase in the relative intensity for Ir(bt)$_2$(acac), but a decrease for the other iridium complexes. In contrast, decreasing the concentration of TPrA instead by two orders of magnitude gave a large increase for each Ir(C^N)$_2$(acac) complex relative to that of [Ru(bpy)$_3$]$^{2+}$. Surprisingly, an even greater increase in the relative intensities of the Ir(C^N)$_2$(acac) complexes was observed when decreasing the concentrations of both starting reactants (*Conditions C* in Table 2.2). Under these conditions, the relative intensity for Ir(pq)$_2$(acac) (I_s/I_{ref} = 81.9) was now well above that reported by Zhou *et al.* (I_s/I_{ref} = 10) and similar to that reported by Kim *et al.* (I_s/I_{ref} = 77).[2a] The intensities for Ir(bt)$_2$(acac) (I_s/I_{ref} = 26.8) and Ir(ppy)$_2$(acac) (I_s/I_{ref} = 0.50) were also greatly increased compared to those obtained using *Conditions A*, but still below those reported by Zhou *et al.*[10] (I_s/I_{ref} = 214 and 0.96, respectively; Table 2.1). It should be noted that the concentrations of metal complex and TPrA used in the comparisons of ECL intensities by Kim *et al.*[2a] and Zhou *et al.*[9-10] were the same or similar to those that we used in *Conditions A* and *B*, and that we only utilised these lower concentrations here as a means to manipulate the generation of key

reaction intermediates to represent the possible effects of a range of other parameters as described above.

(6) *Spectral sensitivity*. For complexes that have a similar spectral distribution, such as the orange-red light emitters: $Ir(pq)_2(acac)$ and $[Ru(bpy)_3]^{2+}$ (Figure 2.3), changes in the sensitivity of the photodetector over the wavelength range will have only minor effects on the relative intensity of the two complexes. In their evaluation of the $Ir(pq)_2(acac)$ complex, Kim *et al.*[2a] obtained spectra with a Princeton Instruments charge-coupled device (CCD) camera and used the integrated area of the spectrum, whereas Zhou *et al.*[9] used an unspecified PMT and integrated the signal over time. Although it could be expected that the CCD-based approach would provide a more consistent response over the wavelengths of the emission bands, this would be unlikely to explain the difference in their reported relative ECL intensities (I_s/I_{ref} of 77 and 10, respectively), due to the similarity of the emission wavelengths of the evaluated and reference complexes.

However, the other three iridium complexes (which emit yellow or green light; Figure 2.3) have a very different spectral distribution to that of $[Ru(bpy)_3]^{2+}$, and photodetectors that have much lower sensitivity in the red region of the spectrum (such as typical photomultiplier tubes) will give artificially high ECL intensities for these complexes relative to the $[Ru(bpy)_3]^{2+}$ reference. In their evaluation of the $Ir(bt)_2(acac)$ and $Ir(ppy)_2(acac)$ complexes, Zhou *et al.*[10] used a MPI-A detector (Xi'an Remax Electronics, China) for ECL measurement, and a Cary Eclipse fluorescence spectrophotometer to collect ECL spectra (without spectral correction). It is unclear which of these instruments was used to obtain the relative ECL intensities, but both contain a photomultiplier tube that will significantly less sensitive to the longer wavelengths of the reference complex. In the evaluation of $Ir(ppy)_3$ by Bruce *et al.*,[3a] they refer to previous papers for the details of the instrumentation, which include a photomultiplier tube (Hamamatsu HC 135) for the measurement of ECL,[37] and a Shimadzu RF-5301 spectrofluorophotometer (without spectral correction) for ECL

spectra.[37b] They do state, however, that the ECL efficiencies were obtained by the literature methods using $[Ru(bpy)_3]^{2+}$ (ϕ_{ECL} = 1) as the standard, and cite a paper in which a charge-coupled device (CCD) camera system was employed,[38] but it is unclear which instrumentation was utilised for the evaluation of Ir(ppy)$_3$.

For our *Conditions A-C*, we used an Ocean Optics spectrometer that exhibits a much flatter spectral response of the region of interest than a PMT. This is seen in the similar λ_{max} of the ECL spectra collected with the CCD spectrometer using a emission slit that provided a 6.5 nm resolution, with the respective photoluminescence spectra obtained with a Cary Eclipse with a emission bandpass of 5 nm, but only after correction of the photoluminescence spectra for the relative spectral sensitivity of the Eclipse (Table 2.2). The artificial hypsochromic shift of the uncorrected photoluminescence emission spectra (particularly Ir(pq)$_2$(acac) and $[Ru(bpy)_3]^{2+}$) results from the poorer sensitivity of the instrument in the red end of the visible range. The Eclipse contains an extended-range multi-alkali PMT (model R928; Hamamatsu), whereas typical bialkali PMTs are even less sensitive in that region.

Conditions D were a repeat of *Conditions C*, except that we replaced the CCD spectrometer with a bialkali PMT (and the acquisition time was reduced). The relative ECL intensity of Ir(pq)$_2$(acac) was similar, due to the similarity of its spectrum with that of the reference complex (Figure 2.3). However, the other three complexes emit light at shorter wavelengths, where the PMT is considerably more sensitive, resulting in an artificial increase in their measured ECL intensities relative to the $[Ru(bpy)_3]^{2+}$. Under these conditions, our I_s/I_{ref} value for Ir(bt)$_2$(acac) was similar to that reported by Zhou *et al.*,[10] but our I_s/I_{ref} for Ir(ppy)$_2$(acac) was far beyond that reported by Zhou *et al.* in the same study.

2.4 Conclusions

The evaluation of ECL I_s/I_{ref} is vulnerable to influence from a range of experimental parameters and in some cases, exceptional intensities reported for new complexes may have been derived using instrumental or chemical conditions that unintentionally disadvantaged the $[Ru(bpy)_3]^{2+}$ reference electrochemiluminophore, such as the electrochemical pulse sequence or the use of photodetectors that are less sensitive towards the red end of the spectrum where the reference complex emits light. However, although the wavelength sensitivity of typical photomultiplier tubes may bias the relative ECL intensities towards electrochemiluminophores that emit light near the blue-end of the spectrum, this comparison may be more practical if the final analytical instrumentation for which the detection system is used exhibits a similar bias. The light-producing reaction pathways identified for the classic $[Ru(bpy)_3]^{2+}$-TPrA co-reactant ECL system are not necessarily all feasible for novel electrochemiluminophores, which is an important consideration for the intended application. For example, in ECL-based immunodiagnostic systems in which the metal-complex labels are immobilised on magnetic microbeads held at an electrode surface, generation of ECL relies predominantly on the diffusion of oxidised TPrA radicals from the electrode to the bound electrochemiluminophores (*i.e.*, Eqn 2, 4, 6 and 8).[8] Eqn 6 and 8 are not feasible for most of the iridium complexes examined in this study. Conversely, in systems in which the metal complex is used for the ECL detection of an amine analyte,[1b, 39] both species can be oxidised at the electrode surface and pathways analogous to Eqns 1-5 become more important. When comparing relative ECL intensities, it is therefore also important to consider the influence of experimental conditions on the relative contribution of multiple reaction pathways that may be available for complexes within the study.

2.5 Experimental Section

2.5.1 Chemicals

[Ru(bpy)$_3$](PF$_6$)$_2$, Ir(ppy)$_3$ and tetrabutylammonium hexafluorophosphate (TBAPF$_6$) were purchased from Sigma-Aldrich (NSW, Australia). Ir(ppy)$_2$(acac), Ir(bt)$_2$(acac) and Ir(pq)$_2$(acac) were purchased from SunaTech (Jiangsu, China). Acetonitrile was from Scharlau (Barcelona, Spain) and was distilled over calcium hydride under nitrogen. Bis(cyclopentadienyl)iron (ferrocene) was purchased from Strem Chemicals (MA, USA).

2.5.2 Absorption and photoluminescence emission spectra

Absorption spectra were obtained using 1 cm pathlength quartz cells with a Cary 300 Bio UV/Vis spectrophotometer (Varian Australia, Vic., Australia). Photoluminescence spectra were collected using a 1cm quartz cuvette with a Cary Eclipse spectrofluorimeter (Varian Australia; 5 nm band pass, 1 nm data interval, PMT voltage: 800 V). Low temperature (77 K) photoluminescence were obtained using an OptistatDN Variable Temperature Liquid Nitrogen Cryostat, with custom-made quartz sample holder. Room temperature and low temperature emission spectra were corrected for the change in instrument sensitivity across the wavelength range under examination, using a correction factor that was established using a quartz-halogen tungsten lamp of standard spectral irradiance (OL 245M, Optronic Laboratories, FL, USA), operated at 6.5A dc from a programmable current source (OL 65A, Optronic Laboratories).

2.5.3 Electrochemistry and ECL

Cyclic voltammetry experiments were performed using an Autolab PGSTAT204 potentiostat (Metrohm Autolab B.V., Netherlands). The electrochemical cell consisted of a cylindrical glass cell with a quartz base and Teflon cover with spill tray.[40] The cell and

accessories were encased in a custom-built light-tight faraday cage. A conventional three-electrode configuration was employed, consisting of a glassy carbon (3 mm diameter) working electrode shrouded in Teflon (CH Instruments, Austin, TX, USA), silver wire reference electrode and platinum wire counter electrode. The metal complexes were prepared at a concentration of 0.25 mM (with 0.1 M TBAPF$_6$ as the supporting electrolyte) in freshly distilled acetonitrile. Prior to each experiment, the working electrode was polished using 0.3 mm and then 0.05 mm alumina with water on a felt pad, sonicated in MilliQ water (1 min), rinsed in freshly distilled acetonitrile and dried with a stream of N$_2$. The solutions were degassed within the electrochemical cell for 15 min. CVs were collected at a scan rate of 0.1 V s^{-1}. Electrochemical potentials were referenced to the ferrocene/ferrocenium (Fc$^{0/+}$) couple measured *in situ* (1 mM) at the end of each experiment. ECL experiments were performed with an Autolab PGSTAT128N potentiostat. The light was detected using an Ocean Optics QE65Pro spectrometer with HC-1 (300 l/mm) grating and Hamamatsu S7031-1006 back-thinned CCD (Quark Photonics, Vic., Australia) *via* optical fibre (1.0 m length, 1.0 mm core diameter) and collimating lens (Ocean Optics 74-UV, 200-2000 nm), positioned under the transparent base of the electrochemical cell described above, and vertically aligned with the face of the working electrode that was 2 mm above the base of the cell. The spectrometer was fitted with a 200 μm entrance slit, which provided a spectral resolution of 6.5 nm (FWHM). Acquisition was triggered using a HR 4000 Break-Out box in conjunction with the potentiostat. The spectra were corrected for the change in instrument sensitivity across the wavelength range (including absorption from the optical fibre and the lens, features in the grating response and the CCD detector response) using correction factors (one for each slit width setting) that were established using an HL-2000 Ocean Optics light source directed onto a WS-1-SL diffuse white reflectance standard. The spectra were integrated to determine the relative ECL intensities. Prior to each experiment, solutions were purged with grade 5 argon within the electrochemical cell for 15 min.

ECL Conditions A: Electrodes: glassy carbon working (3 mm diameter), Ag/AgCl low-leakage reference (Innovative Instruments, FL, USA), and platinum counter. Concentrations: 0.1 mM metal complex, 10 mM TPrA, and 0.1 M $TBAPF_6$ supporting electrolyte. Applied potential: $\{E_{ox} + 0.15\ V\}$ for 0.05 s at 10 Hz, 2 s acquisition time (total of 20 pulses). The entrance slit of the spectrometer was removed and replaced with a round SMA with no slit installed, to increase the proportion of light reaching the CCD detector, resulting in an effective spectral resolution of 30 nm (FWHM).

ECL Conditions B: Electrodes: platinum working (2 mm diameter), silver wire reference, and platinum counter. Concentrations: 0.1 mM complex, 10 mM TPrA, and 0.1 M $TBAPF_6$. Applied potential: $\{E_{ox} + 0.50\ V\}$ for 0.05 s at 10 Hz, 10 s acquisition time (100 pulses). The spectrometer was fitted with a 200 μm entrance slit.

ECL Conditions C: Electrodes: glassy carbon working (3 mm diameter), Ag/AgCl low-leakage reference, and platinum counter. Concentrations: 0.001 mM complex, 0.1 mM TPA, and 0.1 M $TBAPF_6$. Applied potential: $\{E_{ox} + 0.15\ V\}$ for 0.05 s at 10 Hz, 30 s acquisition time (300 pulses). The entrance slit of the spectrometer was removed and replaced with a round SMA as described above.

ECL Conditions D: Electrodes: glassy carbon working (3 mm diameter), Ag/AgCl low-leakage reference, and platinum counter. Concentrations: 0.001 mM complex, 0.1 mM TPA, and 0.1 M $TBAPF_6$. Applied potential: $\{E_{ox} + 0.15\ V\}$ for 0.05 s at 10 Hz, 1 s acquisition time (10 pulses). The CCD spectrometer and fibre optic assembly were replaced with a bialkali photomultiplier tube (ET Enterprises model 9125SB; ETP, NSW, Australia), positioned directly under the transparent base of the electrochemical cell. The PMT was set at a constant voltage of 800 V from a stable power supply (PM20D, ETP) *via* a voltage divider (E637-09, ETP). The output from the PMT was connected to the auxiliary channel of the potentiostat *via* an amplifier (A1, ETP).

Computational methods. DFT calculations were carried out within the Gaussian 09 suite of programs.[41] Ground and triplet state geometries were optimised in the absence of solvent with the mPW1PW91 functional[42] in conjunction with the def2-SVP basis set and associated effective core potential.[43] The mPW1PW91 functional has previously been demonstrated to yield reliable results for such systems.[29, 33b, 44] Stationary points were characterised as minima by calculating the Hessian matrix analytically at the same level of theory. All structures are minima with no imaginary frequencies. Due to difficulties with the D_3 symmetry triplet state of $[Ru(bpy)_3]^{2+}$, a previously reported[45] B3PW91/LANL2DZ calculated structure was used. Single-point energy calculations (including molecular orbital (MO) energies) were carried out with the def2-TZVP basis set and core potential[43] together with DFT functionals with varying amounts of Hartree-Fock exchange: pure functionals PBE,[46] and BP86,[47] the hybrid functionals PBE0,[48] B3LYP,[49] and mPW1PW91,[42] and long range corrected functionals CAM-B3LYP,[50] and B97XD.[51] Solvent effects were included for all single-point energy calculations with acetonitrile for consistency with the experimental system. The polarisable continuum model (PCM)[52] self-consistent reaction field (SCRF) was used together with Truhlar's SMD solvent model.[53] TD-DFT calculations of absorption and emission were calculated at the CAM-B3LYP/def2-SVP level of theory. Absorbance bands were calculated at the singlet-state optimised geometry; 20 singlet and triplet states were calculated with TD-DFT. An SCF convergence criterion of 10-8 a.u. was employed throughout. MO analysis was carried out with the QMForge program.[54]

2.6 Acknowledgements

† The Ir(pq)$_2$(acac) complex has also been utilised for the ECL detection of a wide range of analytes.[55]

§ The ECL efficiency (ϕ_{ECL}; the photons emitted per charge transfer event, but often estimated as the coulometric efficiency, which is the photons generated per charge transfer event in the first potential step) is frequently reported for annihilation ECL systems relative to the absolute value for [Ru(bpy)$_3$]$^{2+}$ in acetonitrile of 0.050.[7, 56] In the case of ECL under solely oxidative conditions with TPrA as co-reactant, the Faradaic charge transfer from the metal complex cannot be distinguished from that of the co-reactant, which is generally present in large excess. Moreover, the oxidised [Ru(bpy)$_3$]$^{3+}$ also reacts with the TPrA co-reactant, which regenerates [Ru(bpy)$_3$]$^{3+}$ in the ground electronic state (Eqn 3).[57] Therefore, comparisons of co-reactant ECL are generally made by relative ECL intensities under identical conditions, using the [Ru(bpy)$_3$]$^{2+}$/TPrA system = 1 as an arbitrary reference. In some cases (e.g., [2a]), this is still referred to as ECL efficiency (ϕ_{ECL}), but it is more appropriate to use the term 'relative co-reactant ECL intensity' (I_s/I_{ref}).

2.7 References

[1]   a) M. M. Richter, *Chem. Rev.* **2004**, *104*, 3003-3036; b) B. A. Gorman, P. S. Francis, N. W. Barnett, *Analyst* **2006**, *131*, 616-639; c) W. Miao, *Chem. Rev.* **2008**, *108*, 2506-2553; d) L. Hu, G. Xu, *Chem. Soc. Rev.* **2010**, *39*, 3275-3304; e) Y. Yuan, S. Han, L. Hu, S. Parveen, G. Xu, *Electrochim. Acta* **2012**, *82*, 484-492; f) X. Zhou, D. Zhu, Y. Liao, W. Liu, H. Liu, Z. Ma, D. Xing, *Nat. Protoc.* **2014**, *9*, 1146-1159; g) K. Muzyka, *Biosens. Bioelectron.* **2014**, *54*, 393-407; h) Z. Liu, W. Qi, G. Xu, *Chem. Soc. Rev.* **2015**, *44*, 3117-3142; i) M. Hesari, Z. Ding, *J. Electrochem. Soc.* **2016**, *163*, H3116-H3131.

[2]   a) J. I. Kim, I.-S. Shin, H. Kim, J.-K. Lee, *J. Am. Chem. Soc.* **2005**, *127*, 1614-1615; b) S. Zanarini, E. Rampazzo, S. Bonacchi, R. Juris, M. Marcaccio, M. Montalti, F.

Paolucci, L. Prodi, *J. Am. Chem. Soc.* **2009**, *131*, 14208-14209; c) S. Zanarini, M. Felici, G. Valenti, M. Marcaccio, L. Prodi, S. Bonacchi, P. Contreras-Carballada, R. M. Williams, M. C. Feiters, R. J. M. Nolte, L. De Cola, F. Paolucci, *Chem. Eur. J.* **2011**, *17*, 4640-4647; d) K. N. Swanick, S. Ladouceur, E. Zysman-Colman, Z. Ding, *Chem. Commun.* **2012**, *48*, 3179-3181; e) G. J. Barbante, E. H. Doeven, E. Kerr, T. U. Connell, P. S. Donnelly, J. M. White, T. Lópes, S. Laird, C. F. Hogan, D. J. D. Wilson, P. J. Barnard, P. S. Francis, *Chem. Eur. J.* **2014**, *20*, 3322-3332; f) A. Kapturkiewicz, *Anal. Bioanal. Chem.* **2016**, In press. DOI 10.1007/s00216-016-9615-8.

[3] a) D. Bruce, M. M. Richter, *Anal. Chem.* **2002**, *74*, 1340-1342; b) B. D. Muegge, M. M. Richter, *Anal. Chem.* **2004**, *76*, 73-77; c) E. H. Doeven, E. M. Zammit, G. J. Barbante, C. F. Hogan, N. W. Barnett, P. S. Francis, *Angew. Chem., Int. Ed.* **2012**, *51*, 4354-4357; d) E. H. Doeven, G. J. Barbante, E. Kerr, C. F. Hogan, J. A. Endler, P. S. Francis, *Anal. Chem.* **2014**, *86*, 2727-2732; e) E. H. Doeven, G. J. Barbante, C. F. Hogan, P. S. Francis, *ChemPlusChem* **2015**, *80*, 456-470.

[4] a) K. Nishimura, Y. Hamada, T. Tsujioka, K. Shibata, T. Fuyuki, *Jpn. J. Appl. Phys., Part 2* **2001**, *40*, L945-L947; b) E. M. Gross, N. R. Armstrong, R. M. Wightman, *J. Electrochem. Soc.* **2002**, *149*, E137-E142; c) A. Kapturkiewicz, G. Angulo, *Dalton Trans.* **2003**, 3907-3913.

[5] a) A. Kapturkiewicz, T.-M. Chen, I. R. Laskar, J. Nowacki, *Electrochem. Commun.* **2004**, *6*, 827-831; b) A. Kapturkiewicz, J. Nowacki, P. Borowicz, *Electrochim. Acta* **2005**, *50*, 3395-3400.

[6] a) S. Lamansky, P. Djurovich, D. Murphy, F. Abdel-Razzaq, H.-E. Lee, C. Adachi, P. E. Burrows, S. R. Forrest, M. E. Thompson, *J. Am. Chem. Soc.* **2001**, *123*, 4304-4312; b) B. W. D'Andrade, M. E. Thompson, S. R. Forrest, *Adv. Mater.* **2002**, *14*, 147-151; c) D. Kolosov, V. Adamovich, P. Djurovich, M. E. Thompson, C. Adachi, *J. Am. Chem. Soc.* **2002**, *124*, 9945-9954.

[7]   W. L. Wallace, A. J. Bard, *J. Phys. Chem.* **1979**, *83*, 1350-1357.

[8]   W. Miao, J.-P. Choi, A. J. Bard, *J. Am. Chem. Soc.* **2002**, *124*, 14478-14485.

[9]   Y. Zhou, W. Li, L. Yu, Y. Liu, X. Wang, M. Zhou, *Dalton Trans.* **2015**, *44*, 1858-1865.

[10]   Y. Zhou, H. Gao, X. Wang, H. Qi, *Inorg. Chem.* **2015**, *54*, 1446-1453.

[11]   J. M. Fernandez-Hernandez, E. Longhi, R. Cysewski, F. Polo, H.-P. Josel, L. De Cola, *Anal. Chem.* **2016**, *88*, 4174-4178.

[12]   a) S. Lamansky, P. Djurovich, D. Murphy, F. Abdel-Razzaq, R. Kwong, I. Tsyba, M. Bortz, B. Mui, R. Bau, M. E. Thompson, *Inorg. Chem.* **2001**, *40*, 1704-1711; b) Y.-Q. Wu, H. Jing, Z.-S. Dong, Q. Zhao, H.-Z. Wu, F.-Y. Li, *Inorg. Chem.* **2011**, *50*, 7412-7420; c) J. Frey, B. F. E. Curchod, R. Scopelliti, I. Tavernelli, U. Rothlisberger, M. K. Nazeeruddin, E. Baranoff, *Dalton Trans.* **2014**, *43*, 5667-5679.

[13]   a) F. G. Gao, A. J. Bard, *J. Am. Chem. Soc.* **2000**, *122*, 7426-7427; b) J. Yu, H. Lin, F. Wang, Y. Lin, J. Zhang, H. Zhang, Z. Wang, B. Wei, *J. Mater. Chem.* **2012**, *22*, 22097-22101; c) S.-H. Ye, T.-Q. Hu, Z. Zhou, M. Yang, M.-H. Quan, Q.-B. Mei, B.-C. Zhai, Z.-H. Jia, W.-Y. Lai, W. Huang, *Phys. Chem. Chem. Phys.* **2015**, *17*, 8860-8869; d) Y. J. Cho, J. Y. Lee, *Adv. Mater.* **2011**, *23*, 4568-4572.

[14]   K. Suzuki, A. Kobayashi, S. Kaneko, K. Takehira, T. Yoshihara, H. Ishida, Y. Shiina, S. Oishi, S. Tobita, *Phys. Chem. Chem. Phys.* **2009**, *11*, 9850-9860.

[15]   E. H. Doeven, E. M. Zammit, G. J. Barbante, P. S. Francis, N. W. Barnett, C. F. Hogan, *Chem. Sci.* **2013**, *4*, 977-982.

[16]   K. Dedeian, P. I. Djurovich, F. O. Garces, G. Carlson, R. J. Watts, *Inorg. Chem.* **1991**, *30*, 1685-1687.

[17]   K. Nakamaru, *J. Chem. Soc. Jpn.* **1982**, *55*, 2697-2705.

[18]   P. I. Djurovich, D. Murphy, M. E. Thompson, B. Hernandez, R. Gao, P. L. Hunt, M. Selke, *Dalton Trans.* **2007**, 3763-3770.

[19] A. Tsuboyama, H. Iwawaki, M. Furugori, T. Mukaide, J. Kamatani, S. Igawa, T. Moriyama, S. Miura, T. Takiguchi, S. Okada, M. Hoshino, K. Ueno, *J. Am. Chem. Soc.* **2003**, *125*, 12971-12979.

[20] B. Beyer, C. Ulbricht, D. Escudero, C. Friebe, A. Winter, L. Gonzalez, U. S. Schubert, *Organometallics* **2009**, *28*, 5478-5488.

[21] Q. Zhao, C.-Y. Jiang, M. Shi, F.-Y. Li, T. Yi, Y. Cao, C.-H. Huang, *Organometallics* **2006**, *25*, 3631-3638.

[22] A. Juris, V. Balzani, P. Belser, A. von Zelewsky, *Helv. Chim. Acta* **1981**, *64*, 2175-2182.

[23] A. Endo, K. Suzuki, T. Yoshihara, S. Tobita, M. Yahiro, C. Adachi, *Chem. Phys. Lett.* **2008**, *460*, 155-157.

[24] T. Hofbeck, H. Yersin, *Inorg. Chem.* **2010**, *49*, 9290-9299.

[25] T. Sajoto, P. I. Djurovich, A. B. Tamayo, J. Oxgaard, W. A. Goddard, M. E. Thompson, *J. Am. Chem. Soc.* **2009**, *131*, 9813-9822.

[26] K. A. King, P. J. Spellane, R. J. Watts, *J. Am. Chem. Soc.* **1985**, *107*, 1431-1432.

[27] F.-C. Chen, S.-C. Chang, G. He, S. Pyo, Y. Yang, M. Kurotaki, J. Kido, *J. Polym. Sci., Part B: Polym. Phys.* **2003**, *41*, 2681-2690.

[28] I.-S. Shin, J. I. Kim, T.-H. Kwon, J.-I. Hong, J.-K. Lee, H. Kim, *J. Phys. Chem. C* **2007**, *111*, 2280-2286.

[29] G. J. Barbante, C. F. Hogan, D. J. D. Wilson, N. A. Lewcenko, F. M. Pfeffer, N. W. Barnett, P. S. Francis, *Analyst* **2011**, *136*, 1329-1338.

[30] N. E. Tokel-Takvoryan, R. E. Hemingway, A. J. Bard, *J. Am. Chem. Soc.* **1973**, *95*, 6582-6589.

[31] P. Szrebowaty, A. Kapturkiewicz, *Chem. Phys. Lett.* **2000**, *328*, 160-168.

[32] S. Campagna, F. Puntoriero, F. Nastasi, G. Bergamini, V. Balzani, *Top. Curr. Chem.* **2007**, *280*, 117-214.

[33] a) T. Joshi, G. J. Barbante, P. S. Francis, C. F. Hogan, A. M. Bond, G. Gasser, L. Spiccia, *Inorg. Chem.* **2012**, *51*, 3302-3315; b) G. J. Barbante, E. H. Doeven, P. S. Francis, B. D. Stringer, C. F. Hogan, P. R. Kheradmand, D. J. D. Wilson, P. J. Barnard, *Dalton Trans.* **2015**, *44*, 8564-8576.

[34] Y. Li, Y. Liu, M. Zhou, *Dalton Trans.* **2012**, *41*, 3807-3816.

[35] a) B. D. Stringer, L. M. Quan, P. J. Barnard, D. J. D. Wilson, C. F. Hogan, *Organometallics* **2014**, *33*, 4860-4872; b) E. Kerr, E. H. Doeven, G. J. Barbante, T. U. Connell, P. S. Donnelly, D. J. D. Wilson, T. D. Ashton, F. M. Pfeffer, P. S. Francis, *Chem. - Eur. J.* **2015**, *21*, 14987-14995.

[36] R. Y. Lai, A. J. Bard, *J. Phys. Chem. A* **2003**, *107*, 3335-3340.

[37] a) J. McCall, C. Alexander, M. M. Richter, *Anal. Chem.* **1999**, *71*, 2523-2527; b) S. R. Workman, Mark M., *Anal. Chem.* **2000**, *72*, 5556-5561.

[38] P. McCord, A. J. Bard, *J. Electroanal. Chem. Interfacial Electrochem.* **1991**, *318*, 91-99.

[39] C. M. Hindson, G. R. Hanson, P. S. Francis, J. L. Adcock, N. W. Barnett, *Chem. Eur. J.* **2011**, *17*, 8018-8022.

[40] E. Kerr, E. H. Doeven, G. J. Barbante, C. F. Hogan, D. J. Hayne, P. S. Donnelly, P. S. Francis, *Chem. Sci.* **2016**, *7*, 5271-5279.

[41] M. J. Frisch, G. W. Trucks, H. B. Schlegel, G. E. Scuseria, M. A. Robb, J. R. Cheeseman, G. Scalmani, V. Barone, B. Mennucci, G. A. Petersson, H. Nakatsuji, M. Caricato, X. Li, H. P. Hratchian, A. F. Izmaylov, J. Bloino, G. Zheng, J. L. Sonnenberg, M. Hada, M. Ehara, K. Toyota, R. Fukuda, J. Hasegawa, M. Ishida, T. Nakajima, Y. Honda, O. Kitao, H. Nakai, T. Vreven, J. J. A. Montgomery, J. E. Peralta, F. Ogliaro, M. Bearpark, J. J. Heyd, E. Brothers, K. N. Kudin, V. N. Staroverov, R. Kobayashi, J. Normand, K. Raghavachari, A. Rendell, J. C. Burant, S. S. Iyengar, J. Tomasi, M. Cossi, N. Rega, J. M. Millam, M. Klene, J. E. Knox, J. B.

Cross, V. Bakken, C. Adamo, J. Jaramillo, R. Gomperts, R. E. Stratmann, O. Yazyev, A. J. Austin, R. Cammi, C. Pomelli, J. W. Ochterski, R. L. Martin, K. Morokuma, V. G. Zakrzewski, G. A. Voth, P. Salvador, J. J. Dannenberg, S. Dapprich, A. D. Daniels, Ö. Farkas, J. B. Foresman, J. V. Ortiz, J. Cioslowski, D. J. Fox, Gaussian, Inc., Wallingford CT, 2009.

[42] C. Adamo, V. Barone, J. Chem. Phys. 1998, 108, 664-675.

[43] F. Weigend, R. Ahlrichs, Phys. Chem. Chem. Phys. 2005, 7, 3297-3305.

[44] a) J. Lin, K. Wu, M. Zhang, J. Comput. Chem. 2009, 30, 2056-2063; b) R. V. Kiran, C. F. Hogan, B. D. James, D. J. D. Wilson, Eur. J. Inorg. Chem. 2011, 4816-4825.

[45] K. Nozaki, K. Takamori, Y. Nakatsugawa, T. Ohno, Inorg. Chem. 2006, 45, 6161-6178.

[46] a) J. P. Perdew, K. Burke, M. Ernzerhof, Phys. Rev. Lett. 1996, 77, 3865-3868; b) J. P. Perdew, K. Burke, M. Ernzerhof, Phys. Rev. Lett. 1997, 78, 1396.

[47] a) A. D. Becke, Phys. Rev. A: Gen. Phys. 1988, 38, 3098-3100; b) J. P. Perdew, Phys. Rev. B 1986, 33, 8822-8824.

[48] C. Adamo, V. Barone, J. Chem. Phys. 1999, 110, 6158-6169.

[49] A. D. Becke, J. Chem. Phys. 1993, 98, 5648-5652.

[50] T. Yanai, D. P. Tew, N. C. Handy, Chem. Phys. Lett. 2004, 393, 51-57.

[51] J.-D. Chai, M. Head-Gordon, Phys. Chem. Chem. Phys. 2008, 10, 6615-6620.

[52] J. Tomasi, B. Mennucci, R. Cammi, Chem. Rev. 2005, 105, 2999-3093.

[53] A. V. Marenich, C. J. Cramer, D. G. Truhlar, J. Phys. Chem. B 2009, 113, 6378-6396.

[54] A. L. Tenderholt.QMForge, Version 2.4, http://qmforge.sourceforge.net

[55] a) I.-S. Shin, Y.-T. Kang, J.-K. Lee, H. Kim, T. H. Kim, J. S. Kim, Analyst 2011, 136, 2151-2155; b) C. Li, S. Zhu, Y. Ding, Q. Song, J. Electroanal. Chem. 2012, 682, 136-140; c) M.-J. Li, Y.-Q. Shi, T.-Y. Lan, H.-H. Yang, G.-N. Chen, J. Electroanal. Chem. 2013, 702, 25-30; d) X. Ni, T. Li, Q. Song, J. Electroanal. Chem. 2014, 719, 30-34; e) Y. Liu, Q. Song, Anal. Methods 2014, 6, 5258-5263.

[56] F.-R. F. Fan, in Electrogenerated Chemiluminescence (Ed.: A. J. Bard), Marcel Dekker, New York, 2004, pp. 23-99.

[57] J. K. Leland, M. J. Powell, J. Electrochem. Soc. 1990, 137, 3127-3131.

Chapter 3: Water-soluble iridium(III) complexes containing tetraethylene glycol derivatised bipyridine ligands for electrogenerated chemiluminescence detection

Lifen Chen,[a] Ben Newman,[a] Luke C. Henderson,[b] Egan H. Doeven,[c] Paul S. Francis*[,a] David J. Hayne*[,b]

[a]School of Life and Environmental Sciences, Faculty of Science, Engineering and Built Environment, Deakin University, Geelong, Victoria 3220, Australia.

[b]Institute for Frontier Materials, Deakin University, Geelong, Victoria 3220, Australia.

[c]Centre for Regional and Rural Futures, Faculty of Science, Engineering and Built Environment, Deakin University, Geelong, Victoria 3220, Australia.

AUTHORSHIP STATEMENT

1. Details of publication and executive author

Title of Publication		Publication details
Water-Soluble Iridium(III) Complexes containing Tetraethylene Glycol Derivatised Bipyridine Ligands for Electrogenerated Chemiluminescence Detection		In preparation for submission
Name of executive author	School/Institute/Division if based at Deakin; Organisation and address if non-Deakin	Email or phone
Professor Paul S. Francis	School of Life and Environmental Sciences	psf@deakin.edu.au

2. Inclusion of publication in a thesis

Is it intended to include this publication in a higher degree by research (HDR) thesis?	Yes	If Yes, please complete Section 3 If No, go straight to Section 4.

3. HDR thesis author's declaration

Name of HDR thesis author if different from above. (If the same, write "as above")	School/Institute/Division if based at Deakin	Thesis title
Lifen Chen	School of Life and Environmental Sciences	Novel iridium(III) complexes for electrogenerated chemiluminescence labeling and detection
If there are multiple authors, give a full description of HDR thesis author's contribution to the publication (for example, how much did you contribute to the conception of the project, the design of methodology or experimental protocol, data collection, analysis, drafting the manuscript, revising it critically for important intellectual content, etc.)		
Major contributions to: conception of project and experimental design; spectroscopic, electrochemical, and electrochemiluminescence laboratory experimentation (both through her own experiments and the guidance and training of Honours student Ben Newman within the laboratory); data analysis and interpretation, and preparation of manuscript under the guidance of PhD supervisors and collaborators, acknowledged by my position as the first author of the manuscript.		
I declare that the above is an accurate description of my contribution to this paper, and the contributions of other authors are as described below.	Signature and date	Signature Redacted by Library 17th March 2019

4. Description of all author contributions

Name and affiliation of author	Contribution(s) (for example, conception of the project, design of methodology or experimental protocol, data collection, analysis, drafting the manuscript, revising it critically for important intellectual content, etc.)
Ben Newman; School of Life and Environmental Sciences, Deakin University	Contributions to chemical synthesis under the supervision of David Hayne and Luke Henderson. Selected spectroscopic and electrochemical experiments, and relevant sections of the manuscript, under the guidance of Lifen Chen and Paul Francis
Luke C. Henderson; Institute for Frontier Materials, Deakin University	Contributions to the synthetic chemistry aspects of the project in conjunction with David Hayne.
Egan H. Doeven; Centre for Regional and Rural Futures, Deakin University	Co-supervision of PhD student Lifen Chen. Contributed to the design of experiments and provided training and guidance in instrumental techniques. Assisted in editing the manuscript.

Paul S. Francis; School of Life and Environmental Sciences, Deakin University	Principal supervision of PhD student Lifen Chen, and co-supervision of Ben Newman. Contribution to conception of project and experimental design. Manuscript editing.
David J. Hayne; Institute for Frontier Materials, Deakin University	Led the design and synthesis of ligands and complexes, and the preparation of synthetic experimental sections of the manuscript. Supervision of Honours student Ben Newman in synthetic aspects of the project.

5. Author Declarations

I agree to be named as one of the authors of this work, and confirm:

vi. *that I have met the authorship criteria set out in the Deakin University Research Conduct Policy,*

vii. *that there are no other authors according to these criteria,*

viii. *that the description in Section 4 of my contribution(s) to this publication is accurate,*

ix. *that the data on which these findings are based are stored as set out in Section 7 below.*

If this work is to form part of an HDR thesis as described in Sections 2 and 3, I further

x. *consent to the incorporation of the publication into the candidate's HDR thesis submitted to Deakin University and, if the higher degree is awarded, the subsequent publication of the thesis by the university (subject to relevant Copyright provisions).*

Name of author	Signature*	Date
Ben Newman		18/03/2019
Luke C. Henderson		17/03/2019
Egan H. Doeven		17/03/2019
Paul S. Francis		17/03/2019
David J. Hayne		19/03/2019

6. Other contributor declarations

I agree to be named as a non-author contributor to this work.

Name and affiliation of contributor	Contribution	Signature* and date

* If an author or contributor is unavailable or otherwise unable to sign the statement of authorship, the Head of Academic Unit may sign on their behalf, noting the reason for their unavailability, provided there is no evidence to suggest that the person would object to being named as author

7. Data storage

The original data for this project are stored in the following locations. (The locations must be within an appropriate institutional setting. If the executive author is a Deakin staff member and data are stored outside Deakin University, permission for this must be given by the Head of Academic Unit within which the executive author is based.)

Data format	Storage Location	Date lodged	Name of custodian if other than the executive author
Electronic data	Ka5.127 and backed up using Dropbox software	Throughout PhD	

This form must be retained by the executive author, within the school or institute in which they are based.

If the publication is to be included as part of an HDR thesis, a copy of this form must be included in the thesis with the publication.

3.1 Abstract

Four cationic heteroleptic iridium(III) complexes containing a 2,2′-bipyridine (bpy) ligand with one or two tetraethylene glycol (TEG) groups attached in the 4 or 4,4′ positions, were synthesized to create new water-soluble electrogenerated chemiluminescence (ECL) luminophores bearing a convenient point of attachment for the development of ECL-labels. The novel TEG-derivatised bipyridines were incorporated into [Ir(C^N)$_2$(R-bpy-R′)]Cl complexes, where C^N = 2-phenylpyridine anion (ppy) or 2-phenylbenzo[d]thiazole anion (bt), through reaction with commercially available ([Ir(C^N)$_2$(µ-Cl)]$_2$ dimers. The novel [Ir(C^N)$_2$(Me-bpy-TEG)]Cl and [Ir(C^N)$_2$(TEG-bpy-TEG)]Cl complexes in aqueous solution largely retained the redox potentials and emission spectra of the parent [Ir(C^N)$_2$(Me-bpy-Me)]PF$_6$ (where Me-bpy-Me = 4,4′methyl-2,2′-bipyridine) luminophores in acetonitrile, and exhibited ECL intensities similar to those of [Ru(bpy)$_3$]$^{2+}$ and the analogous [Ir(C^N)$_2$(pt-TEG]Cl complexes (where pt-TEG = 1-(TEG)-4-(2-pyridyl)-1,2,3-triazole). The distinct spectral distributions of [Ir(ppy)$_2$(Me-bpy-TEG)]$^+$ and [Ir(ppy)$_2$(pt-TEG)]$^+$, which can both be readily adapted for bioconjugation, reveals a viable strategy to create ECL-labels with different emission colours from the same commercial [Ir(ppy)$_2$(µ-Cl)]$_2$ precursor.

3.2 Introduction

Electrogenerated chemiluminescence (ECL) is the process whereby electrochemically oxidised and reduced species undergo subsequent electron transfer reactions to produce electronically excited products that emit light.[1,2] To date, the wide use of ECL across various fields[3,4] has predominantly focused on ruthenium(II) complexes (particularly [Ru(bpy)$_3$]$^{2+}$, where bpy = 2,2′-bipyridine) as the luminophores.[5,6] These complexes are highly soluble in buffered aqueous solution and generally produce ECL in the red/orange region of the electromagnetic spectrum. Cyclometalated iridium(III) complexes have

attracted enormous interest as alternative ECL luminophores to the conventional ruthenium(II) complexes due to their high luminescence efficiencies and wide range of emission colours,[7-10] which not only enables the emission to be shifted into the region where commonly used photomultiplier tubes are most sensitive, but also creates new opportunities for tuneable light-emitting devices and simultaneous multi-analyte detection with spectrally distinct species.

A great number of cyclometalated iridium(III) complexes have been synthesised and many have shown impressive annihilation and/or co-reactant ECL intensities in organic media.[9,11,12] For example, we recently re-examined a promising series of heteroleptic iridium(III) complexes containing an acetylacetonate anion (acac) ligand, with several exhibiting much greater ECL intensities than $[Ru(bpy)_3]^{2+}$ (with tri-n-propylamine (TPrA) co-reactant in acetonitrile solution), although the relative intensities were highly dependent on reaction conditions.[13]

Nevertheless, very few of the iridium(III) complexes examined as ECL luminophores to date are soluble in the aqueous conditions in which most ECL assays are performed.[14] [15-19] As previously reported, the solubility can be improved by incorporating polar functional groups such as sulfonates[20,21] or saccharides[18,22] on one or more ligands of the complex. Li *et al*.,[18] for example, reported intense ECL from a water-soluble bis-cyclometalated iridium(III) complex incorporating a bpy ligand appended with two sugar moieties. Similarly, we utilised bathophenanthroline-disulfonate (BPS) as an ancillary ligand in to increase the solubility of the complexes in aqueous solution.[23,24] However, in most cases, the dissolution of the complexes at relatively high concentrations often still required the addition of some acetonitrile to the aqueous solution, and these approaches do not provide a convenient means to incorporate the luminophores into ECL labels. We recently examined the ECL of several water soluble $[Ir(C^\wedge N)_2(pt)]Cl$ complexes (where $C^\wedge N$ = 2-

phenyl)pyridine anion (ppy) or 2-(2,4-difluorophenyl)pyridine anion (df-ppy), and pt = 4-(2-pyridyl)-1,2,3-triazole) with either a tetraethylene glycol (TEG) or benzyl group attached to the triazole and/or methanesulfonate substituents on the ppy/df-ppy ligands.[25] Although the TEG and methanesulfonate groups improved the solubility of the complexes in water, the complexes with the pt-TEG ligand (Figure 3.1) gave greater co-reactant ECL intensities with TPrA and provide a convenient point of attachment of functional groups for bioconjugation[26] for the future development of iridium(III) complex ECL labels.

$[Ir(df-ppy)_2(pt-TEG)]^+$ $[Ir(ppy-CH_2-SO_3^-)_2(pt-TEG)]^-$
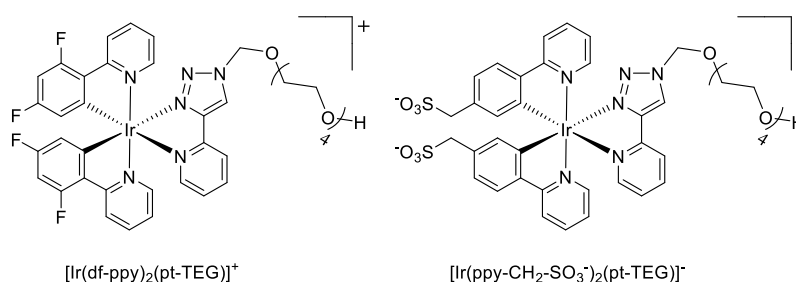
Figure 3.1. $[Ir(C\text{^}N)_2(pt-TEG)]^+$ complexes.[25]

Herein, we prepare four novel $[Ir(C\text{^}N)_2(N\text{^}N)]Cl$ complexes (Figure 3.2), where N^N is bpy with either one or two TEG groups attached in the 4 and 4′ positions (referred to hereafter as Me-bpy-TEG and TEG-bpy-TEG). Through the introduction of the TEG group(s) onto the commonly used bpy ligand, iridium(III) complexes previously studied in organic solvents can be examined in buffered aqueous solution. We incorporate the Me-bpy-TEG and TEG-bpy-TEG ligands into heteroleptic iridium(III) complexes with ppy or 2-phenylbenzo[d]thiazole anion (bt) ligands by reacting the bipyridine derivatives with commercially available $([Ir(C\text{^}N)_2(\mu-Cl)]_2$ dimers. We evaluate the influence of the TEG group(s) on the parent luminophore by comparing their spectroscopic and electrochemical properties with the corresponding $[Ir(C\text{^}N)_2(Me-bpy-Me)]^+$ complexes, and compare their co-reactant ECL intensities to the analogous water-soluble $[Ir(C\text{^}N)_2(pt-TEG)]^+$ complexes and $[Ru(bpy)_3]^{2+}$.

[Ir(bt)$_2$(TEG-bpy-TEG)]$^+$ [Ir(bt)$_2$(Me-bpy-TEG)]$^+$

[Ir(ppy)$_2$(TEG-bpy-TEG)]$^+$ [Ir(ppy)$_2$(Me-bpy-TEG)]$^+$
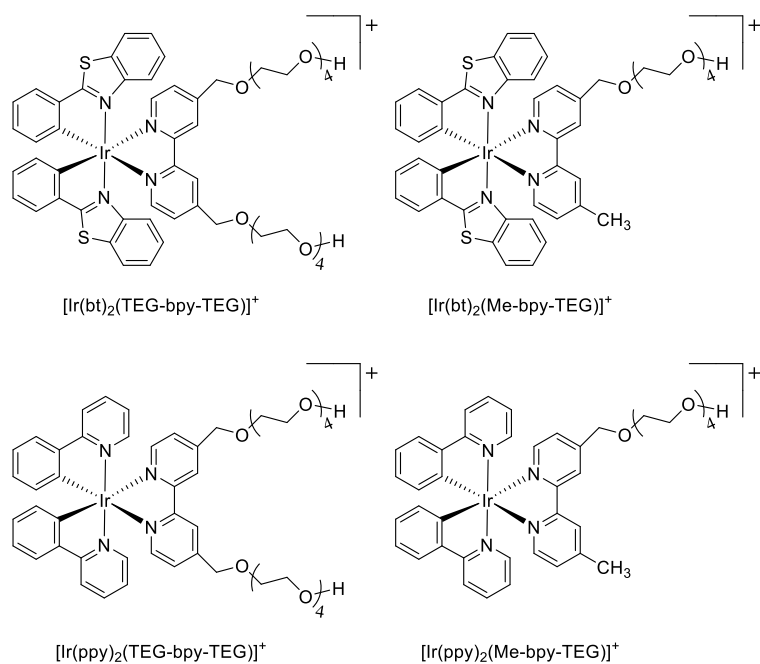
Figure 3.2. Novel iridium(III) complexes containing a 2,2′-bipyridine ligand with one or two tetraethylene glycol groups.

3.3 Results and Discussion

To prepare the complexes shown in Figure 3.2, the chloro-bridged iridium(III) dimers ([Ir(C^N)$_2$(μ-Cl)]$_2$, where C^N = ppy or bt) were initially reacted with bpy derivatives furnished with either one or two TEG groups (Me-bpy-TEG (**L^1**) and TEG-bpy-TEG (**L^2**)). The bipyridine ligands were prepared using TEG mono protected with a trityl group and functionalised using tosyl chloride to afford a suitable leaving group to react with hydroxyl methyl bipyridine derivatives (Scheme 3.1).
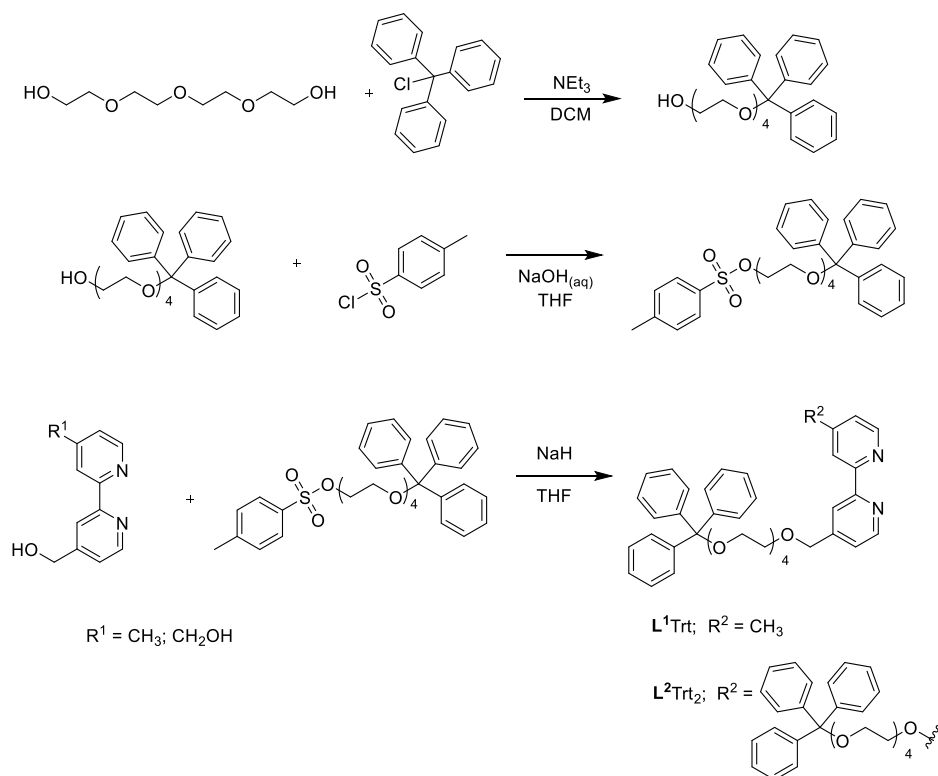
Scheme 3.1. Synthesis of trityl protected bipyridine ligands (L^1Trt and L^2Trt$_2$).

Trifluoroacetic acid was used to deprotect L^1Trt followed by acid/base extraction to give L^1, but L^2 proved difficult to isolate by this method, so L^2Trt$_2$ was used directly to form iridium(III) dimers. The trityl groups were then removed from the bis-TEGTrt$_2$ complexes to give [Ir(C^N$_2$)(TEG-bpy-TEG)]Cl by stirring in methanolic hydrochloric acid afforded by addition of acetyl chloride to methanol. Precipitation of complexes from dichloromethane occurred upon addition of diethyl ether allowing isolation by centrifugation. The [Ir(C^N$_2$)(Me-bpy-TEG)]Cl and [Ir(C^N$_2$)(TEG-bpy-TEG)]Cl complexes were sufficiently soluble for the preparation of aqueous stock solutions at 1 mM.

3.3.1 UV-Vis absorption and photoluminescence spectra

UV-vis absorption spectra of the four novel iridium(III) complexes and [Ru(bpy)$_3$]$^{2+}$ were examined at 10 μM in water (Figure 3.3) and the peak maxima were compared to the [Ir(C^N)$_2$(Me-bpy-Me)]$^+$ analogues at the same concentration in acetonitrile (Table 3.1). The two [Ir(C^N)$_2$(TEG-bpy-TEG)]$^+$ complexes showed similar absorption spectra to their

[Ir(C^N)$_2$(Me-bpy-TEG)]$^+$ counterparts in water, although the absorbances for the [Ir(C^N)$_2$(TEG-bpy-TEG)]$^+$ species were higher. In general, complexes with the ppy ligands exhibited strong $\pi \rightarrow \pi^*$ LC transitions (λ = 240–300 nm), while the complexes with bt ligands exhibited more prominent charge-transfer (λ = 300 nm and above).[27] The peak maxima were somewhat similar to those of corresponding [Ir(C^N)$_2$(Me-bpy-Me)]$^+$ complexes in acetonitrile (Table 3.1).
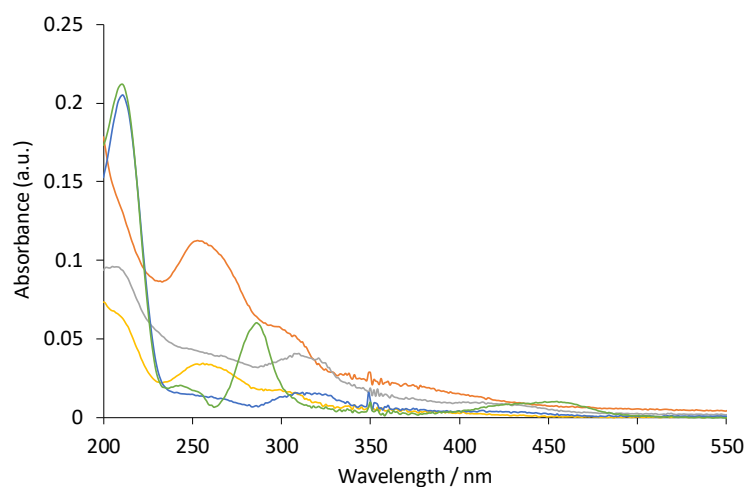
Figure 3.3. UV-vis absorbance spectra obtained for [Ir(bt)$_2$(TEG-bpy-TEG)]$^+$ (grey line), [Ir(bt)$_2$(Me-bpy-TEG)]$^+$ (blue line), [Ir(ppy)$_2$(TEG-bpy-TEG)]$^+$ (orange line), [Ir(ppy)$_2$(Me-bpy-TEG)]$^+$ (yellow line) and [Ru(bpy)$_3$]$^{2+}$ (green line), at a concentration of 10 μM in water at ambient temperature.

The photoluminescence spectra of the four novel complexes ([Ir(ppy)$_2$(TEG-bpy-TEG)]Cl, [Ir(bt)$_2$(TEG-bpy-TEG)]Cl, [Ir(ppy)$_2$(Me-bpy-TEG)]Cl and [Ir(bt)$_2$(Me-bpy-TEG)]Cl) and the archetype ECL metal complex [Ru(bpy)$_3$]$^{2+}$ were initially examined at room temperature at 10 μM in aqueous solution (Figure 3.4). The peak maxima were also compared to those of the previously reported Ir(ppy)$_2$(Me-bpy-Me)]PF$_6$ and [Ir(bt)$_2$(Me-bpy-Me)]PF$_6$ complexes[28-30] at the same concentration in acetonitrile (Table 3.1).

Table 3.1. UV-Vis absorbance and luminescence peak maxima of the metal complexes at room temperature and low temperature.

Complex	λ_{abs} (nm)	λ_{em} (r.t.)[a] / nm	λ_{em} (85 K)[b] / nm
[Ir(bt)$_2$(TEG-bpy-TEG)]Cl	258, 310, ~360(br)	531, 568, 619	517, 557, 599
[Ir(bt)$_2$(Me-bpy-TEG)]Cl	214, 258, 307, ~400(br)	531, 567, 613	
[Ir(bt)$_2$(Me-bpy-Me)]PF$_6$	256, 408(br), 468(br)	528, 568, 615	516, 558, 606
[Ir(ppy)$_2$(TEG-bpy-TEG)]Cl	213, 316, ~420(br)	628	471, 511(sh), 533
[Ir(ppy)$_2$(Me-bpy-TEG)]Cl	213, 318, ~420(br)	623	
[Ir(ppy)$_2$(Me-bpy-Me)]PF$_6$	208, 269, 321, 411(br)	590	473, 511, 533
[Ru(bpy)$_3$]Cl$_2$	215, 290, 445	629	

[a]10 μM in water, except for the two [Ir(C^N)$_2$(Me-bpy-Me)]PF$_6$ complexes where were prepared at 10 μM in acetonitrile. [b]5 μM in 4:1 (v/v) ethanol:methanol. sh = shoulder. br = broad.
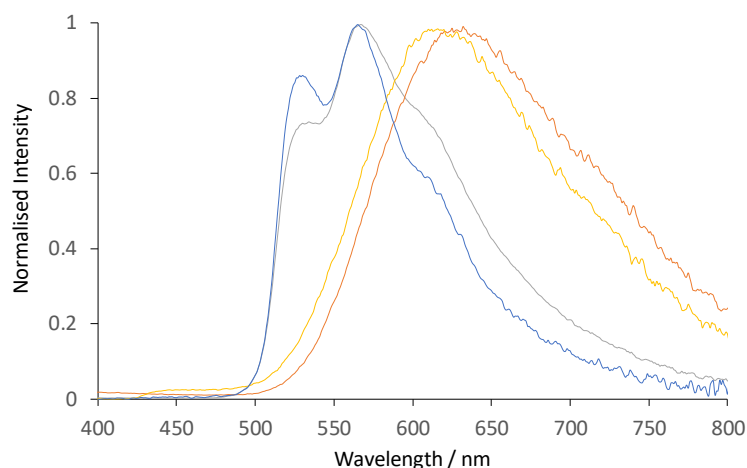
Figure 3.4. Normalised luminescence emission spectra obtained for [Ir(bt)$_2$(TEG-bpy-TEG)]$^+$ (grey line), [Ir(bt)$_2$(Me-bpy-TEG)]$^+$ (blue line), [Ir(ppy)$_2$(TEG-bpy-TEG)]$^+$ (orange line), and [Ir(ppy)$_2$(Me-bpy-TEG)]$^+$ (yellow line), at 10 μM in water at ambient temperature.

The three [Ir(bt)$_2$(N^N)]$^+$ complexes exhibited similar peak maxima (Table 3.1). There were differences in the relatively intensity of the three major emission bands (Figure 3.4), but the overall emission colours of the two novel complexes in water and the Me-bpy-Me analogue

in acetonitrile were visually a similar green (Figure 3.5, second, fourth and seventh cuvette from the left). The luminescence of heteroleptic iridium(III) complexes has previously been attributed to mixed ligand-centred (^{3}LC ($\pi \rightarrow \pi^*$) and metal-to-ligand charge-transfer ^{3}MLCT (dπ(Ir)$\rightarrow\pi^*$(C^N)) transitions.[31] The vibronic fine structure observed in the emission spectra of the bt complexes are consistent with a significant $\pi \rightarrow \pi^*$ contribution to the luminescence.

The two novel [Ir(ppy)$_2$(N^N)]$^+$ complexes in water exhibited single broad emission peaks (Figure 3.4) that were red-shifted from that of [Ir(ppy)$_2$(Me-bpy-Me)]$^+$ in acetonitrile by over 30 nm (Table 3.1). The closely related [Ir(ppy)$_2$(bpy)]$^+$ complex has previously been shown to exhibit solvatochromic shifts[32,33][34] due to an unusually high barrier for relaxation to the lowest energy excited state (^{3}MLCT$_{(bpy)}$), where contributions from higher energy bands are promoted in less polar solvents. The absence of a red-shift in the [Ir(bt)$_2$(N^N)]$^+$ complexes and the similar peak maxima for the two [Ir(ppy)$_2$(N^N)]$^+$ complexes with either one or two TEG groups, indicates that the red-shift in these complexes can be attributed to a similar solvatochromic effect. It is possible that some aggregation of the complexes occurs, considering they possess a hydrophilic core with highly polar side chain, which may enhance this effect.[33] The lower emission intensities of the [Ir(ppy)$_2$(TEG-bpy-TEG)]$^+$, [Ir(ppy)$_2$(Me-bpy-TEG)]$^+$ and [Ru(bpy)$_3$]$^{2+}$ complexes in water (Figure 3.5) compared to the [Ir(ppy)$_2$(Me-bpy-Me)]$^+$ in acetonitrile, under a UV lamp, are in part due to the lower sensitivity of the camera (and eye) at 623-629 nm compared to 590 nm. Quantitative comparisons of photoluminescence intensities or quantum yields were not undertaken as they are not well correlated with ECL intensities.[23]
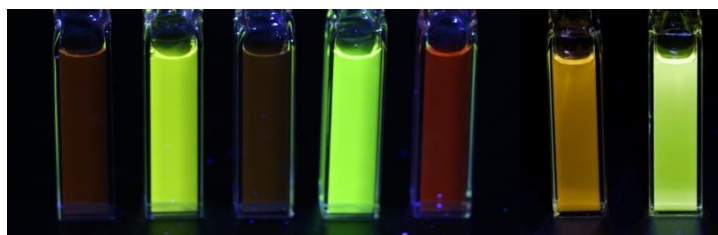
Figure 3.5. Left: [Ir(ppy)$_2$(TEG-bpy-TEG)]Cl, [Ir(bt)$_2$(TEG-bpy-TEG)]Cl, [Ir(ppy)$_2$(Me-bpy-TEG)]Cl, [Ir(bt)$_2$(Me-bpy-TEG)]Cl and [Ru(bpy)$_3$]Cl$_2$, in water at a concentration of 0.1 mM. Right: Ir(ppy)$_2$(Me-bpy-Me)]PF$_6$ and [Ir(bt)$_2$(Me-bpy-Me)]PF$_6$ at 0.1 mM in acetonitrile.

The photoluminescence spectra of the two [Ir(C^N)$_2$(TEG-bpy-TEG)]$^+$ complexes (where C^N is bt or ppy) were examined at 85 K (Figure 3.6). The solutions were prepared in 4:1 (v/v) ethanol:methanol, which is commonly used for low-temperature spectra.[13]
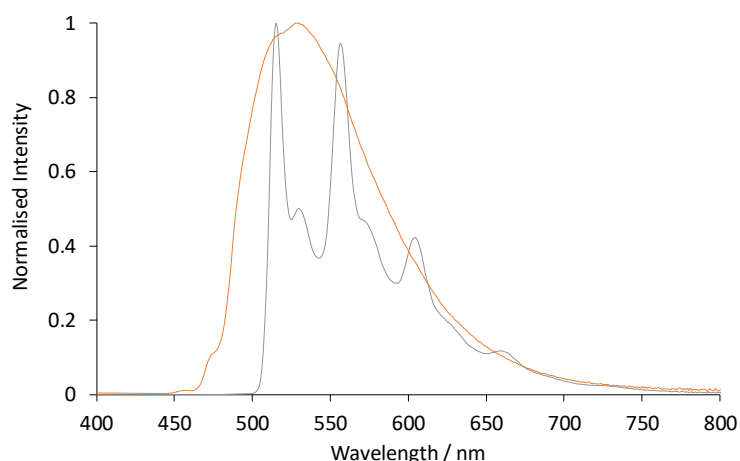
Figure 3.6. Normalised photoluminescence emission spectra obtained for [Ir(bt)$_2$(TEG-bpy-TEG)]$^+$ (grey line), and [Ir(ppy)$_2$(TEG-bpy-TEG)]$^+$ (orange line), at 5 μM in 4:1 (v/v) ethanol:methanol at low-temperature (85 K).

Low-temperature spectra generally show greater detail of vibrational energy levels, and allow for a more accurate estimation of the energy gap (E_{0-0}) between the lowest vibrational levels of the ground and lowest excited state.[35] The low temperature spectrum for [Ir(bt)$_2$(TEG-bpy-TEG)]$^+$ is highly structured (Figure 3.6), even more than at room temperature (Figure 3.4), and was in close agreement with that of [Ir(bt)$_2$(Me-bpy-Me)]$^+$ (Table 3.2). The highest energy peak at 517 nm corresponds to an E_{0-0} energy of 2.4 eV. The

broad emission spectrum produced by [Ir(ppy)$_2$(TEG-bpy-TEG)]$^+$ at low temperature is unusual for an iridium(III) complex, but the peak maxima are nearly identical to those of [Ir(ppy)$_2$(Me-bpy-Me)]$^+$, and the highest energy band at 471/473 nm is well over 100 nm blue-shifted from the room-temperature maxima. This is further confirmation that, like [Ir(ppy)$_2$(bpy)]$^+$, these complexes exhibit simultaneous emissions from multiple bands. Although this complicates the approximation of the E_{0-0}, comparison with previous interpretation of emission spectra of [Ir(ppy)$_2$(bpy)]$^+$,[32-34] enables it to be also estimated as 2.4 eV.

3.3.2 Voltammetry

Cyclic voltammetry (CV) experiments were initially conducted using buffered aqueous solutions to mimic the analytical conditions for which they were designed (Figure 3.7, black lines). No reverse peaks are seen as the oxidation of the four novel complexes appears irreversible in an aqueous environment, which is most likely due to the tendency of iridium complexes to generate electrochemically unstable oxidised or reduced species, in addition the poor solubility of the complexes and/or reaction products in aqueous solution that can cause electrode fouling. This behavior has been observed for various iridium complexes in aqueous solutions in the literature, thus was not investigated in detail. The electrochemical reversibility of the luminophore is important for intense and efficient ECL, as the luminophore can participate in the light emitting process many times in a single potential pulse or CV scan (under conditions of excess co-reactant). The electrochemical irreversibility of the iridium complexes studied is most likely a factor in the relatively weak light emission observed, with respect to the complexes QY and the standard Ru(bpy)$_3^{2+}$ complex. In the Chapter 4, Ru(bpy)$_3^{2+}$ based assays and iridium-complex based ECL assays were compared, and the experiments further demonstrated that the irreversibility of iridium complexes is most likely a key factor in limiting their analytical application. The cyclic

voltammetry (CV) experiments and square wave voltammetry (swv) were both conducted to get the positions of the oxidation peaks. The shape of the cyclic voltammograms made assigning peak potentials difficult, so squarewave voltammetry (Figure 3.7, orange lines) was also conducted to inform the positions of the oxidation peaks (Table 3.3).
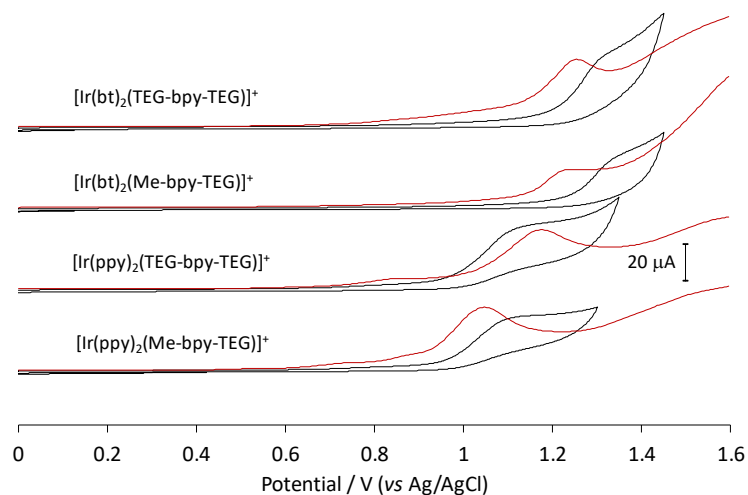
Figure 3.7. Squarewave voltammetry,and cyclic voltammetry traces obtained for the four novel iridium(III) complexes at a concentration of 1 mM. 0.005 V step, 0.02 V amplitude, 25 Hz, scan rate: 0.1 V/s. The electrochemical parameters were determined by using a three-electrode system. All solutions were prepared in either deionised water with a 0.1 M phosphate buffer electrolyte adjusted to pH 7.5, or dry acetonitrile with 0.1 M $TBAPF_6$ electrolyte, and were degassed with nitrogen for 5 min. Glass carbon electrode was used as working electrode, Pt wire and either a 'leakless' Ag/AgCl reference or Ag wire pseudo-reference were used as counter electrode, and reference electrode.

Table 3.3. Oxidation and reduction potentials of the complexes.

Complex	E_p^{ox} (V vs Ag/AgCl)[a]	$E^{0'}$ (ox) (V vs Fc$^{+/0}$)[b]	$E^{0'}$ (red) (V vs Fc$^{+/0}$)[b]
[Ir(bt)$_2$(TEG-bpy-TEG)]Cl	1.25	1.02	-1.73
[Ir(bt)$_2$(Me-bpy-TEG)]Cl	1.22	1.00	-1.79
[Ir(bt)$_2$(Me-bpy-Me)]PF$_6$	-	1.03	-1.79
[Ir(ppy)$_2$(TEG-bpy-TEG)]Cl	0.84, 1.18	0.86	-1.79
[Ir(ppy)$_2$(Me-bpy-TEG)]Cl	0.73, 1.04	0.86	-1.81
[Ir(ppy)$_2$(Me-bpy-Me)]PF$_6$	-	0.85	-1.86
[Ru(bpy)$_3$](PF$_6$)$_2$	-	0.89	-1.73

[a]1 mM in buffered aqueous solution. [b]0.1 mM in acetonitrile with 0.1 M TBAPF$_6$ electrolyte.

The mechanism of co-reactant ECL depends on both the oxidation and reduction of the metal complex, so it is important that both are characterised. The reduction of the complexes, however, is obscured in voltammetric experiments due to the reduction of solvent, so these potentials were determined in acetonitrile and referenced to the ferrocenium/ferrocene couple (Figure 3.8). This internal electrochemical reference is more reliable that the reference electrode potential and provides a more accurate comparison to the previously reported potentials of related iridium complexes that were not sufficiently soluble in an aqueous buffer (Table 3.3). The additional oxidation peak at ~0.6 V (vs Fc$^{+/0}$) in the traces in Figure 3.8 arises from the chloride counter ion of these complexes. This peak could be removed by converting the compounds to their hexafluorophosphate salts, but this was deemed unnecessary for the project.

The values obtained for the three [Ir(bt)$_2$(N^N)]$^+$ complexes were very similar (oxidation potentials within 30 mV and reduction potentials within 60 mV). Those obtained for the three [Ir(ppy)$_2$(N^N)]$^+$ complexes were also consistent (oxidation potentials within

10 mV and reduction potentials within 70 mV). The oxidation peaks can be attributed to the metal-centered oxidation process, and the reduction peaks can be attributed to ligand-centered reduction processes. The similarity of these potentials indicates that the presence of TEG moieties on the bpy ligand has little effect on the electrochemical properties of the complex.
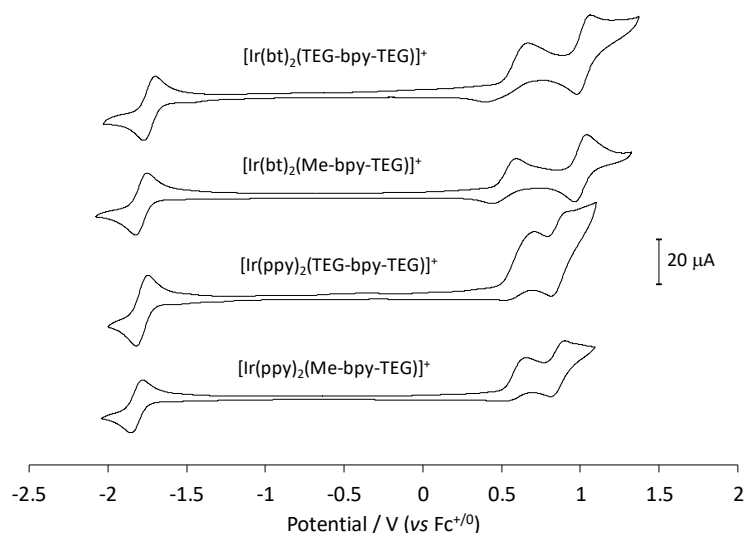
Figure 3.8. Cyclic voltammetry traces for the four novel iridium(III) complexes at 1 mM in acetonitrile with 0.1 M TBAPF6 electrolyte.

3.3.3 Electrogenerated chemiluminescence

The ECL intensities of the $[Ir(C\wedge N)_2(N\wedge N)]^+$ complexes containing a Me-bpy-TEG or TEG-bpy-TEG ligand in buffered aqueous solution using TPrA as a co-reactant were compared with those of the analogous complexes with pt-TEG ligand (Note: the synthesis and characterisation of the $[Ir(ppy)_2(pt-TEG]^+$ and $[Ir(bt)_2(pt-TEG)]^+$ complex is included in the following chapter of this thesis). To remove the bias of the large differences in sensitivity of typical photomultiplier tubes towards the emission wavelengths of these complexes, we used the integrated area of ECL spectra collected using a CCD spectrometer for these comparisons. Figure 3.9 shows the ECL intensities relative to that of the $[Ru(bpy)_3]^{2+}$ complex under the same conditions.

The co-reactant ECL intensities of iridium(III) complexes relative to $[Ru(bpy)_3]^{2+}$ can be highly dependent on instrumental and chemical conditions.[13,25] Using an applied potential pulse 0.1 s, the co-reactant ECL intensities of most of the $[Ir(C^\wedge N)_2(N^\wedge N)]^+$ complexes were greater than that of $[Ru(bpy)_3]^{2+}$ (Figure 3.9a), but when the pulse time was increased to 0.5 s (Figure 3.9b) the intensities were below that of $[Ru(bpy)_3]^{2+}$. Nevertheless, the trend in intensities between the $[Ir(C^\wedge N)_2(N^\wedge N)]^+$ complexes was similar at the two pulse times. The intensities of the $[Ir(C^\wedge N)_2(Me\text{-}bpy\text{-}TEG)]^+$ complexes were between 1.2- and 2.2-fold those of the $[Ir(C^\wedge N)_2(TEG\text{-}bpy\text{-}TEG)]^+$.
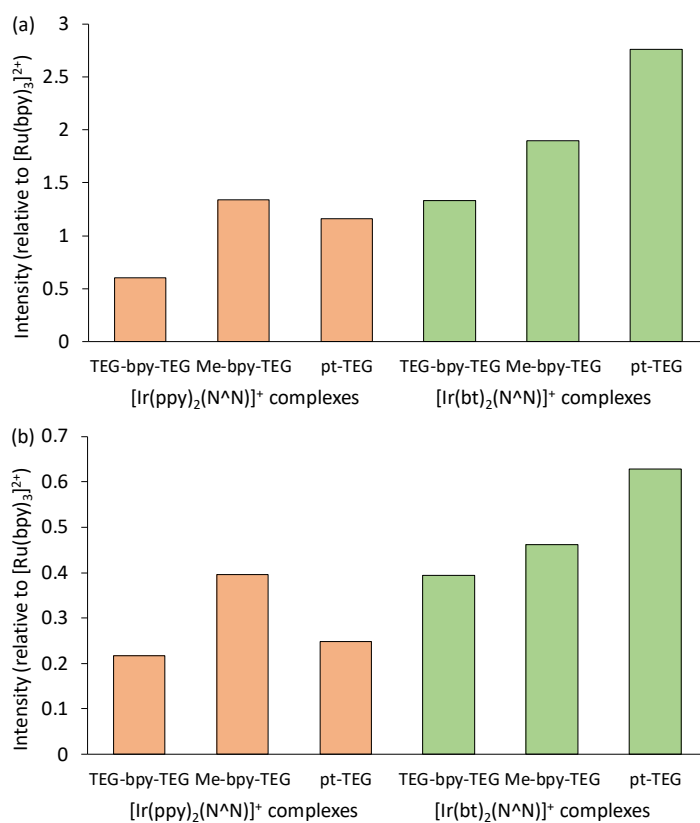
Figure 3.9. Relative ECL intensities (integrated area of ECL spectra obtained using a CCD spectrometer) of water-soluble $[Ir(C^\wedge N)_2(N^\wedge N)]^+$ complexes at 10 μM in a 0.1 M phosphate buffer with 10 mM TPrA, using an applied potential of E_p^{ox} + 0.1 V for each complex for (a) 0.1 s or (b) 0.5 s.

The ECL spectra of the $[Ir(C^\wedge N)_2(Me\text{-}bpy\text{-}TEG)]^+$ and $[Ir(C^\wedge N)_2(TEG\text{-}bpy\text{-}TEG)]^+$ complexes (Figure 3.10) were in good agreement with their photoluminescence emission

spectra (Figure 3.4), taking into account the lower resolution of the CCD spectrometer used to collect the ECL spectra. The spectral distribution of $[Ir(bt)_2(pt\text{-}TEG)]^+$ is similar to that of $[Ir(bt)_2(Me\text{-}bpy\text{-}TEG)]^+$ and $[Ir(bt)_2(TEG\text{-}bpy\text{-}TEG)]^+$, but emission of $[Ir(ppy)_2(pt\text{-}TEG)]^+$ is considerably blue-shifted from $[Ir(ppy)_2(Me\text{-}bpy\text{-}TEG)]^+$ and $[Ir(ppy)_2(TEG\text{-}bpy\text{-}TEG)]^+$ (Figure 3.10). One practical outcome of this shift is that much greater ECL intensities will be measured with $[Ir(ppy)_2(pt\text{-}TEG)]^+$ than with $[Ir(ppy)_2(Me\text{-}bpy\text{-}TEG)]^+$ or $[Ir(ppy)_2(TEG\text{-}bpy\text{-}TEG)]^+$ when using photomultiplier tubes that are much more sensitive towards shorter wavelengths of light within the visible region. On the other hand, as both the Me-bpy-TEG and pt-TEG ligands can be readily adapted for bioconjugation, this shows a viable strategy to create two ECL-labels with distinctly different emission colours from the same commercial $[Ir(ppy)_2(\mu\text{-}Cl)]_2$ dimer that provide similar ECL intensities using a CCD spectrometer to distinguish their emissions.
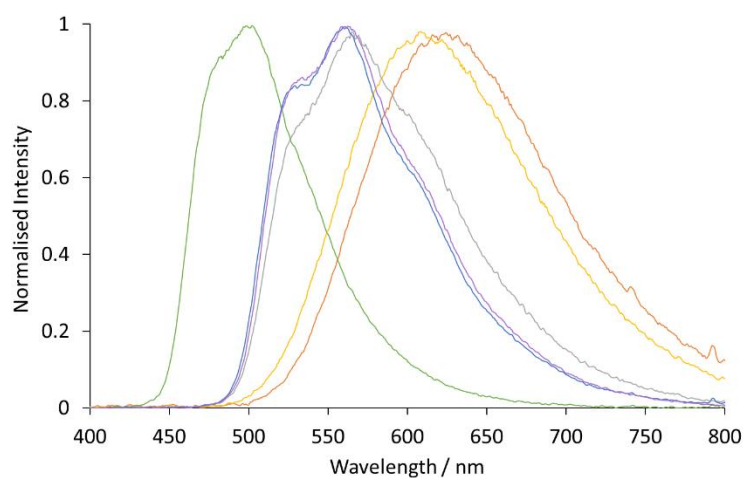
Figure 3.10. Normalised ECL spectra obtained for $[Ir(bt)_2(TEG\text{-}bpy\text{-}TEG)]^+$ (grey line), $[Ir(bt)_2(Me\text{-}bpy\text{-}TEG)]^+$ (blue line), $[Ir(bt)_2(pt\text{-}TEG)]^+$ (purple line), $[Ir(ppy)_2(TEG\text{-}bpy\text{-}TEG)]^+$ (orange line), and $[Ir(ppy)_2(Me\text{-}bpy\text{-}TEG)]^+$ (yellow line) and $[Ir(ppy)_2(pt\text{-}TEG)]^+$ (green line) at 10 μM in 0.1 M phosphate buffer with 10 mM TPrA co-reactant, using an applied potential of E_p^{ox} + 0.1 V for each complex for 0.1 s.

3.4 Conclusions

Four [Ir(C^N)$_2$(N^N)]Cl complexes in which C^N = ppy or bt, and C^N = bpy with either one or two TEG groups attached in the 4 and 4′ positions, were successfully synthesised with acceptable yields for all reaction steps. Characterisation of the complexes showed that the introduction of one or two the TEG groups to the bpy ligand of iridium(III) complexes is a viable strategy to enhance their solubility in aqueous solution while retaining the electrochemical and spectroscopic properties of the parent luminophore, and providing a convenient attachment point for the future development of ECL labels for bioconjugation in affinity based assays.

3.5 Experimental

3.5.1 Chemicals

Tris(2,2′-bipyridine)ruthenium(II) hexafluorophosphate ([Ru(bpy)$_3$](PF$_6$)$_2$), tetrabutylammonium hexafluorophosphate (TBAPF$_6$; electrochemical grade) was purchased from Sigma-Aldrich (NSW, Australia). Bis(cyclopentadienyl)iron (ferrocene; Fc) was purchased from Strem Chemicals (MA, USA). Reagents and solvents were purchased from various commercial sources and used without further purification. The iridium(III) dimer precursors were purchased from SunaTech (China). NMR spectra were acquired on a Bruker Biospin AV400 spectrometer or a Bruker Biospin AV500 spectrometer. ^{1}H NMR spectra were acquired at 400 MHz or 500 MHz, and ^{13}C{^{1}H} NMR spectra were acquired at 100 MHz or 126 MHz. All NMR spectra were recorded at 298 K. Chemical shifts were referenced to residual solvent peaks and are quoted in parts per million (ppm), relative to tetramethylsilane (Si(CH$_3$)$_4$).

3.5.2 Synthesis

1,1,1-triphenyl-2,5,8,11-tetraoxatridecan-13-ol
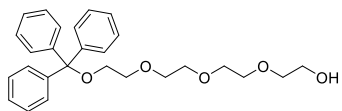
Trityl chloride (4.85 g, 17.4 mmol) in dichloromethane (80 mL) was added dropwise to a mixture of tetraethylene glycol (33.1 g, 170.6 mmol) and triethylamine (8 mL, 57.4 mmol) in dichloromethane (200 mL). After the addition was complete, the reaction mixture was stirred for 2 days at ambient temperature. The mixture was washed with saturated sodium carbonate (200 mL), dH_2O (3 × 200 mL) then brine (200 mL) before being dried ($MgSO_4$). The solvent was removed under reduced pressure to afford a yellow oil (6.95 g, 15.9 mmol, 91%). ^1H NMR (500 MHz; CD_3CN): δ 7.47-7.44 (m, 6H), 7.34-7.31 (m, 6H), 7.28-7.24 (m, 3H), 3.62-3.55 (m, 12H), 3.48-3.46 (m, 2H), 3.14 (dd, J = 5.4, 4.3, 2H). $^{13}C\{^1H\}$ NMR (101 MHz, CD_3CN) δ 145.27, 129.55, 128.82, 128.05, 87.35, 73.30, 71.43, 71.27, 71.24, 71.12, 71.09, 64.39, 61.95.

1,1,1-triphenyl-2,5,8,11-tetraoxatridecan-13-yl 4-methylbenzenesulfonate
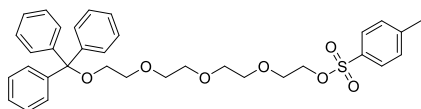
A mixture of 1,1,1-triphenyl-2,5,8,11-tetraoxatridecan-13-ol (3.51 g, 8.1 mmol) in tetrahydrofuran (100 mL) was cooled to 0 °C. Sodium hydroxide (8 M, 25 mL) was added followed by dropwise addition of tosylchloride (1.85 g, 9.7 mmol) in tetrahydrofuran (80mL). The reaction was left to warm to ambient temperature and stirred overnight. Brine (100 mL) was added to the mixture which was then extracted with dichloromethane (3 × 75 mL). The combined organic extracts were dried ($MgSO_4$) and the solvent was removed under reduced pressure to afford a yellow oil (4.58 g, 7.6 mmol, 91%). ^1H NMR (500 MHz; CD_3CN): δ 7.78-7.75 (m, 2H), 7.46-7.44 (m, 6H), 7.42-7.40 (m, 2H), 7.33-7.30 (m, 6H),

7.27-7.23 (m, 3H), 4.08-4.06 (m, 2H), 3.61-3.54 (m, 8H), 3.53-3.51 (m, 2H), 3.49-3.47 (m, 2H), 3.14-3.12 (m, 2H), 2.41 (s, 3H). ^{13}C{^{1}H} NMR (101 MHz, CD$_3$CN) δ 146.34, 145.26, 133.79, 131.00, 129.54, 128.82, 128.77, 128.05, 87.34, 71.42, 71.25, 71.20, 71.11, 70.94, 69.17, 64.39, 21.65.

L^1Trt
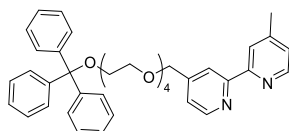
A mixture of 4-(hydroxymethyl)-4′-methyl-2,2′-bipyridine (458 mg, 2.3 mmol) and sodium hydride (60% oil dispersion, 190 mg, 4.8 mmol) was heated at reflux in tetrahydrofuran (dry, 50 mL). After 1.5 h, 1,1,1-triphenyl-2,5,8,11-tetraoxatridecan-13-yl 4-methylbenzenesulfonate (1662 mg, 2.8 mmol) was added and the reaction mixture was stirred at reflux for 20 h. The reaction mixture was cooled to ambient temperature before methanol was added to quench excess sodium hydride. A solid was observed and remove by filtration then the solvent was removed from the filtrate under reduced pressure. The residue was purified by flash chromatography (SiO$_2$, 0→50% ethyl acetate in dichloromethane) to afford the product as a viscous yellow oil after removal of the solvent under reduced pressure (940 mg, 1.5 mmol, 65%). ^{1}H NMR (400 MHz; CD$_3$CN): δ 8.57 (d, J = 4.9, 1H), 8.49 (d, J = 5.0, 1H), 8.36 (s, 1H), 8.26 (s, 1H), 7.44 (m, 6H), 7.31 (m, 7H), 7.30 (m, 4H), 4.62 (s, 2H), 3.61 (m, 14H), 3.11 (t, J = 4.8, 2H), 2.42 (s, 3H). ^{13}C{^{1}H} NMR (101 MHz, CD$_3$CN) δ 156.97, 156.57, 150.10, 150.02, 149.95, 149.27, 145.20, 129.47, 128.74, 127.97, 125.74, 122.77, 122.33, 119.58, 87.26, 71.99, 71.38, 71.23, 71.21, 71.07, 71.04, 71.00, 64.32, 21.20.

_L¹_ (Me-bpy-TEG)

L^1 (Me-bpy-TEG)
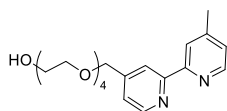
A mixture of 4-methyl-4′-(15,15,15-triphenyl-2,5,8,11,14-pentaoxapentadecyl)-2,2′-bipyridine (940 mg, 1.52 mmol) and trifluoroacetic acid (2 mL) was set stirring in dichloromethane (20 mL) at ambient temperature. After 1 h the mixture was extracted with 1 M hydrochloric acid (3 × 30 mL) and the combined aqueous extracts were adjusted to pH 9 by careful addition of solid potassium carbonate. The aqueous phase was then extracted with ethyl acetate (3 × 30 mL) and the combined organic extracts were dried and the solvent removed under reduced pressure to afford a yellow oil (229 mg, 0.61 mmol, 40%). ^{1}H NMR (400 MHz, CD$_3$CN) δ 8.61 (dd, J = 5.0, 0.7 Hz, 1H), 8.51 (dd, J = 5.0, 0.5 Hz, 1H), 8.35 (dd, J = 1.6, 0.8 Hz, 1H), 8.28 – 8.24 (m, 1H), 7.34 (ddd, J = 7.3, 4.0, 3.2 Hz, 1H), 7.26 – 7.21 (m, 1H), 4.66 (s, 2H), 3.70 – 3.51 (m, 14H), 3.49 – 3.44 (m, 2H), 2.46 (d, J = 20.2 Hz, 3H). ^{13}C{^{1}H} NMR (101 MHz, CD$_3$CN) δ 157.01, 156.57, 150.19, 149.93, 149.80, 149.43, 128.65, 125.78, 122.95, 122.45, 119.71, 73.10, 72.04, 70.97, 70.91, 70.88, 70.84, 70.74, 61.69, 21.20.

Synthesis of 4,4′-bis(ethoxycarbonyl)-2,2′-bipyridine
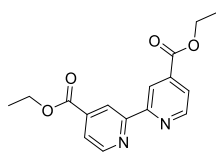
A mixture of 2,2′-bipyridine-4,4′-dicarboxylic acid (5.08 g, 20.8 mmol) and sulphuric acid (10 mL) was heated at reflux in ethanol (200 mL). After 24 h the reaction mixture was cooled to ambient temperature then poured into ice water (100 mL) and adjusting to pH 7 by addition of solid potassium carbonate. The solvent volume was lessened under reduced pressure and the mixture was extracted with dichloromethane (150 mL). The organic phase

was washed with dH$_2$O (3 × 100 mL) then brine (100 mL) before drying (MgSO$_4$) and removal of the solvent a under reduced pressure to afford a colourless solid (4.85 g, 16.1 mmol, 77%). 1H NMR (400 MHz, CDCl$_3$) δ 8.95 (s, 1H), 8.86 (s, 1H), 7.91 (d, J = 4.2 Hz, 1H), 4.46 (q, J = 7.1 Hz, 2H), 1.44 (t, J = 7.1 Hz, 3H). ^{13}C{^{1}H} NMR (101 MHz, CDCl$_3$) δ 165.24, 156.46, 150.15, 139.22, 123.47, 120.79, 62.09, 14.42.

Synthesis of 4,4′-bis(hydroxymethyl)-2,2′-bipyridine
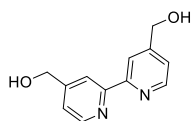
A mixture of 4,4′-bis(ethoxycarbonyl)-2,2′-bipyridine (2.80 g, 9.3 mmol) in ethanol (150 mL) was set stirring and sodium borohydride (3.83 g, 85 mmol) was added portion-wise. After stirring for 16 h at ambient temperature excess sodium borohydride was quenched by addition of an aqueous solution of saturated ammonium chloride. The reaction mixture was filtered to remove solids and the solvent volume was lessened under reduced pressure. The mixture was washed with ethyl acetate (6 × 100 mL) and the combined organic extracts were washed with brine. The organic phase was dried (MgSO$_4$) and the solvent removed under reduced pressure to afford a colourless solid (1.51 g, 7.0 mmol, 75%). ^{1}H NMR (400 MHz, DMSO) δ 8.60 (d, J = 5.0 Hz, 1H), 8.39 (s, 1H), 7.37 (d, J = 4.9 Hz, 1H), 5.52 (t, J = 5.8 Hz, 1H), 4.63 (d, J = 5.7 Hz, 2H). ^{13}C NMR (101 MHz, DMSO) δ 155.21, 152.83, 148.96, 121.40, 117.75, 61.71.

L^{2}Trt$_2$
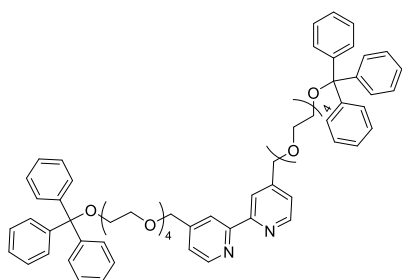
A mixture of 4,4′-bis(hydroxymethyl)-2,2′-bipyridine (254 mg, 1.2 mmol) and sodium hydride (60% oil dispersion, 70 mg, 1.8 mmol) was heated at reflux in tetrahydrofuran (dry, 50 mL). After 1.5 h, 1,1,1-triphenyl-2,5,8,11-tetraoxatridecan-13-yl 4-methylbenzenesulfonate (1693 mg, 2.9 mmol) was added and the reaction mixture was stirred at reflux for 20 h. The reaction mixture was cooled to ambient temperature before methanol was added to quench residual sodium hydride. The reaction mixture was filtered to remove any solids and the solvent was removed under reduced pressure. The resultant residue was taken up in ethyl acetate (100 mL) and washed with dH_2O (3 × 100 mL) then brine (100 mL). The organic phase was dried ($MgSO_4$) and the solvent was removed under reduced pressure then the residue was purified by column chromatography (SiO_2, 0→10% methanol in ethyl acetate) to afford a yellow oil (939 mg, 0.89 mmol, 74%). ^1H NMR (400 MHz, CD_3CN) δ 8.57 (d, 2H), 8.37 (d, 2H), 7.49 – 7.40 (m, 12H), 7.32 (s, 2H), 7.32 – 7.27 (m, 12H), 7.26 – 7.20 (m, 6H), 4.06 (q, 2H), 3.68 – 3.49 (m, 30H), 3.16 – 3.06 (m, 4H). $^{13}C\{^1H\}$ NMR (126 MHz, CD_3CN) δ 156.83, 150.16, 145.23, 129.51, 128.79, 128.01, 122.92, 119.60, 87.29, 70.99, 64.36, 60.95.

General method for synthesis of iridium complexes

Approximately one molar equivalent of chloro-bridged iridium dimer and two equivalents of ligand were added to a flask. A solvent mixture of dichloromethane and methanol (1:1 v/v) was added and the mixture was sparged with N_2 for 20 min then sealed, shielded from light and heated at 50 °C for 20 h. Any solid that remained in the reaction mixture was removed by centrifuge and the supernatant was filtered through filter aid (celite). The solvent was removed under reduced pressure and the residue was taken up in a minimum of dichloromethane and a precipitate was formed after addition of diethyl ether. The precipitate was isolated by centrifuge and washed with diethyl ether (× 3) then dried *in vacuo*.

[Ir(bt)₂(Me-bpy-TEG)]Cl
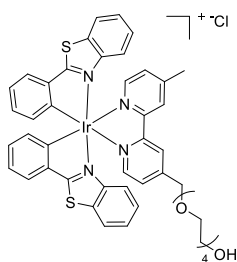
The dimer [Ir(bt)₂(μ-Cl)]₂ (239 mg, 0.18 mmol) and **L¹** (132 mg, 0.35 mmol) were reacted according to the general method. The product was isolated as an orange powder (250 mg, 0.24 mmol, 69%). ¹H NMR (500 MHz, CD₃CN) δ 8.52 (s, 1H), 8.44 (s, 1H), 8.03 (t, J = 7.1 Hz, 3H), 7.92 (dd, J = 8.5, 7.0 Hz, 3H), 7.52 (d, J = 5.6 Hz, 1H), 7.38 (t, J = 7.4 Hz, 3H), 7.12 (dt, J = 21.1, 7.6 Hz, 4H), 6.87 (t, J = 7.5 Hz, 2H), 6.40 (dd, J = 7.5, 4.9 Hz, 2H), 6.24 (dd, J = 8.4, 4.2 Hz, 2H), 4.77 (s, 2H), 3.65 (ddd, J = 8.4, 6.4, 3.5 Hz, 4H), 3.55 – 3.44 (m, 10H), 3.39 – 3.35 (m, 2H), 2.54 (s, 3H). ¹³C{¹H} NMR (126 MHz, CD₃CN) δ 182.47, 182.44, 157.42, 156.99, 154.26, 153.66, 151.66, 151.64, 151.57, 151.10, 150.13, 150.11, 141.47, 141.43, 134.19, 134.15, 132.84, 132.67, 132.63, 130.38, 129.05, 129.00, 127.75, 127.20, 127.04, 127.02, 126.39, 124.94, 124.12, 122.93, 73.28, 71.35, 71.15, 71.11, 71.07, 71.05, 70.99, 70.96, 61.76, 21.49.

[Ir(ppy)₂(Me-bpy-TEG)]Cl
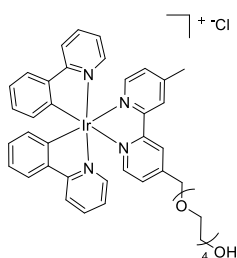
The dimer [Ir(ppy)₂(-Cl)]₂ (193 mg, 0.18 mmol) and **L¹** (128 mg, 0.34 mmol) were reacted according to the general method. The product was isolated as a yellow powder (243 mg, 0.27 mmol, 79%). ¹H NMR (500 MHz, CD₃CN) δ 8.58 (s, 1H), 8.50 (s, 1H), 8.06 (d, J = 8.1 Hz, 2H), 7.89 (d, J = 5.6 Hz, 1H), 7.86 – 7.76 (m, J = 11.7, 6.1 Hz, 5H), 7.61 (dd, J = 12.2, 5.7 Hz, 2H), 7.45 (d, J = 5.6 Hz, 1H), 7.31 (d, J = 5.6 Hz, 1H), 7.03 (t, J = 7.0 Hz, 4H), 6.90

(t, J = 7.4 Hz, 2H), 6.27 (dd, J = 7.5, 4.4 Hz, 2H), 4.75 (s, 2H), 3.72 – 3.63 (m, 4H), 3.59 – 3.45 (m, J = 29.1, 5.3 Hz, 10H), 3.41 (t, J = 4.9 Hz, 2H), 2.53 (s, 3H). 13C NMR (126 MHz, CD$_3$CN) δ 168.44, 168.41, 156.82, 156.39, 153.53, 152.98, 151.65, 151.61, 151.18, 150.73, 150.13, 150.05, 145.07, 145.03, 139.43, 132.53, 132.50, 131.29, 131.28, 129.98, 126.87, 126.52, 125.83, 125.81, 124.44, 124.43, 123.38, 123.37, 123.17, 120.80, 120.77, 73.29, 71.34, 71.16, 71.14, 71.12, 71.05, 70.99, 70.96, 61.74, 21.43.

[Ir(ppy)$_2$(L^{2}Trt$_2$)]Cl
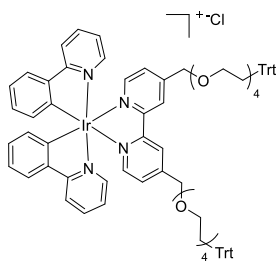
The dimer [Ir(ppy)$_2$(μ-Cl)]$_2$ (71.7 mg, 0.0.067 mmol) and **L**^{2}Trt$_2$ (118 mg, 0.112 mmol) were reacted according to the general method. The product was isolated as a yellow powder (106 mg, 0.067 mmol, 60%). ^{1}H NMR (400 MHz, CD$_3$CN) δ 8.56 – 8.42 (m, 4H), 8.03 (dd, 6H), 7.97 – 7.73 (m, 8H), 7.60 – 7.52 (m, 12H), 7.41 – 7.18 (m, 12H), 7.08 – 6.85 (m, 6H), 6.27 (t, 4H), 4.71 (dd, 4H), 3.58 (dt, 32H). ^{13}C{^{1}H} NMR (126 MHz, CD$_3$CN) δ 151.21, 145.19, 139.41, 128.03, 126.98, 125.84, 124.39, 123.44, 120.81, 73.28, 70.71, 64.22, 61.86.

[Ir(bt)$_2$(L^{2}Trt$_2$)]Cl
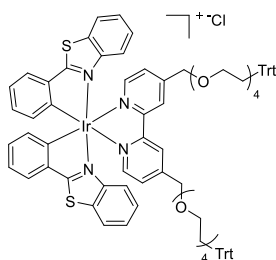
The dimer [Ir(bt)$_2$(μ-Cl)]$_2$ (111 mg, 0.086 mmol) and **L**^{2}Trt$_2$ (162 mg, 0.15 mmol) were reacted as per the general method. The product was isolated as an orange powder (168 mg, 0.099 mmol, 66%). ^{1}H NMR (400 MHz, CD$_3$CN) δ 8.48 (s, 2H), 8.04 (dd, 4H), 7.92 (d, 2H), 7.55 (d, 2H), 7.39 (t, 2H), 7.13 (dd, 4H), 6.89 (t, 2H), 6.40 (d, 2H), 6.24 (d, 2H), 4.78 (s,

4H), 3.65 (dd, 8H), 3.58 – 3.33 (m, 26H). ^{13}C{^{1}H} NMR (126 MHz, CD$_3$CN)   182.04, 156.81, 153.84, 151.16, 149.68, 141.01, 133.74, 132.44, 132.22, 128.62, 127.34, 126.86, 126.61, 124.50, 123.74, 122.64, 72.81, 70.43, 61.41.

General procedure for trityl deprotection of [Ir(C^N)$_2$(L^{2}Trt$_2$)]Cl complexes

The trityl protected complex was set stirring in methanol (15 mL) and the mixture was cooled to 0 °C before acetyl chloride (0.4 mL) was added. The mixture stirred and allowed to warm to ambient temperature for a total of 10 h. The solvent was removed under reduced pressure and the residue was taken up a in a minimum of dichloromethane. A precipitate was formed upon addition of diethyl ether which was isolated by centrifugation and washed with diethyl ether (×3) then dried *in vacuo*.

[Ir(ppy)$_2$(TEG-bpy-TEG)]Cl
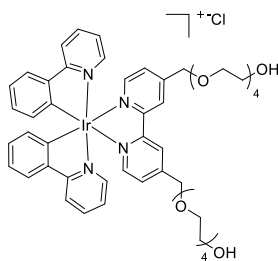
The complex [Ir(ppy)$_2$(L^{2}Trt$_2$)]Cl (90 mg, 0.057 mmol) was reacted according to the general procedure for trityl deprotection to afford a yellow solid (51 mg, 0.046 mmol, 81%). ^{1}H NMR (400 MHz, CD$_3$CN) δ 8.52 (s, 2H), 8.03 (dd, 2H), 7.97 – 7.77 (m, 6H), 7.62 (d, 2H), 7.48 (d, 2H), 7.04 (t, 4H), 6.91 (t, 2H), 6.28 (d, 2H), 4.76 (s, 4H), 3.76 – 3.38 (m, 32H). ^{13}C {^{1}H} NMR (126 MHz, CD$_3$CN)   168.53, 156.59, 153.44, 151.29, 150.18, 145.29, 139.47, 132.53, 131.13, 126.99, 125.84, 124.46, 123.36, 120.81, 73.28, 70.85, 61.86.

[Ir(bt)₂(TEG-bpy-TEG)]Cl
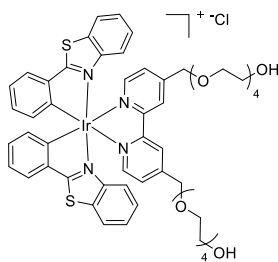
The complex [Ir(bt)2(bpy-(TEG-Trt)₂)]Cl (101 mg, 0.059 mmol) was reacted according to the general procedure for trityl deprotection to afford an orange solid (53 mg, .043 mmol, 73%). ^{1}H NMR (400 MHz, CD₃CN) δ 8.47 (s, 2H), 8.16 – 8.00 (m, 4H), 7.92 (d, 2H), 7.56 (t, 2H), 7.39 (t, 1H), 7.12 (dd, 4H), 6.88 (t, 2H), 6.40 (d, 2H), 6.24 (d, 2H), 4.76 (d, 4H), 3.65 (dd, 9H), 3.59 – 3.30 (m, 25H). ^{13}C{^{1}H} NMR (126 MHz, CD₃CN)   182.04, 156.81, 153.84, 151.16, 149.68, 141.01, 133.74, 132.33, 128.62, 127.34, 126.74, 124.50, 123.74, 122.64, 72.81, 70.87, 61.41.

3.5.3 Absorbance and emission spectra

Absorbance spectra were obtained using a Cary 300 Bio UV/Vis spectrophotometer (Agilent, USA). Quartz cuvettes with a path length of 1 cm were used for all measurements. All room temperature photoluminescence spectra were collected using a Cary Eclipse spectrofluorometer (5 nm band pass, 1 nm data interval, PMT: 600 V). Quartz cuvettes with a path length of 1 cm were used for all measurements. Low temperature spectra were obtained using an OptistatDN Variable Temperature Liquid Nitrogen Cryostat (Oxford Instruments) with custom-made quartz sample holder, placed within the Eclipse sample chamber. Low temperature spectra were collected at 85 K to avoid damage to the spectroscopic cuvettes near 77 K.[35] No difference was observed in the λ_{max} at 77 K and 85 K for complexes such as [Ru(bpy)₃]$^{2+}$ under these conditions.[35]

In both the low temperature and room temperature data, there is a wavelength dependence of the detector response. To account for this, a correction factor (established using a quartz-

halogen tungsten lamp of standard spectral irradiance) was applied to both room temperature and low temperature emission spectra. All room temperature experiments were performed with deionised water or acetonitrile, and all low temperature experiments performed in an ethanol:methanol (4:1) glass.

3.5.4 Electrochemistry and ECL

An Autolab PGSTAT204 or PGSTAT128N potentiostat (Metrohm Autolab B.V., Netherlands) was used to perform cyclic voltammetry, squarewave voltammetry (0.005 V step, 0.02 V amplitude, 25 Hz), and chronoamperometry (CA). The system comprised of a flat-bottomed glass electrochemical cell with a Teflon custom-built lid designed for a three-electrode system. The electrodes were a glassy carbon working (CH instruments), Pt wire counter, and either a 'leakless' Ag/AgCl reference or Ag wire pseudo-reference. This configuration positioned the working electrode 2 mm from the bottom of the cell. Experiments were conducted with the electrochemical cell housed in a Faraday cage. All experiments were referenced to $Fc^{+/0}$ *in situ* (at equimolar concentration to the analyte). The working electrode was polished on a felt pad with 0.05 μm alumina powder prior to use. A small blowtorch was used to polish the platinum and silver electrodes prior to use. All solutions were prepared in either deionised water with a 0.1 M phosphate buffer adjusted to pH 7.5, or dry acetonitrile with 0.1 M $TBAPF_6$ electrolyte, and were degassed with nitrogen for 5 min. ECL spectra were collected using a QE65pro Ocean Optics CCD *via* optical fibre and collimating lens positioned below the base of the electrochemical cell. Each acquisition was triggered by the potentiostat in conjunction with a HR4000 Break-Out box. Relative ECL intensities were averages of two replicates using the integrated areas under the spectra.

3.6 Acknowledgements

3.7 References

(1)   Bard, A. J. *Electrogenerated chemiluminescence*; CRC Press, 2004.

(2)   Miao, W. *Chemical Reviews* **2008**, *108*, 2506-2553.

(3)   Zhan, Y.; Luo, F.; Guo, L.; Qiu, B.; Lin, Y.; Li, J.; Chen, G.; Lin, Z. *ACS Sensors* **2017**, *2*, 1684-1691.

(4)   Zhang, J.-D.; Lu, L.; Zhu, X.-F.; Zhang, L.-J.; Yun, S.; Duanmu, C.-S.; He, L. *ACS Sensors* **2018**, *3*, 2351-2358.

(5)   Della Ciana, L.; Zanarini, S.; Perciaccante, R.; Marzocchi, E.; Valenti, G. *The Journal of Physical Chemistry C* **2010**, *114*, 3653-3658.

(6)   Hai-Juan, L.; Shuang, H.; Lian-Zhe, H.; Guo-Bao, X. *Chinese Journal of Analytical Chemistry* **2009**, *37*, 1557-1565.

(7)   Fiorani, A.; Valenti, G.; Iurlo, M.; Marcaccio, M.; Paolucci, F. *Current Opinion in Electrochemistry* **2018**, *8*, 31-38.

(8)   Kapturkiewicz, A. *Analytical and Bioanalytical Chemistry* **2016**, *408*, 7013-7033.

(9)   Kim, J. I.; Shin, I.-S.; Kim, H.; Lee, J.-K. *Journal of the American Chemical Society* **2005**, *127*, 1614-1615.

(10) Muegge, B. D.; Richter, M. M. *Analytical Chemistry* **2004**, *76*, 73-77.

(11) Bruce, D.; Richter, M. M. *Analytical Chemistry* **2002**, *74*, 1340-1342.

(12) Kapturkiewicz, A.; Angulo, G. *Dalton Transactions* **2003**, 3907-3913.

(13) Chen, L.; Doeven, E. H.; Wilson, D. J.; Kerr, E.; Hayne, D. J.; Hogan, C. F.; Yang, W.; Pham, T. T.; Francis, P. S. *ChemElectroChem* **2017**, *4*, 1797-1808.

(14) Li, C.; Lin, J.; Guo, Y.; Zhang, S. *Chemical Communications* **2011**, *47*, 4442-4444.

(15) Fernandez-Hernandez, J. M.; Longhi, E.; Cysewski, R.; Polo, F.; Josel, H.-P.; De Cola, L. *Analytical Chemistry* **2016**, *88*, 4174-4178.

(16) Zhou, Y.; Xie, K.; Leng, R.; Kong, L.; Liu, C.; Zhang, Q.; Wang, X. *Dalton Transactions* **2017**, *46*, 355-363.

(17) Kim, H. J.; Lee, K.-S.; Jeon, Y.-J.; Shin, I.-S.; Hong, J.-I. *Biosensors & Bioelectronics* **2017**, *91*, 497-503.

(18) Li, M.-J.; Jiao, P.; Lin, M.; He, W.; Chen, G.-N.; Chen, X. *Analyst* **2011**, *136*, 205-210.

(19) Shin, I.-S.; Kang, Y.-T.; Lee, J.-K.; Kim, H.; Kim, T. H.; Kim, J. S. *Analyst* **2011**, *136*, 2151-2155.

(20) Kiran, R. V.; Hogan, C. F.; James, B. D.; Wilson, D. J. *European Journal of Inorganic Chemistry* **2011**, *2011*, 4816-4825.

(21) Jia, J.; Fei, H.; Zhou, M. *Electrophoresis* **2012**, *33*, 1397-1401.

(22) Li, M. J.; Jiao, P.; He, W.; Yi, C.; Li, C. W.; Chen, X.; Chen, G. N.; Yang, M. *European Journal of Inorganic Chemistry* **2011**, *2011*, 197-200.

(23) Barbante, G. J.; Doeven, E. H.; Kerr, E.; Connell, T. U.; Donnelly, P. S.; White, J. M.; Lopes, T.; Laird, S.; Wilson, D. J.; Barnard, P. J. *Chemistry–A European Journal* **2014**, *20*, 3322-3332.

(24) Kiran, R. V.; Zammit, E. M.; Hogan, C. F.; James, B. D.; Barnett, N. W.; Francis, P. S. *Analyst* **2009**, *134*, 1297-1298.

(25) Kerr, E.; Doeven, E. H.; Barbante, G. J.; Connell, T. U.; Donnelly, P. S.; Wilson, D. J.; Ashton, T. D.; Pfeffer, F. M.; Francis, P. S. *Chemistry–A European Journal* **2015**, *21*, 14987-14995.

(26) Connell, T. U.; James, J. L.; White, A. R.; Donnelly, P. S. *Chemistry–A European Journal* **2015**, *21*, 14146-14155.

(27) Tamayo, A. B.; Garon, S.; Sajoto, T.; Djurovich, P. I.; Tsyba, I. M.; Bau, R.; Thompson, M. E. *Inorganic Chemistry* **2005**, *44*, 8723-8732.

(28) Lepeltier, M.; Kwok-Ming Lee, T.; Kam-Wing Lo, K.; Toupet, L.; Le Bozec, H.; Guerchais, V. *European Journal of Inorganic Chemistry* **2005**, *2005*, 110-117.

(29) Zanoni, K. P.; Kariyazaki, B. K.; Ito, A.; Brennaman, M. K.; Meyer, T. J.; Murakami Iha, N. Y. *Inorganic Chemistry* **2014**, *53*, 4089-4099.

(30) Kang, T.-S.; Mao, Z.; Ng, C.-T.; Wang, M.; Wang, W.; Wang, C.; Lee, S. M.-Y.; Wang, Y.; Leung, C.-H.; Ma, D.-L. *Journal of Medicinal Chemistry* **2016**, *59*, 4026-4031.

(31) Brooks, J.; Babayan, Y.; Lamansky, S.; Djurovich, P. I.; Tsyba, I.; Bau, R.; Thompson, M. E. *Inorganic Chemistry* **2002**, *41*, 3055-3066.

(32) King, K.; Spellane, P.; Watts, R. J. *Journal of the American Chemical Society* **1985**, *107*, 1431-1432.

(33) Wu, S.-H.; Ling, J.-W.; Lai, S.-H.; Huang, M.-J.; Cheng, C. H.; Chen, I.-C. *The Journal of Physical Chemistry A* **2010**, *114*, 10339-10344.

(34) Alrawashdeh, L. R.; Cronin, M. P.; Woodward, C. E.; Day, A. I.; Wallace, L. *Inorganic Chemistry* **2016**, *55*, 6759-6769.

(35) Soulsby, L. C.; Hayne, D. J.; Doeven, E. H.; Chen, L.; Hogan, C. F.; Kerr, E.; Adcock, J. L.; Francis, P. S. *ChemElectroChem* **2018**, *5*, 1543-1547.

Chapter 4: A conceptual framework for the development of iridium(III) complex based electrogenerated chemiluminescence labels

Lifen Chen,[a,†] David J. Hayne,*[a,†] Egan H. Doeven,[b] Johnny Agugiaro,[c] David J.D. Wilson,[c] Luke C. Henderson,[d] Timothy U. Connell,[e,‡] Ryan Nai,[b] Richard Alexander,[b] Serena Carrara,[c] Conor F. Hogan,[c] Paul S. Donnelly,[f] Paul S. Francis*[a,c]

[a]School of Life and Environmental Sciences, Faculty of Science, Engineering and Built Environment, Deakin University, Geelong, Victoria 3220, Australia.

[b]Centre for Regional and Rural Futures, Faculty of Science, Engineering and Built Environment, Deakin University, Geelong, Victoria 3220, Australia.

[c]Department of Chemistry and Physics, La Trobe Institute for Molecular Science, La Trobe University, Melbourne, Victoria 3086, Australia.

[d]Institute for Frontier Materials, Deakin University, Geelong, Victoria 3220, Australia.

[e]Manufacturing Business Unit, Commonwealth Scientific and Industrial Research Organisation (CSIRO), Clayton, Victoria 3168, Australia.

[f]School of Chemistry and Bio21 Molecular Science and Biotechnology Institute, The University of Melbourne, Melbourne 3010, Australia.

[†]These authors contributed equally.

[‡]Current affiliation: RMIT University, Melbourne, Victoria 3001 Australia.

AUTHORSHIP STATEMENT

1. Details of publication and executive author

Title of Publication		Publication details
A Conceptual Framework for the Development of Iridium(III) Complex-based Electrogenerated Chemiluminescence Labels		Submitted for publication
Name of executive author	School/Institute/Division if based at Deakin; Organisation and address if non-Deakin	Email or phone
Professor Paul S. Francis	School of Life and Environmental Sciences	psf@deakin.edu.au

2. Inclusion of publication in a thesis

Is it intended to include this publication in a higher degree by research (HDR) thesis?	Yes	If Yes, please complete Section 3 If No, go straight to Section 4.

3. HDR thesis author's declaration

Name of HDR thesis author if different from above. (If the same, write "as above")	School/Institute/Division if based at Deakin	Thesis title
Lifen Chen	School of Life and Environmental Sciences	Novel iridium(III) complexes for electrogenerated chemiluminescence labeling and detection
If there are multiple authors, give a full description of HDR thesis author's contribution to the publication (for example, how much did you contribute to the conception of the project, the design of methodology or experimental protocol, data collection, analysis, drafting the manuscript, revising it critically for important intellectual content, etc.)		
Major contributions to conception of project and experimental design, primary responsibility for the analytical, electrochemical, and electrochemiluminescence laboratory experimentation (including the ECL-based RNA hybridisation assay), data analysis and interpretation, and preparation of manuscript under the guidance of PhD supervisors, acknowledged by my position as the first author of the manuscript.		
I declare that the above is an accurate description of my contribution to this paper, and the contributions of other authors are as described below.	Signature and date	Signature Redacted by Library 14th March 2019

4. Description of all author contributions

Name and affiliation of author	Contribution(s) (for example, conception of the project, design of methodology or experimental protocol, data collection, analysis, drafting the manuscript, revising it critically for important intellectual content, etc.)
David J. Hayne; School of Life and Environmental Sciences and Institute for Frontier Materials, Deakin University	In conjunction with Tim Connell, Paul Donnelly and Luke Henderson, led the design and synthesis of ligands, complexes and ECL labels. Contributed to the preparation of synthetic experimental sections of the manuscript. Assisted in editing the manuscript.
Egan H. Doeven; Centre for Regional and Rural Futures, Deakin University	Co-supervision of PhD student Lifen Chen. Contributed to the design of experiments (through discussion with Lifen Chen, Paul Francis, and David Hayne) and provided training in instrumental techniques. Assisted in editing the manuscript.
Johnny Agugiaro; La Trobe Institute for Molecular Science, La Trobe University	Implementation of computational methods and interpretation of computational data under the supervision of David J. D. Wilson.

David J. D. Wilson; La Trobe Institute for Molecular Science, La Trobe University	Supervision of computational methods and contributions to interpretation of computational data.
Luke C. Henderson; Institute for Frontier Materials, Deakin University	Supervision and advice in the design and completion of synthetic chemistry aspects of the project.
Timothy U. Connell; Commonwealth Scientific and Industrial Research Organisation (CSIRO), Australia.	Contributed to the synthesis of iridium complexes and the preparation of synthetic experimental sections of the manuscript. Assisted in editing the manuscript.
Yi Heng Nai; Centre for Regional and Rural Futures, Deakin University	Preparation of the RNA probes and contribution to the design of the RNA hybridisation assay. Contributions to the preparation of relevant aspects of the manuscript.
Richard Alexander; Centre for Regional and Rural Futures, Deakin University	Design and fabrication of analytical components for ECL detection in the RNA hybridisation assay.
Serena Carrara; La Trobe Institute for Molecular Science, La Trobe University	Experiments required for the ECL-based sandwich immunoassay for C-reactive protein (CRP) and contributed to the photophysical characterization of iridium complexes. Assisted in editing the manuscript.
Conor F. Hogan; La Trobe Institute for Molecular Science, La Trobe University	Provided expertise in interpretation of electrochemical data and the design of certain ECL experiments within the project, and advice on specific technical aspects of the manuscript.
Paul S. Donnelly; Bio21, University of Melbourne.	Guidance in the synthesis and characterisation of iridium complexes. Assisted in editing the manuscript.
Paul S. Francis; School of Life and Environmental Sciences, Deakin University	Principal supervision of PhD student Lifen Chen. Contribution to conception of project and experimental design (through discussion with Lifen Chen, David Hayne and Egan Doeven). Manuscript editing.

5. Author Declarations

I agree to be named as one of the authors of this work, and confirm:

xi. that I have met the authorship criteria set out in the Deakin University Research Conduct Policy,

xii. that there are no other authors according to these criteria,

xiii. that the description in Section 4 of my contribution(s) to this publication is accurate,

xiv. that the data on which these findings are based are stored as set out in Section 7 below.

If this work is to form part of an HDR thesis as described in Sections 2 and 3, I further

xv. consent to the incorporation of the publication into the candidate's HDR thesis submitted to Deakin University and, if the higher degree is awarded, the subsequent publication of the thesis by the university (subject to relevant Copyright provisions).

Name of author	Signature*	Date
David J. Hayne		15/03/2019
Egan H. Doeven		15/03/2019
Johnny Agugiaro		17/03/2019

David J. D. Wilson		14/03/2019
Luke C. Henderson		14/03/2019
Timothy U. Connell		15/03/2019
Yi Heng Nai		18/03/2019
Richard Alexander		18/03/2019
Serena Carrara		14/03/2019
Conor F. Hogan		15/03/2019
Paul S. Donnelly		15/03/2019
Paul S. Francis		14/03/2019

6. Other contributor declarations

I agree to be named as a non-author contributor to this work.

Name and affiliation of contributor	Contribution	Signature* and date

* If an author or contributor is unavailable or otherwise unable to sign the statement of authorship, the Head of Academic Unit may sign on their behalf, noting the reason for their unavailability, provided there is no evidence to suggest that the person would object to being named as author

7. Data storage

The original data for this project are stored in the following locations. (The locations must be within an appropriate institutional setting. If the executive author is a Deakin staff member and data are stored outside

Deakin University, permission for this must be given by the Head of Academic Unit within which the executive author is based.)

Data format	Storage Location	Date lodged	Name of custodian if other than the executive author
Electronic data	Ka5.127 and backed up using Dropbox software	Throughout PhD	

This form must be retained by the executive author, within the school or institute in which they are based.

If the publication is to be included as part of an HDR thesis, a copy of this form must be included in the thesis with the publication.

4.1 Abstract

Translation of the highly promising electrogenerated chemiluminescence (ECL) properties of Ir(III) complexes (with tri-*n*-propylamine (TPrA) as a co-reactant) into a new generation of ECL labels for ligand binding assays necessitates the introduction of functionality suitable for bioconjugation. Modification of the ligands, however, can affect not only the photophysical and electrochemical properties of the complex, but also the reaction pathways available to generate light. Through a combined theoretical and experimental study, we reveal the limitations of conventional approaches to the design of electrochemiluminophores and introduce a new class of ECL label, $[Ir(C\char`^N)_2(pt\text{-}TOxT\text{-}Sq)]^+$ (where $C\char`^N$ is a range of possible cyclometalating ligands, and pt-TOxT-Sq is a pyridyltriazole ligand with trioxatridecane chain and squarate amide ethyl ester), which outperformed commercial Ir(III) complex labels in two commonly used assay formats. Predicted limits on the redox potentials and emission wavelengths of Ir(III) complexes capable of generating ECL *via* the dominant pathway applicable in microbead supported ECL assays were experimentally verified by measuring the ECL intensities of the parent luminophores at different applied potentials, and comparing the ECL responses for the corresponding labels under assay conditions. This study provides a framework to tailor ECL labels for specific assay conditions and a fundamental understanding of the ECL pathways that will underpin exploration of new luminophores and co-reactants.

4.2 Introduction

Electrogenerated chemiluminescence (ECL) has been widely adopted over the past few decades for affinity/ligand binding assays,[1] with ~2 billion tests now performed each year on commercial ECL instrumentation for clinical diagnostics, life science research, food testing and biodefense applications.[2] Remarkably, despite the extensive on-going research into new approaches and applications, the vast majority of ECL-based assays published in

the open literature and all commercial systems still rely on a single orange luminophore: tris(2,2′-bipyridine)ruthenium(II) ($[Ru(bpy)_3]^{2+}$; Fig. 4.1).[1]

The underlying principles of this detection chemistry were established through an extensive series of investigations that included the inception of 'co-reactant' ECL,[3] in which the oxidation of a sacrificial species such as tri-*n*-propylamine (TPrA) forms the chemi-excitation source (Scheme 4.1a), and the elucidation of an alternative pathway to the excited luminophore (Scheme 4.1b)[4] that has been shown to be the dominant light-producing mechanism within typical ECL-based assays immobilized on microbeads.[5] ECL labels for bioconjugation were created by adding suitable functional groups to both or one pyridine rings of a single ligand (see Fig. 4.1), which exert only minor influence on the electrochemical and photophysical properties of the luminophore.[6]
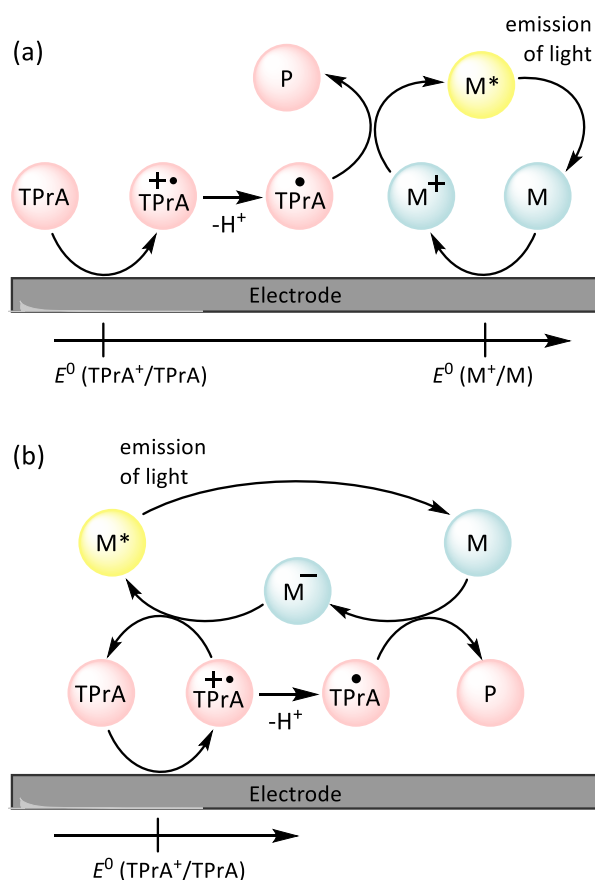
Scheme 4.1. Co-reactant ECL mechanisms involving (a) electrochemical oxidation the tri-*n*-propylamine co-reactant (TPrA) and metal complex (M; $[Ru(bpy)_3]^{2+}$), or (b) oxidation of the co-reactant only,[4, 7] where

TPrA$^{+\bullet}$ is an aminium radical cation, TPrA$^{\bullet}$ is a neural α-amino alkyl radical, and P is its oxidation products. The additional 'catalytic route' involving oxidation of TPrA by M$^+$, and an 'annihilation' pathway, in which the excited state is generated from the reaction of M$^+$ (from Scheme 1a) with M$^-$ (from Scheme 1b), are shown in Scheme 4.S1 in the Supporting Information.
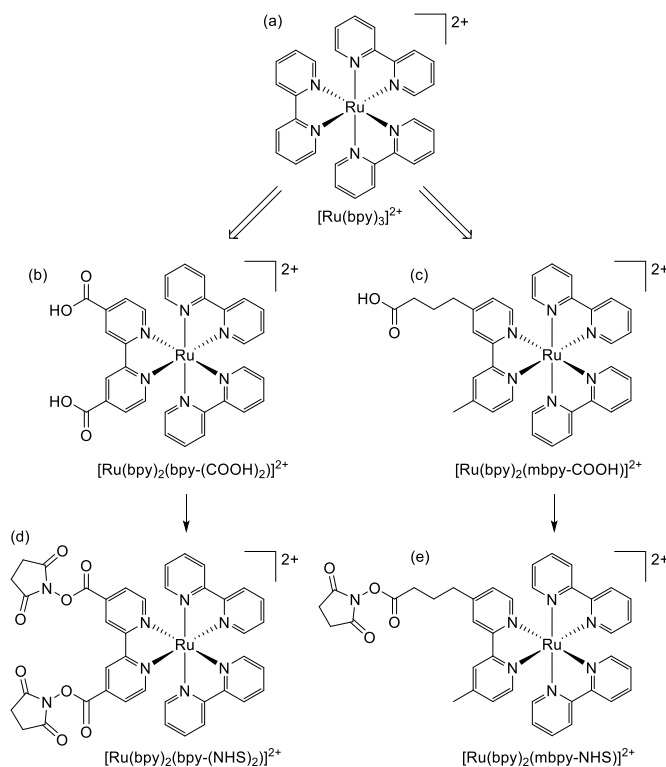
Fig. 4.1. (a) The parent luminophore, tris(2,2′-bipyridine)ruthenium(II); (b,c) Examples of derivatives containing (b) two[8] or (c) one[5a, 6, 9] functional group for bioconjugation. The single binding group separated from the luminophore by an alkyl chain is the approach that has been adopted in commercial ECL systems. Carboxylic acid functionality is common, but other groups, such as amines, maleimides, hydrazides, and phosphoramidites have also been used.[10] (d,e) The carboxylic acids are converted to more reactive *N*-hydroxysuccinimide (NHS) esters for binding to amines (such as lysine units of proteins).[9a]

Cyclometalated iridium(III) complexes (e.g., Fig. 4.2a,b,c) have emerged as promising candidates for a new generation of ECL labels.[1c, 11] Compared to the traditional Ru(II) polypyridine chelates, the Ir(III) complexes exhibit much greater quantum yields (offering enhanced analytical performance) and their emission wavelengths and electrochemical potentials can be readily manipulated through changes in ligand structure,[12] creating

exciting opportunities for multi-color and/or potential-resolved multiplexed ECL systems.[13] However, despite over a decade of exploration of the co-reactant ECL of Ir(III) complexes with these goals in mind, the properties of the most promising luminophores have not been effectively translated into ECL labels for the extensive range of possible bioassays, which we attribute to several major limitations:

(1) The available Ir(III) complexes are generally far less soluble in water than $[Ru(bpy)_3]^{2+}$, and so their ECL properties have almost exclusively been evaluated under conditions that are not compatible with those of the bioassays.[11a, 14]

(2) Most ligands utilized in Ir(III) complexes do not have readily available derivatives with functional groups suitable for bioconjugation and consequently, very few of the promising Ir(III) complexes have been adapted into labels. Of the few that have been created, the predominant approach has been to replace one ligand with the same bipyridine derivatives that have been used in the $[Ru(bpy)_3]^{2+}$-based labels (e.g., Fig. 4.2d).[13i, 15] However, this appears to limit the range of electrochemical potentials, emission wavelengths and ECL intensities of the complexes.

(3) The two dominant ECL reaction pathways (Schemes 4. 1a and 1b) elucidated for $[Ru(bpy)_3]^{2+}$ (with TPrA as co-reactant)[4] are not necessarily both feasible for all Ir(III) complexes,[16] which has implications for their effectiveness under assay conditions. This has not been considered in the previous development of Ir(III)-based ECL labels.

We sought to devise a framework for the development of ECL labels from Ir(III) complex luminophores in which each of the above challenges are addressed. With this in mind, we selected a pyridyltriazole ancillary ligand (Fig. 4.2c) as the scaffold for the novel ECL labeling complexes. This ligand class exhibits several favorable properties for ECL

detection,[17] including simple 'click chemistry' preparation[18] that provides a versatile point for derivatization or attachment.[19]

De Cola and co-workers explored various $[Ir(C^N)_2(pt-R)]^+$ complexes (Fig. 4.2c; where C^N = ppy or df-ppy, and R = methyl, phenyl, benzyl, adamantyl, β-cyclodextrin and other groups) for photoluminescence,[20] light emitting electrochemical cells[21] and ECL[17a] applications. The $[Ir(df-ppy)_2(pt-R)]^+$ species exhibited a deeper blue emission than most charged Ir(III) complexes, and intense co-reactant ECL under aprotic and aqueous conditions. Similarly, we have shown that $[Ir(df-ppy)_2(ptb)]^+$ (Fig. 4.2c; C^N = df-ppy; R = Bn) exhibits more intense co-reactant ECL than related blue luminophores $Ir(df-ppy)_3$ and $[Ir(df-ppy)_2(ptp)]^+$ (where ptp = 3-phenyl-1,2,4-triazol-5-ylpyridinato) in acetonitrile,[17b] which we exploited in foundational investigations of multicolor annihilation ECL.[22] Using an analogous synthetic strategy, we prepared a highly water-soluble derivative $[Ir(df-ppy)_2(pt-TEG)]^+$ (Fig. 4.2c; C^N = df-ppy; R = tetraethylene glycol (TEG)) that provided more intense co-reactant ECL[17c, 23] and chemiluminescence[24] than related Ir(III) complexes in buffered aqueous solution.
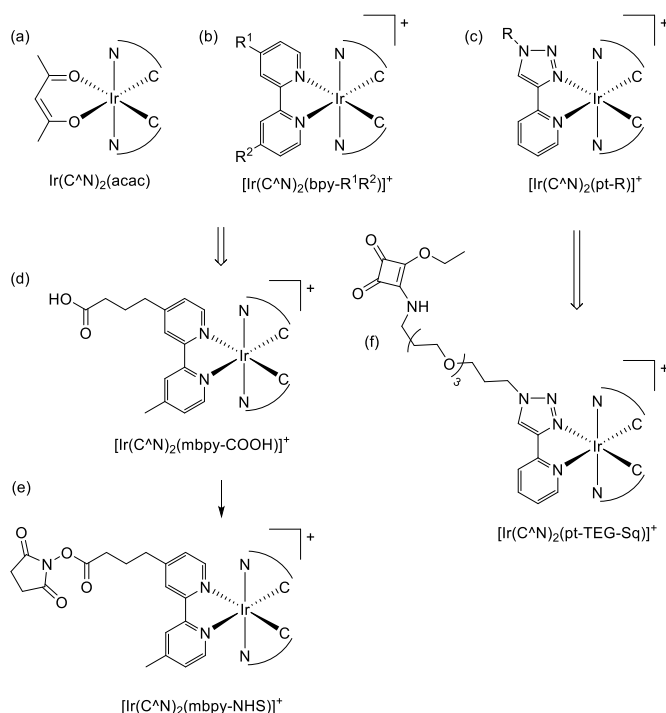
Fig. 4.2. The conceptual development of $[Ir(C{\wedge}N)_2(L)]^+$ complex ECL labels from the early promising examinations of (a) neutral heteroleptic iridium(III) complexes such as $Ir(C{\wedge}N)_2(acac)$, where $C{\wedge}N$ = 2-phenylpyridine (ppy), 2-phenylbenzo[d]thiazole (bt), 2-phenylisoquinoline (piq) or various other ligands.[11a, 14] (b) A representative example of the wider class of cationic $[Ir(C{\wedge}N)_2(N{\wedge}N)]^+$ complexes, the co-reactant ECL of many of which has also been examined.[25] (c) More recently reported analogues incorporating various 1-substituted-4-(2-pyridyl)-1,2,3-triazole ligand, which show promising properties for ECL.[17a, b, 22a] (d) The most common approach to convert neutral and cationic Ir(III) complexes into ECL labels has been to substitute one ligand for the same carboxylic acid bipyridine derivative as that used in Ru(II) labels (see Fig. 4.1).[13i, 15] (e) As with the Ru(II)-based labels shown in Fig. 4.1, the carboxylic acids are converted to the corresponding NHS esters for binding to amines. (f) The alternative design for ECL labels described herein.

Although most prior studies of the ECL of $[Ir(C{\wedge}N)_2(pt\text{-}R)]^+$ complexes have focused on developing efficient blue luminophores (such as $[Ir(df\text{-}ppy)_2(ptb)]^+$; λ_{em} = 453, 481 nm),[17] we have previously observed efficient red photoluminescence (λ_{em} = 592, 632 nm) from $[Ir(piq)_2(ptb)]^+$ (where piq = 1-phenylisoquinoline),[26] indicating that the emission of these complexes can be tuned over a wide range *via* simple modifications to the $C{\wedge}N$ ligands. Moreover, in our previous development of luminescent Ir(III) complexes for live cell imaging,[27] we explored several strategies for their covalent attachment to biomolecules, involving the introduction of maleimide, *N*-hydroxysuccinimide activated ester, or squarate ethyl ester (Fig. 4.2f; $C{\wedge}N$ = ppy or 2-phenylquinoline (pq)) functional groups.

We now draw together these advances to overcome several barriers to the adoption of promising iridium-complex electrochemiluminophores to labeling in bioassay. This includes an in-depth examination of the influence of bioconjugation ligands on Ir(III) complex luminophores, a simple synthetic approach to prepare analogues suitable for organic solvents or aqueous conditions, the creation of novel ECL labels, and the evaluation of the new labels within two common ECL-based bioassay formats.

4.3 Results and Discussion

4.3.1 Comparison of luminophores

The electrochemical properties in acetonitrile solution were investigated by cyclic voltammetry using ferrocene/ferrocenium as an internal standard, as shown in Table 4.1. Peak positions were determined using the peak picking algorithm in the Nova software package, or, under some conditions, by drawing a manual baseline (where automatic picking was difficult or inaccurate). Unless otherwise specified, the potential specified is the formal potential ($E_{1/2}$), calculated from the average of the oxidation and reduction peaks of the specified couple. Electrochemiluminophore efficiency is fundamentally dependent on both its redox potentials and excited state character. In the case of heteroleptic iridium(III) complexes, these parameters can be readily tuned through even subtle modifications of ligand structure, to stabilize or destabilize the frontier molecular orbitals with some degree of selectivity.[11, 28] Early exploration of Ir(C^N)$_2$(acac) complexes showed high ECL efficiencies with a wide range of emission colors, in reactions with radical anions of aromatic nitriles.[29] Efficient co-reactant ECL from Ir(C^N)$_2$(acac) complexes with TPrA as a co-reactant has also been demonstrated,[25a, 30] but little attention has been paid to the influence of their different redox potentials on the competing light-producing reaction pathways (Scheme 4.1). Moreover, the effects of replacing ancillary ligands such as acac with those suitable for bioconjugation (ECL-labeling) must also be considered. To understand these effects, we initially conducted an experimental and theoretical study of the relevant properties of twelve iridium(II) complexes. This included: (i) four commercially available Ir(C^N)$_2$(acac) complexes (Fig. 4.2a), where C^N = piq, bt, ppy and df-ppy, which exhibit red, yellow, green and blue luminescence, respectively; (ii) four [Ir(C^N)$_2$(dm-bpy)]$^+$ complexes (Fig. 4.2b; R and R′ = Me), with the same C^N ligands, as the parent luminophores of complexes with bpy-based ligands for bioconjugation (Fig.4.2e), and (iii) four [Ir(C^N)$_2$(ptb)]$^+$ complexes (Fig. 4.2c; R = Bn) containing the parent luminophore of

the proposed [Ir(C^N)$_2$(pt-TEG-Sq)]$^+$ labeling complexes. The model luminophores were employed because they were commercially available or readily synthesized and they avoided complications from the reactive peripheral functionality of their labelling derivatives[6] when assessing the properties of the luminophore. The [Ir(C^N)$_2$(dm-bpy)]$^+$ and [Ir(C^N)$_2$(ptb)]$^+$ complexes containing piq, ppy and df-ppy ligands have previously been reported,[17b, 21, 26, 31] but the two bt analogues were prepared in this study for the first time.

The properties of the Ir(C^N)$_2$(acac) complexes (Table 4.1 and Fig. 4.3, S4.1-S4.6) were in good agreement with those reported across prior studies.[14b, 32] DFT calculations on Ir(C^N)$_2$(acac) complexes indicate that the HOMO is predominantly localized on the phenyl ring of the C^N ligands and the metal center, the LUMO is on the C^N ligand (Fig. S4.7), and the observed luminescence (Fig. 4.4) originates from mixed metal-to-ligand and intra-ligand charge transfer (^{3}MLCT/^{3}ILCT) excited states.[33] As the acac ligand has minimal direct involvement in the frontier molecular orbitals, trends in spectroscopic and electrochemical properties across the four complexes mirror those of their homoleptic Ir(C^N)$_3$ counterparts.[14b, 17b, 34]

Table 4.1. Selected spectroscopic and electrochemical properties of Ir(C^N)$_2$(acac), [Ir(C^N)$_2$(dm-bpy)]+, and

	Photoluminescence			Electrochemical potentials (*vs* Fc$^{+/0}$)				
	λ_{max}/nm$^{a, b}$	λ_{max} (85 K)/nm^{b,c}	E_{0-0}/eV^d	E_{ox}/V^e	E_{red}/V^e	E_{ox}*/V^f	E_{red}*/V^f	I_{ECL}^{g}
[Ru(bpy)$_3$]$^{2+}$	**620**	**581**, 629, 685(sh)	2.13	0.89	−1.73, −1.92, −2.15	−1.24	0.40	1
Ir(piq)$_2$(acac)	**633**	**604**, 655, 716	2.05	0.43	−2.12, −2.34	−1.62	−0.07	2.05
Ir(bt)$_2$(acac)	**565**, 605	**546**, 592, 645	2.27	0.58	−2.24	−1.69	0.03	0.81
Ir(ppy)$_2$(acac)	**525**	**501**, 537	2.48	0.42	−2.59	−2.06	−0.11	0.015
Ir(df-ppy)$_2$(acac)	**491**	**471**, 504, 542(sh)	2.63	0.73	−2.44, −2.68	−1.90	0.19	0.17
[Ir(piq)$_2$(dm-bpy)]$^+$	595, **631**	**581**, 594(sh), 631, 687, 758(sh)	2.13	0.84	−1.85, −2.14, −2.36	−1.29	0.28	0.76
[Ir(bt)$_2$(dm-bpy)]$^+$	526, **566**	**515**, 529, 557, 573(sh), 605, 626(sh), 661	2.41	0.99	−1.83, −2.26	−1.42	0.58	0.66
[Ir(ppy)$_2$(dm-bpy)]$^+$	**592**	475(sh),^{h} **509**, 531	2.44	0.85	−1.86, −2.46	−1.59	0.58	0.27
[Ir(df-ppy)$_2$(dm-bpy)]$^+$	**524**	**450**, 482, 508, 518, 549(sh), 564(sh)	2.76	1.16	−1.80, −2.48	−1.60	0.96	0.89
[Ir(piq)$_2$(ptb)]$^+$	594, **633**	**581**, 594(sh), 631, 687, 758(sh)	2.13	0.86	−1.98, −2.19, −2.51	−1.27	0.15	0.43
[Ir(bt)$_2$(ptb)]$^+$	526, **565**	**515**, 528(sh), 556, 572(sh), 604, 659	2.41	1.02	−2.06, −2.27	−1.39	0.35	0.34
[Ir(ppy)$_2$(ptb)]$^+$	**477**, 509	**471**, 487, 495(sh), 506, 536, 549(sh), 585(sh)	2.63	0.87	−2.18	−1.74	0.43	0.10
[Ir(df-ppy)$_2$(ptb)]$^+$	454, **482**	**448**, 480, 506, 516	2.77	1.18	−2.12	−1.49	0.55	0.18

[Ir(C^N)$_2$(ptb)]+ complexes in acetonitrile.

^{a}Metal complexes at 10 μM in acetonitrile at ambient temperature. ^{b}Corrected for the change in instrument sensitivity over the wavelength range. ^{c}Metal complexes at 5 μM in ethanol:methanol (4:1) at 85 K (sh = shoulder). ^{d}Energy gap between the zeroth vibrational levels of the ground and excited states, estimated from the highest energy peak of the low-temperature emission spectrum. ^{e}Metal complexes at 0.25 mM in acetonitrile with 0.1 TBAPF$_6$ supporting electrolyte; scan rate: 0.1 V/s. ^{f}Excited state potentials based on the ground state potentials and E_{0-0}.[35] ^{g}ECL intensities relative to [Ru(bpy)$_3$]$^{2+}$ (10 μM metal complex, 10 mM TPrA, 0.1 M TBAPF$_6$ supporting electrolyte; 10 s pulse, 10 Hz). ^{h}Shoulder arising from the characteristic rigidochromic blueshift of [Ir(ppy)$_2$(N^N)]$^+$ complexes (where N^N = bpy or a derivative) involving contribution to the emission from a higher energy excited state.[36]

Ir(ppy)$_2$(acac) exhibits green luminescence (Fig. 4.4a) and the highest LUMO energy of the four complexes, which is seen in its most negative reduction potential (Fig. 4.3). The electron-withdrawing fluoro substituents of Ir(df-ppy)$_2$(acac) strongly stabilize the HOMO

and to a lesser extent the LUMO, with corresponding positive shifts in associated electrochemical potentials and a hypsochromic shift to give its characteristic blue emission. The bt ligand also lowers the energy of the frontier orbitals compared to ppy, but with a slightly lesser effect on the HOMO, resulting in a yellow emission. The structure in this emission can be attributed to the greater proportion of the LUMO on the phenyl ring of the C^N ligands. The extended aromaticity of the piq ligand greatly stabilizes the LUMO through its low lying π^* orbital, but the HOMO energy is relatively unchanged, resulting in a large bathochromic shift into the red region
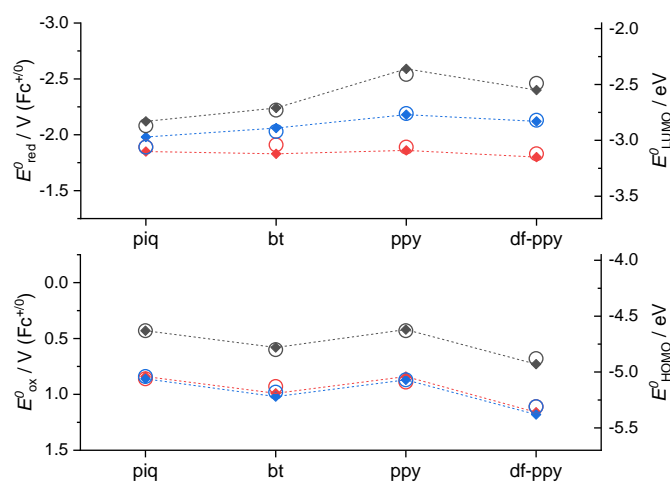
Fig. 4.3. Effects of ligand structure on electrochemical properties (solid diamonds; left axes) and calculated MO energies (open circles; right axes; BP86/def2-TZVP calculations), for Ir(C^N)$_2$(acac) (grey symbols), [Ir(C^N)$_2$(dm-bpy)]$^+$ (red symbols), and [Ir(C^N)$_2$(ptb)]$^+$ (blue symbols) complexes, where C^N = piq, bt, ppy, or df-ppy. The upper graph shows reduction potentials and LUMO energies, and the lower graph shows oxidation potentials and HOMO energies.
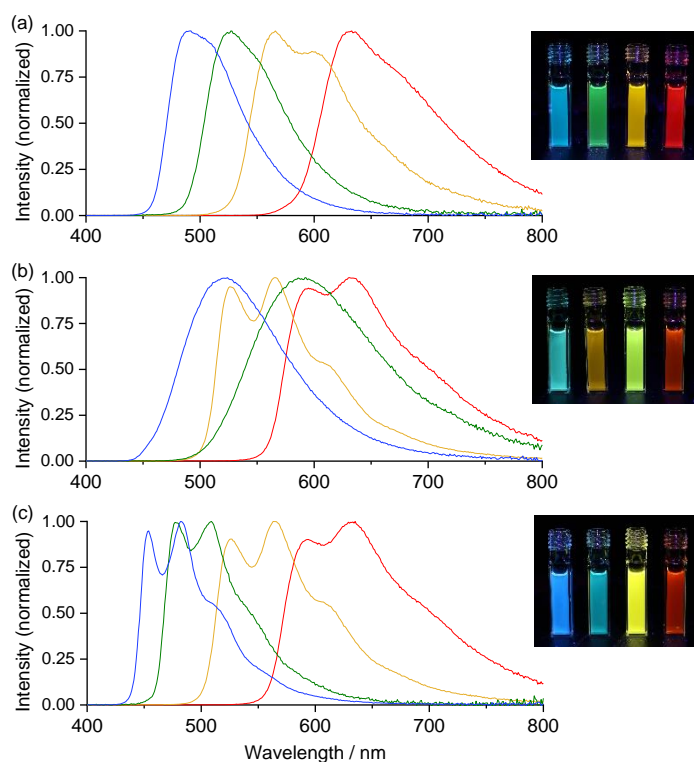
Fig. 4.4. Photoluminescence emission spectra (corrected) of (a) Ir(C^N)$_2$(acac), (b) [Ir(C^N)$_2$(dm-bpy)]$^+$, and (c) [Ir(C^N)$_2$(ptb)]$^+$ complexes, where C^N = df-ppy (blue lines), ppy (green lines), bt (yellow lines), or piq (red lines), at a concentration of 10 μM in acetonitrile. The inset photos show the emissions under UV light, with the complexes (0.1 mM in acetonitrile) containing df-ppy, ppy, bt, and then piq ligands in cuvettes from left to right.

If the ancillary acac ligand is replaced by dm-bpy, the HOMO is stabilized by ~0.4 eV (observed as commensurate increases in the oxidation potentials; Fig. 4.3b) but remains on the metal and C^N ligands (Fig. S4.7 and Table S4.5). The low-lying π* orbital of the dm-bpy ligand, however, is now the dominant contributor to the LUMO level of the df-ppy, ppy, and bt complexes, although both the dm-bpy and two piq ligands contribute to the LUMO of the [Ir(piq)$_2$(dm-bpy)]$^+$ complex. This results in a similar reduction potential for all four [Ir(C^N)$_2$(dm-bpy)]$^+$ complexes at ~1.83 ±0.03 V *vs* Fc$^{+/0}$ (Fig. 4.3a). As Ir(ppy)$_2$(acac) has the highest energy LUMO, the influence of the dm-bpy ligand on the emission spectra is most prominent for [Ir(ppy)$_2$(dm-bpy)]$^+$. This changes the order of emission energy from df-ppy > ppy > bt > piq in Ir(C^N)$_2$(acac) complexes (Fig. 4.4a) to df-ppy > bt > ppy > piq in

[Ir(C^N)$_2$(dm-bpy)]$^+$ complexes (Fig. 4.4b). Moreover, the near identical LUMO energies narrows the difference in emission wavelengths between the four complexes, reducing the possible selectivity of multi-color ECL systems.

The HOMOs calculated for the [Ir(C^N)$_2$(ptb)]$^+$ complexes had similar energies to those of their [Ir(C^N)$_2$(dm-bpy)]$^+$ counterparts (Fig. 4.3b), and were again distributed on the metal center and C^N ligands. The LUMOs, however, were intermediate in energy between those of the Ir(C^N)$_2$(acac) and [Ir(C^N)$_2$(dm-bpy)]$^+$ complexes. The order of emission energies matched that of the Ir(C^N)$_2$(acac) complexes (Fig. 4.4c). The difference in the λ_{max} between the blue and red emitters is 151 nm (or 140 nm if the highest energy peaks are compared), which is much greater than that of the [Ir(C^N)$_2$(ptb)]$^+$ complexes (71 nm), and similar to that of the Ir(C^N)$_2$(acac) complexes (142 nm).

The co-reactant ECL intensities of iridium complexes relative to [Ru(bpy)$_3$]$^{2+}$ are highly dependent on instrumental and chemical conditions, such as co-reactant concentration, the applied potential pulse time, and sensitivity of the photodetector in different regions of the spectrum.[14b] The conditions used to obtain the ECL intensities in Table 4. 1 (shown relative to [Ru(bpy)$_3$]$^{2+}$) were based on those previously employed, which provide a conservative evaluation.[14b] In the case of the Ir(C^N)$_2$(acac) complexes, the red and yellow emitters exhibited greater intensities (2.05 and 0.81) than the green and blue emitters (0.015 and 0.17), but it should be noted that the CCD detector provides a fairly even response across the wavelength range and other commonly used photodetectors (such as photomultiplier tubes) exhibit much greater sensitivity in the blue and green regions. The ECL intensities of the [Ir(C^N)$_2$(dm-bpy)]$^+$ and [Ir(C^N)$_2$(ptb)]$^+$ complexes were distributed over narrower ranges (0.27-0.89 and 0.10-0.43, respectively).

The above characterizations allow us to assess the feasibility of the ECL reaction pathways shown in Schemes 1a and 1b for these Ir(III) complexes. This is critical, because

studies of the ECL of $[Ru(bpy)_3]^{2+}$ with TPrA co-reactant have shown that the conditions of some assays heavily favor one ECL pathway over others.[4-5, 37] The requirements can be visualized using the graphs shown in Fig. 4.5a-d,[16] in which the electrochemical potential for oxidation and reduction of the metal complex is plotted against the excited state energy (shown as the λ_{max} from low temperature emission spectra). Overlaid on these graphs are the redox potential requirements of the two ECL pathways. Line (i) is the oxidation potential of TPrA. For complexes with an oxidation potential above this line, reaction 1 is favorable. This 'catalytic route'[4] provides an efficient means to generate $TPrA^{+\bullet}$,[38] but it is not essential for ECL, because TPrA is also electrochemically oxidized.

Line (ii) represents the oxidation potential that the metal complex requires to attain its electronically excited state *via* reaction 2 (from Scheme 4.1a). As can be seen in the curve of this line, the energy demands become greater as the emission wavelength becomes shorter (*i.e.*, blue-shifted luminophores must possess higher oxidation potentials to generate ECL *via* Scheme 4.1a). This requirement for Scheme 4.1a, which we referred to in our previous work as the 'ECL wall of energy sufficiency',[39] was met by all of the metal complexes under investigation (Fig. 4.5a-c).

$$M^+ + TPrA \rightarrow M + TPrA^{+\bullet} \qquad\qquad (1)$$

$$M^+ + TPrA^{\bullet} \rightarrow M^* + P \qquad\qquad (2)$$

To generate ECL *via* Scheme 1b, the metal complex must first be able to be reduced by $TPrA^{\bullet}$ (reaction 3) and then react with $TPrA^{+\bullet}$ with sufficient excess energy to generate the electronically excited luminophore (reaction 4). These requirements are met in complexes with a reduction potential above line (iii) and below line (iv) in Fig. 4.5a-c. (*i.e.*, the green colored region of the graph).

$$M + TPrA^{\bullet} \rightarrow M^- + P \qquad\qquad (3)$$

$$M^- + TPrA^{+\bullet} \rightarrow M^* + TPrA \qquad (4)$$

Of the Ir(C^N)$_2$(acac) and [Ir(C^N)$_2$(dm-bpy)]$^+$ complexes (Fig 4.5a and 4.5b), only the red emitters with piq ligands clearly satisfy the criteria for generating ECL with TPrA *via* Scheme 4.1b. It should be noted, however, that there are numerous sources of error in these predictions[16] and borderline cases (such [Ir(bt)$_2$(dm-bpy)]$^+$ and [Ir(ppy)$_2$(dm-bpy)]$^+$) as should be treated with caution. Of the [Ir(C^N)$_2$(ptb)]$^+$ complexes, both [Ir(piq)$_2$(ptb)]$^+$ and [Ir(bt)$_2$(ptb)]$^+$ satisfy the criteria for generating ECL *via* Scheme 1b.
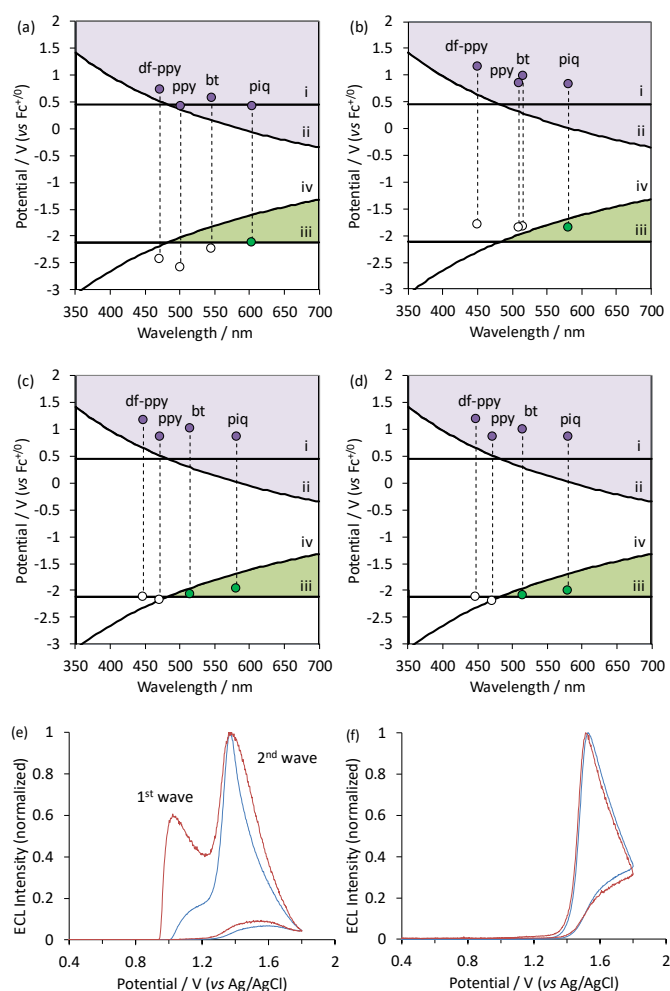
Fig. 4.5. (a-d) Plots of redox potentials versus low-temperature emission wavelengths (E_{0-0}) for (a) Ir(C^N)$_2$(acac), (b) [Ir(C^N)$_2$(dm-bpy)]$^+$, (c) [Ir(C^N)$_2$(ptb)]$^+$, and (d) [Ir(C^N)$_2$(pt-TEG)]$^+$, overlaid on graphs depicting the redox potential requirements of key steps of the ECL mechanisms shown in Schemes 1a and 1b, indicating which ECL pathway(s) are feasible for each complex. Lines i-iv show the redox potential

requirements for reactions 1-4, respectively. (e-f) Normalized ECL intensity during an applied potential sweep from 0 V to 1.8 V and back to 0 V (*vs* Ag|AgCl) for (e) [Ir(bt)$_2$(pt-TEG)]$^+$ and (f) [Ir(df-ppy)$_2$(pt-TEG)]$^+$ at 1 μM (blue lines) and 0.1 μM (red lines) in buffer (ProCell) solution containing TPrA as a co-reactant (plots for [Ir(piq)$_2$(pt-TEG)]$^+$ and [Ir(ppy)$_2$(pt-TEG)]$^+$ are shown in Supporting Information), providing experimental confirmation of the predictions made in Fig. 4.5d under the aqueous conditions commonly used in ECL assays.

4.3.2 Water soluble [Ir(C^N)$_2$(pt-TEG)]$^+$ complexes

The click chemistry synthesis of pyridyltriazole ligands provides an exceedingly simple approach to introduce functional groups that improve the solubility of the Ir(III) complex.[17a, 20, 24, 40] Using this approach, we prepared [Ir(C^N)$_2$(pt-TEG)]$^+$ (Fig. 4.2c, C^N = piq, bt, ppy, df-ppy; R = TEG), with chloride counter ions instead of hexafluorophosphate, for evaluation under conditions akin to those of typical ECL assays. The electrochemical properties of iridium metal complexes Ir(C^N)$_2$(acac), Ir(C^N)$_2$(ptb), Ir(C^N)$_2$(dm-bpy) and [Ir(C^N)$_2$(pt-TEG)]$^+$ in acetonitrile were investigated by cyclic volatmmetrey using ferrocene/ferrocenium as the internal standard. Peak positions were determined using the peak picking algorithm in the Nova software package, or, under some conditions, by drawing a manual baseline (where automatic picking was difficult or inaccurate). Unless otherwise specified, the potential specified is the formal potential (E$_{1/2}$), calculated from the average of the oxidation and reduction peaks of the specified couple. The oxidation potentials of the complexes in phosphate buffer were determined by square-wave volammetry. The datas were summarized in Table 4.2.

The electrochemical potentials of the [Ir(C^N)$_2$(pt-TEG)]$^+$ complexes (*vs* Fc$^{+/0}$) matched those of [Ir(C^N)$_2$(ptb)]$^+$ in acetonitrile (Fig. S4.6) and the oxidation potentials of the [Ir(C^N)$_2$(pt-TEG)]$^+$ complexes in buffered aqueous solution (*vs* Ag|AgCl) exhibited a similar trend (Table 4.2). The luminescence λ_{max} of [Ir(C^N)$_2$(pt-TEG)]$^+$ in water and [Ir(C^N)$_2$(ptb)]$^+$ in acetonitrile at ambient temperature were near identical, as was their λ_{max}

at low temperature in 4:1 ethanol:methanol (Fig. S4.4 and S4.5, Tables 4.1 and 4.2). The ECL intensities of the $[Ir(C{\wedge}N)_2(pt\text{-}TEG)]^+$ complexes in buffered aqueous solution, however, were greater than those of $[Ir(C{\wedge}N)_2(ptb)]^+$ in acetonitrile, relative to that of $[Ru(bpy)_3]^{2+}$ under each set of conditions.

Due to the similar properties of the $[Ir(C{\wedge}N)_2(ptb)]^+$ and $[Ir(C{\wedge}N)_2(pt\text{-}TEG)]^+$ complexes, the same predictions (Fig. 4.5d) were made for the feasibility of the two ECL reaction mechanisms (Schemes 4.1a and 4.1b), where $[Ir(piq)_2(pt\text{-}TEG)]^+$ and $[Ir(bt)_2(pt\text{-}TEG)]^+$ are anticipated to generate ECL (with TPrA co-reactant) *via* both pathways, whereas $[Ir(ppy)_2(pt\text{-}TEG)]^+$ and $[Ir(df\text{-}ppy)_2(pt\text{-}TEG)]^+$ are limited to Scheme 4.1a. We sought validation for these predictions using the 'two-wave' ECL experiment that was utilized by Bard and co-workers[4] in their elucidation of Scheme 4.1b for $[Ru(bpy)_3]^{2+}$, in which the ECL intensity is monitored during a voltammetric sweep from low to high anodic potentials. Scheme 1b is initiated at the oxidation potential for TPrA, whereas Scheme 4.1a also requires electrochemical oxidation of the metal complex, which in the case of the $[Ir(C{\wedge}N)_2(pt\text{-}TEG)]^+$ complexes, occurs at considerably higher potentials (Fig. 4.5d). The two 'waves' of ECL intensity corresponding to the oxidation of TPrA and the metal complex (Table 4.2) for $[Ir(bt)_2(pt\text{-}TEG)]^+$ (Fig. 4.5e) and $[Ir(piq)_2(pt\text{-}TEG)]^+$ (Fig. S4.8b), and the single wave of ECL associated with the oxidation of $[Ir(df\text{-}ppy)_2(pt\text{-}TEG)]^+$ (Fig. 4.5f) and $[Ir(ppy)_2(pt\text{-}TEG)]^+$ (Fig. S4.8a) in aqueous buffered solution support the prediction made for each complex based on electrochemical potentials and emission energies. Bard and co-workers observed that a lower concentration of $[Ru(bpy)_3]^{2+}$ favored the first wave of ECL (*via* Scheme 4.1b), which we also observed for $[Ir(bt)_2(pt\text{-}TEG)]^+$ (Fig. 4.5e) adding further evidence of the competing ECL pathways of this complex. We note here that interpretation of ECL intensity profiles during voltammetric experiments without considering the energy requirements of the competing ECL pathways (as depicted in Fig.

4.5a-d) can be misleading, as other factors can contribute. The ECL of Ir(ppy)$_3$ with TPrA, for example, is strongly inhibited at high over-potentials,[13d, e] which has been attributed to oxidative quenching of the excited state Ir(ppy)$_3$* by TPrA$^{\bullet+}$. Moreover, De Cola and co-workers[14a] observed more than two maxima in the ECL of Ir(pph)$_2$(pic) (where pph = phenylphenanthridine; pic = picolinate) and TPrA, which is yet to be understood.

Table 4.2. Selected spectroscopic and electrochemical properties of [Ir(C^N)$_2$(pt-TEG)]$^+$ complexes.

	Photoluminescence				Electrochemical potentials			
	λ_{max}/nm[a,b]	λ_{max} (85 K)/nm[b,c]	E_{0-0}/eV[d]	ϕ_{PL} (%)[e]	E_{ox}/V (vs Ag|AgCl)[f]	E_{ox}/V (vs Fc$^{+/0}$)[g]	E_{red}/V (vs Fc$^{+/0}$)[g]	I_{ECL}[h]
[Ru(bpy)$_3$]$^{2+}$	**625**	**581**, 629	2.13	3	1.09	0.89	−1.73, −1.92, −2.15	1
[Ir(piq)$_2$(pt-TEG)]$^+$	596, **628**	**580**, 629, 684	2.14	9	1.15	0.86	−2.01, −2.23	0.86
[Ir(bt)$_2$(pt-TEG)]$^+$	526, **562**	**515**, 557, 604, 659	2.41	23	1.28	1.01	−2.08	2.76
[Ir(ppy)$_2$(pt-TEG)]$^+$	475, **505**	**471**, 506, 536	2.63	14	1.08	0.86	−2.20	1.57
[Ir(df-ppy)$_2$(pt-TEG)]$^+$	452, **481**	**448**, 480, 507	2.77	19	1.44	1.20	−2.13	0.26

[a]Metal complexes at 10 μM in water at ambient temperature. [b]Corrected for the change in instrument sensitivity over the wavelength range. [c]Metal complexes at 5 μM in ethanol:methanol (4:1) at 85 K. [d]Energy gap between the zeroth vibrational levels of the ground and excited states, estimated from the highest energy peak of the low-temperature emission spectrum. [e]Photoluminescence quantum yield in 'ProCell' phosphate buffer used in commercial ECL instruments. [f]Metal complexes at 0.5 mM in 0.1 M phosphate buffer solution (pH 7.5); squarewave voltammetry; 5 mV step, 0.02 amplitude, 25 Hz. [g]Metal complexes at 0.25 mM in acetonitrile with 0.1 TBAPF$_6$; cyclic voltammetry; scan rate: 0.1 V/s. [h]ECL intensities relative to [Ru(bpy)$_3$]$^{2+}$ (10 μM metal complex in acetonitrile, 10 mM TPrA phosphate buffer (pH 7.5); 10 s pulse, 10 Hz).

4.3.3 New ECL labels

Using the synthetic strategies outlined in our preparation of [Ir(ppy)$_2$(pt-TEG-Sq)]$^+$ for live cell photoluminescence imaging[27] (details in Supporting Information), we adapted the promising [Ir(C^N)$_2$(pt-TEG)]$^+$ electrochemiluminophores (Fig 4.2c, R = TEG) for ECL labelling. Conventional ECL labels with carboxylic acid functionality (*e.g.*, Fig. 4.1b,c and

4.2d) for attachment to amine groups require initial conversion to the NHS esters, which can only be stored for short periods of time at low temperature. In contrast, the squarate ethyl ester functionality of the novel $[Ir(C^\wedge N)_2(pt\text{-}TEG\text{-}Sq)]^+$ ECL labels (Fig. 4.2f) does not require further activation, and the labels can be stored at room temperature for extended periods of time. The emission spectra and electrochemical properties of the $[Ir(C^\wedge N)_2(pt\text{-}TEG\text{-}Sq)]^+$ and commercial $[Ir(C^\wedge N)_2(mbpy\text{-}COOH)]^+$ labels (Table 4.3 and Fig. S4.9) were closely aligned to those of their parent luminophores, $[Ir(C^\wedge N)_2(pt\text{-}TEG)]^+$ (Table 4. 2) and $[Ir(C^\wedge N)_2(dm\text{-}bpy)]^+$ (Table 4.1), respectively. Similar to water-soluble complexes $[Ir(C^\wedge N)_2(pt\text{-}TEG)]+$, the electrochemical properties of $[Ir(C^\wedge N)_2(pt\text{-}TEG\text{-}Sq)]^+$ and commercial $[Ir(C^\wedge N)_2(mbpy\text{-}COOH)]^+$ labels in acetonitrile solution were investigated by cyclic volatmmertry using ferrocene/ferrocenium as the internal standard at a scan rate of 0.1 V/s. The values of the formal oxidation potential E_{ox}/V (*vs* $Fc^{+/0}$) and formal reduction potential E_{red}/V (*vs* $Fc^{+/0}$) were summarized in Table 4.3. Peak positions were determined using the peak picking algorithm in the Nova software package, or, under some conditions, by drawing a manual baseline (where automatic picking was difficult or inaccurate). Unless otherwise specified, the potential specified is the formal potential ($E_{1/2}$), calculated from the average of the oxidation and reduction peaks of the specified couple. Potentials that are from one peak only (irreversible redox processes) are highlighted. All the complexes showed one oxidation wave at the potential range between 1.16 V and 0.84 V with reduction wave at the potential range between -2.56 V and -1.78 V. Comparing the potentials of $[Ir(C^\wedge N)_2(pt\text{-}TEG\text{-}Sq)]^+$ and commercial $[Ir(C^\wedge N)_2(mbpy\text{-}COOH)]^+$ labels, we found that the ancillary ligand does not have significant effects on the potentials. For example, $[Ir(piq)_2(bpy\text{-}COOH)]^+$ can be oxidized at the potential of 0.85 V, which was nealy the same as $[Ir(piq)_2(pt\text{-}TEG\text{-}Sq)]^+$, where the oxidation potential was 0.87 V. The photoluminescence quantum yields (ϕ_{PL}) and emission lifetimes (τ) for the $[Ir(C^\wedge N)_2(pt\text{-}TEG\text{-}Sq)]^+$ labels were greater than those of their commercial analogues (Table 4.3).

To complete our examination of the influence of the electrochemical and spectroscopic properties on the ECL of Ir(III) complexes in the context of the reaction pathways available to each luminophore, we compared the relative ECL intensities of the bioconjugated $[Ir(C^{\wedge}N)_2(pt\text{-}TEG\text{-}Sq)]^+$ and $[Ir(C^{\wedge}N)_2(mbpy\text{-}COOH)]^+$ labels in two different of modes of bioassay. The first was a sandwich hybridization RNA assay on magnetic bead support, and the second was a C-reactive protein (CRP) sandwich immunoassay with the capture monoclonal antibody (mAb) immobilized onto a gold electrode.

Table 4.3. Selected spectroscopic and electrochemical properties of ECL labels.

ECL label[a]	Photoluminescence			Electrochemical potentials	
	$\lambda_{max}/nm^{b,c}$	ϕ_{PL} (%)^{b,d}	$\tau/ns^{b,e}$	E_{ox}/V (vs Fc$^{+/0}$)^f	E_{red}/V (vs Fc$^{+/0}$)^f
$[Ru(bpy)_2(mbpy\text{-}COOH)]^{2+}$	**632**	4.9	311	0.84	−1.78, −1.96, −2.24
$[Ir(piq)_2(bpy\text{-}COOH)]^+$	592(sh), **640**	10.4	378	0.85	−1.90, −2.17
$[Ir(bt)_2(mbpy\text{-}COOH)]^+$	530(sh), **572**, 615(sh)	5.9	174	1.04	−1.87, −2.28
$[Ir(ppy)_2(mbpy\text{-}COOH)]^+$	**606**	2.0	398	0.84	−1.87
$[Ir(df\text{-}ppy)_2(mbpy\text{-}COOH)]^+$	**533**	2.7	392	1.16	−1.84, −2.49
$[Ir(piq)_2(pt\text{-}TEG\text{-}Sq)]^+$	590(sh), **632**	11.8	927	0.87	−2.01, −2.22, −2.56
$[Ir(bt)_2(pt\text{-}TEG\text{-}Sq)]^+$	526, **564**	26.7	1051	1.01	−2.11, −2.35, −2.56
$[Ir(ppy)_2(pt\text{-}TEG\text{-}Sq)]^+$	476, **503**	8.8	308	0.86	−2.22
$[Ir(df\text{-}ppy)_2(pt\text{-}TEG\text{-}Sq)]^+$	453, **483**, 515	15.7	559	1.16	−2.14

[a]The chemical structure of $[Ru(bpy)_2(mbpy\text{-}COOH)]^{2+}$ is shown in Fig. 4.1c; the $[Ir(C^{\wedge}N)_2(mbpy\text{-}COOH)]^+$ labels are depicted by Fig. 4.2d, except that the piq complex does not contain the 4-methyl group, and the bt complex contains a 4′-carboxy instead of 4′-carboxypropyl group on the bpy-based ligand (due to the availability of the different commercial labels at the time of the study); and the $[Ir(C^{\wedge}N)_2(pt\text{-}TEG\text{-}Sq)]^+$ labels are depicted by Fig. 4.2f. [b]The ECL labels were dissolved in DMF (1 mM) and diluted to 10 μM in a 0.1 M PBS solution (pH 7.4). [c]Corrected for the change in instrument sensitivity over the wavelength range. [d]Photoluminescence quantum yield. [e]Emission lifetime. [f]ECL labels at 0.25 mM in acetonitrile with 0.1 TBAPF$_6$; cyclic voltammetry; scan rate: 0.1 V/s. Peaks associated with the counter ion or labelling functional group not listed.

In the sandwich RNA hybridization assay, the target was mixed with a capture probe bound to streptavidin coated magnetic beads (2.8 μm diameter), and a detection probe with ECL

label, and heated to 45 ℃ for 15 min. The beads were then washed, resuspended in ProCell solution (a phosphate buffer enriched with TPrA and various surfactants with a confidential specific chemical composition, which has specially designed and optimized for ECL assays in commercial systems), and dispersed above a screen-printed electrode in an in-house-fabricated holder (Fig. S4.10) containing a magnet to move the beads to the electrode surface. The ECL was initiated by applying 1.4 V *vs* Ag|AgCl at the working electrode for 10 s and measured using a silicon photomultiplier (Fig. S4.11).

Bard and co-workers' elucidation of an alternative ECL reaction pathway of the $[Ru(bpy)_3]^{2+}$ luminophore with TPrA co-reactant[4] revealed Scheme 1b as the dominant light-producing pathway of the magnetic bead-supported assays of the commercial ECL instruments. In these assays, only an infinitesimal fraction of ECL-labels are held with the nanometric electron tunneling distance from the electrode surface required for their direct oxidation (required for Scheme 4.1a).[4, 5b, 41] Diffusion of the TPrA radicals, however, allows chemi-excitation of the $[Ru(bpy)_3]^{2+}$ luminophores (Scheme 4.1b) at much greater (micrometric) distances from the electrode surface.

Based on the above considerations of the parent luminophores of the ECL labels (Fig. 4.5), the reaction pathway depicted in Scheme 4.1b should only be feasible for the novel red and yellow emitters ($[Ir(piq)_2(pt\text{-}TEG\text{-}Sq)]^+$ and $[Ir(bt)_2(pt\text{-}TEG\text{-}Sq)]^+$) and the commercial red emitter ($[Ir(piq)_2(bpy\text{-}COOH)]^+$). As shown in Fig. 4.6a, comparison of the ECL signal-to-blank (S/B) ratios for the different labels for the same target RNA concentration and assay conditions shows that these labels gave the greatest response. The commercial bt analogue, for which the parent luminophore was considered a borderline case (Fig. 4.5b), also showed a minor response. The two $[Ir(C\text{\textasciicircum}N)_2(pt\text{-}TEG\text{-}Sq)]^+$ labels gave superior S/B ratios than their commercial counterparts, but the response with $[Ir(piq)_2(pt\text{-}TEG\text{-}Sq)]^+$ was still 3-fold poorer than that of $[Ru(bpy)_2(mbpy\text{-}COOH)]^{2+}$.
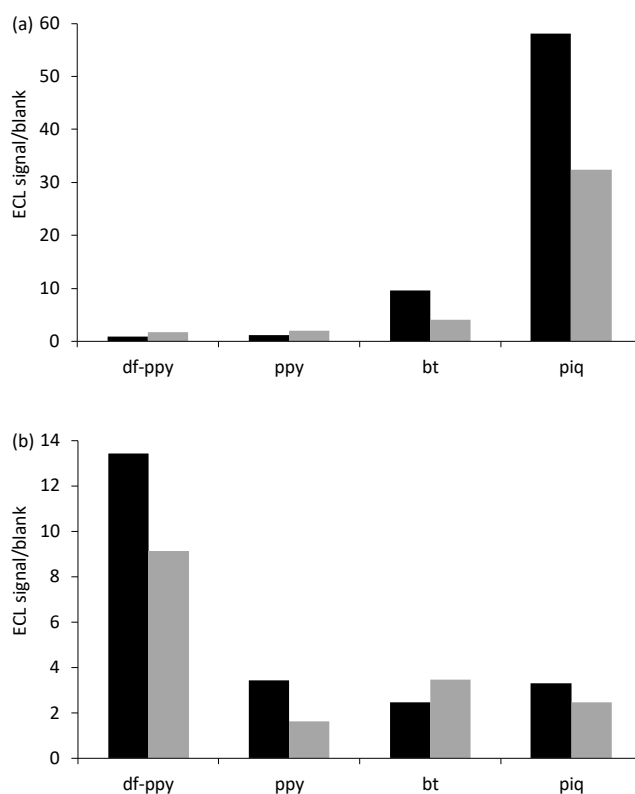
Fig. 4.6. ECL signal/blank ratio for (a) the detection of target RNA by sandwich hybridization assay on a magnetic bead support, and (b) the detection of C-reactive protein by sandwich immunoassay with the capture monoclonal antibody immobilized on a gold electrode, using $[Ir(C^\wedge N)_2(pt\text{-}TEG\text{-}Sq)]^+$ (black columns) or $[Ir(C^\wedge N)_2(mbpy\text{-}COOH)]^+$ (grey columns) ECL labels.

For the $[Ir(piq)_2(pt\text{-}TEG\text{-}Sq)]^+$, $[Ir(bt)_2(pt\text{-}TEG\text{-}Sq)]^+$, $[Ir(piq)_2(bpy\text{-}COOH)]^+$ and $[Ru(bpy)_2(mbpy\text{-}COOH)]^{2+}$ labels, the reactions depicted in Scheme 1b are exergonic, but considerable variation in ECL responses were observed in the RNA assay due to differences in the efficiencies of (i) excitation (dependent on the relative rate of reactions leading to the excited state in addition to various 'dark' reactions), and (ii) emission (which can be estimated from the photoluminescence quantum yield, although the excited state may also be vulnerable to quenching from reactive oxidation products of the co-reactant in some cases[13d]). As the quantum yield of the labels decreased in the order: $[Ir(bt)_2(pt\text{-}TEG\text{-}Sq)]^+$ > $[Ir(piq)_2(pt\text{-}TEG\text{-}Sq)]^+$ > $[Ir(piq)_2(bpy\text{-}COOH)]^+$ > $[Ru(bpy)_2(mbpy\text{-}COOH)]^{2+}$ (Table 4.3), the excitation efficiency appears to be the dominant factor. It is therefore not surprising that most of Ir(III) complexes reported to exhibit the greatest ECL intensities to date have

129

exhibited red luminescence and reduction potentials that would place them in the same regions of Fig. 4.5 as the $[Ru(bpy)_3]^{2+}$ complex, even though they were not evaluated under bead-based assay conditions that would limit the ECL pathway to that depicted Scheme 4.1b. Examples include $Ir(pq)_2(acac)$ (λ_{em} = 609 nm, $E^{0\prime}$ = 0.57 V and -2.05 V vs $Fc^{+/0}$),[25a] $Ir(pph)_2(pic)$ (λ_{em} = 649 nm, $E^{0\prime}$ = 0.61 V and -1.94 V vs $Fc^{+/0}$),[14a] and $[Ir(dmpq)_2(mbpy\text{-}COOH)]^+$ (λ_{em} = 590 nm, $E^{0\prime}$ = 0.78 V and -1.66 V vs $Fc^{+/0}$),[15b] where dmpq = 3,5-dimethylphenyl)quinoline.

For assays in which the Ru(II)/Ir(III) complex luminophore can diffuse to the electrode or is immobilized in very close proximity to the electrode surface, co-reactant ECL with TPrA is feasible via Scheme 4.1a (with possible involvement of Scheme 4.S1a), but only if a sufficient potential is applied to oxidize the metal complex, and the reaction between the oxidized complex and TPrA$^{\bullet}$ is sufficiently exergonic to populate the excited state responsible for the emission (reaction 2). As illustrated by Fig. 4.5a-d, all metal complexes examined in this study meet this requirement. The potentials required to oxidize these metal complexes are generally greater than that for TPrA, and so the pathway depicted in Scheme 4.1b (and Scheme 4.S1b) may also contribute to the overall ECL intensity for complexes meeting its requirements (described above).

In our second assay, the capture antibody was covalently immobilized on a monolayer of 16-mercaptohexadecanoic acid on a gold electrode, which was incubated with the target CRP and then the detection antibody. The electrode was then introduced to an electrochemical cell containing ProCell solution and the ECL was initiated using a voltammetric sweep (0.05 V/s) from +0.5 V to +1.5/1.6 V (vs Ag|AgCl) and measured using photomultiplier tube (S20 multi-alkali photocathode) module. The ECL labels in this assay are much closer to the electrode than the vast majority of those in the bead-based approach, but still outside the electron tunneling region.[4, 41] O'Reilly $et\ al.$,[42] however, developed a

similar assay (CRP by sandwich immunoassay; capture antibody absorbed on a Pt electrode; detection antibody with $[Ru(bpy)_2(N^N)]^{2+}$-type ECL label) and found evidence that the dominant reaction pathway involved oxidation of the label (Scheme 4.1a) and the catalytic oxidation of TPrA (Scheme 4.S1a). Electron hopping[37, 41] between redox active sites was noted as a possibility, but the authors favored an explanation based on the fast rate of charge transfer for the metal complex label.[42]

As shown in Fig. 4.6b, comparison of the ECL signal-to-blank (S/B) ratios for the different labels under the same CRP assay conditions shows that the two blue emitter labels ($[Ir(df-ppy)_2(pt-TEG-Sq)]^+$ and $[Ir(df-ppy)_2(mbpy-COOH)]^+$, which both require oxidation to generate ECL, gave the greatest response. Moreover, the S/B ratio for the novel ($[Ir(df-ppy)_2(pt-TEG-Sq)]^+$ ECL label was only 15% lower than that of $[Ru(bpy)_2(mbpy-COOH)]^{2+}$.

4.4 Conclusions

This exploration of spectroscopic, electrochemical and ECL properties of analogous series of $Ir(C^N)_2(acac)$, $[Ir(C^N)_2(dm-bpy)]^+$, $[Ir(C^N)_2(ptb)]^+$, $[Ir(C^N)_2(pt-TEG)]^+$, $[Ir(C^N)_2(mbpy-COOH)]^+$, and $[Ir(C^N)_2(pt-TEG-Sq)]^+$ complexes has provided a new understanding of the translation of promising Ir(III) complexes to ECL labelling, whilst at the same time introducing a new class of ECL label. As the possibility of multi-colored or potential-resolved ECL systems has been the main driver for the exploration of Ir(III) ECL systems, we selected a group of common C^N ligands (df-ppy, ppy, bt and piq) that would impart a wide range of properties. This highlighted the effects of modifying the ancillary ligand for ECL labeling purposes, the availability of ECL reaction pathways, and the implications on the performance of ECL labels in different assay formats.

Adaption of promising $Ir(C^N)_2(acac)$ complexes for ECL labelling through the common approach of replacing the ancillary ligand with 2,2′-bipyridine derivatives

introduces a low-lying π* LUMO that contracts the spread of emission colors over a series of complexes, which will be detrimental for multi-color applications. The change is most prominent in complexes with the furthest negative reduction potentials (*i.e.*, the highest LUMO energies). Of the Ir(C^N)$_2$(acac) complexes examined in this study, this was the ppy complex, and the change in ancillary ligand to dm-bpy visibly switched the order of emission energies with the Ir(bt)$_2$(acac) complex. These effects can be largely ameliorated with alternative ancillary ligands such as pyridyltriazole ligands, which can be prepared by simple click chemistry procedures to access more water-soluble analogues and functionality suitable for labelling, without significant modification to the properties of the luminophore.

Graphical representations of the key energy requirements of the competing ECL reactions elucidated for the [Ru(bpy)$_3$]$^{2+}$ complex with TPrA as a co-reactant show fundamental limits on the redox potentials and emission wavelengths of complexes that can generate ECL through a mechanism involving oxidation of only the TPrA co-reactant (Scheme 4.1b). Most importantly in the context of developing multi-color ECL systems, the 'window' of reduction potentials enabling this pathway becomes narrower as emission energy increases, and it does not extend across the entire visible region. Plotting the redox potentials and (low-temperature) emissions of the Ir(III) complexes on these graphs enables simple prediction of the feasible ECL pathways, which for the [Ir(C^N)$_2$(pt-TEG)]$^+$ complexes was supported by the relative ECL intensity at different applied potentials under aqueous conditions relevant to bioassay.

The practical outcome of this limitation is seen in the bead-based assay, in which only some of the Ir(III) complexes (those for which Scheme 4.1b is feasible) result in a significant ECL signal for the target analyte. This provides the simplest experimental verification of Bard and co-workers' reasoning[4] (supported by a range of experiments and simulations by other groups[5b, 41, 43]). The requirements for the dominant ECL reaction

pathway for bead-based assays using [Ru(bpy)$_3$]$^{2+}$ with TPrA as co-reactant. Examination of a greater range of electrochemiluminophores with this approach will enable the energy boundaries (carrying considerable error due to the difficulty in establishing the redox potentials of TPrA and TPrA$^{\bullet}$) to be clarified. Moreover, this approach will be valuable for the evaluation of alternative co-reactants in conjunction with various metal complexes (which may extend the reduction potential window further into the blue region of spectrum), as previous studies[44] have predominantly focused on [Ru(bpy)$_3$]$^{2+}$, and not under bioconjugated assay conditions. Assays in which the metal complex can diffuse to the electrode surface, or is immobilized within a few nanometers of the electrode, or where electrons can be transferred over greater distances from the metal complex to the electrode, are not subject to the above limitations. In these cases, the effectiveness of the label is defined only by the efficiency of its excitation and emission under the specific assay conditions, and the relative sensitivity of the photodetector towards that luminophore.

The novel [Ir(C^N)$_2$(pt-TEG-Sq)]$^+$ ECL labels were obtained through a more convenient and versatile synthetic approach and provided superior ECL responses to the commercial [Ir(C^N)$_2$(mbpy-COOH)]$^+$ analogues in both assays. In both assays, the ECL was less intense than that of the conventional [Ru(bpy)$_2$(mbpy-COOH)]$^{2+}$ label, but assay conditions have been optimized specifically for the [Ru(bpy)$_3$]$^{2+}$-based labels since the inception of the technique, and there is considerable scope to improve the relative performance of the Ir(III) complex labels, in areas such as TPrA concentration and electrochemical pulse time.[14b] Despite a few alternative co-reactants providing greater ECL intensities with [Ru(bpy)$_3$]$^{2+}$ under specific conditions, TPrA remains the 'gold standard' co-reactant for ECL assays. Other co-reactants, however, may provide superior ECL performance from various Ir(III) complexes. Finally, the ability through DFT calculations to predict the influence of changes in ligand structure on the redox and luminescence character

of the complex, and consider these changes with respect to the energy requirements of various ECL pathways, will enable the design of superior Ir(III) complex ECL labels with specific emission colors and targeting different reaction pathways.

4.5 Experimental

4.5.1 Chemicals

Tris(2,2′-bipyridine)ruthenium(II) hexafluorophosphate ([Ru(bpy)$_3$](PF$_6$)$_2$), tetrabutylammonium hexafluorophosphate (TBAPF$_6$; electrochemical grade) was purchased from Sigma-Aldrich (NSW, Australia). Tris(2,2′-bipyridine)ruthenium(II) chloride hexahydrate ([Ru(bpy)$_3$]Cl$_2$.6H$_2$O), and bis(cyclopentadienyl)iron (ferrocene; Fc) was purchased from Strem Chemicals (MA, USA). The four Ir(C^N)(acac) complexes and five ECL labels (bis(2,2′-bipyridyl)(4-methyl-4′-carboxypropyl-2,2′-bipyridyl)ruthenium(II) hexafluorophosphate ([Ru(bpy)$_2$(mbpy-COOH)](PF$_6$)$_2$), bis(4,6-difluoro-2-(2-pyridyl)phenyl-C^2,N)(4-methyl-4′-carboxypropyl-2,2'-bipyridyl)iridium(III) chloride ([Ir(df-ppy)$_2$(mbpy-COOH)]Cl), bis(2-phenylpyridine-C^2,N)(4-carboxypropyl-2,2′-bipyridyl)iridium(III) hexafluorophosphate ([Ir(ppy)$_2$(mbpy-COOH)](PF$_6$)), bis(2-phenylbenzothiazole-C^2,N)(4-methyl-4′-carboxy-2,2′-bipyridyl) iridium(III) chloride ([Ir(bt)$_2$(mbpy-COOH)]Cl), bis(1-phenylisoquinoline)(4-methyl-4'-carboxypropyl-2,2′-bipyridyl)iridium(III) chloride ([Ir(piq$_2$(bpy-COOH)]Cl)) were purchased from SunaTech (Jiangsu, China). Acetonitrile (Scharlau, Spain) and was distilled over calcium hydride under a nitrogen atmosphere and collected as needed. Syntheses of the pt-TEG and pt-TEG-Sq ligands, the [Ir(C^N)$_2$(dm-bpy)](PF$_6$), [Ir(C^N)$_2$(ptb)](PF$_6$) and [Ir(C^N)$_2$(pt-TEG)]Cl complexes, and the [Ir(C^N)$_2$(pt-TEG-Sq)]$^+$ ECL labels (where C^N = piq, bt, ppy, or df-ppy) are described in the Supporting Information. The solubility of the [Ir(C^N)$_2$(pt-TEG)]$^+$ complexes was approximately 1 mM [Ir(bt)$_2$(pt-TEG)]$^+$ and [Ir(ppy)$_2$(pt-TEG)]$^+$ and 0.5

mM [Ir(df-ppy)$_2$(pt-TEG)]$^+$ in water, and 0.1 mM [Ir(piq)$_2$(pt-TEG)]$^+$ in water with 10% acetonitrile. Stock [Ir(C^N)$_2$(pt-TEG)]$^+$ solutions were subsequently prepared at 0.1 mM.

4.5.2 Photophysical measurements

For the characterization of Ir(C^N)$_2$(acac), [Ir(C^N)$_2$(dm-bpy)](PF$_6$), [Ir(C^N)$_2$(ptb)](PF$_6$) and [Ir(C^N)$_2$(pt-TEG)]Cl complexes, absorption spectra were obtained with a Cary 300 Bio UV/Vis spectrophotometer (Varian Australia, Vic., Australia) with 1 cm pathlength quartz cuvettes. Emission spectra were measured on a Cary Eclipse fluorescence spectrometer (Varian Australia; 5 nm band pass, 1 nm data interval, PMT voltage: 800 V). Metal complexes were prepared at a concentration of 10 μM in deionized water or freshly distilled acetonitrile. For the low temperature emission spectra, the complexes were prepared at 0.5 μM in ethanol:methanol (4:1) and cooled to 85 K using an OptistatDN Variable Temperature Liquid Nitrogen Cryostat equipped with custom-made quartz sample holder. The low temperature spectra were collected at 85 K to avoid damage to the spectroscopic cuvettes near 77 K observed during our previous study[14b] and by others.[45] No significant difference in the λ_{max} for metal complexes such as [Ru(bpy)$_3$]$^{2+}$ and Ir(ppy)$_3$ between 77 K and 85 K was observed under these instrumental conditions.[22b] All emission spectra were corrected by standard correction curves established using a quartz halogen tungsten lamp.

For the characterization of [Ir(C^N)$_2$(pt-TEG-Sq)]$^+$ and other ECL labels, the complexes were dissolved in DMF (1 mM) and diluted to 10 μM in a 0.1 M PBS solution (pH = 7.4). Steady-state emission spectra were collected on a Nanolog (HORIBA Jobin Yvon IBH) spectrofluorometer. A 450 W xenon-arc lamp was used to excite the complexes using a 1200 g/mm grating blazed at 330 nm excitation monochromators, a 1200 g/mm grating blazed at a 500 nm emission monochromator, and a thermoelectrically cooled TBX picosecond single-photon detector. Emission and excitation spectra were corrected for

source intensity, gratings, and detector response. Lifetimes were measured using the time correlated single photon counting (TCSPC) option on the spectrometer and correlated by a time-to-amplitude converter (TAC) in forward TAC mode. A nanoled laser (λ_{ex} = 344 nm or 451 nm) was pulsed at a 100 kHz, signals were collected using a FluoroHub counter and the data was analyzed using DAS6 software (HORIBA Jobin Yvon IBH). Spectra for absolute quantum yields were measured at room temperature (22 $\pm$ 2 ℃) with a Quanta-phi HORIBA Scientific 6 in. diameter integrating sphere connected to the Nanolog via optical fibers. The complexes were excited using a 450 W xenon lamp and detected with a liquid nitrogen cooled Symphony II (Model SII-1LS-256−06) CCD.

4.5.3 Electrochemistry

An Autolab PGSTAT204 potentiostat (Metrohm Autolab B.V., Netherlands) with a conventional three-electrode system housed in a custom-made light-tight faraday cage was used. The electrochemical cell contained a glassy carbon working electrode (3 mm diameter), platinum counter electrode, and a low leakage Ag|AgCl (3.4 M) (Innovative Instruments, Fl, USA) or silver wire reference electrode. Cyclic voltammograms were performed at a scan rate of 0.1 V/s and metal complex concentration of 0.25 mM with a supporting electrolyte of 0.1 M TBAPF$_6$ in freshly distilled acetonitrile. The glassy carbon electrode was polished using 0.3 and 0.05 μm alumina powder, sonicated in water and then distilled acetonitrile, and dried before use. Prior to analysis, solutions were deoxygenated for 15 min (using Argon). Potentials were referenced to the ferrocenium/ferrocene redox couple. All electrochemical experiments were carried out at room temperature. Square wave voltammetric measurements were performed using 0.5 mM metal complex in 0.1 M phosphate buffer (pH 7.5), with 5 mV step, 25 Hz frequency, 0.02 V amplitude and 100 mV/s scan rate.

4.5.4 Electrochemiluminescence

ECL experiments were performed using the same electrochemical cell configuration as described above, and the light emitted near the working electrode surface was detected using a photomultiplier tube (PMT; Electron Tubes model 9124B; ETP, NSW, Australia) positioned under the cell, or a CCD spectrometer (QE65Pro, Ocean Optics, FL, USA) interfaced with the cell using a collimating lens (74-UV, Ocean Optics) and optic fiber (1.0 m, 1.0 mm core diameter; Ocean Optics). Acquisition was synchronized with the electrochemical experiment by sending a trigger from the potentiostat to the HR4000 (Ocean Optics) break out box. Comparisons of co-reactant ECL intensities (integrated peak area) between Ir(III) complexes and $[Ru(bpy)_3]^{2+}$ were performed using chronoamperometry (potential of E_{pa} + 0.1 V, 10 s pulse time, 10 Hz), with the CCD spectrometer, and metal complex concentration of 10 μM. The 'two-wave' ECL experiments involved a voltammetric sweep from 0 V to 1.8 V vs Ag|AgCl followed by the reverse sweep back to 0 V, with the resulting ECL measured by PMT. The ECL detection for each bioassay is described in later sections.

4.5.5 Conversion of carboxylic acid ECL labels to N-hydroxysuccinimide (NHS) esters

N,N'-dicyclohexylcarbodiimide (DCC, 146 mmol; Sigma Aldrich, >99%) and NHS (146 mmol; Sigma Aldrich, 98%) were dissolved in 1.5 mL chilled (water ice-bath), dried (molecular sieves) DMF (Sigma Aldrich, molecular biology grade) with stirring. To this solution, 28 mmol of $[Ru(bpy)_2(mbpy-COOH)]^{2+}$ (Fig. 4.1c) or $[Ir(C\wedge N)_2(mbpy-COOH)]^+$ (Fig. 4.2d) dissolved in 0.5 mL dry, chilled DMF was added. The mixture was stirred on ice for 30 min, before returning to room temperature (22 ℃) and stirring was continued for 5 h. The reaction mixture was the chilled (-18 ℃), and the solids were removed by centrifugation. The $[Ru(bpy)_2(mbpy-NHS)]^{2+}$ and $[Ir(C\wedge N)_2(mbpy-NHS)]^+$ solutions were stored at -20 ℃ in a desiccator. The $[Ir(C\wedge N)_2(pt-TEG-Sq)]^+$ labels (Fig. 4.2e) did not require this step.

4.5.6 Assay 1: Sandwich hybridization RNA assay on magnetic bead support

NASBA and purification of target RNA amplicon. The RNA fragment used in the sandwich hybridization assay was the amplicon that resulted from the Nucleic Acid Sequence Based Amplification (NASBA) of viral-like particles (VLP) RNA. We packaged an artificial sequence into MS2 capsid, which created the VLPs to serve as a model for carrying target sequence of interest in this study. The VLPs were prepared as previously described.[46] VLP RNA purification was performed using spin column based Qiagen RNeasy RNA isolation kit as per the manufacturer's protocol. The amplification process was performed using commercial NASBA reagent from Life Science Advance Technologies (St. Petersburg, FL, USA). Briefly, the final 20 µL reaction buffer mixture (LRB) consists of 40 mM Tris HCl (pH 8.5), 70 mM KCl, 12 mM $MgCl_2$, 15% dimethyl sulfoxide, 5 mM dithiothreitol (DTT), 1 mM dNTP mixture, 2 mM ATP, CTP and UTP mixture, 1.5 mM GTP, 0.5 mM ITP, 0.2 µM of P1 and P2 primers (Integrated DNA Technologies, IL, USA) and purified VLP RNA (10 ng/µL). The NASBA reaction was initiated by addition of enzyme cocktail (LEM) containing three enzymes, namely 6.4 U AMV Reverse Transcriptase (AMV-RT), 32 U T7 RNA polymerase, and 0.1 U ribonuclease H, and the NASBA mixture was incubated at 41 ℃ for 60 min. To obtain purified NASBA RNA amplicon, the NASBA reaction mixture was subjected to lithium chloride-cold ethanol RNA precipitation method by as per the manufacturers recommendation (AM9480; Thermo Fisher, Mulgrave, VIC, Australia) and standardized using UV spectroscopy (Nanodrop 2000; Thermo Fisher) to give 1 pmol/µL concentration in 10 mM Tris EDTA (pH 7.5). The RNA samples were stored at –80 ℃ until required. Primers and NASBA amplicon fragment sequences are detailed in Table S4.7.

Attachment of the capture probe to the magnetic beads. 40 µL (400 µg) of Dynabeads M-280 Streptavidin (MB) were washed with binding buffer (20 mM Tris HCl, pH 8, 0.5 M

NaCl) by vortexing and magnetic separation, then resuspended in 100 μL of binding buffer at 4 mg/mL, the capture probe (CP) was bound to the MB by adding 20 μL of CP solution (10 μM) to the bead solution and incubating for 20 min at room temperature with gentle mixing. Excess CP was removed by washing the beads three times in binding buffer, followed by resuspension in 200 μL binding buffer (2 mg/mL). The CP@MB solution was stored at 4 ℃ and was stable for several weeks.

Conjugation of ECL labels with the detection probe. The detection probe (as purchased) was resuspended to a concentration of 500 μM in 100 mM sodium borate buffer (pH 8). 100 μL (50 nmol) of this solution was combined with 1000 nmol of the complex (20-fold excess, 80 μL at 12.5 mM) $[Ru(bpy)_2(mbpy-NHS)]^{2+}$ or $[Ir(C^\wedge N)_2(mbpy-NHS)]^+$ in DMF and 620 μL 100 mM borate buffer. The solution was shielded from ambient light with aluminum foil, and reacted at room temperature for 24 h on a rotating mixer. The labelled oligo was washed and purified as described by Zhou *et al*.,[8c] before being resuspended in nuclease free water at 20 μM. The concentration of the labelled oligo was measured using a Nanodrop 2000 UV-Vis spectrophotometer and the purity was checked by RP-HPLC. When necessary, the labelled oligo was further purified by collecting the appropriate fraction eluted from the column and precipitating the labelled oligo by solvent evaporation and salt precipitation before re-suspension. The $[Ir(C^\wedge N)_2(pt-TEG-Sq)]^+$ labels were attached to the oligo and purified in a similar manner, except the complex concentration was 10 mM in acetonitrile, and 800 μL additional borate buffer was added. If the solution turned cloudy on the combination of the complex and oligo or borate buffer, acetonitrile (<100 μL) was added dropwise until the solution turned clear. The analytical and semi-preparative HPLC was performed using an Agilent Technologies 1260 Infinity LC system (CA, USA) with a Phenomenex Luna 5μ C18(2) 100Å column (150 × 4.6 mm) (CA, USA). The mobile phase was a solvent gradient using solvent A (0.1% ammonium acetate in deionized water) and

solvent B (acetonitrile) at a total flow rate of 1 mL/min. The oligo labeled with the Ru complex was examined and purified using a gradient of 5%→100% solvent B over 40 min. The oligos labelled with iridium complexes were examined and purified using a gradient of 5%→100% solvent B over 20 min. For semi-preparative RP-HPLC, samples were made up to approximately 20 μM in acetonitrile and loaded onto the column at a maximum injection volume of 100 μL.

Assay procedure. 7 μL of CP@MB (2 mg/mL), 1 μL of detection probe (20 μM, 20 pmol) and differing amounts of target RNA solution were mixed in a PCR tube and made up to 20 μL final volume using binding buffer. The sample was heated to 45 °C for 15 min to allow RNA hybridisation to occur. The beads were then washed two times using binding buffer with 5% T-20 and 0.1% T-100 detergent, removing excess detection probe. The beads were then resuspended in ProCell solution (Roche Diagnostics Australia), before dispersing above the working electrode of a Zensor screen printed electrode, mounted in a custom-made holder (Fig. S4.10) pre-filled with 80 μL ProCell solution. The magnet (3 × 4 mm diameter rod shaped N42 rare earth; Aussie Magnets, Australia) positioned behind the electrode ensured the beads were rapidly collected at the surface of the working electrode for analysis. The ECL was detected using an 3 × 3 mm silicon photon multiplier (SiPM; ASD-RGB3S-P; AdvanSiD, Italy) interfaced with an ASD-EP-EB-N amplifier board (AdvanSiD; Fig. S4.11). The SPE holder and photodetector were housed in a light-tight Faraday cage. An Autolab PGSTAT 101 (Metrohm Autolab B.V.) potentiostat with NOVA software was used to apply a single-step chronoamperometry experiment (1.4 V *vs* Ag|AgCl for 10 s) and record the electrochemical signals. Data from the SiPM was recorded and processed using an eDAQ401 (eDAQ, Australia) data recording unit using the supplied eDAQ Chart software.

4.5.7 Assay 2: C-reactive protein sandwich immunoassay on a gold electrode

Attachment of the capture antibody to the electrode. Fabrication of the immunosensor was adapted from a previously described procedure.[42, 47] A gold electrode (Au) was polished with a 0.03 μm alumina/water slurry on a polishing cloth to a mirror finish, followed by sonicating and rinsing with distilled water. A self-assembled monolayer (SAM) was formed by dipping the electrode for 48 h in an ethanol solution containing 1 mM 16-mercaptohexadecanoic acid (MHDA). The Au/MHDA electrode was then treated in a mixture of 5 mM 1-ethyl-3-[3-dimethylaminopropyl] carbodiimide hydrochloride (EDC) and 15 mM sulfo-*N*-hydroxy succinimide in Dulbecco's phosphate buffered saline (DPBS) solution for 20 min at room temperature, to activate the carboxylic acids groups of the MHDA. The custom capture monoclonal antibody (mAb) mAbTJ229, was covalently immobilized on the Au/MHA electrode by incubating the modified electrode in a 0.1 M PBS solution (pH 7.4) containing 100 μg/mL stock for approximately 1 h at 37°C. After coating with the capture mAb, individual, independently prepared Au/MHA/mAb electrodes were incubated with Fetal Bovine Serum for 1 h at 4 °C to block the non-specific binding sites.

Conjugation of ECL labels with the detection antibody. The Ir(III) complex was dissolved in DMF (0.01 M) and 10 μL was added to an Eppendorf tube containing 1 mL 0.1 M PBS solution (pH = 7.4) of the monoclonal antibody mAbTJ330 (100 μg/mL) and slowly stirred at 4 °C for 4 h. The reaction mixture was purified by different cycles of centrifugation using an ultra-centrifugal tube with a cut-off of 30K.

Assay procedure. The Au/MHA electrodes with immobilized capture antibody were incubated with 10 ng/mL CRP solution for 1 h at 37 °C. The functionalized electrodes were then immersed in a PBS solution containing the soluble labelled detection antibody (100 μg/mL stock) for 1 h at 37 °C and again washed. A custom system was used for ECL

characterization, consisting in an electrochemical cell based on modified gold-disk working electrode shrouded in Teflon (CH Instruments, Austin, TX, USA, 3 mm diameter), which were closely facing (a few millimeters) the photomultiplier tube (PMT) module (Sens-Tech model P30A-05, ETP, NSW, Australia). The PMT signal was amplified by TA-GI-74 Ames Photonics Inc. amplifier (Model D7280) and controlled by a CHI660C Electrochemical Workstation (CH Instruments, Inc., Austin, TX, USA). The RE employed was an Ag|AgCl (1M KCl) from CHI-Instruments and was separated from the catholyte by a glass frit. A platinum wire served as the CE. ProCell solution (Roche Diagnostics Australia) was used as the aqueous solvent and source of TPrA. The solutions were scanned at 0.05 V/s from +0.5 V to +1.5/+1.6 V (according to the oxidation potential of the different complexes).

4.6 Acknowledgements

4.7 References

1. (a) Li, L.; Chen, Y.; Zhu, J.-J., Recent advances in electrochemiluminescence analysis. *Anal. Chem.* **2017,** *89*, 358-371; (b) Khonsari, Y. N.; Sun, S., Recent trends in electrochemiluminescence aptasensors and their applications. *Chem. Commun.* **2017,** *53*, 9042-9054; (c) Liu, Z.; Qi, W.; Xu, G., Recent advances in electrochemiluminescence. *Chem. Soc. Rev.* **2015,** *44*, 3117-3142; (d) Muzyka, K.,

Current trends in the development of the electrochemiluminescent immunosensors. *Biosens. Bioelectron.* **2014,** *54*, 393-407; (e) Hu, L.; Xu, G., Applications and trends in electrochemiluminescence. *Chem. Soc. Rev.* **2010,** *39*, 3275-3304; (f) Miao, W., Electrogenerated chemiluminescence and its biorelated applications. *Chem. Rev.* **2008,** *108*, 2506-2553.

2. (a) Roche Diagnostics Products and Solutions 2017. http://www.cobas.com/content/dam/cobas_com/pdf/lists/products-and-solutions.pdf; (b) Meso Scale Diagnostics https://www.mesoscale.com/en/technical_resources/our_technology/multi-array.

3. (a) Rubinstein, I.; Bard, A. J., Electrogenerated chemiluminescence. 37. Aqueous ECL systems based on tris(2,2'-bipyridine)ruthenium(2+) and oxalate or organic acids. *J. Am. Chem. Soc.* **1981,** *103*, 512-516; (b) Leland, J. K.; Powell, M. J., Electrogenerated chemiluminescence: an oxidative-reduction type ECL reaction sequence using tripropyl amine. *J. Electrochem. Soc.* **1990,** *137*, 3127-3131.

4. Miao, W.; Choi, J.-P.; Bard, A. J., Electrogenerated chemiluminescence 69: the tris(2,2'-bipyridine)ruthenium(II), $(Ru(bpy)_3^{2+})$/tri-*n*-propylamine (TPrA) system revisited - a new route involving TPrA$^{\bullet+}$ cation radicals. *J. Am. Chem. Soc.* **2002,** *124*, 14478-14485.

5. (a) Komori, K.; Takada, K.; Hatozaki, O.; Oyama, N., Electrochemiluminescence of Ru(II) complexes immobilized on a magnetic microbead surface: distribution of magnetic microbeads on the electrode surface and effect of azide ion. *Langmuir* **2007,** *23*, 6446-6452; (b) Sentic, M.; Milutinovic, M.; Kanoufi, F.; Manojlovic, D.; Arbault, S.; Sojic, N., Mapping electrogenerated chemiluminescence reactivity in space: mechanistic insight into model systems used in immunoassays. *Chem. Sci.* **2014,** *5*, 2568-2572.

6.   Barbante, G. J.; Hogan, C. F.; Wilson, D. J. D.; Lewcenko, N. A.; Pfeffer, F. M.; Barnett, N. W.; Francis, P. S., Simultaneous control of spectroscopic and electrochemical properties in functionalised electrochemiluminescent tris(2,2'-bipyridine)ruthenium(II) complexes. *Analyst* **2011,** *136*, 1329-1338.

7.   Valenti, G.; Fiorani, A.; Li, H.; Sojic, N.; Paolucci, F., Essential role of electrode materials in electrochemiluminescence applications. *ChemElectroChem* **2016,** *3*, 1990-1997.

8.   (a) Bard, A. J.; Whitesides, G. M. Luminescent metal chelate labels and means for detection. 8602734, 19851030., 1986; (b) Xu, L.; Li, Y.; Wu, S.; Liu, X.; Su, B., Imaging latent fingerprints by electrochemiluminescence. *Angew. Chem., Int. Ed.* **2012,** *51*, 8068-8072, S8068/1-S8068/17; (c) Zhou, X.; Zhu, D.; Liao, Y.; Liu, W.; Liu, H.; Ma, Z.; Xing, D., Synthesis, labeling and bioanalytical applications of a tris(2,2'-bipyridyl)ruthenium(II)-based electrochemiluminescence probe. *Nat. Protoc.* **2014,** *9*, 1146-1159; (d) Liao, Y.; Zhou, X.; Fu, Y.; Xing, D., Linear Ru(bpy)$_3^{2+}$−polymer as a universal probe for sensitive detection of biomarkers with controllable electrochemiluminescence signal-amplifying ratio. *Anal. Chem.* **2017,** *89*, 13016-13023.

9.   (a) Blackburn, G. F.; Shah, H. P.; Kenten, J. H.; Leland, J.; Kamin, R. A.; Link, J.; Peterman, J.; Powell, M. J.; Shah, A.; Talley, D. B.; Tyagi, S. K.; Wilkins, E.; Wu, T.-G.; Massey, R. J., Electrochemiluminescence detection for development of immunoassays and DNA probe assays for clinical diagnostics. *Clin. Chem.* **1991,** *37*, 1534-1539; (b) Carrara, S.; Arcudi, F.; Prato, M.; Cola, L. D., Amine-rich nitrogen-doped carbon nanodots as a platform for self-enhancing electrochemiluminescence. *Angew. Chem. Int. Ed.* **2017,** *56*, 4757-4761; (c) Valenti, G.; Scarabino, S.; Goudeau, B.; Lesch, A.; Jović, M.; Villani, E.; Sentic, M.; Rapino, S.; Arbault, S. p.; Paolucci,

F.; Sojic, N., Single cell electrochemiluminescence imaging: from the proof-of-concept to disposable device-based analysis. *J. Am. Chem. Soc.* **2017,** *139*, 16830-16837.

10. (a) Debad, J. D.; Glezer, E. N.; Wohlstadter, J.; Sigal, G. B.; Leland, J. K., Clinical and Biological Applications of ECL. In *Electrogenerated Chemiluminescence*, Bard, A. J., Ed. Marcel Dekker: New York, 2004; pp 359-396; (b) Gorman, B. A.; Francis, P. S.; Barnett, N. W., Tris(2,2'-bipyridyl)ruthenium(II) chemiluminescence. *Analyst* **2006,** *131*, 616-639.

11. (a) Kapturkiewicz, A., Cyclometalated iridium(III) chelates—a new exceptional class of the electrochemiluminescent luminophores. *Anal. Bioanal. Chem.* **2016,** *408*, 7013-7033; (b) Laird, S.; Hogan Conor, F., Electrochemiluminescence of Iridium Complexes. In *Iridium(III) in Optoelectronic and Photonics Applications, 1st edn*, Zysman-Colman, E., Ed. John Wiley & Sons, Inc.: Chichester, UK, 2017; pp 359-414.

12. (a) Lowry, M. S.; Bernhard, S., Synthetically tailored excited states: phosphorescent, cyclometalated iridium(III) complexes and their applications. *Chem.-Eur. J.* **2006,** *12*, 7970-7977; (b) Ladouceur, S.; Zysman-Colman, E., A comprehensive survey of cationic iridium(III) complexes bearing nontraditional ligand chelation motifs. *Eur. J. Inorg. Chem.* **2013**, 2985-3007; (c) Housecroft, C. E.; Constable, E. C., Over the LEC rainbow: Colour and stability tuning of cyclometallated iridium(III) complexes in light-emitting electrochemical cells. *Coord. Chem. Rev.* **2017,** *350*, 155-177.

13. (a) Bruce, D.; Richter, M. M., Green electrochemiluminescence from ortho-metalated tris(2-phenylpyridine)iridium(III). *Anal. Chem.* **2002,** *74*, 1340-1342; (b) Muegge, B. D.; Richter, M. M., Multicolored electrogenerated chemiluminescence from ortho-metalated iridium(III) systems. *Anal. Chem.* **2004,** *76*, 73-77; (c) Doeven, E. H.; Zammit, E. M.; Barbante, G. J.; Hogan, C. F.; Barnett, N. W.; Francis, P. S., Selective

excitation of concomitant electrochemiluminophores: tuning emission color by electrode potential. *Angew. Chem., Int. Ed.* **2012,** *51*, 4354-4357; (d) Doeven, E. H.; Zammit, E. M.; Barbante, G. J.; Francis, P. S.; Barnett, N. W.; Hogan, C. F., A potential-controlled switch on/off mechanism for selective excitation in mixed electrochemiluminescent systems. *Chem. Sci.* **2013,** *4*, 977-982; (e) Doeven, E. H.; Barbante, G. J.; Kerr, E.; Hogan, C. F.; Endler, J. A.; Francis, P. S., Red-green-blue electrogenerated chemiluminescence utilizing a digital camera as detector. *Anal. Chem.* **2014,** *86*, 2727-2732; (f) Doeven, E. H.; Barbante, G. J.; Hogan, C. F.; Francis, P. S., Potential-resolved electrogenerated chemiluminescence for the selective detection of multiple luminophores. *ChemPlusChem* **2015,** *80*, 456-470; (g) Li, H.; Bouffier, L.; Arbault, S.; Kuhn, A.; Hogan, C. F.; Sojic, N., Spatially-resolved multicolor bipolar electrochemiluminescence. *Electrochem. Commun.* **2017,** *77*, 10-13; (h) Wang, Y.-Z.; Xu, C.-H.; Zhao, W.; Guan, Q.-Y.; Chen, H.-Y.; Xu, J.-J., Bipolar electrode based multicolor electrochemiluminescence biosensor. *Anal. Chem.* **2017,** *89*, 8050-8056; (i) Gao, H.; Dang, Q.; Xia, S.; Zhao, Y.; Qi, H.; Gao, Q.; Zhang, C., Highly selective electrogenerated chemiluminescence biosensor for simultaneous detection of matrix metalloproteinase-2 and matrix metalloproteinase-7 in cell secretions. *Sens. Actuators, B* **2017,** *253*, 69-76; (j) Wang, Y.-Z.; Ji, S.-Y.; Xu, H.-Y.; Zhao, W.; Xu, J.-J.; Chen, H.-Y., Bidirectional electrochemiluminescence color switch: an application in detecting multimarkers of prostate cancer. *Anal. Chem.* **2018,** *90*, 3570-3575; (k) Guo, W.; Ding, H.; Gu, C.; Liu, Y.; Jiang, X.; Su, B.; Shao, Y., Potential-resolved multicolor electrochemiluminescence for multiplex immunoassay in a single sample. *J. Am. Chem. Soc.* **2018,** *140*, 15904-15915.

14. (a) Fernandez-Hernandez, J. M.; Longhi, E.; Cysewski, R.; Polo, F.; Josel, H.-P.; De Cola, L., Photophysics and electrochemiluminescence of bright cyclometalated Ir(III) complexes in aqueous solutions. *Anal. Chem.* **2016,** *88*, 4174-4178; (b) Chen, L.;

Doeven, E. H.; Wilson, D. J. D.; Kerr, E.; Hayne, D. J.; Hogan, C. F.; Yang, W.; Pham, T. T.; Francis, P. S., Co-reactant electrogenerated chemiluminescence of iridium(III) complexes containing an acetylacetonate ligand. *ChemElectroChem* **2017,** *4*, 1797-1808.

15. (a) Li, C.; Lin, J.; Guo, Y.; Zhang, S., A novel electrochemiluminescent reagent of cyclometalated iridium complex-based DNA biosensor and its application in cancer cell detection. *Chem. Commun.* **2011,** *47*, 4442-4444; (b) Zhou, Y.; Xie, K.; Leng, R.; Kong, L.; Liu, C.; Zhang, Q.; Wang, X., Highly efficient electrochemiluminescence labels comprising iridium(III) complexes. *Dalton Trans.* **2017,** *46*, 355-363; (c) Zhao, Y.; Luo, Y.; Li, T.; Song, Q., Au NPs driven electrochemiluminescence aptasensors for sensitive detection of fumonisin B1. *RSC Adv.* **2014,** *4*, 57709-57714.

16. Kerr, E.; Doeven, E. H.; Wilson, D. J. D.; Hogan, C. F.; Francis, P. S., Considering the chemical energy requirements of the tri-*n*-propylamine co-reactant pathways for the judicious design of new electrogenerated chemiluminescence detection systems. *Analyst* **2016,** *141*, 62-69.

17. (a) Zanarini, S.; Felici, M.; Valenti, G.; Marcaccio, M.; Prodi, L.; Bonacchi, S.; Contreras-Carballada, P.; Williams, R. M.; Feiters, M. C.; Nolte, R. J. M.; De Cola, L.; Paolucci, F., Green and blue electrochemically generated chemiluminescence from click chemistry-customizable iridium complexes. *Chem. Eur. J.* **2011,** *17*, 4640-4647; (b) Barbante, G. J.; Doeven, E. H.; Kerr, E.; Connell, T. U.; Donnelly, P. S.; White, J. M.; Lớpes, T.; Laird, S.; Hogan, C. F.; Wilson, D. J. D.; Barnard, P. J.; Francis, P. S., Understanding electrogenerated chemiluminescence efficiency in blue-shifted iridium(III)-complexes: an experimental and theoretical study. *Chem. Eur. J.* **2014,** *20*, 3322-3332; (c) Kerr, E.; Doeven, E. H.; Barbante, G. J.; Connell, T. U.; Donnelly, P. S.; Wilson, D. J. D.; Ashton, T. D.; Pfeffer, F. M.; Francis, P. S., Blue

electrogenerated chemiluminescence from water-soluble iridium complexes containing sulfonated phenylpyridine or tetraethylene glycol derivatised triazolylpyridine ligands. *Chem. - Eur. J.* **2015,** *21*, 14987-14995.

18. (a) Beyer, B.; Ulbricht, C.; Escudero, D.; Friebe, C.; Winter, A.; Gonzalez, L.; Schubert, U. S., Phenyl-1H-[1,2,3]triazoles as new cyclometalating ligands for iridium(III) complexes. *Organometallics* **2009,** *28*, 5478-5488; (b) Scattergood, P. A.; Sinopoli, A.; Elliott, P. I. P., Photophysics and photochemistry of 1,2,3-triazole-based complexes. *Coord. Chem. Rev.* **2017,** *350*, 136-154; (c) Hosseinnejad, T.; Ebrahimpour-Malmir, F.; Fattahi, B., Computational investigations of click-derived 1,2,3-triazoles as keystone ligands for complexation with transition metals: a review. *RSC Adv.* **2018,** *8*, 12232-12259.

19. Connell, T. U.; Donnelly, P. S., Labelling proteins and peptides with phosphorescent d^6 transition metal complexes. *Coord. Chem. Rev.* **2017**, DOI: 10.1016/j.ccr.2017.12.001.

20. Felici, M.; Contreras-Carballada, P.; Vida, Y.; Smits, J. M.; Nolte, R. J.; De Cola, L.; Williams, R. M.; Feiters, M. C., Ir(III) and Ru(II) complexes containing triazole-pyridine ligands: luminescence enhancement upon substitution with beta-cyclodextrin. *Chem. - Eur. J.* **2009,** *15*, 13124-13134.

21. Mydlak, M.; Bizzarri, C.; Hartmann, D.; Sarfert, W.; Schmid, G.; De Cola, L., Positively charged iridium(III) triazole derivatives as blue emitters for light-emitting electrochemical cells. *Adv. Funct. Mater.* **2010,** *20*, 1812-1820.

22. (a) Kerr, E.; Doeven, E. H.; Barbante, G. J.; Hogan, C. F.; Bower, D.; Donnelly, P. S.; Connell, T. U.; Francis, P. S., Annihilation electrogenerated chemiluminescence of mixed metal chelates in solution: modulating emission colour by manipulating the energetics. *Chem. Sci.* **2015,** *6*, 472-479; (b) Soulsby, L. C.; Hayne, D. J.; Doeven, E.

H.; Wilson, D. J. D.; Agugiaro, J.; Connell, T. U.; Chen, L.; Hogan, C. F.; Kerr, E.; Adcock, J. L.; Donnelly, P. S.; White, J. M.; Francis, P. S., Mixed annihilation electrogenerated chemiluminescence of iridium(III) complexes. *Phys. Chem. Chem. Phys.* **2018,** *20*, 18995-19006.

23. Doeven, E. H.; Barbante, G. J.; Harsant, A. J.; Donnelly, P. S.; Connell, T. U.; Hogan, C. F.; Francis, P. S., Mobile phone-based electrochemiluminescence sensing exploiting the 'USB On-The-Go' protocol. *Sens. Actuators, B* **2015,** *216*, 608-613.

24. Smith, Z. M.; Kerr, E.; Doeven, E. H.; Connell, T. U.; Barnett, N. W.; Donnelly, P. S.; Haswell, S. J.; Francis, P. S., Analytically useful blue chemiluminescence from a water-soluble iridium(III) complex containing a tetraethylene glycol functionalised triazolylpyridine ligand. *Analyst* **2016,** *141*, 2140-2144.

25. (a) Kim, J. I.; Shin, I.-S.; Kim, H.; Lee, J.-K., Efficient electrogenerated chemiluminescence from cyclometalated iridium(III) complexes. *J. Am. Chem. Soc.* **2005,** *127*, 1614-1615; (b) Yu, L.; Huang, Z.; Liu, Y.; Zhou, M., Photophysics, electrochemistry and electrochemiluminescence of water-soluble biscyclometalated iridium (III) complexes. *J. Organomet. Chem.* **2012,** *718*, 14-21; (c) Ladouceur, S.; Swanick, K. N.; Gallagher-Duval, S.; Ding, Z.; Zysman-Colman, E., Strongly blue luminescent cationic iridium(III) complexes with an electron-rich ancillary ligand: evaluation of their optoelectronic and electrochemiluminescence properties. *Eur. J. Inorg. Chem.* **2013,** *2013*, 5329-5343.

26. Connell, T. U.; White, J. M.; Smith, T. A.; Donnelly, P. S., Luminescent iridium(III) cyclometalated complexes with 1,2,3-triazole "Click" ligands. *Inorg. Chem.* **2016,** *55*, 2776-2790.

27. Connell, T. U.; James, J. L.; White, A. R.; Donnelly, P. S., Protein labelling with versatile phosphorescent metal complexes for live cell luminescence imaging. *Chem. - Eur. J.* **2015,** *21*, 14146-14155.

28. Haghighatbin, M. A.; Laird, S. E.; Hogan, C. F., Electrochemiluminescence of cyclometalated iridium (III) complexes. *Curr. Opin. Electrochem.* **2018,** *8*, 52-59.

29. (a) Kapturkiewicz, A.; Chen, T.-M.; Laskar, I. R.; Nowacki, J., Electrochemiluminescence studies of the cyclometalated iridium(III) complexes with substituted 2-phenylbenzothiazole ligands. *Electrochem. Commun.* **2004,** *6*, 827-831; (b) Kapturkiewicz, A.; Nowacki, J.; Borowicz, P., Electrochemiluminescence studies of the cyclometalated iridium(III) L_2Ir(acetyl acetonate) complexes. *Electrochim. Acta* **2005,** *50*, 3395-3400.

30. (a) Li, C.; Lin, J.; Yang, X.; Wan, J., Efficient electrochemiluminescent cyclometalated iridium(III) complexes: Synthesis, photophysical and electrochemiluminescent properties. *J. Organomet. Chem.* **2011,** *696*, 2445-2450; (b) Zhou, Y.; Li, W.; Yu, L.; Liu, Y.; Wang, X.; Zhou, M., Highly efficient electrochemiluminescence from iridium(III) complexes with 2-phenylquinoline ligand. *Dalton Trans.* **2015,** *44*, 1858-1865; (c) Zhou, Y.; Gao, H.; Wang, X.; Qi, H., Electrogenerated chemiluminescence from heteroleptic iridium(III) complexes with multicolor emission. *Inorg. Chem.* **2015,** *54*, 1446-1453.

31. (a) Lowry, M. S.; Hudson, W. R.; Pascal, R. A., Jr.; Bernhard, S., Accelerated luminophor discovery through combinatorial synthesis. *J. Am. Chem. Soc.* **2004,** *126*, 14129-14135; (b) Liu, S.-J.; Zhao, Q.; Fan, Q.-L.; Huang, W., A series of red-light-emitting ionic iridium complexes: structures, excited state properties, and application in electroluminescent devices. *Eur. J. Inorg. Chem.* **2008**, 2177-2185; (c) Zanoni, K. P. S.; Kariyazaki, B. K.; Ito, A.; Brennaman, M. K.; Meyer, T. J.; Murakami Iha, N. Y.,

Blue-green iridium(III) emitter and comprehensive photophysical elucidation of heteroleptic cyclometalated iridium(III) complexes. *Inorg. Chem.* **2014,** *53*, 4089-4099; (d) Kuramochi, Y.; Ishitani, O., Iridium(III) 1-phenylisoquinoline complexes as a photosensitizer for photocatalytic CO_2 reduction: a mixed system with a Re(I) catalyst and a supramolecular photocatalyst. *Inorg. Chem.* **2016,** *55*, 5702-5709; (e) Kang, T. K.; Kang, C. H.; Lee, J.; Kim, S. H.; Kim, B. H.; Lee, W.-Y., Electrogenerated chemiluminescence from newly synthesized α-diimine-ligated heteroleptic iridium(III) complexes. *J. Electroanal. Chem.* **2016,** *775*, 83-90.

32. (a) Bronstein, H. A.; Finlayson, C. E.; Kirov, K. R.; Friend, R. H.; Williams, C. K., Investigation into the Phosphorescence of a Series of Regioisomeric Iridium(III) Complexes. *Organometallics* **2008,** *27*, 2980-2989; (b) Baranoff, E.; Curchod, B. F. E.; Frey, J.; Scopelliti, R.; Kessler, F.; Tavernelli, I.; Rothlisberger, U.; Gratzel, M.; Nazeeruddin, M. K., Acid-induced degradation of phosphorescent dopants for OLEDs and its application to the synthesis of tris-heteroleptic iridium(III) bis-cyclometalated complexes. *Inorg. Chem.* **2012,** *51*, 215-224; (c) Lepeltier, M.; Dumur, F.; Wantz, G.; Vila, N.; Mbomekalle, I.; Bertin, D.; Gigmes, D.; Mayer, C. R., Red phosphorescent organic light-emitting diodes (PhOLEDs) based on a heteroleptic cyclometalated Iridium (III) complex. *J. Lumin.* **2013,** *143*, 145-149; (d) Frey, J.; Curchod, B. F. E.; Scopelliti, R.; Tavernelli, I.; Rothlisberger, U.; Nazeeruddin, M. K.; Baranoff, E., Structure-property relationships based on Hammett constants in cyclometalated iridium(III) complexes: their application to the design of a fluorine-free FIrPic-like emitter. *Dalton Trans.* **2014,** *43*, 5667-5679.

33. (a) Lamansky, S.; Djurovich, P.; Murphy, D.; Abdel-Razzaq, F.; Kwong, R.; Tsyba, I.; Bortz, M.; Mui, B.; Bau, R.; Thompson, M. E., Synthesis and characterization of phosphorescent cyclometalated iridium complexes. *Inorg. Chem.* **2001,** *40*, 1704-1711;

(b) Liu, T.; Xia, B.-H.; Zhou, X.; Zheng, Q.-C.; Pan, Q.-J.; Zhang, H.-X., Theoretical studies of the spectroscopic properties of blue emitting iridium complexes. *Theor. Chem. Acc.* **2008,** *121*, 155-164; (c) Gu, X.; Fei, T.; Zhang, H.; Xu, H.; Yang, B.; Ma, Y.; Liu, X., Tuning the emission color of iridium(III) complexes with ancillary ligands: a combined experimental and theoretical study. *Eur. J. Inorg. Chem.* **2009**, 2407-2414; (d) Younker, J. M.; Dobbs, K. D., Correlating experimental photophysical properties of iridium(III) complexes to spin-orbit coupled TDDFT predictions. *J. Phys. Chem. C* **2013,** *117*, 25714-25723.

34. (a) Deaton, J. C.; Young, R. H.; Lenhard, J. R.; Rajeswaran, M.; Huo, S., Photophysical properties of the series fac- and mer-(1-phenylisoquinolinato-N^C$^{2'}$)$_x$(2-phenylpyridinato-N^C$^{2'}$)$_{3-x}$iridium(III) (x = 1-3). *Inorg. Chem.* **2010,** *49*, 9151-9161; (b) Wang, R.; Liu, D.; Ren, H.; Zhang, T.; Wang, X.; Li, J., Homoleptic tris-cyclometalated iridium complexes with 2-phenylbenzothiazole ligands for highly efficient orange OLEDs. *J. Mater. Chem.* **2011,** *21*, 15494-15500.

35. Jones, W. E., Jr.; Fox, M. A., Determination of excited-state redox potentials by phase-modulated voltammetry. *J. Phys. Chem.* **1994,** *98*, 5095-5099.

36. Wu, S.-H.; Ling, J.-W.; Lai, S.-H.; Huang, M.-J.; Cheng, C. H.; Chen, I. C., Dynamics of the Excited States of [Ir(ppy)$_2$bpy]$^+$ with Triple Phosphorescence. *J. Phys. Chem. A* **2010,** *114*, 10339-10344.

37. Valenti, G.; Rampazzo, E.; Bonacchi, S.; Petrizza, L.; Marcaccio, M.; Montalti, M.; Prodi, L.; Paolucci, F., Variable doping induces mechanism swapping in electrogenerated chemiluminescence of Ru(bpy)$_3^{2+}$ core−shell silica nanoparticles. *J. Am. Chem. Soc.* **2016,** *138*, 15935-15942.

38. Kanoufi, F.; Zu, Y.; Bard, A. J., Homogeneous oxidation of trialkylamines by metal complexes and its impact on electrogenerated chemiluminescence in the trialkylamine/Ru(bpy)$_3$$^{2+}$ system. *J. Phys. Chem. B* **2001,** *105*, 210-216.

39. (a) Stringer, B. D.; Quan, L. M.; Barnard, P. J.; Wilson, D. J. D.; Hogan, C. F., Iridium complexes of N-heterocyclic carbene ligands: investigation into the energetic requirements for efficient electrogenerated chemiluminescence. *Organometallics* **2014,** *33*, 4860-4872; (b) Quan, L. M.; Stringer, B. D.; Haghighatbin, M.; Agugiaro, J.; J. Barbante, G.; Wilson, D. J.; Hogan, C. F.; Barnard, P., Tuning the electrochemiluminescent properties of iridium complexes of N-heterocyclic carbene ligands. *Dalton Trans.* **2018**, Ahead of Print.

40. Truong, J.; Spilstead, K. B.; Barbante, G. J.; Doeven, E. H.; Wilson, D. J. D.; Barnett, N. W.; Henderson, L. C.; Altimari, J. M.; Hockey, S. C.; Zhou, M.; Francis, P. S., Chemiluminescence detection with water-soluble iridium(III) complexes containing a sulfonate-functionalised ancillary ligand. *Analyst* **2014,** *139*, 6028-6035.

41. Imai, K.; Valenti, G.; Villani, E.; Rapino, S.; Rampazzo, E.; Marcaccio, M.; Prodi, L.; Paolucci, F., Numerical simulation of doped silica nanoparticle electrochemiluminescence. *J. Phys. Chem. C* **2015,** *119*, 26111-26118.

42. O'Reilly, E. J.; Conroy, P. J.; Hearty, S.; Keyes, T. E.; O'Kennedy, R.; Forster, R. J.; Dennany, L., Electrochemiluminescence platform for the detection of C-reactive proteins: application of recombinant antibody technology to cardiac biomarker detection. *RSC Adv.* **2015,** *5*, 67874-67877.

43. Svir, I.; Oleinick, A.; Klymenko, O. V.; Amatore, C., Strong and unexpected effects of diffusion rates on the generation of electrochemiluminescence by amine/transition-metal(II) systems. *ChemElectroChem* **2015,** *2*, 811-818.

44. (a) Liu, X.; Shi, L.; Niu, W.; Li, H.; Xu, G., Environmentally friendly and highly sensitive ruthenium(II) tris(2,2'-bipyridyl) electrochemiluminescent system using 2-(dibutylamino)ethanol as co-reactant. *Angew. Chem., Int. Ed.* **2007,** *46*, 421-424; (b) Han, S.; Niu, W.; Li, H.; Hu, L.; Yuan, Y.; Xu, G., Effect of hydroxyl and amino groups on electrochemiluminescence activity of tertiary amines at low tris(2,2'-bipyridyl)ruthenium(II) concentrations. *Talanta* **2010,** *81*, 44-47; (c) Kebede, N.; Francis, P. S.; Barbante, G. J.; Hogan, C. F., Electrogenerated chemiluminescence of tris(2,2'-bipyridine)ruthenium(II) using common biological buffers as co-reactant, pH buffer and supporting electrolyte. *Analyst* **2015,** *140*, 7142-7145; (d) Kitte, S. A.; Wang, C.; Li, S.; Zholudov, Y.; Qi, L.; Li, J.; Xu, G., Electrogenerated chemiluminescence of tris(2,2'-bipyridine)ruthenium(II) using *N*-(3-aminopropyl)diethanolamine as coreactant. *Anal. Bioanal. Chem.* **2016,** *408*, 7059-7065; (e) Fiorani, A.; Irkham; Valenti, G.; Paolucci, F.; Einaga, Y., Electrogenerated chemiluminescence with peroxydisulfate as a coreactant using boron doped diamond electrodes. *Anal. Chem.* **2018,** *90*, 12959-12963.

45. Mallet, C.; Bolduc, A.; Bishop, S.; Gautier, Y.; Skene, W. G., Unusually high fluorescence quantum yield of a homopolyfluorenylazomethine – towards a universal fluorophore. *Phys. Chem. Chem. Phys.* **2014,** *16*, 24382-24390.

46. Wei, Y.; Yang, C.; Wei, B.; Huang, J.; Wang, L.; Meng, S.; Zhang, R.; Li, J., RNase-resistant virus-like particles containing long chimeric RNA sequences produced by two-plasmid coexpression system. *J. Clin. Microbiol.* **2008,** *46*, 1734-1740.

47. Spain, E.; Carrara, S.; Adamson, K.; Ma, H.; O'Kennedy, R.; Cola, L. D.; Forster, R. J., Cardiac troponin I: ultrasensitive detection using faradaic electrochemical impedance. *ACS Omega* **2018,** *3*, 17116-17124.

Chapter 5: Conclusions and future work

In Chapter 2, a series of iridium complexes that have been reported by researchers in the past with a wide range of reported ECL intensities relative to $Ru(bpy)_3^{2+}$ were re-examined. Experiments were carried out under a range of conditions to reconcile the factors that can contribute to ECL intensity and highlight the variability that can be introduced from the experimental method used to determine the ECL performance of a complex. This study revealed several sources for the large discrepancies in reported ECL intensity of the complexes relative to $Ru(bpy)_3^{2+}$, including possible decomposition of the complex, changes to the electrode surface, the influence of solvent and reactant concentration, as well as the instrumental setup and experimental approach. This work has shown the importance of considering all of these parameters in the evaluation of ECL luminophores.

In Chapter 3, a set of novel highly water-soluble iridium complexes containing polyethylene glycol (TEG) functionalized bipyridine (bpy) ligands were synthesized and their co-reactant ECL evaluated in aqueous solution. The introduction of one or two the TEG groups to the bpy ligand of iridium(III) complexes was shown to be a viable strategy to enhance the solubility of these complexes in aqueous solution while retaining the electrochemical and spectroscopic properties of the parent luminophore, and providing a convenient attachment point for the future development of ECL labels for bioconjugation in affinity based assays. The novel $[Ir(C\wedge N)_2(Me\text{-}bpy\text{-}TEG)]Cl$ and $[Ir(C\wedge N)_2(TEG\text{-}bpy\text{-}TEG)]Cl$ complexes exhibited ECL intensities close to those of $[Ru(bpy)_3]^{2+}$, indicating that these iridium complexes could be excellent ECL labels. Although iridium complex ECL labels with different emission colors have previously been generated by modification of the cyclometallating $(C\wedge N)$ ligands, this study showed a viable strategy to create two ECL-labels with similar ECL intensities and distinctly different emission colors from the same commercial $[Ir(C\wedge N)_2(\mu\text{-}Cl)]_2$ dimer.

In Chapter 4, a new approach to the development of iridium complex ECL labels incorporating a bioconjugatable squarate group was presented. This strategy provided not only a more convenient synthetic approach but also superior ECL intensities and a wider range of emission colors from red to blue. This study provided new insight into the key energy requirements of the competing ECL reactions with iridium complexes, which showed the fundamental limits on the redox potentials and emission wavelengths of complexes that can generate ECL through a mechanism involving oxidation of only the TPrA co-reactant. Most importantly in the context of developing multi-colour ECL systems, the 'window' of reduction potentials enabling this pathway becomes narrower as emission energy increases, and it does not extend across the entire visible region. This limitation is particularly important for bead-based assays, in which the generation of ECL is only feasible for certain iridium complexes meeting the energy requirements. Examination of a greater range of metal complexes with this approach will enable these energy boundaries to be clarified. The approaches outlined in this study should also be exploited to evaluate alternative co-reactants in conjunction with various metal complex luminophores, as previous studies have focused on $[\text{Ru(bpy)}_3]^{2+}$, and not under bioconjugated assay conditions.

The research presented in this thesis provides a new platform for the translation of iridium complexes showing promising ECL properties into real-world analytical applications. This work will continue with the application of the new ECL labels described in Chapters 3 and 4 in innovative highly sensitive, multi-color and/or potential-resolved ECL systems for a wide range of future analytical applications.

Appendices

Appendix I

Supporting Information: Co-reactant electrogenerated chemiluminescence of iridium(III) complexes containing an acetylacetonate ligand

Figure S2.1. Photoluminescence emission spectra of **Ir(ppy)₃**. Solid lines: low temperature (77 K); Dashed lines: room temperature. Grey lines: uncorrected; Coloured lines: corrected for the difference in instrumental sensitivity over the wavelength range. Details (r.t.): λ_{ex} = 350 nm; filters: Ex: 250-395 nm, Em: 430-1100 nm; concentration: 10 μM in acetonitrile. (77 K): λ_{ex} = 378 nm; filters: Ex: 250-395 nm, Em: 430-1100 nm; concentration: 5 μM in 4:1 (v/v) ethanol:methanol.

Figure S2.2. Photoluminescence emission spectra of **Ir(ppy)₂(acac)** in acetonitrile. Solid lines: low temperature (77 K); Dashed lines: room temperature. Grey lines: uncorrected; Coloured lines: corrected for the difference in instrumental sensitivity over the wavelength range. Details (r.t.): λ_{ex} = 350 nm; filters: Ex: 250-395 nm, Em: 430-1100 nm; concentration: 10 μM in acetonitrile. (77 K): λ_{ex} = 300 nm; filters: Ex: 250-395 nm, Em: 360-1100 nm; concentration: 5 μM in 4:1 (v/v) ethanol:methanol.

Figure S2.3. Photoluminescence emission spectra of **Ir(bt)₂(acac)** in acetonitrile. Solid lines: low temperature (77 K); Dashed lines: room temperature. Grey lines: uncorrected; Coloured lines: corrected for the difference in instrumental sensitivity over the wavelength range. Details (r.t.): λ_{ex} = 350 nm; filters: Ex: 250-395 nm, Em: 430-1100 nm; concentration: 10 μM in acetonitrile. (77 K): λ_{ex} = 329 nm; filters: Ex: 250-395 nm, Em: 360-1100 nm; concentration: 5 μM in 4:1 (v/v) ethanol:methanol.

Figure S2.4. Photoluminescence emission spectra of **Ir(pq)₂(acac)** in acetonitrile. Solid lines: low temperature (77 K); Dashed lines: room temperature. Grey lines: uncorrected; Coloured lines: corrected for the difference in instrumental sensitivity over the wavelength range. Details (r.t.): λ_{ex} = 350 nm; filters: Ex: 250-395 nm, Em: 430-1100 nm; concentration: 10 µM in acetonitrile. (77 K): λ_{ex} = 345 nm; filters: Ex: 250-395 nm, Em: 430-1100 nm; concentration: 5 µM in 4:1 (v/v) ethanol:methanol.

Figure S2.5. Photoluminescence emission spectra of **[Ru(bpy)$_3$](PF$_6$)$_2$** in acetonitrile. Solid lines: low temperature (77 K); Dashed lines: room temperature. Grey lines: uncorrected; Coloured lines: corrected for the difference in instrumental sensitivity over the wavelength range. Details (r.t.): λ_{ex} = 450 nm; filters: Ex: 335-620 nm, Em: 430-1100 nm; concentration: 10 μM in acetonitrile (500-800 nm shown). (77 K): λ_{ex} = 292 nm; filters: Ex: 250-395 nm, Em: 430-1100; concentration: 5 μM in 4:1 (v/v) ethanol:methanol.

Figure S2.6. BP86/def2-TZVP ground-state singlet molecular orbital surfaces.

	Ir(ppy)$_3$	Ir(ppy)$_2$(acac)	Ir(bt)$_2$(acac)	Ir(pq)$_2$(acac)	[Ru(bpy)$_3$]$^{2+}$
LUMO					
HOMO					
HOMO-1					
HOMO-2					

Figure S2.7. BP86/def2-TZVP calculated triplet spin density surfaces.

Ir(ppy)$_3$	Ir(ppy)$_2$(acac)	Ir(bt)$_2$(acac)	Ir(pq)$_2$(acac)	[Ru(bpy)$_3$]$^{2+}$

Figure S2.8. Contribution of metal centre to LUMO in: (1) Ir(ppy)$_3$; (2) Ir(ppy)$_2$(acac); (3) Ir(bt)$_2$(acac); (4) Ir(pq)$_2$(acac); and (5) [Ru(bpy)$_3$]$^{2+}$.

Figure S2.9. Comparison of energies of: HOMO-LUMO gap; room temperature ECL (at λ_{max}); low temperature photoluminescence (at λ_{max}); and electrochemical ΔE (oxidation-reduction potentials); for (1) Ir(ppy)$_3$; (2) Ir(ppy)$_2$(acac); (3) Ir(bt)$_2$(acac); (4) Ir(pq)$_2$(acac); and (5) [Ru(bpy)$_3$]$^{2+}$. The HOMO-LUMO gaps were found to be strongly dependent on the proportion of Hartree-Fock exchange in the functional. As a result, the BP86 results (pure exchange-correlation functional without Hartree-Fock exchange) shown here represent a lower bound of DFT calculated values.

Appendix II

Supporting Information: A conceptual framework for the development of iridium(III) complex-based electrogenerated chemiluminescence labels

Scheme 1. Additional ECL pathways

Synthesis and characterization

    $[Ir(C\wedge N)_2(dm\text{-}bpy)](PF_6)$ and $[Ir(C\wedge N)_2(ptb)](PF_6)$ complexes

    $[Ir(C\wedge N)_2(pt\text{-}TEG)]Cl$ complexes

    pt-TOxT-Sq ligand

    $[Ir(C\wedge N)_2(pt\text{-}TOxT\text{-}Sq)]^+$ ECL labels

Additional data for $Ir(C\wedge N)_2(acac)$, $[Ir(C\wedge N)_2(dm\text{-}bpy)]^+$, $[Ir(C\wedge N)_2(ptb)]^+$, and $[Ir(C\wedge N)_2(pt\text{-}TEG)]^+$

    Figure S4.1. UV-Vis absorption spectra

    Figures S4.2-S4.5. Ambient and low temperature photoluminescence emission spectra

    Figure S4.6. Cyclic voltammograms

    Tables S4.1-S4.4. Calculated MO energies

    Figure S4.7. Contribution to the respective MOs

    Table S4.5-S4.6. Contour plots

    Figure S4.8. ECL intensity during potential sweeps

Figure S4.9. Photoluminescence emission spectra of ECL labels

Table S4.7. Primers and NASBA amplicon fragment sequences

Figure S4.10. 3D drawing and photograph of the custom screen-printed electrode (SPE) holder

Figure S4.11. Photograph of the cell holder

NMR spectra

Scheme S4.1. (a) The 'catalytic route' of co-reactant ECL involving oxidation of TPrA by M^+, and (b) an alternative ECL pathway[1] in which the excited state is generated from the reaction between M^+ and M^-. The contribution of these pathways to the overall emission intensity is expected to be small when low concentrations of the metal complex are used.

Synthesis of [Ir(C^N)₂(dm-bpy)](PF₆) and [Ir(C^N)₂(ptb)](PF₆) complexes

Reagents and solvents were purchased from commercial sources and used without further purification. The iridium(III) dimer precursors were purchased from SunaTech (China). NMR spectra were acquired on a Bruker Biospin AV400 spectrometer. ^{1}H NMR spectra were acquired at 400 MHz, and ^{13}C{^{1}H} NMR spectra were acquired at 100 MHz. All NMR spectra were recorded at 298 K. Chemical shifts were referenced to residual solvent peaks and are quoted in terms of parts per million (ppm), relative to tetramethylsilane (Si(CH₃)₄). Electrospray ionization mass spectra (ESI-MS) were acquired using a Thermo Scientific Exactive Plus Orbitrap Mass Spectrometer.

[Ir(piq)₂(dm-bpy)](PF₆): The dimer [Ir(piq)₂(μ-Cl)]₂ (150 mg, 118 μmol) and 4,4′-dimethyl-2,2′-bipyridine (50 mg, 271 μmol) were suspended in a 3:1 mixture of dichloromethane and methanol and heated at reflux whilst stirred in darkness under an inert atmosphere for 16 h. The solution was cooled to ambient temperature and a large excess of KPF₆ was added and the mixture stirred for a further 24 h. The mixture was filtered to remove solid KPF₆ and the filtrate was concentrated under reduced pressure. The residue was redissolved in a minimum amount of acetonitrile and filtered through filter aid (Celite). To this solution was added a saturated aqueous solution of ammonium hexafluorophosphate until precipitation of a brightly colored solid began to occur. The mixture was allowed to stir in darkness for 16 h, and the product then collected by filtration and washed with water, cold ethanol and diethyl ether to yield the product as a dark brown precipitate (114 mg, 52%). ^{1}H NMR (400 MHz; CD₂Cl₂): δ 8.98 (m, 1H), 8.32 (m, 2H), 7.92 (m, 1H), 7.80 (m, 2H), 7.68 (d, J = 5.8 Hz, 1H), 7.41 (d, J = 6.4 Hz, 1H), 7.34 (d, J = 6.4 Hz, 1H), 7.20 (1H, J = 5.1 Hz, d), 7.14 (t, J = 7.6 Hz 1H), 6.90 (t, J = 7.4 Hz, 1H), 6.34 (d, J = 8.1 Hz, 1H), 2.57 (s, 3H). ESI-MS (positive ion). Calcd for C₄₂H₃₂IrN₄ ([M]$^+$): m/z 785.226. Found m/z 785.2264.

[Ir(bt)₂(dm-bpy)](PF₆): The dimer [Ir(bt)$_2$(μ-Cl)]$_2$ (150 mg, 116 μmol) and 4,4′-dimethyl-2,2′-bipyridine (47 mg, 255 μmol) were suspended in a 3:1 mixture of dichloromethane and methanol and heated at reflux whilst stirred in darkness under an inert atmosphere for 16 h. The solution was cooled to ambient temperature and a large excess of KPF₆ was added and the mixture stirred for a further 24 h. The mixture was filtered to remove solid KPF₆ and the filtrate was concentrated under reduced pressure. The crude product was then recrystallized from ethanol to yield the product as an orange solid (119 mg, 54%). ^{1}H NMR (400 MHz; CD$_2$Cl$_2$): δ 8.23 (s, 1H), 7.95 (d, J = 5.6 Hz, 1H), 7.90 (d, J = 8.0 Hz, 1H), 7.85 (d, J = 7.6 Hz, 1H), 7.37 (t, J = 7.4 Hz, 1H), 7.30 (d, J = 5.6 Hz, 1H), 7.09-7.14 (m, 2H), 6.88 (td, J = 7.5, 1.2 Hz, 1H), 6.41 (d, J = 7.6 Hz, 1H), 6.24 (d, J = 8.4 Hz, 1H), 2.59 (s, 3H). ^{13}C{^{1}H} NMR (100 MHz; CD$_2$Cl$_2$): δ 181.8, 156.8, 153, 150.9, 150.7, 149.8, 140.8, 133.9, 132.6, 132.1, 129.6, 128.6, 127.3, 126.5, 125.6, 124, 123.7, 118.3, 21.8. ESI-MS (positive ion). Calcd for C$_{38}$H$_{28}$IrN$_4$S$_2^+$ ([M]$^+$): m/z 797.139. Found m/z 757.1393.

[Ir(ppy)₂(dm-bpy)](PF₆): The dimer [Ir(ppy)$_2$(μ-Cl)]$_2$ (150 mg, 140 μmol) and 4,4′-dimethyl-2,2′-bipyridine (57 mg, 309 μmol) were suspended in a 3:1 mixture of dichloromethane and methanol and heated at reflux whilst stirred in darkness under an inert atmosphere for 16 h. The solution was cooled to ambient temperature and a large excess of KPF₆ was added and the mixture stirred for a further 24 h. The mixture was filtered to remove solid KPF₆ and the filtrate was concentrated under reduced pressure. The crude product was then recrystallized from isopropanol to yield the product as a pale yellow solid (181 mg, 78%). ^{1}H NMR (400 MHz; CD$_2$Cl$_2$): δ 8.31 (s, 1H), 7.95 (d, J = 8.2 Hz, 1H), 7.82 (d, J = 5.6 Hz, 1H), 7.78 (td, J = 7.8, 1.5 Hz, 1H), 7.73 (dd, J = 7.8, 0.9 Hz, 1H), 7.51 (d, J = 5.7 Hz, 1H), 7.23 (d, J = 5.5 Hz, 1H), 7.06 (td, J = 7.5, 1.1 Hz, 1H), 7.00 (ddd, J = 7.4, 5.9, 1.4 Hz, 1H), 6.92 (td, J = 7.5, 1.4 Hz, 1H), 6.32 (d, J = 7.6 Hz, 1H), 2.58 (s, 3H). ESI-MS (positive ion). Calcd for C$_{34}$H$_{28}$IrN$_4$ ([M]$^+$): m/z 685.194. Found m/z 685.1949.

[Ir(df-ppy)$_2$(dm-bpy)](PF$_6$): The dimer [Ir(df-ppy)$_2$(μ-Cl)]$_2$ (150 mg, 123 μmol) and 4,4′-dimethyl-2,2′-bipyridine (50 mg, 271 μmol) were suspended in a 3:1 mixture of dichloromethane and methanol and heated at reflux whilst stirred in darkness under an inert atmosphere for 16 h. The solution was cooled to ambient temperature and a large excess of KPF$_6$ was added and the mixture stirred for a further 24 h. The mixture was filtered to remove solid KPF$_6$ and the filtrate was concentrated under reduced pressure. The crude product was then recrystallized from isopropanol to yield the product as a pale yellow solid (165 mg, 74%). ^{1}H NMR (400 MHz; CD$_2$Cl$_2$): δ 8.37 (s, 1H), 8.32 (d, J = 8.4 Hz, 1H), 7.82 (m, 2H), 7.50 (d, J = 5.7 Hz, 1H), 7.29 (d, J = 5.7 Hz, 1H), 7.05 (m, 1H), 6.62 (ddd, J = 12.5, 9.2, 2.4 Hz, 1H), 5.75 (dd, J = 8.4, 2.3 Hz, 1H), 2.61 (s, 3H). ESI-MS (positive ion). Calcd for C$_{34}$H$_{24}$F$_4$IrN$_4$$^+$ ([M]$^+$): m/z 757.157. Found m/z 757.1575.

[Ir(piq)$_2$(ptb)](PF$_6$): This complex was synthesized according to the previously published procedure.[2] The dimer [Ir(piq)$_2$(μ-Cl)]$_2$ (150 mg, 118 μmol) and 2-(1-(benzyl)-1H-1,2,3-triazol-4-yl)pyridine (56 mg, 236 μmol) were suspended in a 3:1 mixture of dichloromethane and methanol. Starting materials typically solubilized within 1 h. Reactions were stirred in darkness under an inert atmosphere for 16 h. The solvents were then removed, and the residue dissolved in acetonitrile and filtered through a filter aid (Celite). The solvent was then removed by evaporation under reduced pressure and the residue redissolved in a minimum amount of ethanol and filtered through filter aid (Celite). To this solution was added a saturated aqueous solution of ammonium hexafluorophosphate until precipitation of a brightly colored solid began to occur. The mixture was allowed to stir in darkness for 16 h, and the product was then collected by filtration and washed with water, cold ethanol, ether, and lastly pentane, and then dried *in vacuo* to yield the product as an orange solid (153 mg, 66 %). ^{1}H NMR spectra was consistent with the literature values. ^{1}H NMR (400 MHz; CD$_2$Cl$_2$): δ 9.00 (m, 2H), 8.62 (s, 1H), 8.33 (m, 2H), 8.12 (d, J = 7.9 Hz, 1H), 7.91-8.00 (m,

3H), 7.84-7.99 (m, 4H), 7.69 (d, J = 5.6 Hz, 1H), 7.60 (d, J = 6.4 Hz, 1H), 7.39 (t, J = 6.9 Hz, 2H), 7.09-7.33 (m, 9H), 6.93 (t, J = 7.4 Hz, 1H), 6.84 (t, J = 7.4 Hz, 1H), 6.51 (d, J = 7.6 Hz, 1H), 6.32 (d, J = 7.6 Hz, 1H), 5.57 (s, 2H). ESI-MS (positive ion). Calcd for $C_{44}H_{32}IrN_6^+$ ([M]$^+$): m/z 837.231. Found m/z 837.2410.

[Ir(bt)$_2$(ptb)](PF$_6$): The dimer [Ir(bt)$_2$(μ-Cl)]$_2$ (150 mg, 116 μmol) and 2-(1-(benzyl)-1H-1,2,3-triazol-4-yl)pyridine (55 mg, 232 μmol) were suspended in a 3:1 mixture of dichloromethane and methanol. Starting materials typically solubilized within 1 h. Reactions were stirred in darkness under an inert atmosphere for 16 h. The solvents were then removed and the residue dissolved in acetonitrile and filtered through a filter aid (Celite). The solvent was then removed by evaporation under reduced pressure and the residue redissolved in a minimum amount of ethanol and filtered through filter aid (Celite). To this solution was added a saturated aqueous solution of ammonium hexafluorophosphate until precipitation of a brightly colored solid began to occur. The mixture was allowed to stir in darkness for 16 h, and the product was then collected by filtration and washed with water, cold ethanol, ether, and lastly pentane, and then dried *in vacuo* to yield the product as a dark yellow solid (191 mg, 83%). ^{1}H NMR (400 MHz; CD$_2$Cl$_2$): δ 8.67 (s, 1H), 8.06 (dq, J = 8.0, 0.8 Hz, 1H), 8.00 (td, J = 7.8, 1.6 Hz, 1H), 7.94 (dq, J = 5.5, 0.8 Hz, 1H), 7.90 (dq, J = 8.1, 0.6 Hz, 1H), 7.87 (dq, J = 8.1, 0.6 Hz, 1H), 7.84 (m, 1H), 7.80 (m, 1H), 7.32-7.43 (m, 6H), 7.25-7.29 (m, 2H), 7.11 (td, J = 7.6, 1.2 Hz, 1H), 7.03-7.08 (m, 2H), 6.95 (ddd, J = 8.5, 7.3, 1.3 Hz, 1H), 6.88 (td, J = 7.6, 1.5 Hz, 1H), 6.82 (td, J = 7.6, 1.5 Hz, 1H), 6.48 (d, J = 7.7 Hz, 1H), 6.40 (d, J = 8.4 Hz, 1H), 6.37 (d, J = 7.8 Hz, 1H), 6.08 (d, J = 8.3 Hz, 1H), 5.65 (d, J = 14.8 Hz, 1H), 5.55 (d, J = 14.8 Hz, 1H). ^{13}C{^{1}H}

NMR (100 MHz; CD$_2$Cl$_2$): δ 182.2, 181.3, 151.1, 150.6, 150.2, 150.0, 149.7 (2C), 146.4, 141.3, 140.9, 140.6, 134.2, 134.0 (2C), 132.5, 132.0 (2C), 131.9, 129.9 (2C), 129.8, 128.6 (3C), 128.5, 127.3, 127.2, 126.7, 126.6, 126.4 (2C), 124.0, 123.9, 123.8, 123.5, 123.4, 118.7,

118.0, 56.5. ESI-MS (positive ion). Calcd for $C_{40}H_{28}IrN_6S_2^+$ ([M]$^+$): m/z 849.144. Found m/z 849.1458.

[Ir(ppy)$_2$(ptb)](PF$_6$): This complex was synthesized according to the previously published procedure.[2] The dimer [Ir(ppy)$_2$(μ-Cl)]$_2$ (150 mg, 140 μmol) and 2-(1-(benzyl)-1H-1,2,3-triazol-4-yl)pyridine (66 mg, 280 μmol) were suspended in a 3:1 mixture of dichloromethane and methanol. Starting materials typically solubilized within 1 h. Reactions were stirred in darkness under an inert atmosphere for 16 h. The solvents were then removed and the residue dissolved in acetonitrile and filtered through a filter aid (Celite). The solvent was then removed by evaporation under reduced pressure and the residue redissolved in a minimum amount of ethanol and filtered through filter aid (Celite). To this solution was added a saturated aqueous solution of ammonium hexafluorophosphate until precipitation of a brightly colored solid began to occur. The mixture was allowed to stir in darkness for 16 h, and the product was then collected by filtration and washed with water, cold ethanol, ether, and lastly pentane, and then dried *in vacuo* to yield the product as a yellow solid (197 mg, 80%). ^{1}H NMR spectra was consistent with the literature values. ^{1}H NMR (400 MHz; CD$_2$Cl$_2$): δ 8.62 (s, 1H), 8.11 (d, J = 7.9 Hz, 1H), 7.99 (dt, J = 7.9, 1.6 Hz, 1H), 7.95 (t, 8.8 Hz, 2H), 7.76-7.84 (m, 3H), 7.69-7.74 (m, 2H), 7.67 (d, J = 5.8 Hz, 1H), 7.49 (d, J = 5.8 Hz, 1H), 7.38-7.42 (m, 3H), 7.26-7.34 (m, 3H), 7.00-7.09 (m, 3H), 6.98 (ddd, J = 7.5, 5.8, 1.4 Hz, 1H), 6.93 (td, J = 7.5, 1.3 Hz, 1H), 6.88 (td, J = 7.5, 1.3 Hz, 1H), 6.32 (dd, J = 7.7, 0.6 Hz, 1H), 6.31 (dd, J = 7.6, 0.8 Hz, 1H), 5.62 (m, 2H). ESI-MS (positive ion). Calcd for $C_{36}H_{28}IrN_6^+$ ([M]$^+$): m/z 737.200. Found m/z 737.2012.

[Ir(df-ppy)$_2$(ptb)](PF$_6$): This complex was synthesized according to the previously published procedure.[2] The dimer [Ir(df-ppy)$_2$(μ-Cl)]$_2$ (100 mg, 82 μmol) and 2-(1-(benzyl)-1H-1,2,3-triazol-4-yl)pyridine (39 mg, 165 μmol) were suspended in a 3:1 mixture of dichloromethane and methanol. Starting materials typically solubilized within 1 h. Reactions

were stirred in darkness under an inert atmosphere for 16 h. The solvents were then removed and the residue dissolved in acetonitrile and filtered through a filter aid (Celite). The solvent was then removed by evaporation under reduced pressure and the residue redissolved in a minimum amount of ethanol and filtered through filter aid (Celite). To this solution was added a saturated aqueous solution of ammonium hexafluorophosphate until precipitation of a brightly colored solid began to occur. The mixture was allowed to stir in darkness for 16 h, and the product was then collected by filtration and washed with water, cold ethanol, ether, and lastly pentane, and then dried *in vacuo* to yield the product as a yellow solid (126 mg, 80%). ^{1}H NMR spectra was consistent with the literature values. ^{1}H NMR (400 MHz; CDCl$_3$): δ 8.80 (s, 1H), 8.30 (t, J = 10.5 Hz, 2H), 8.22 (d, J = 7.9 Hz, 1H), 8.00 (td, J = 7.9, 1.5 Hz, 1H), 7.79-7.83 (m, 3H), 7.61 (d, J = 5.8 Hz, 1H), 7.45 (d, J = 5.8 Hz, 1H), 7.36 (s, 5H), 7.32 (m, 1H), 7.11 (ddd, J = 7.3, 5.9, 1.3 Hz, 1H), 7.01 (ddd, J = 7.3, 5.9, 1.3 Hz, 1H), 6.55 (m, 2H), 5.73 (dd, J = 8.5, 2.5 Hz, 1H), 5.68 (dd, J = 8.5, 2.3 Hz, 1H), 5.58 (s, 2H). ESI-MS (positive ion). Calcd for C$_{36}$H$_{24}$F$_4$IrN$_6^+$ ([M]$^+$): m/z 808.162. Found m/z 808.1638.

Synthesis of pt-TEG ligand and [Ir(C^N)$_2$(pt-TEG)]Cl complexes

The iridium(III) dimer precursors were purchased from SunaTech (China). The ligand pt-TEG was synthesized according to the previously reported procedure.[3] Nuclear magnetic resonance (NMR) spectra were acquired on a Jeol 400 spectrometer or a Bruker Ascend 500 spectrometer. ^{1}H NMR spectra were acquired at 400 MHz or 500 MHz, ^{13}C{^{1}H} NMR spectra were acquired at 101 MHz or 126 MHz, and ^{19}F NMR acquired at 471 MHz. All NMR spectra were recorded at 298 K. ^{1}H and ^{13}C{^{1}H} chemical shifts are referenced to residual solvent peaks and quoted in ppm relative to TMS. ^{19}F NMR signals are quoted relative to an internal standard of trifluoroacetic acid. HRMS spectra were recorded on an Agilent 6510 ESI-TOF LC/MS Mass Spectrometer.

2-(2-(2-(2-hydroxyethoxy)ethoxy)ethoxy)ethyl 4-methylbenzenesulfonate:
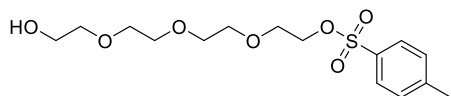
A solution of sodium hydroxide (0.70 g, 17.5 mmol) in H_2O (4 mL) was added to a solution of tetraethylene glycol (20 mL, 116 mmol) in THF (4 mL, 0 °C). A mixture of tosyl chloride (2.12 g, 11.1 mmol) in THF (4 mL) was added dropwise over 1 h to the mixture and was stirred for a further 3.5 h at 0 °C. The mixture was added to iced water (100 mL) and extracted with DCM (3 ×50 mL). The combined organic extracts were washed (H_2O, 2 ×30 mL) then dried ($MgSO_4$) and the solvent was removed under reduced pressure to afford a slightly yellow oil (3.66g, 91%), ^{1}H NMR (400 MHz; $CDCl_3$): δ 7.81-7.79 (m, 2H, Ar*H*), 7.35-7.33 (m, 2H, Ar*H*), 4.17-4.15 (m, 2H, C*H*$_2$), 3.72-3.58 (m, 15H, C*H*$_2$), 2.44 (s, 3H, C*H*$_3$). ^{13}C{^{1}H} NMR (101 MHz; $CDCl_3$): δ 144.9, 133.0, 129.9, 128.1, 72.5, 70.8, 70.7, 70.6, 70.4, 69.3, 68.8, 61.8, 21.7.

2-(2-(2-(2-azidoethoxy)ethoxy)ethoxy)ethan-1-ol:
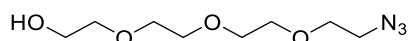
A mixture of the product above (3.56 g, 9.83 mmol) and sodium azide (1.47 g, 22.6 mmol) in ethanol (60 mL) was stirred at 70 °C for 16 h. The solution was let cool to ambient temperature before H_2O (50 mL) was added and the solvent volume was reduced under reduced pressure. The aqueous mixture was extracted with ethyl acetate (3 ×50 mL) and the combined organic extracts were dried ($MgSO_4$). The solvent was removed under reduced pressure and the residue purified by column chromatography (SiO_2, 100% DCM → 5% MeOH) to afford a slightly yellow oil (1.30g, 60%). ^{1}H NMR (400 MHz; $CDCl_3$): δ 3.68 (t, *J* = 4.6 Hz, 2H), 3.64 (m, 10H), 3.57 (t, *J* = 4.6 Hz, 2H), 3.36 (t, *J* = 5.0 Hz, 2H), 2.77 (s, 1H). ^{13}C{^{1}H} NMR (101 MHz; $CDCl_3$): δ 72.6, 70.7, 70.7, 70.6, 70.3, 70.0, 61.7, 50.7.

pt-TEG:[3b]
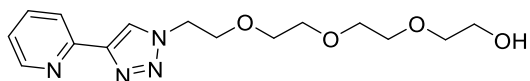
To a solution of the azide (0.57 g, 2.6 mmol) in a 2:1 mixture of DMSO/H$_2$O (3 mL) was added 2-ethynylpyridine (0.33 g, 3.23 mmol), CuSO$_4$.5H$_2$O (15 mg, 2 mol%) and sodium ascorbate (0.10 g, 20 mol%). The mixture was stirred at ambient temperature for 20 h before the reaction was quenched by addition of 1M EDTA in NH$_4$OH (50 mL). The mixture was extracted with DCM (3 × 50 mL) and the combined organic extracts were dried (MgSO$_4$) and the solvent was removed under reduced pressure. The residue was purified by column chromatography (SiO$_2$, 100% DCM → 5% MeOH) to afford a yellow oil (0.50 g, 60%). ^{1}H NMR (400 MHz; CDCl$_3$) δ 8.56 (ddd, J = 4.9, 1.8, 1.0 Hz, 1H), 8.41 (s, 1H), 8.18 (dt, J = 8.0, 1.1 Hz, 1H), 7.81 – 7.75 (m, 1H), 7.23 (ddd, J = 7.5, 4.9, 1.2 Hz, 1H), 4.64 – 4.59 (m, 2H), 3.92 (dd, J = 5.4, 4.8 Hz, 2H), 3.72 (dd, J = 5.3, 3.9 Hz, 2H), 3.67 – 3.57 (m, 10H). ^{13}C{^{1}H} NMR (101 MHz, CDCl$_3$) δ 150.3, 149.1, 147.8, 137.5, 123.8, 123.0, 120.6, 72.7, 70.8, 70.7, 70.6, 70.4, 69.6, 61.8, 50.6.

[Ir(piq)$_2$(pt-TEG)]Cl: The dimer [Ir(piq)$_2$(μ-Cl)]$_2$ (229 mg, 0.2 mmol) and the ligand pt-TEG (117 mg, 0.4 mmol) were suspended in a stirred solution of dichloromethane and methanol (3:1 v/v, 10 mL). Full dissolution occurred within 1 h and the solution was allowed to stir in the dark for 14 h. The solution was concentrated under reduced pressure and the residue was taken up in a minimum of dichloromethane then diethyl ether was added until the mixture became cloudy. The mixture was stored at -20 °C overnight to afford an orange powder. The solid was isolated by filtration, washed with diethyl ether and dried *in vacuo* to afford an orange powder (189 mg, 56%). ^{1}H NMR (400 MHz; CDCl$_3$): δ 10.38 (s, 1H), 9.02 (d, J = 7.9 Hz, 1H), 8.95 (ddd, J = 10.5, 6.9, 3.4 Hz, 2H), 8.24 (dd, J = 10.4, 5.9 Hz, 2H), 8.01 (td, J = 7.8, 1.5 Hz, 1H), 7.93-7.87 (m, 2H), 7.79-7.72 (m, 4H), 7.58-7.53

(m, 2H), 7.41-7.37 (m, 2H), 7.32-7.28 (m, 1H), 7.18-7.14 (m, 1H), 7.12-7.08 (m, 1H), 7.06-7.02 (m, 1H), 6.90-6.86 (m, 1H), 6.83-6.79 (m, 1H), 6.39 (dd, J = 7.7, 1.1 Hz, 1H), 6.30-6.28 (m, 1H), 4.70-4.61 (m, 2H), 3.94 (ddd, J = 13.0, 6.4, 4.2 Hz, 1H), 3.71 (dd, J = 6.0, 3.0 Hz, 2H), 3.64-3.45 (m, 11H). $^{13}C\{^{1}H\}$ NMR (101 MHz; CDCl$_3$): δ 169.6, 168.8, 153.7, 150.2, 150.1, 149.6, 148.4, 145.8, 145.6, 141.4, 140.5, 139.9, 137.2, 137.1, 132.6, 132.5, 131.7, 131.7, 130.8, 130.6, 130.3, 130.1, 129.3, 128.7, 128.6, 127.7, 127.5, 127.2, 126.9, 126.4, 125.9, 124.9, 122.3, 122.0, 121.0, 121.5, 77.4, 72.8, 70.6, 70.6, 70.4, 70.2, 68.4, 61.5, 52.0. ESI-MS (positive ion). Calcd for C$_{45}$H$_{42}$IrN$_6$O$_4^+$ ([M]$^+$): m/z 923.29. Found m/z 923.2500.

[Ir(bt)$_2$(pt-TEG)]Cl: The dimer [Ir(bt)$_2$(μ-Cl)]$_2$ (247 mg, 0.2 mmol) and the ligand pt-TEG (124 mg, 0.4 mmol) were stirred in a mixture of dichloromethane and methanol (3:1 v/v, 10 mL) and the solution was allowed to stir in the dark for 14 h. Some solid was still present and was removed by centrifugation and the supernatant was decanted off and retained. The supernatant was concentrated under reduced pressure and the residue was taken up in a minimum of dichloromethane then PET spirits (bp 40-60 °C) was added until the mixture became cloudy. The mixture was stored at -20 °C overnight to afford a yellow crystalline solid. The solid was isolated by filtration, washed with PET spirits and dried *in vacuo* to afford a yellow crystalline powder (154 mg, 42%). ^{1}H NMR (400 MHz; DMSO-d$_6$): δ 9.40 (s, 1H), 8.44 (d, J = 8.0 Hz, 1H), 8.25 (m, 3H,), 8.01 (d, J = 7.7 Hz, 1H), 7.91 (d, J = 7.6 Hz, 1H,), 7.87 (d, J = 5.5 Hz, 1H), 7.66 (m, 1H), 7.46 (m, 1H), 7.42 (m, 1H), 7.29 (m, 1H), 7.14 (m, 2H), 7.02 (m, 1H), 6.93 (m, 1H), 6.83 (m, 1H), 6.35 (m, 2H), 6.28 (d, J = 7.7 Hz, 1H), 6.08 (d, J = 8.4 Hz, 1H), 4.73 (m, 2H), 3.82 (m, 2H), 3.45 (m, 13H,). $^{13}C\{^{1}H\}$ NMR (101 MHz; DMSO-d$_6$): δ 181.5, 180.8, 150.0, 149.7, 148.7, 148.5, 148.4, 146.6, 140.8, 140.4, 140.2, 132.9, 132.8, 132.0, 131.3, 131.2 (2C), 131.2, 128.3, 128.0, 127.6, 127.3, 127.0, 126.4, 126.1, 125.9, 124.7, 124.6, 123.2, 122.8, 122.7, 117.5, 116.6, 72.3, 69.7, 69.6, 69.6,

69.6, 68.4, 60.1, 51.9. ESI-MS (positive ion). Calcd for $C_{41}H_{38}IrN_6O_4S_2^+$ ([M]$^+$): m/z 935.20. Found m/z 935.1620.

[Ir(ppy)$_2$(pt-TEG)]Cl: The chlorido-bridged dimer [Ir(ppy)$_2$(μ-Cl)]$_2$ (132 mg, 123 μmol) and the ligand pt-TEG (80 mg, 247 μmol) were suspended in a stirred solution of dichloromethane and methanol (3:1 v/v, 5 mL). Full dissolution occurred within 1 h and the solution was allowed to stir in the dark for 14 h. The solvent was removed under reduced pressure and the residue redissolved in acetonitrile (3 mL) and filtered through Celite filter aid. The filtrate was evaporated under reduced pressure to dryness and diethyl ether (20 mL) added. The suspension was sonicated for 15 min and the precipitate collected by filtration and copiously washed with diethyl ether and pentane. The crude solid was purified *via* silica gel chromatography with a gradient of methanol (0-10%) in dichloromethane. The collated fractions were evaporated under reduced pressure and to yield the product as a yellow powder (188 mg, 89%). ^{1}H NMR (500 MHz; CDCl$_3$): δ 10.46 (s, 1H), 9.04 (d, J = 8.0 Hz, 1H), 8.04 (td, J = 7.8, 1.5 Hz, 1H), 7.90 (m, 2H), 7.78-7.74 (m, 3H), 7.70 (dd, J = 5.8, 0.7 Hz, 1H), 7.67-7.64 (m, 2H), 7.50 (dd, J = 5.8, 0.7 Hz, 1H), 7.22 (ddd, J = 7.6, 5.6, 1.3 Hz, 1H), 7.07 (ddd, J = 7.3, 5.9, 1.4 Hz, 1H), 7.03 (td, J = 7.5, 1.0 Hz, 1H), 7.00-6.97 (m, 2H), 6.91 (td, J = 7.4, 1.2 Hz, 1H), 6.87 (td, J = 7.4, 1.2 Hz, 1H), 4.77-4.68 (m, 2H), 4.05-3.99 (m, 2H), 3.76-3.66 (m, 4H), 3.68-3.57 (m, 8H). ^{13}C NMR (126 MHz; CDCl$_3$): δ 168.4, 167.6, 150.3, 150.1, 149.5, 149.4, 148.5, 148.4, 146.6, 143.8, 143.6, 139.8, 137.8, 137.7, 131.9, 131.7, 130.6, 130, 129.3, 125.8, 124.7, 124.6, 124.2, 123.3, 122.8, 122.6, 122.1, 119.4, 119.3, 72.6, 70.5 (2C), 70.4, 70.1, 68.3, 61.4, 51.8. ESI-MS (positive ion). Calcd for $C_{37}H_{42}N_6O_4Ir^+$ ([M]$^+$): m/z 823.258. Found m/z 823.2571.

[Ir(df-ppy)$_2$(pt-TEG)]Cl: The chlorido-bridged dimer [Ir(df-ppy)$_2$(μ-Cl)]$_2$ (340 mg, 280 μmol) and the ligand pt-TEG (182 mg, 564 μmol) were suspended in a stirred solution of dichloromethane and methanol (3:1 v/v, 5 mL). Full dissolution occurred within 1 h and

the solution was allowed to stir in the dark for 14 h. The solvent was removed under reduced pressure and the residue redissolved in acetonitrile (3 mL) and filtered through Celite filter aid. The filtrate was evaporated under reduced pressure to dryness and diethyl ether (20 mL) added. The suspension was sonicated for 15 min and the precipitate collected by filtration and copiously washed with diethyl ether and pentane. The solid was dried *in vacuo* to give the complex as a light-yellow powder (380 mg, 73%). ^{1}H NMR (500 MHz; CDCl$_3$): δ 9.16 (s, 1H), 8.40 (d, J = 8.0 Hz, 1H), 8.28 (t, J = 10.0 Hz, 2H), 8.01 (t, J = 7.8 Hz, 1H), 7.80 (m, 3H), 7.65 (d, J = 5.7 Hz, 1H), 7.50 (d, J = 5.7 Hz, 1H), 7.31 (t, J = 6.6 Hz, 1H), 7.15 (t, J = 6.7 Hz, 1H), 7.05 (t, J = 6.7 Hz, 1H), 6.55 (m, 1H), 6.48 (m, 1H), 5.71 (d, J = 7.7 Hz, 1H), 5.66 (d, J = 8.0 Hz, 1H), 4.69-4.58 (m, 2H), 3.95-3.89 (m, 2H), 2.69 (broad s, 1H). ^{13}C NMR (101 MHz; CDCl$_3$): 165.1 (m, CF), 164.5 (m, CF), 164.2 (m, CF), 162.6 (m, CF), 162.0 (m), 160.0 (m), 153.9 (d), 150.2, 150.0 (d), 149.7, 149.4, 148.7, 148.4, 140.7, 139.1, 139.0, 129.7, 127.9 (m, 2C), 126.4, 125.2, 123.9, 123.7 (d), 123.5 (d), 123.3, 114.2 (m, 2C), 99.1 (m, 2C), 77.4, 72.8, 70.6, 70.5, 70.2, 68.4, 61.4, 52.2. ^{19}F NMR (376 MHz; CDCl$_3$): -106.3 (m, 1F), -107.2 (m, 1F), -109.2 (m, 1F), -110.1 (m, 1F). Calcd for C$_{37}$H$_{34}$F$_4$N$_6$O$_4$Ir^{+} ([M]$^{+}$): *m/z* 895.221. Found *m/z* 895.2184.

Synthesis of the pt-TOxT-Sq ligand

General

Reagents and solvents were purchased from various commercial sources and used without further purification. NMR spectra were acquired on a Jeol 400 spectrometer or a Bruker Ascend 500 spectrometer. ^{1}H NMR spectra were acquired at 400 MHz or 500 MHz, ^{13}C{^{1}H} NMR spectra were acquired at 101 MHz or 126 MHz, and ^{19}F NMR acquired at 471 MHz. All NMR spectra were recorded at 298 K. Chemical shifts were referenced to residual solvent peaks and are quoted in terms of parts per million (ppm), relative to tetramethylsilane (Si(CH$_3$)$_4$); ^{19}F NMR signals are quoted relative to an internal standard of

trifluoroacetic acid. Electrospray ionization mass spectra (ESI-MS) were acquired using a Thermo Scientific Exactive Plus Orpitrap Mass Spectrometer.

Synthesis of 1-amino,13-(Boc-amino)-4,7,10-trioxatridecane:[3a]
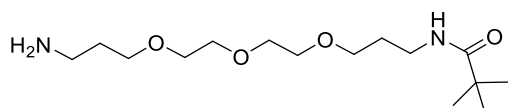
To a solution of 4,7,10-trioxa-1,13-tridecanediamine (18.2 g, 82.5 mmol) in 1,4-dioxane (150 mL) a solution of Boc_2-O (3.00 g, 13.8 mmol) in 1,4-dioxane (80 mL) was added dropwise at ambient temperature over 16 h. The solution was stirred for a further 30 h before the solvent was removed under reduced pressure and the residue taken up in H_2O. The aqueous mixture was extracted with dichloromethane (8 × 80 mL) and the combined organic extracts were washed with brine (2 × 200 mL). The organic phase was then dried ($MgSO_4$), filtered and the solvent removed under reduced and the product isolated as a yellow oil after the residue was purified by silica gel chromatography using a solvent gradient of 100% dichloromethane → 10% methanol/2% aq. ammonia/88% dichloromethane (2.96 g, 9.23 mmol, 67%). ^{1}H NMR (400 MHz; $CDCl_3$): δ 5.17 (s, 1H), 3.63-3.49 (m, 12H), 3.19 (m, 2H), 2.80 (m, 1H), 2.46 (s, 3H), 1.73 (m, 4H), 1.41 (s, 9H).

1-azido, 13-(Boc-amino)-4,7,10-trioxatridecane:[3a]
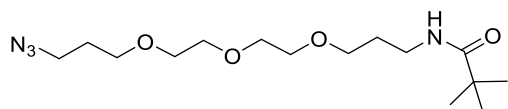
A flask containing sodium azide (6.04 g, 93.0 mmol), H_2O (30 mL) and dichloromethane (75 mL) was cooled to 0 °C and triflic anhydride (3 mL, 18.0 mmol) was added dropwise. After 15 min the mixture was stirred vigorously at ambient temperature for 3.5 h. The organic layer was separated and the aqueous layer was back extracted with dichloromethane (2×20mL). The combined organic extracts were washed with sat. Na_2CO_3. The organic

phase was then added dropwise to 1-amino,13-(Boc-amino)-4,7,10-trioxatridecane (2.92 g, 9.12 mmol), K_2CO_3 (2.59 g, 18.7 mmol) and $CuSO_4.5H_2O$ (cat.) in a methanol/water (90 mL/60mL) solvent mixture. The mixture was stirred vigorously for 3 days before the organic phase was separated, washed with H_2O (2×40 mL) and the aqueous phases were back extracted with dichloromethane (2×40 mL). The combined organic extracts were dried ($MgSO_4$), filtered and the solvent removed under reduced pressure. The residue was loaded onto a silica column and eluted with a gradient of 100% dichloromethane→4%methanol/96% dichloromethane to afford a slightly yellow oil (1.99 g, 5.74 mmol, 63%). ^{1}H NMR (400 MHz; $CDCl_3$): δ 4.98 (s, 1H), 3.65-3.51 (m, 12H), 3.38 (t, J = 6.7 Hz, 2H), 3.21 (m, 2H), 1.84 (m, 2H), 1.74 (m, 2H), 1.42 (s, 9H). {^{1}H}^{13}C NMR (101 MHz; $CDCl_3$): δ 156.1, 79.0, 70.7, 70.7, 70.5, 70.3, 69.7, 68.0, 48.5, 38.7, 29.7, 29.2, 28.5.

2-(1-(13-(Boc-amino)-4,7,10-trioxatridecyl)-1H-1,2,3-triazol-4-yl)pyridine:[3a]
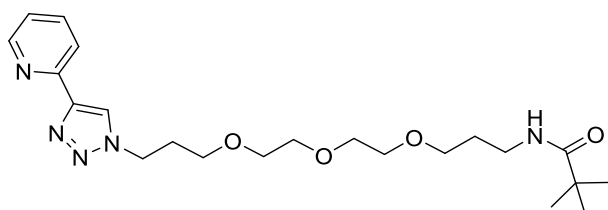
A mixture of 1-azido,13-(Boc-amino)-4,7,10-trioxatridecane (1.95 g, 5.62 mmol), 2-ethynylpyridine (0.65 g, 6.26 mmol) and sodium ascorbate (20 mol%) was set stirring in DMSO/H_2O (2:1, 3 mL) then $CuSO_4.5H_2O$ (2 mol%) was added. After 5 days H_2O was added (40 mL) and the mixture was extracted with dichloromethane (3×30 mL). The organic phase was washed with brine, dried ($MgSO_4$) and filtered then the solvent was removed under reduced pressure and any remaining DMSO was removed *in vacuo*. The residue was purified by silica gel chromatography using ethyl acetate as the eluent to afford a yellow oil (2.36 g, 5.44 mmol, 97%). ^{1}H NMR (400 MHz; $CDCl_3$): δ 8.57 (ddd, J = 4.9, 1.8, 1.0 Hz, 1H), 8.18 (s, 1H), 8.16 (t, J = 1.0 Hz, 1H), 7.77 (td, J = 7.8, 1.8 Hz, 1H), 7.22 (ddd, J = 7.5, 4.9, 1.2 Hz, 1H), 5.01 (br, 1H), 4.55 (t, J = 6.8 Hz, 2H), 3.66-3.59 (m, 8H), 3.50 (dt, J =

16.0, 5.9 Hz, 4H), 3.21 (q, J = 6.1 Hz, 2H), 1.75 (dd, J = 12.7, 6.4 Hz, 4H), 1.42 (s, 9H).

$\{^1H\}$ ^{13}C NMR (101 MHz; CDCl$_3$): δ 156.1, 150.5, 149.5, 148.3, 137.0, 122.9, 122.6, 120.3, 70.7, 70.6, 70.5, 70.3, 69.7, 67.2, 47.4, 38.6, 30.3, 29.8, 29.7, 28.5.

pt-TOxT-Sq:
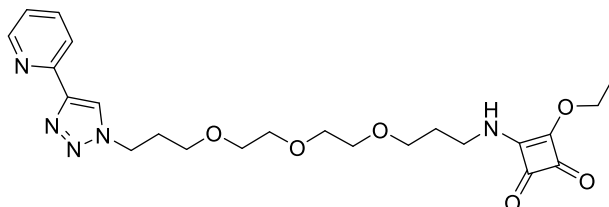
A mixture of 2-(1-(13-(Boc-amino)-4,7,10-trioxatridecyl)-1H-1,2,3-triazol-4-yl)pyridine (0.656 g, 1.44 mmol) and trifluoroacetic acid (2 mL) in acetonitrile (10 mL) was set stirring at 50 ℃. After 2.5 h the reaction was cooled to ambient temperature and potassium carbonate was cautiously added to adjust the reaction mixture to pH 7. The reaction mixture was added dropwise to a round bottom flask containing 3,4-diethoxy-3-cyclobutene-1,2-dione (0.737 g, 4.33 mmol) and potassium carbonate (3.43 g, 24.8 mmol) in acetonitrile (25 mL). The reaction mixture was then stirred for 18 h before being filtered through celite and the solvent was removed affording a yellow residue. The residue was washed with dichloromethane, the washings were retained, and the solvent volume reduced before purification by column chromatography (SiO$_2$, DCM→10%MeOH/DCM) to afford a light-yellow oil (0.625 g, 1.32 mmol, 92%). ^1H NMR (500 MHz; CD$_3$CN): δ 8.56 (d, J = 4.6 Hz, 1H), 8.27 (s, 1H), 8.07 (d, J = 7.9 Hz, 1H), 7.82 (td, J = 7.7, 1.7 Hz, 1H), 7.27 (ddd, J = 7.5, 4.9, 1.0 Hz, 1H), 4.65 (m, 2H), 4.50 (t, J = 6.9 Hz, 2H), 3.54 (m, 14H), 2.15 (dq, J = 13.4, 7.0 Hz, 3H), 1.78 (q, J = 6.2 Hz, 2H), 1.38 (t, J = 6.5 Hz, 3H). $^{13}C\{^1H\}$ NMR (126 MHz; CD$_3$CN): δ 190.2, 151.5, 150.6, 148.8, 137.9, 123.9, 123.8, 123.7, 120.5, 71.1, 70.9, 70.9, 70.1, 69.2, 69.0, 68.0, 48.2, 43.0, 31.0, 16.1.

Synthesis of the [Ir(C^N)$_2$(pt-TOxT-Sq)]$^+$ ECL labels:

General procedure[4]

A mixture of the appropriate iridium precursor and **pt-TOxT-Sq** was set stirring in a solvent mixture of methanol/dichloromethane (3:1). The reaction was stirred overnight at ambient temperature and the solvent was removed after TLC confirmed the reaction was complete. The solvent was removed under reduced pressure. The residue was taken up in a minimum of dichloromethane and diethyl ether was layered on top. A residue settled at the bottom of the flask after storing at -20 ℃ for 72 h. The supernatant was decanted off and the residue was washed with diethyl ether ($\times$3). A solid was isolated by filtration after trituration of the residue with diethyl ether.

[Ir(ppy)$_2$(pt-TOxT-Sq)]Cl. The chlorido-bridged dimer [Ir(ppy)$_2$(μ-Cl)]$_2$ was reacted as detailed in the general procedure affording a yellow powder (0.473 g, 0.47 mmol, 75%). ^{1}H NMR (500 MHz; CD$_3$CN): δ 9.40 (m, 1H), 8.41-8.37 (m, 1H), 8.05 (m, 3H), 7.86-7.74 (m, 6H), 7.63 (d, J=5.3 Hz, 1H), 7.34 (ddd, J =7.4, 5.8, 1.3 Hz, 1H), 7.10 (ddd, J = 7.3, 6.0, 1.3, 1H), 7.04 (m, 2H), 6.92 (m, 2H), 6.81 (td, J = 7.4, 1.1 Hz, 1H), 6.26 (m, 2H), 4.64 (m, 2H), 4.51 (m, 2H), 3.45 (m, 15H), 2.08 (q, J = 6.2 Hz, 2H), 1.78 (q, J = 6.4 Hz, 2H), 1.35 (m, 3H). ^{13}C{^{1}H} NMR (126 MHz; CD$_3$CN): δ 168.6, 168.2, 151.1, 150.8, 150.7, 150.2, 149.4, 147.7, 145.3, 145.3, 140.7, 139.5, 139.4, 132.8, 132.4, 131.2, 130.6, 128.3, 127.5, 125.8, 125.3, 124.6, 124.3, 124.0, 123.5, 123.1, 120.7, 120.6, 71.0, 70.9, 70.8, 70.8, 70 .0, 69.1, 67.6, 50.4, 30.5, 16.2. ESI-MS (positive ion). Calcd for C$_{45}$H$_{47}$IrN$_7$O$_6$ ([M]$^+$): m/z 974.322. Found m/z 974.3229.

[Ir(bt)$_2$(pt-TOxT-Sq)]Cl. The chlorido-bridged dimer [Ir(bt)$_2$(μ-Cl)]$_2$ was reacted as detailed in the general procedure affording a yellow powder (0.320 g, 0.29 mmol, 52%). ^{1}H NMR (400 MHz; CD$_3$CN): δ 9.16 (s, 1H), 8.26 (d, J = 7.9 Hz, 1H), 8.06 (m, 3H), 7.95 (m, 2H), 7.84 (m, 1H), 7.40 (m, 3H), 7.27 (m, 1H), 7.11 (m, 2H), 7.03 (td, J= 7.5, 1.0 Hz, 1H), 6.89 (td, J = 7.5, 1.3 Hz, 1H), 6.80 (td, J = 7.5, 1.3 Hz, 1H), 6.55 (d, J= 8.3 Hz, 1H), 6.47 (d,

J = 7.6 Hz, 1H), 6.36 (d, J = 7.6 Hz, 1H), 6.16 (d, J = 8.4 Hz, 1H), 4.62 (d, J = 6.3 Hz, 2H), 4.54 (t, J = 6.5 Hz, 2H), 3.37 (m, 14H), 3.02 (s, 1H), 2.03 (q, J = 6.1 Hz, 2H), 1.71 (q, J = 6.3 Hz, 2H), 1.34 (t, J = 14.1 Hz, 3H). ^{13}C{^{1}H} NMR (101 MHz; CD$_3$CN): δ 182.7, 182.1, 151.7, 151.2, 150.9, 150.1, 150.1, 149.8, 147.5, 141.9, 141.5, 141.3, 134.4, 134.4, 132.8, 132.6, 132.6, 132.2, 129.2, 128.9, 128.6, 128.0, 127.7, 127.2, 126.9, 124.9, 124.8, 124.3, 123.9, 123.8, 119.1, 118.3, 70.9, 70.9, 70.8, 70.0, 69.1, 67.2, 50.5, 42.9, 42.6, 31.6, 31.0, 30.6, 18.8, 16.1. ESI-MS (positive ion). Calcd for C$_{49}$H$_{47}$IrN$_7$O$_6$S$_2^+$ ([M]$^+$): m/z 1086.266. Found m/z 1086.2673.

[Ir(piq)$_2$(pt-TOxT-Sq)]Cl. The chlorido-bridged dimer [Ir(piq)$_2$(μ-Cl)]$_2$ was reacted as detailed in the general procedure affording an orange powder (0.547 g, 0.49 mmol, 93%). ^{1}H NMR (400 MHz; [CD$_3$CN]): δ 9.14 (s, 1H), 9.01 (m, 2H), 8.38 (d, J = 8.0 Hz, 1H), 8.31 (m, 2H), 8.02 (m, 3H,), 7.83 (m, 4H), 7.70 (m, 1H), 7.67 (d, J = 6.4 Hz), 7.54 (d, J = 6.4 Hz, 1H), 7.49 (d, J = 6.4 Hz, 1H), 7.43 (d, J = 6.4 Hz, 1H), 7.31 (ddd, J = 7.7, 5.6, 1.3 Hz, 1H), 7.13 (ddd, J = 8.2, 7.2, 1.2 Hz, 1H), 7.04 (ddd, J = 8.2, 7.1, 1.2 Hz, 1H), 6.89 (td, J = 7.4, 1.2 Hz, 1H), 6.77 (td, J = 7.4, 1.2 Hz, 1H), 6.42 (d, J = 7.5 Hz, 1H), 6.28 (dd, J = 7.7, 1.1 Hz, 1H), 4.62 (m, 2H), 4.46 (t, J = 6.8 Hz, 2H), 3.32 (m, 15H), 1.98 (dd, J = 6.5, 5.2 Hz, 2H), 1.73 (q, J = 6.4 Hz, 2H), 1.33 (t, J = 7.1 Hz, 3H). ^{13}C{^{1}H} NMR (101 MHz; [CD$_3$CN]): δ 169.5, 169.2, 154.3, 151.2, 151.0, 150.4, 149.2, 146.8, 146.7, 142.4, 141.8, 140.7, 138.1, 138.0, 133.3, 133.1, 132.8, 132.8, 131.7, 131.3, 131.2, 130.6, 129.9, 129.8, 128.6, 128.5, 128.1, 127.7, 127.6, 127.1, 127.0, 123.9, 123.3, 122.9, 122.8, 122.6, 70.9, 70.8, 70.7, 70.0, 69.0, 67.3, 50.3, 30.3, 16.1. ESI-MS (positive ion). Calcd for C$_{53}$H$_{51}$IrN$_7$O$_6$ ([M]$^+$): m/z 1074.353. Found m/z 1074.3534.

[Ir(df-ppy)$_2$(pt-TOXT-Sq)]Cl. The chlorido-bridged dimer [Ir(df-ppy)$_2$(μ-Cl)]$_2$ was reacted as detailed in the general procedure affording a yellow powder (0.276 g, 0.25 mmol, 61%). ^{1}H NMR (500 MHz; CD$_3$CN): δ 9.50 (m, 1H), 8.44 (m, 1H), 8.30 (m, 2H), 8.10 (m, 1H),

7.89 (m, 3H), 7.76 (m, 1H), 7.66 (m, 1H), 7.39 (m, 1H), 7.13 (m, 2H), 6.66 (m, 2H), 5.73 (ddd, J = 24.1, 8.7, 2.3 Hz, 2H), 4.63 (m, 2H), 4.54 (m, 2H), 3.45 (m, 15H), 2.09 (q, J = 6.2 Hz, 2H), 1.78 (q, J = 6.4 Hz, 2H), 1.36 (m, 3H). $^{13}C\{^1H\}$ NMR (126 MHz; CD3CN): δ 164.7 (m, CF), 163.4 (m, CF), 162.8 (m, CF), 161.0 (m, CF), 154.9 (m, CF), 151.9 (m, CF), 151.6, 151.0, 150.7, 150.3, 141.3, 140.5, 140.5, 128.4, 128.0, 125.1, 124.8, 124.7, 124.54, 124.5, 124.3, 124.2, 114.8 (m, CF), 99.6 (m, CF), 71.0, 70.9, 70.8, 70.79, 70.0, 69.2, 67.6, 57.9, 50.6, 30.4, 18.8, 16.2. ^{19}F NMR (471 MHz; CD$_3$CN): δ -106.18 (d, J = 10.6, 1F), -107.06 (d, J = 9.6, 1F), -108.07 (d, J = 10.5, 1F), -108.87 (d, J = 10.2, 1F). ESI-MS (positive ion). Calcd for C$_{45}$H$_{43}$F$_4$IrN$_7$O$_6$$^+$ ([M]$^+$): *m/z* 1046.284. Found *m/z* 1046.2845.

Additional data
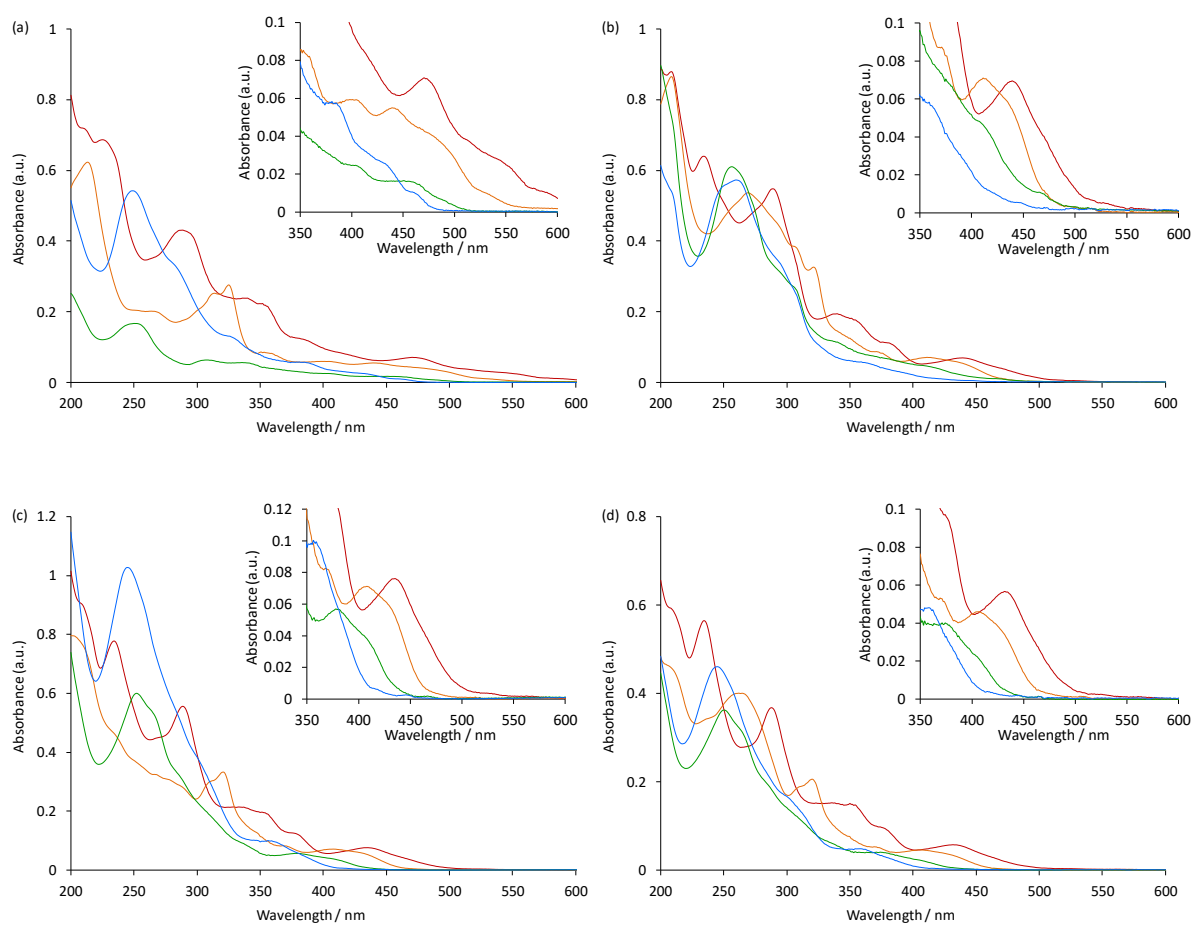
Figure S4.1. UV-Vis absorption spectra of (a) Ir(C^N)$_2$(acac), (b) [Ir(C^N)$_2$(dm-bpy)]$^+$, (c) [Ir(C^N)$_2$(ptb)]$^+$, and (d) [Ir(C^N)$_2$(pt-TEG)]$^+$, where C^N = piq (red lines), bt (orange lines), ppy (green lines) or df-ppy (blue lines). The metal complexes were prepared at a concentration of 10 μM in acetonitrile (a-c) or water (d). The insets show lowest energy absorption bands.
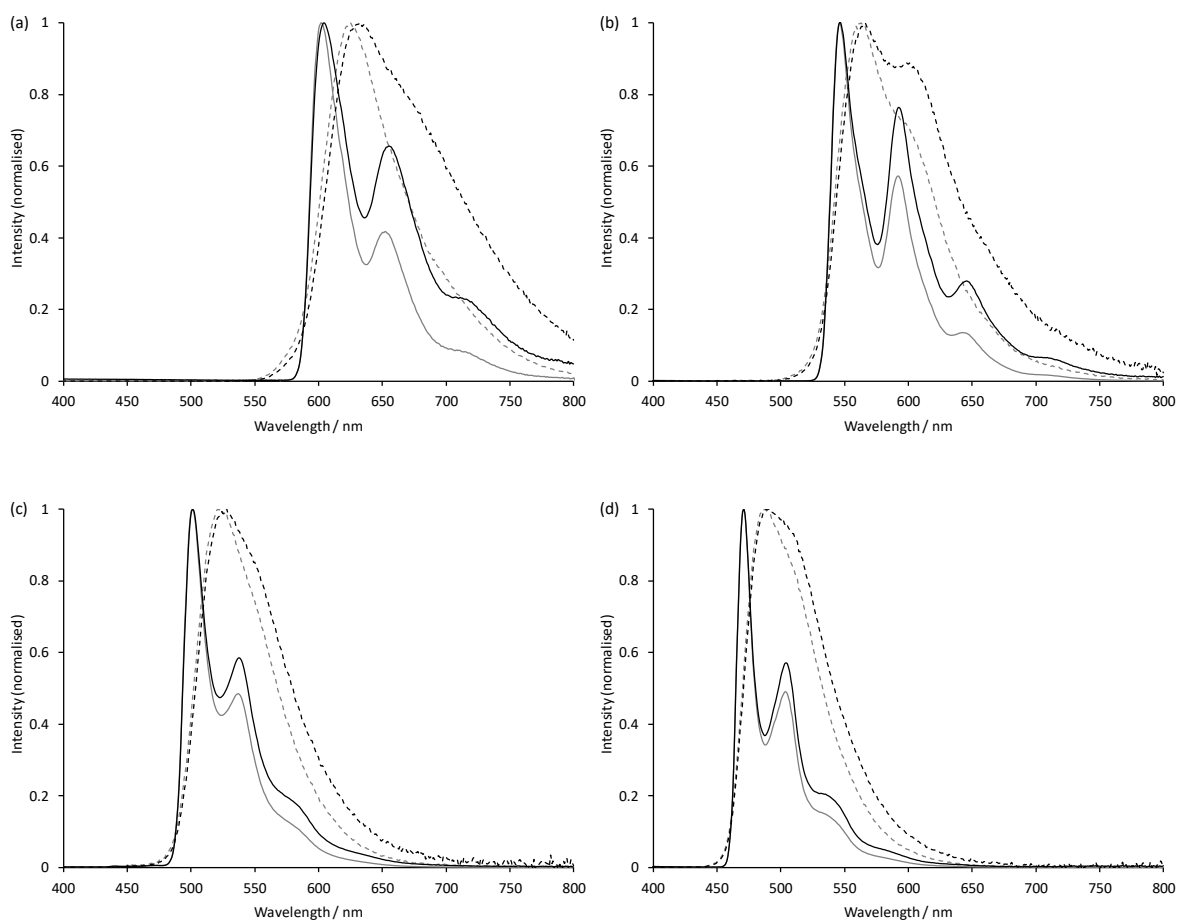
Figure S4.2. Normalized photoluminescence emission spectra of (a) Ir(piq)$_2$(acac), (b) Ir(bt)$_2$(acac), (c) Ir(ppy)$_2$(acac), and (d) Ir(df-ppy)$_2$(acac). Black lines: corrected spectra at 85 K (solid) and room temperature (dashed). Grey lines: uncorrected spectra at 85 K (solid) and room temperature (dashed). Conditions: 85 K spectra: 5 μM in 4:1 (v/v) ethanol:methanol; excitation wavelengths (λ_{ex}) were between 300 and 342 nm. Room temperature spectra: 10 μM in acetonitrile; λ_{ex} = 350 nm.
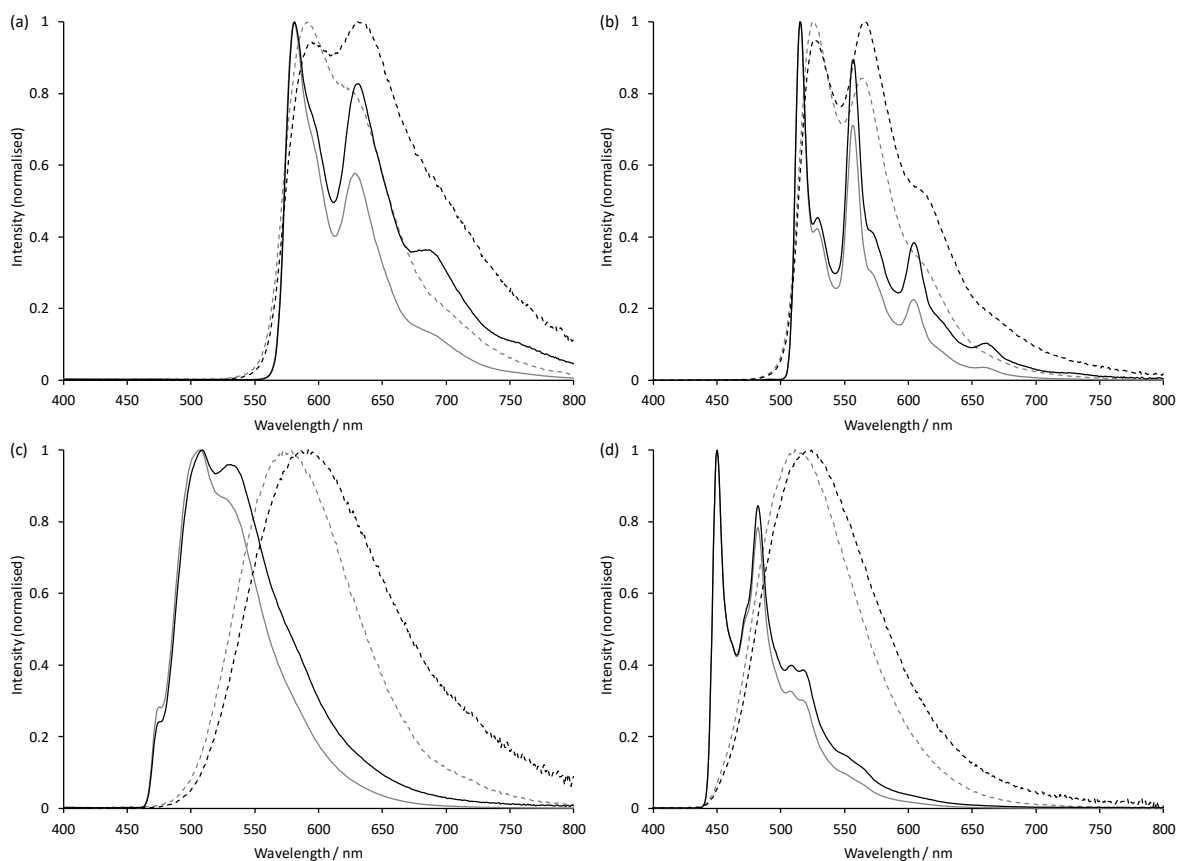
Figure S4.3. Normalized photoluminescence emission spectra of (a) [Ir(piq)$_2$(dm-bpy)]$^+$, (b) [Ir(bt)$_2$(dm-bpy)]$^+$, (c) [Ir(ppy)$_2$(dm-bpy)]$^+$, and (d) [Ir(df-ppy)$_2$(dm-bpy)]$^+$. Black lines: corrected spectra at 85 K (solid) and room temperature (dashed). Grey lines: uncorrected spectra at 85 K (solid) and room temperature (dashed). Conditions: 85 K spectra: 5 μM in 4:1 (v/v) ethanol:methanol; λ_{ex} = 295-374 nm. Room temperature spectra: 10 μM in acetonitrile; λ_{ex} = 350 nm.
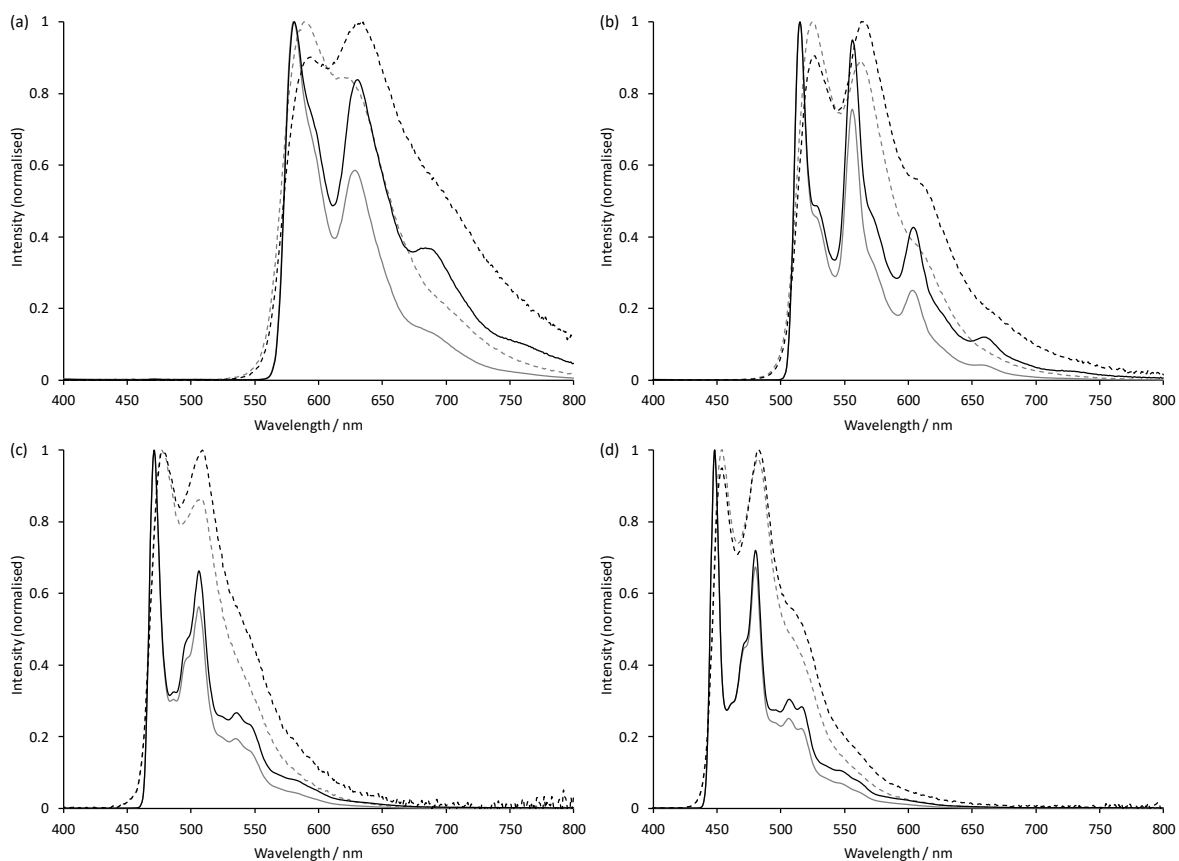
Figure S4.4. Normalized photoluminescence emission spectra of (a) $[Ir(piq)_2(ptb)]^+$, (b) $[Ir(bt)_2(ptb)]^+$, (c) $[Ir(ppy)_2(ptb)]^+$, and (d) $[Ir(df\text{-}ppy)_2(ptb)]^+$. Black lines: corrected spectra at 85 K (solid) and room temperature (dashed). Grey lines: uncorrected spectra at 85 K (solid) and room temperature (dashed). Conditions: 85 K spectra: 5 μM in 4:1 (v/v) ethanol:methanol; λ_{ex} = 290-324 nm. Room temperature spectra: 10 μM in acetonitrile; λ_{ex} = 350 nm.
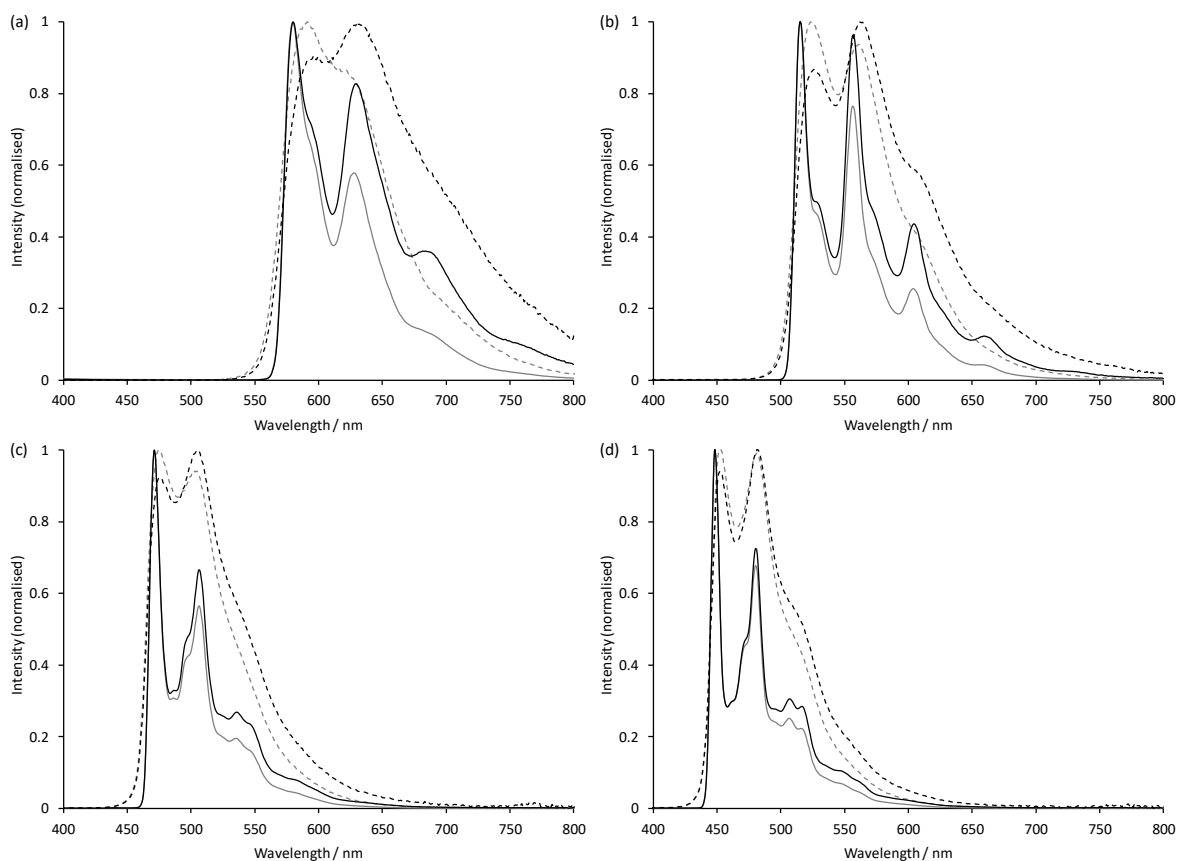
Figure S4.5. Normalized photoluminescence emission spectra of (a) [Ir(piq)$_2$(pt-TEG)]$^+$, (b) [Ir(bt)$_2$(pt-TEG)]$^+$, (c) [Ir(ppy)$_2$(pt-TEG)]$^+$, and (d) [Ir(df-ppy)$_2$(pt-TEG)]$^+$. Black lines: corrected spectra at 85 K (solid) and room temperature (dashed). Grey lines: uncorrected spectra at 85 K (solid) and room temperature (dashed). Conditions: 85 K spectra: 5 μM in 4:1 (v/v) ethanol:methanol; λ_{ex} = 267-324 nm. Room temperature spectra: 10 μM in water; λ_{ex} = 340 nm.
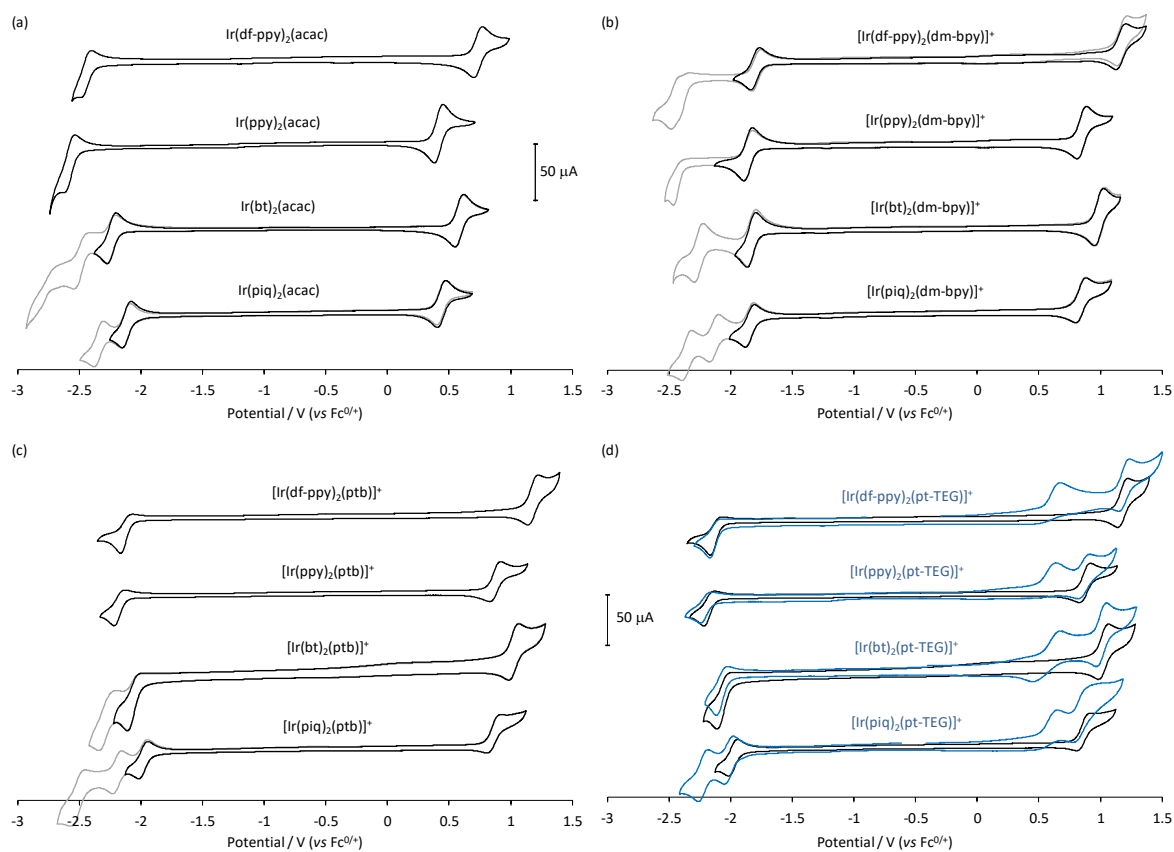
Figure S4.6. Cyclic voltammograms for (a) Ir(C^N)$_2$(acac), (b) [Ir(C^N)$_2$(dm-bpy)]$^+$, (c) [Ir(C^N)$_2$(ptb)]$^+$, and (d) [Ir(C^N)$_2$(pt-TEG)]$^+$ (blue lines) overlaid on those for [Ir(C^N)$_2$(ptb)]$^+$ (black lines). The grey plots show selected further reduction peaks. Metal complexes were prepared at a concentration of 0.25 mM in acetonitrile with 0.1 M TBAPF$_6$ supporting electrolyte. The additional peaks at ~0.65 V in the CVs for the [Ir(C^N)$_2$(pt-TEG)]$^+$ complexes are due to their chloride counter ions.

Table S4.1. Calculated MO energies (eV; BP86/def2-TZVP) for Ir(C^N)$_2$(acac) complexes in acetonitrile.

	Ir(piq)$_2$(acac)	Ir(bt)$_2$(acac)	Ir(ppy)$_2$(acac)	Ir(df-ppy)$_2$(acac)
LUMO+3	-1.92	-1.56	-1.97	-1.99
LUMO+2	-2.01	-2.04	-1.98	-2.05
LUMO+1	-2.78	-2.73	-2.40	-2.48
LUMO	-2.87	-2.73	-2.41	-2.49
HOMO	-4.63	-4.80	-4.63	-4.88
HOMO-1	-4.91	-4.99	-4.91	-5.06
HOMO-2	-5.22	-5.37	-5.26	-5.45
HOMO-3	-5.50	-5.61	-5.69	-5.76
HOMO-LUMO GAP	1.76	2.07	2.22	2.39

Table S4.2. Calculated MO energies (eV; BP86/def2-TZVP) for [Ir(C^N)$_2$(dm-bpy)]$^+$ complexes in acetonitrile.

	[Ir(piq)$_2$(dm-bpy)]$^+$	[Ir(bt)$_2$(dm-bpy)]$^+$	[Ir(ppy)$_2$(dm-bpy)]$^+$	[Ir(df-ppy)$_2$(dm-bpy)]$^+$
LUMO+3	-2.29	-2.22	-2.30	-2.34
LUMO+2	-2.86	-2.85	-2.47	-2.55
LUMO+1	-2.98	-2.92	-2.56	-2.63
LUMO	-3.06	-3.04	-3.06	-3.12
HOMO	-5.06	-5.13	-5.09	-5.31
HOMO-1	-5.29	-5.53	-5.31	-5.52
HOMO-2	-5.48	-5.62	-5.56	-5.72
HOMO-3	-5.75	-5.97	-5.95	-5.94
HOMO-LUMO GAP	2.00	2.09	2.03	2.19

Table S4.3. Calculated MO energies (eV; BP86/def2-TZVP) for [Ir(C^N)$_2$(ptb)]$^+$ complexes in acetonitrile.

	[Ir(piq)$_2$(ptb)]$^+$	[Ir(bt)$_2$(ptb)]$^+$	[Ir(ppy)$_2$(ptb)]$^+$	[Ir(df-ppy)$_2$(ptb)]$^+$
LUMO+3	-2.27	-2.23	-2.31	-2.34
LUMO+2	-2.74	-2.77	-2.53	-2.62
LUMO+1	-2.91	-2.87	-2.60	-2.66
LUMO	-3.06	-2.92	-2.76	-2.82
HOMO	-5.04	-5.18	-5.07	-5.31
HOMO-1	-5.50	-5.58	-5.57	-5.75
HOMO-2	-5.51	-5.69	-5.63	-5.78
HOMO-3	-5.85	-6.00	-5.90	-6.01
HOMO-LUMO GAP	1.98	2.26	2.31	2.49

Table S4.4. Calculated MO energies (BP86/def2-TZVP) for [Ir(C^N)$_2$(pt-TEG)]$^+$ complexes in water.

	[Ir(piq)$_2$(pt-TEG)]$^+$	[Ir(bt)$_2$(pt-TEG)]$^+$	[Ir(ppy)$_2$(pt-TEG)]$^+$	[Ir(df-ppy)$_2$(pt-TEG)]$^+$
LUMO+3	-2.20	-2.17	-2.25	-2.27
LUMO+2	-2.70	-2.72	-2.51	-2.58
LUMO+1	-2.94	-2.84	-2.57	-2.63
LUMO	-2.98	-2.90	-2.71	-2.76
HOMO	-5.03	-5.15	-5.04	-5.26
HOMO-1	-5.40	-5.53	-5.54	-5.70
HOMO-2	-5.52	-5.65	-5.58	-5.71
HOMO-3	-5.80	-5.97	-5.88	-5.95
HOMO-LUMO GAP	2.05	2.25	2.33	2.50
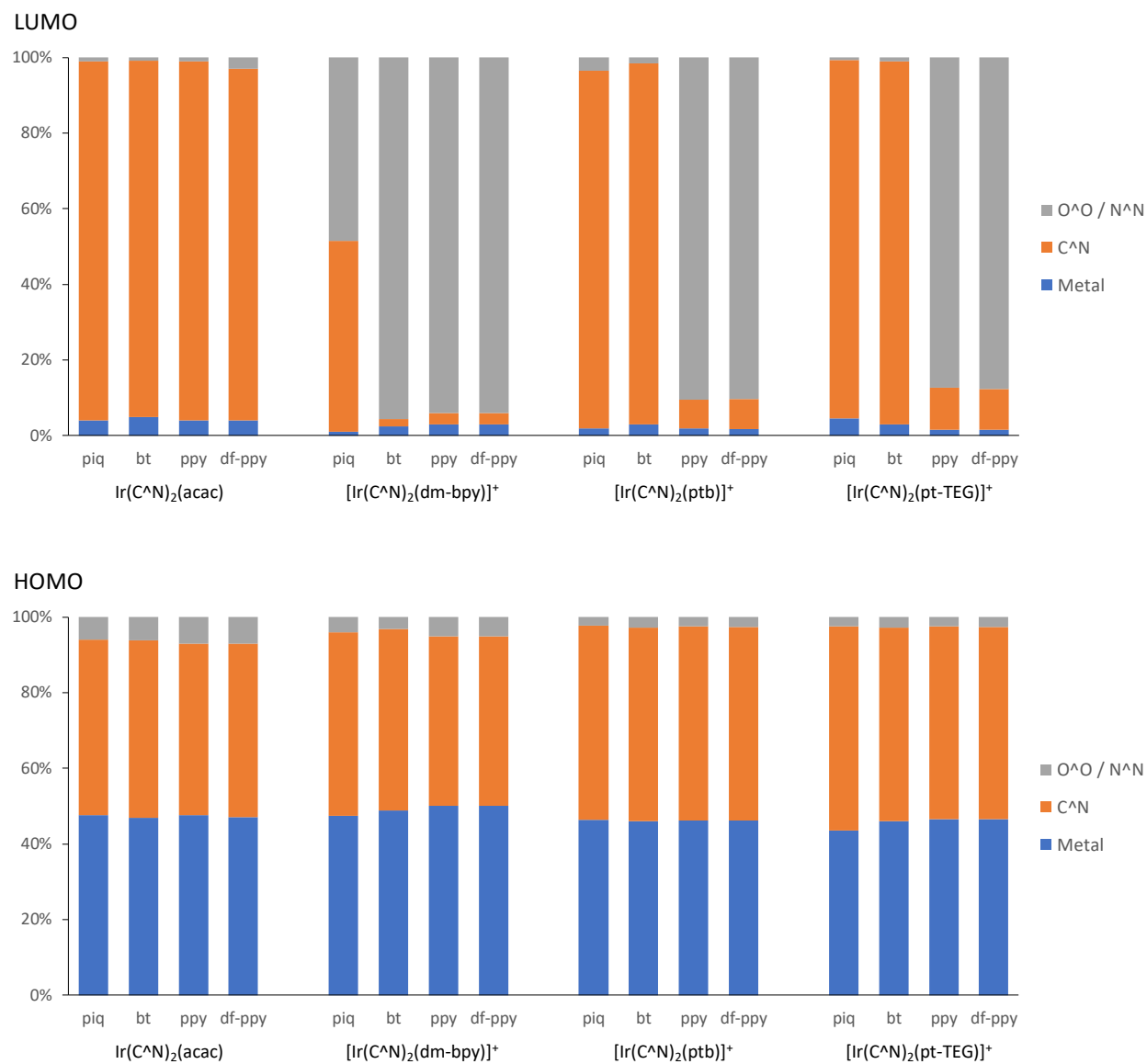
Figure S4.7. Contribution to the respective MOs (BP86/def2-TZVP) of the metal and ligands in Ir(C^N)$_2$(acac), [Ir(C^N)$_2$(dm-bpy)]$^+$, [Ir(C^N)$_2$(ptb)]$^+$, and [Ir(C^N)$_2$(pt-TEG)]$^+$ complexes, where C^N = piq, bt, ppy, or df-ppy.

Table S4.5. Contour plots for $[Ru(bpy)_3]^{2+}$, $Ir(C^\wedge N)_2(acac)$, $[Ir(C^\wedge N)_2(dm\text{-}bpy)]^+$ and $[Ir(C^\wedge N)_2(ptb)]^+$ complexes in acetonitrile.

	HOMO	LUMO
$[Ru(bpy)_3]^{2+}$		
$Ir(piq)_2(acac)$		
$Ir(bt)_2(acac)$		
$Ir(ppy)_2(acac)$		
$Ir(df\text{-}ppy)_2(acac)$		

[Ir(piq)₂(dm-bpy)]⁺		
[Ir(bt)₂(dm-bpy)]⁺		
[Ir(ppy)₂(dm-bpy)]⁺		
[Ir(df-ppy)₂(dm-bpy)]⁺		
[Ir(piq)₂(ptb)]⁺		

[Ir(bt)₂(ptb)]⁺		
[Ir(ppy)₂(ptb)]⁺		
[Ir(df-ppy)₂(ptb)]⁺		
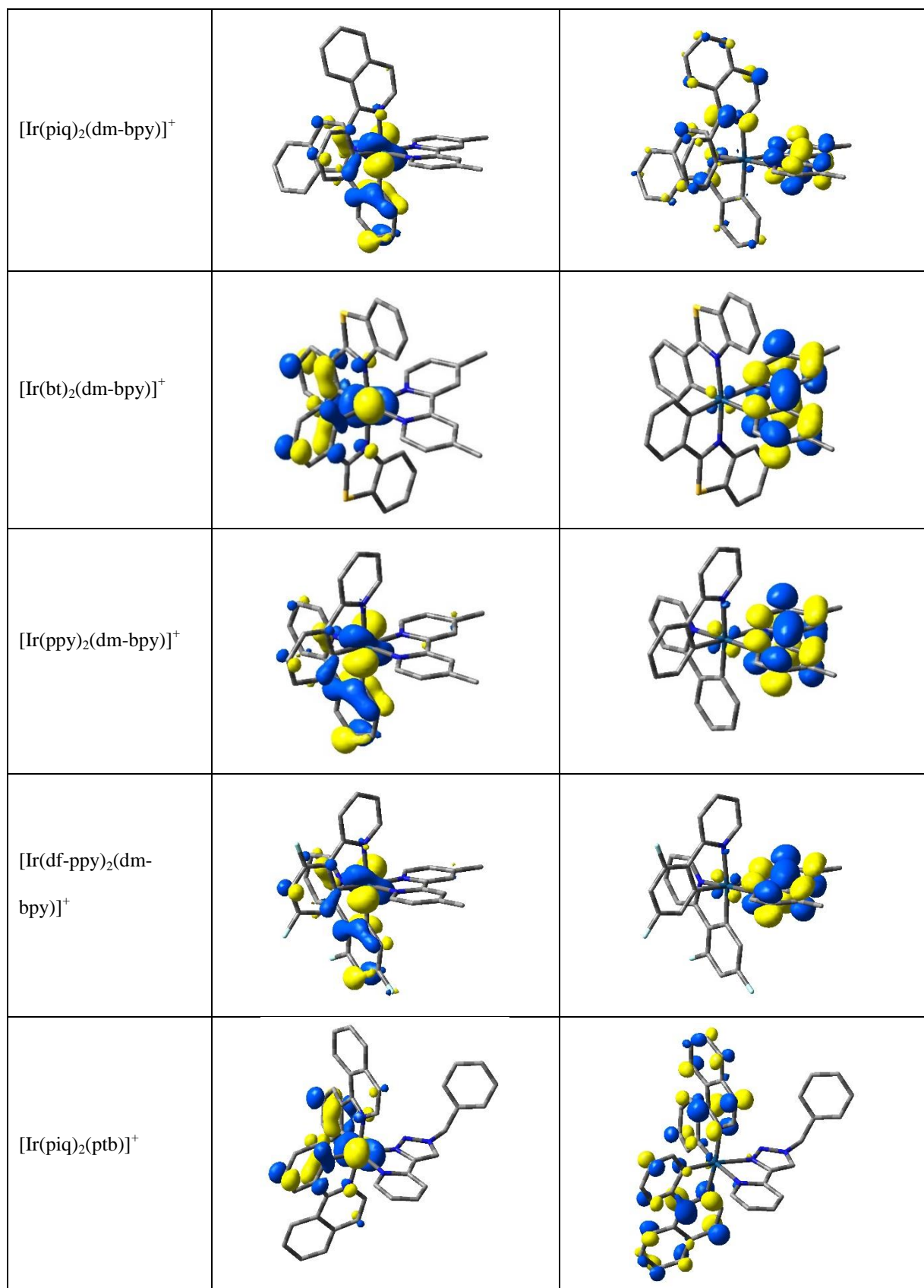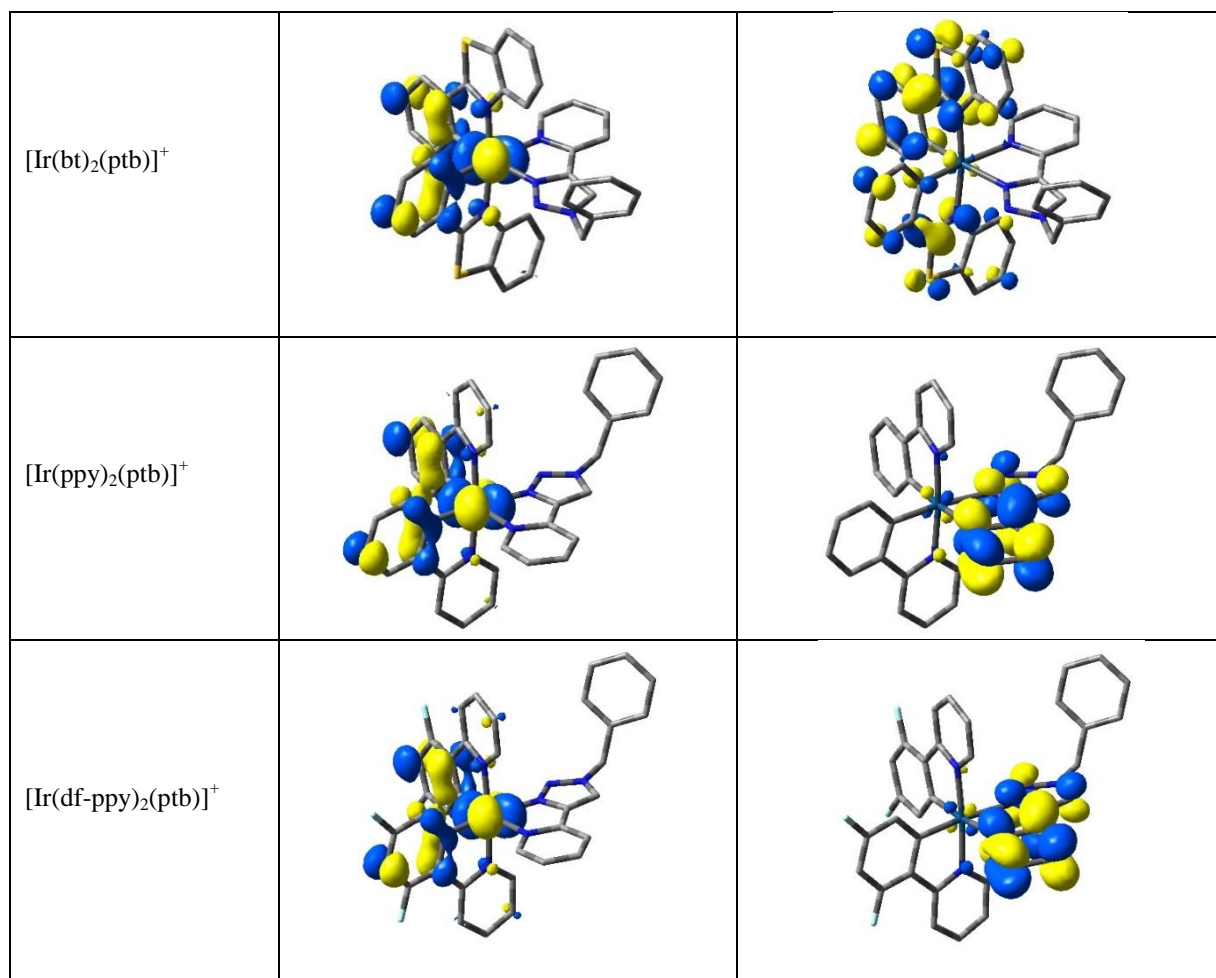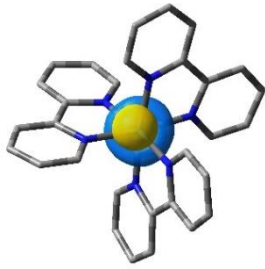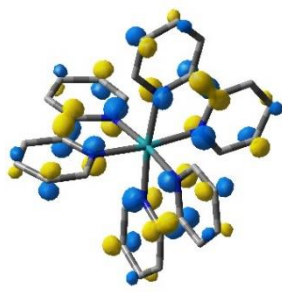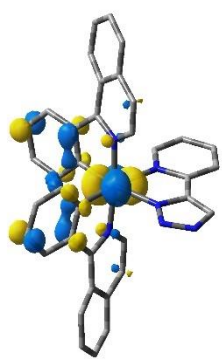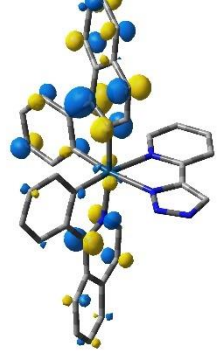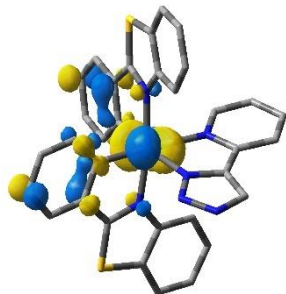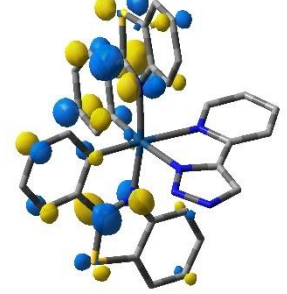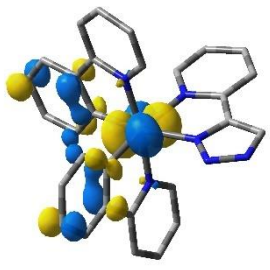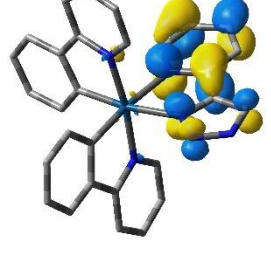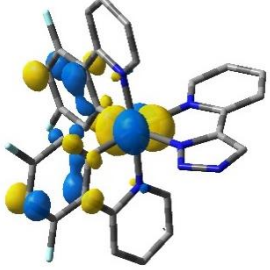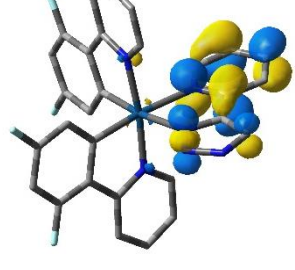
Table S4.6. Contour plots for $[Ru(bpy)_3]^{2+}$ and the $[Ir(C^\wedge N)_2(pt\text{-}TEG)]^+$ complexes in water. The hydrogen atoms and TEG chain have been omitted for clarity.

	HOMO	LUMO
$[Ru(bpy)_3]^{2+}$		
$[Ir(piq)_2(pt\text{-}TEG)]^+$		
$[Ir(bt)_2(pt\text{-}TEG)]^+$		
$[Ir(ppy)_2(p\text{-}TEG)]^+$		
$[Ir(df\text{-}ppy)_2(p\text{-}TEG)]^+$		
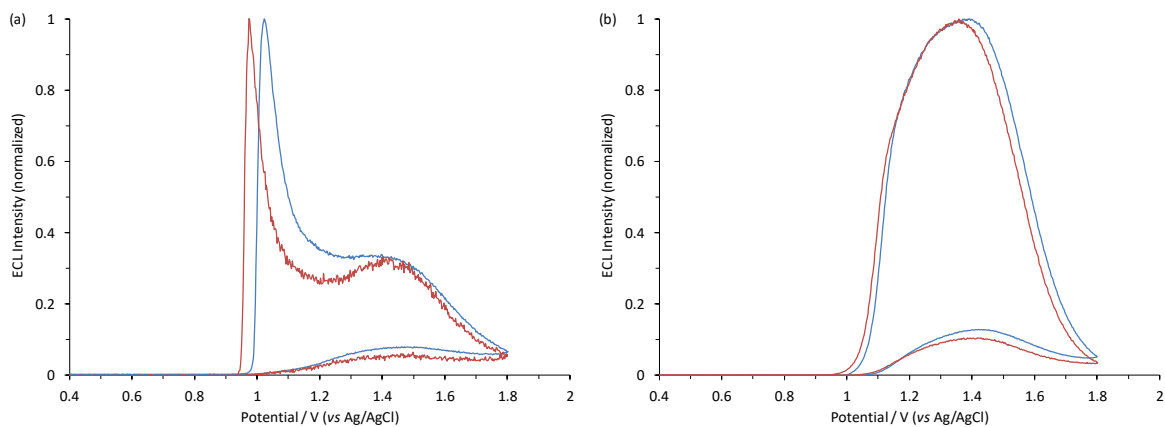
Figure S4.8. Normalized ECL intensity during an applied potential sweep from 0 V to 1.8 V and back to 0 V (*vs* Ag/AgCl) for (a) [Ir(piq)$_2$(pt-TEG)]$^+$ and (b) [Ir(ppy)$_2$(pt-TEG)]$^+$ at 1 μM (blue lines) and 0.1 μM (red lines) in (ProCell) phosphate buffer solution containing TPrA as a co-reactant.
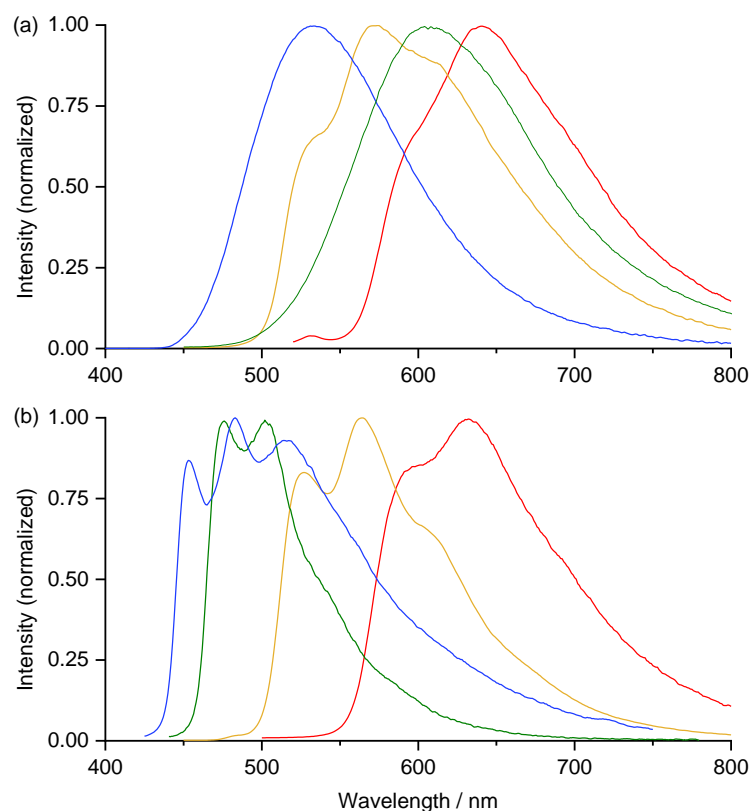
Figure S4.9. Photoluminescence emission spectra (corrected) of (a) [Ir(C^N)$_2$(mbpy-COOH)]$^+$, and (b) [Ir(C^N)$_2$(pt-TOxT-Sq)]$^+$ labels, where C^N = df-ppy (blue lines), ppy (green lines), bt (yellow lines), or piq (red lines), at a concentration of 10 μM in phosphate buffer.

Table S4.7. Primers and NASBA amplicon fragment sequences.

	Sequences (5' - 3' orientation)
P1[a]	***AAT TTC TAA TAC GAC TCA CTA TAG GGA A***<u>GT GCC ATC CGA TAA CAG</u>
P2[b]	***GAT GCA AGG TCG CAT ATG AG***<u>A GCC TTA CCG TAG TGT ACT A</u>
Detection probe	Amino-C6-GAT GCA AGG TCG CAT ATG AG
Capture probe	GAC AAT TTC GGG TGG GTT CC-Biotin TEG
NASBA amplicon (176 nt)	GGGAA<u>GUGCC AUCCGAUAAC AGGACGAUCG CAC</u>GGAACCC ACCCGAAAUU GUCGGUGGUACUUAUCGUCC AGGUGUAUCG AAAGUGCGUG AAUAAAUACG CUUUUGCUAG CGAGGGAGCUAAUGCUGCCC UGGAGU<u>UAGU ACACUACGGU AAGGCU</u>*CUCA UAUGCGACCU UGCAUC*

[a]Primer 1 consists of a 3' terminal sequence that is target specific (underlined) and a 5' terminal T7 promoter sequence (bold) that can be recognized by T7 RNA polymerase. [b]Primer 2 consists of a 3' terminal target specific sequence (underlined) and 5' terminal ECL detection probe sequence (bold).
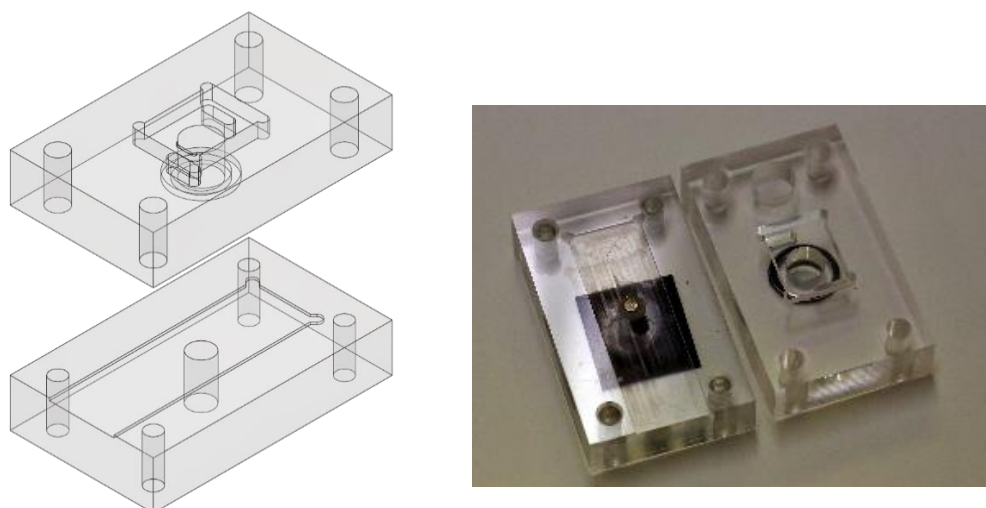
Figure S4.10. 3D drawing and photograph of the custom screen-printed electrode (SPE) holder, which was designed using SolidWorks 2015 CAD package (Dassault Systems, France). G-code CNC toolpaths were created using Siemens NX 10 CAD/CAM package (Siemens, Germany). The holders were machined from 10 mm thick cast poly(methylmethacrylate) (PMMA) sheets (Resi-Plex, Australia) using a Datron M7HP CNC mill (Datron AG, Germany). They were designed to house Zensor TE-100 SPE (eDAQ, Australia) which consist of carbon ink working (3 mm diameter) and counter electrodes, and an Ag|AgCl based ink reference electrode. These electrodes have been shown to have characteristics well suited for ECL-based analytical methods.[5] To perform ECL assays using paramagnetic particles, the holders incorporated a 3 ×4 mm diameter rod shaped N42 rare earth magnet (Aussie Magnets, Australia) beneath the working electrode.

Figure S4.11. Photograph of the cell holder containing magnet and Zensor SPE, coupled with the silicon photomultiplier detector (ASD-RGB3S-P; AdvanSiD, Italy) and ASD-EP-EB-N amplifier board (AdvanSiD).

NMR spectra of [Ir(C^N)₂(dm-bpy)](PF₆) and [Ir(C^N)₂(ptb)](PF₆) complexes

¹H NMR spectrum of [Ir(bt)₂(dm-bpy)](PF₆)
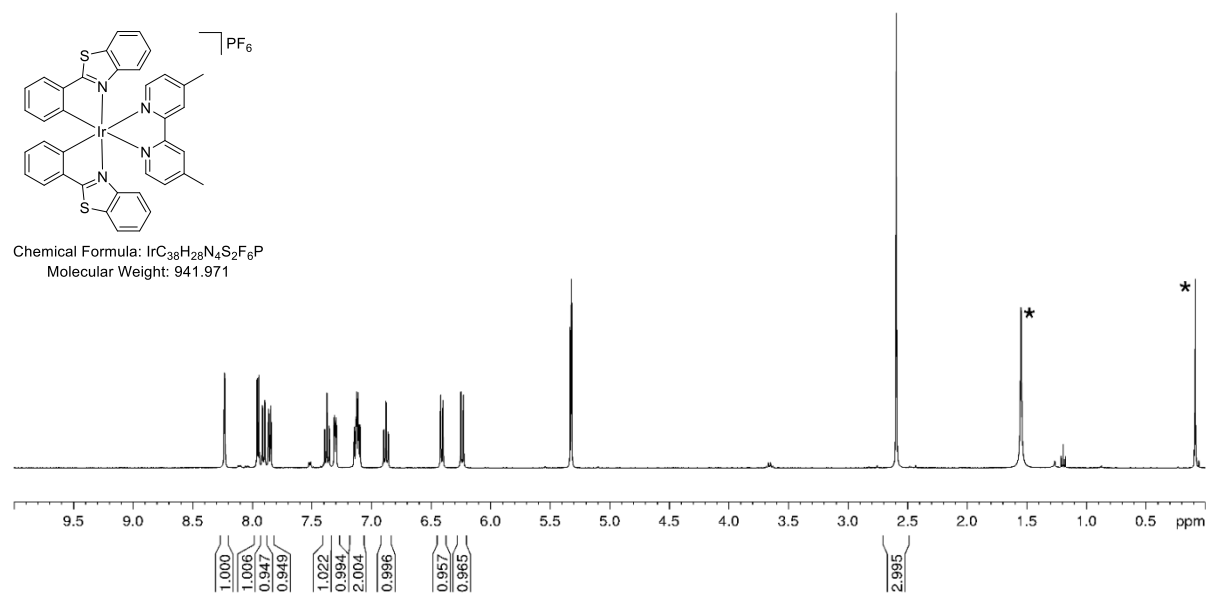
Chemical Formula: IrC₃₈H₂₈N₄S₂F₆P
Molecular Weight: 941.971

¹H NMR (400 MHz; CD₂Cl₂): δ 8.23 (s, 1H), 7.95 (d, J = 5.6 Hz, 1H), 7.90 (d, J = 8.0 Hz, 1H), 7.85 (d, J = 7.6 Hz, 1H), 7.37 (t, J = 7.4 Hz, 1H), 7.30 (d, J = 5.6 Hz, 1H), 7.09-7.14 (m, 2H), 6.88 (td, J = 7.5, 1.2 Hz, 1H), 6.41 (d, J = 7.6 Hz, 1H), 6.24 (d, J = 8.4 Hz, 1H), 2.59 (s, 3H).

$^{13}C\{^1H\}$ NMR spectrum of [Ir(bt)$_2$(dm-bpy)](PF$_6$)

Chemical Formula: IrC$_{38}$H$_{28}$N$_4$S$_2$F$_6$P
Molecular Weight: 941.971
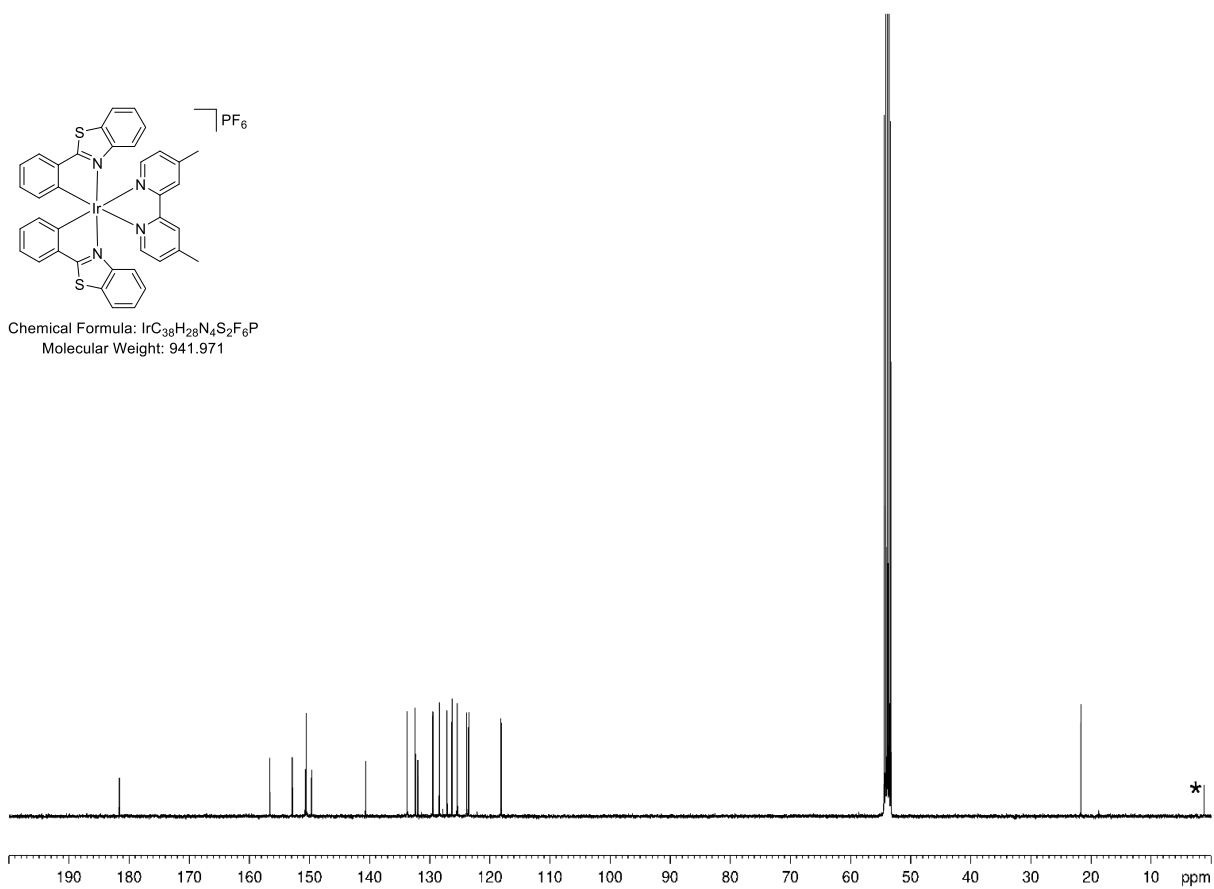
$^{13}C\{^1H\}$ NMR (100 MHz; CD$_2$Cl$_2$): δ 181.8, 156.8, 153.0, 150.9, 150.7, 149.8, 140.8, 133.9, 132.6, 132.1, 129.6, 128.6, 127.3, 126.5, 125.6, 124.0, 123.7, 118.3, 21.8.

¹H NMR spectrum of [Ir(piq)₂(dm-bpy)](PF₆)

^{1}H NMR spectrum of [Ir(piq)$_2$(dm-bpy)](PF$_6$)
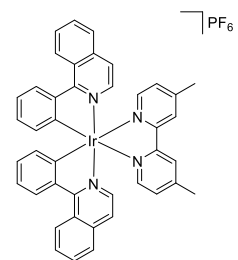
Chemical Formula: IrC$_{42}$H$_{32}$N$_4$F$_6$P
Molecular Weight: 929.927
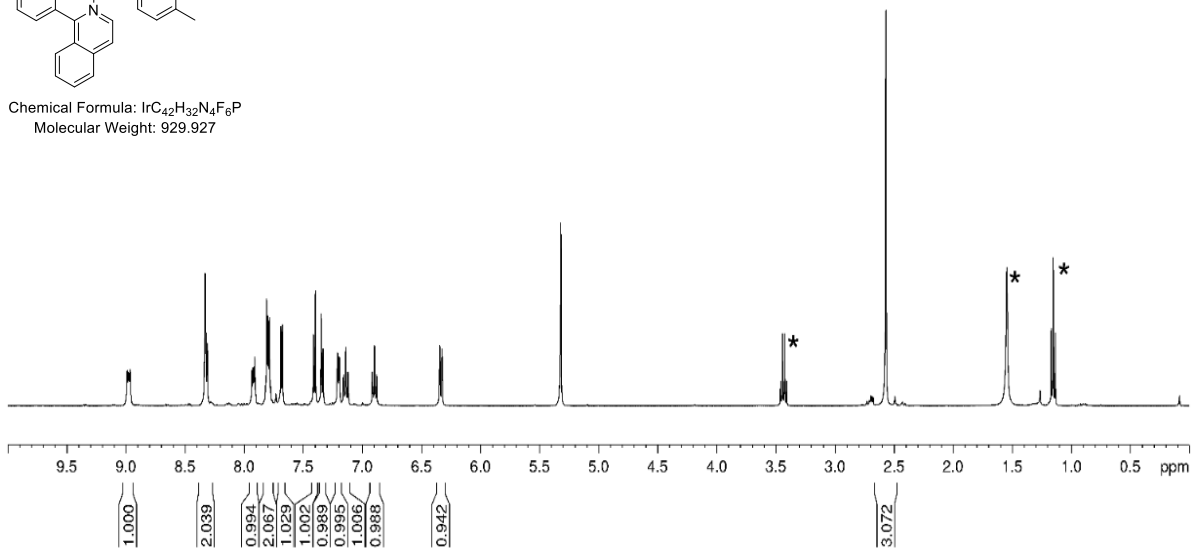
^{1}H NMR (400 MHz; CD$_2$Cl$_2$): δ 8.98 (m, 1H), 8.32 (m, 2H), 7.92 (m, 1H), 7.80 (m, 2H), 7.68 (d, J = 5.8 Hz, 1H), 7.41 (d, J = 6.4 Hz, 1H), 7.34 (d, J = 6.4 Hz, 1H), 7.20 (1H, J = 5.1 Hz, d), 7.14 (t, J = 7.6 Hz 1H), 6.90 (t, J = 7.4 Hz, 1H), 6.34 (d, J = 8.1 Hz, 1H), 2.57 (s, 3H).

¹H NMR spectrum of [Ir(ppy)$_2$(dm-bpy)](PF$_6$)
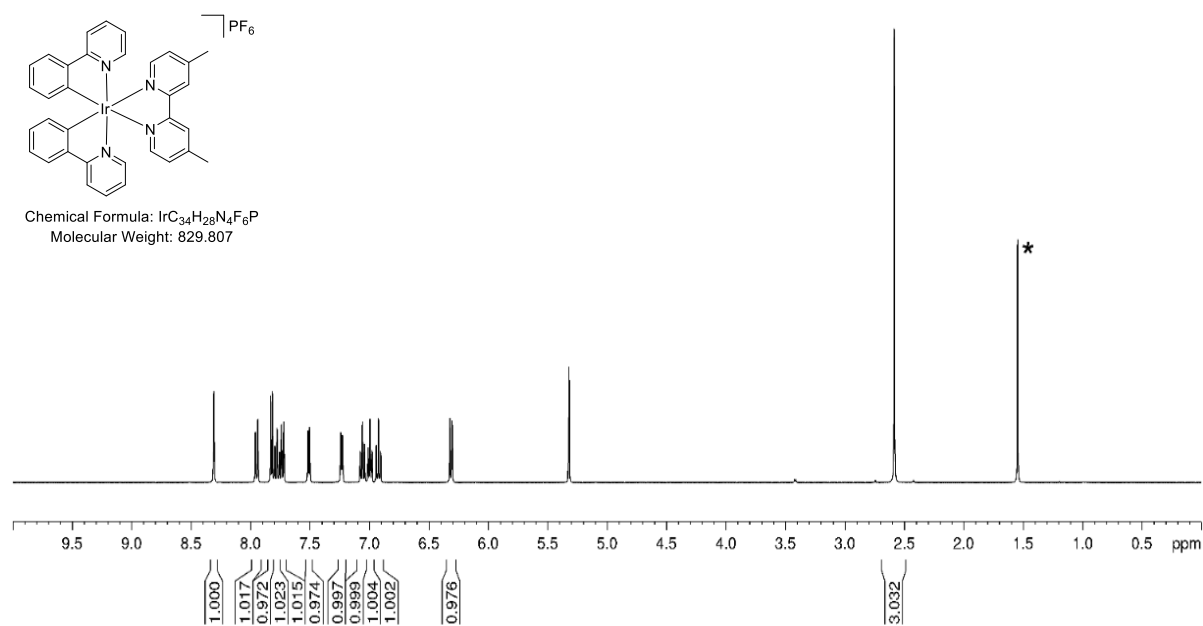
Chemical Formula: IrC$_{34}$H$_{28}$N$_4$F$_6$P
Molecular Weight: 829.807

¹H NMR (400 MHz; CD$_2$Cl$_2$): δ 8.31 (s, 1H), 7.95 (d, *J* = 8.2 Hz, 1H), 7.82 (d, *J* = 5.6 Hz, 1H), 7.78 (td, *J* = 7.8, 1.5 Hz, 1H), 7.73 (dd, *J* = 7.8, 0.9 Hz, 1H), 7.51 (d, *J* = 5.7 Hz, 1H), 7.23 (d, *J* = 5.5 Hz, 1H), 7.06 (td, *J* = 7.5, 1.1 Hz, 1H), 7.00 (ddd, *J* = 7.4, 5.9, 1.4 Hz, 1H), 6.92 (td, *J* = 7.5, 1.4 Hz, 1H), 6.32 (d, *J* = 7.6 Hz, 1H), 2.58 (s, 3H).

^{1}H NMR spectrum of [Ir(df-ppy)$_2$(dm-bpy)](PF$_6$)
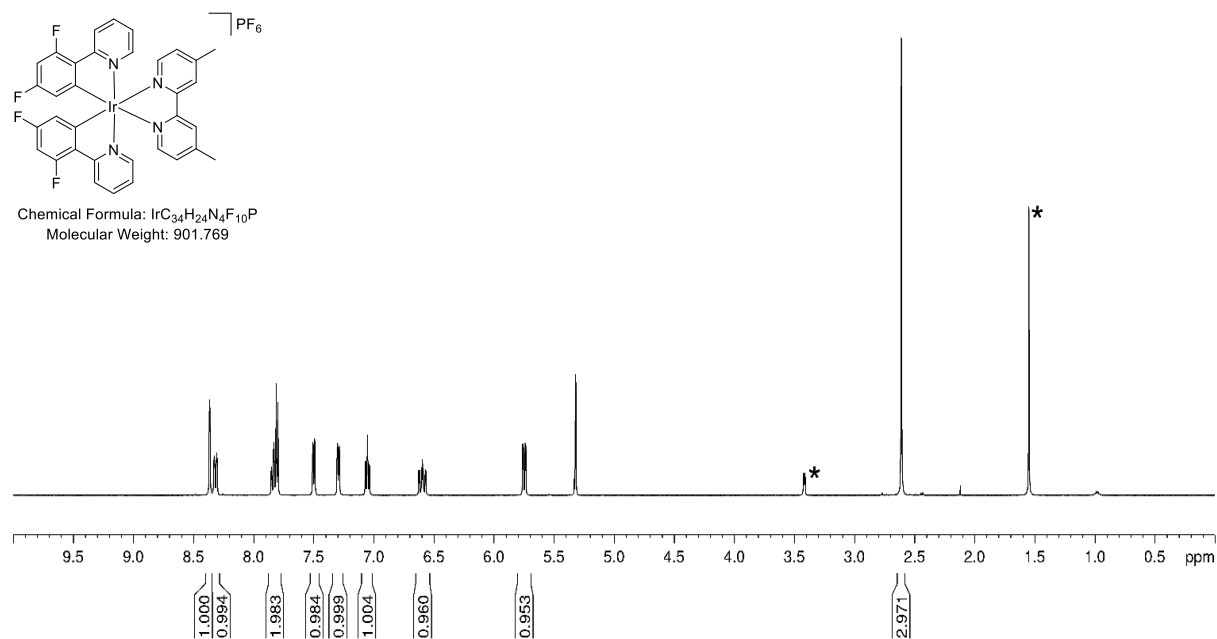
Chemical Formula: IrC$_{34}$H$_{24}$N$_4$F$_{10}$P
Molecular Weight: 901.769

^{1}H NMR (400 MHz; CD$_2$Cl$_2$): δ 8.37 (s, 1H), 8.32 (d, J = 8.4 Hz, 1H), 7.82 (m, 2H), 7.50 (d, J = 5.7 Hz, 1H), 7.29 (d, J = 5.7 Hz, 1H), 7.05 (m, 1H), 6.62 (ddd, J = 12.5, 9.2, 2.4 Hz, 1H), 5.75 (dd, J = 8.4, 2.3 Hz, 1H), 2.61 (s, 3H).

¹H NMR spectrum of [Ir(bt)₂(ptb)](PF₆)
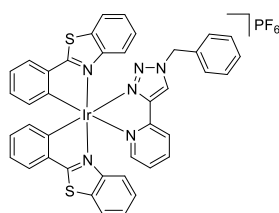
Chemical Formula: IrC$_{40}$H$_{28}$N$_6$S$_2$F$_6$P
Molecular Weight: 994.007
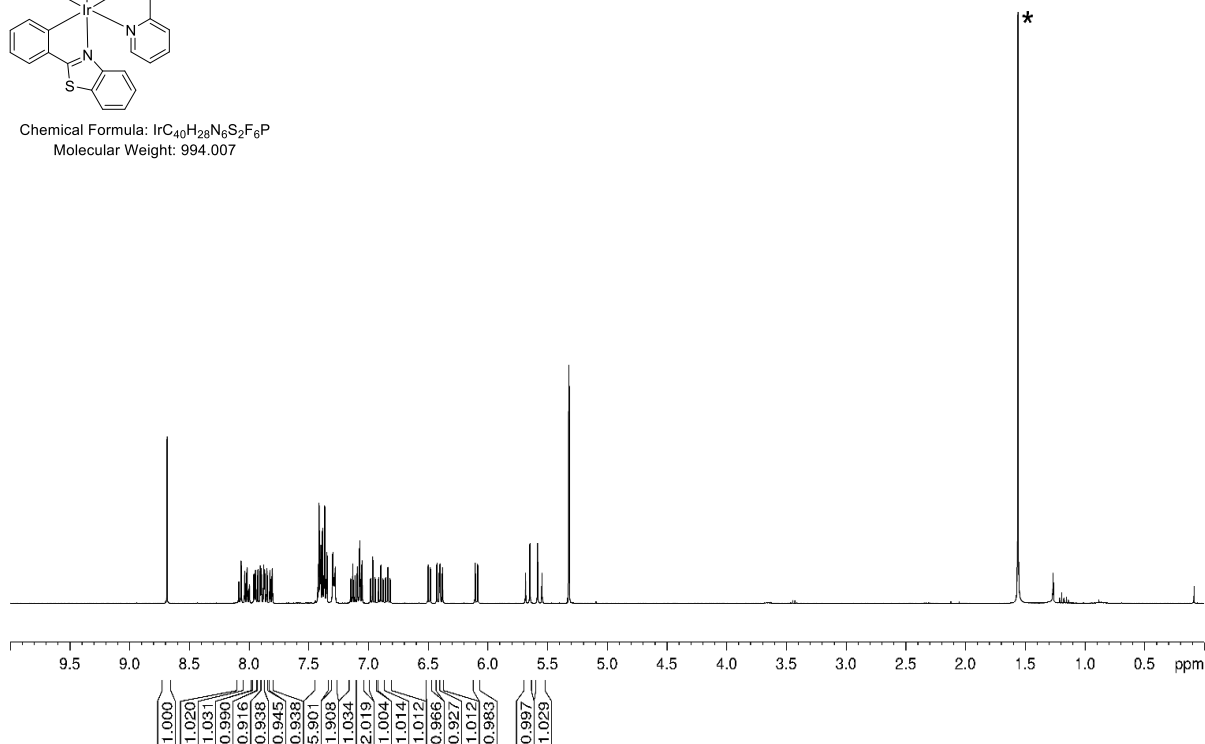
^{1}H NMR (400 MHz; CD$_2$Cl$_2$): δ 8.67 (s, 1H), 8.06 (dq, J = 8.0, 0.8 Hz, 1H), 8.00 (td, J = 7.8, 1.6 Hz, 1H), 7.94 (dq, J = 5.5, 0.8 Hz, 1H), 7.90 (dq, J = 8.1, 0.6 Hz, 1H), 7.87 (dq, J = 8.1, 0.6 Hz, 1H), 7.84 (m, 1H), 7.80 (m, 1H), 7.32-7.43 (m, 6H), 7.25-7.29 (m, 2H), 7.11 (td, J = 7.6, 1.2 Hz, 1H), 7.03-7.08 (m, 2H), 6.95 (ddd, J = 8.5, 7.3, 1.3 Hz, 1H), 6.88 (td, J = 7.6, 1.5 Hz, 1H), 6.82 (td, J = 7.6, 1.5 Hz, 1H), 6.48 (d, J = 7.7 Hz, 1H), 6.40 (d, J = 8.4 Hz, 1H), 6.37 (d, J = 7.8 Hz, 1H), 6.08 (d, J = 8.3 Hz, 1H), 5.65 (d, J = 14.8 Hz, 1H), 5.55 (d, J = 14.8 Hz, 1H).

¹³C{¹H} NMR spectrum of [Ir(bt)₂(ptb)](PF₆)

Chemical Formula: IrC$_{40}$H$_{28}$N$_6$S$_2$F$_6$P
Molecular Weight: 994.007
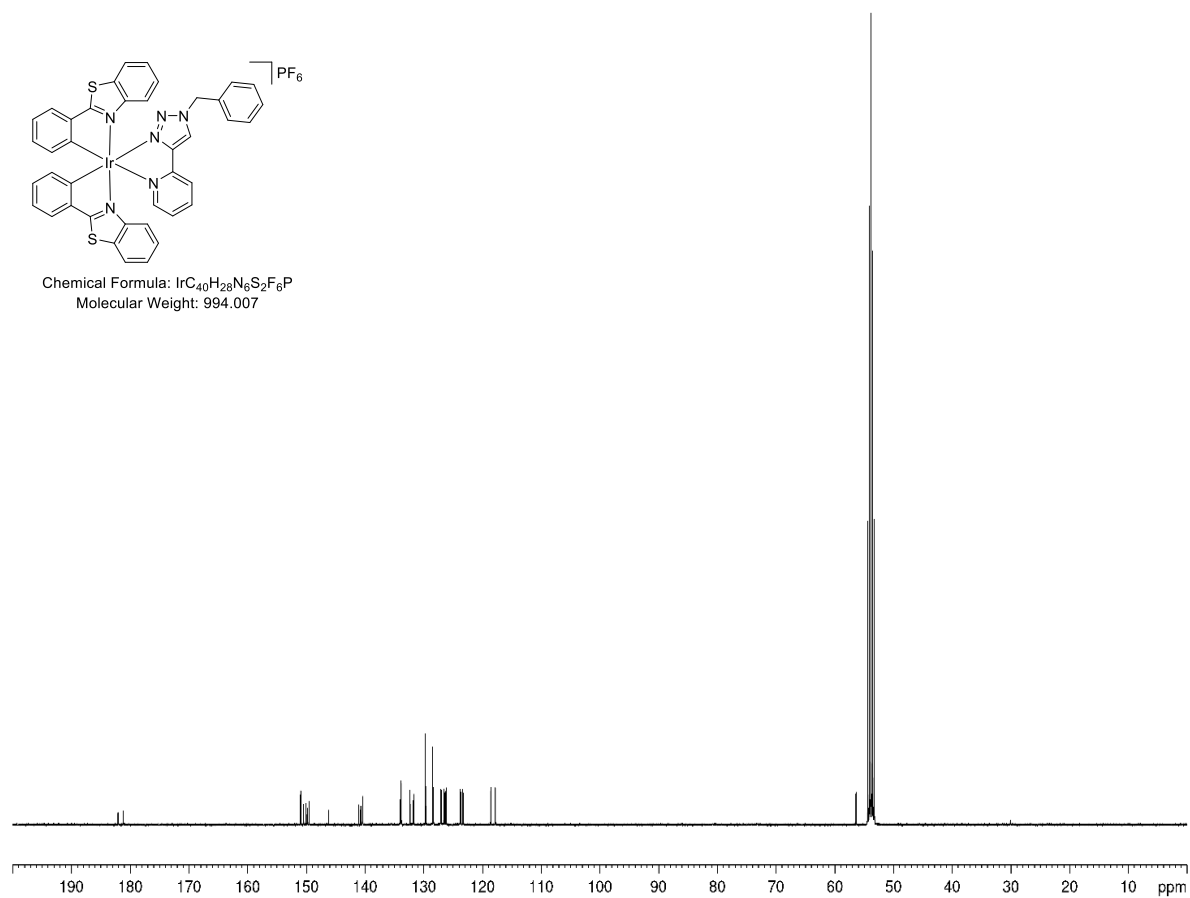
^{13}C{^{1}H} NMR (100 MHz; CD$_2$Cl$_2$): δ 182.2, 181.3, 151.1, 150.6, 150.2, 150, 149.7 (2C), 146.4, 141.3, 140.9, 140.6, 134.2, 134.0 (2C), 132.5, 132.0 (2C), 131.9, 129.9 (2C), 129.8, 128.6 (3C), 128.5, 127.3, 127.2, 126.7, 126.6, 126.4 (2C), 124, 123.9, 123.8, 123.5, 123.4, 118.7, 118, 56.5.

¹H NMR spectrum of [Ir(piq)₂(ptb)](PF₆)
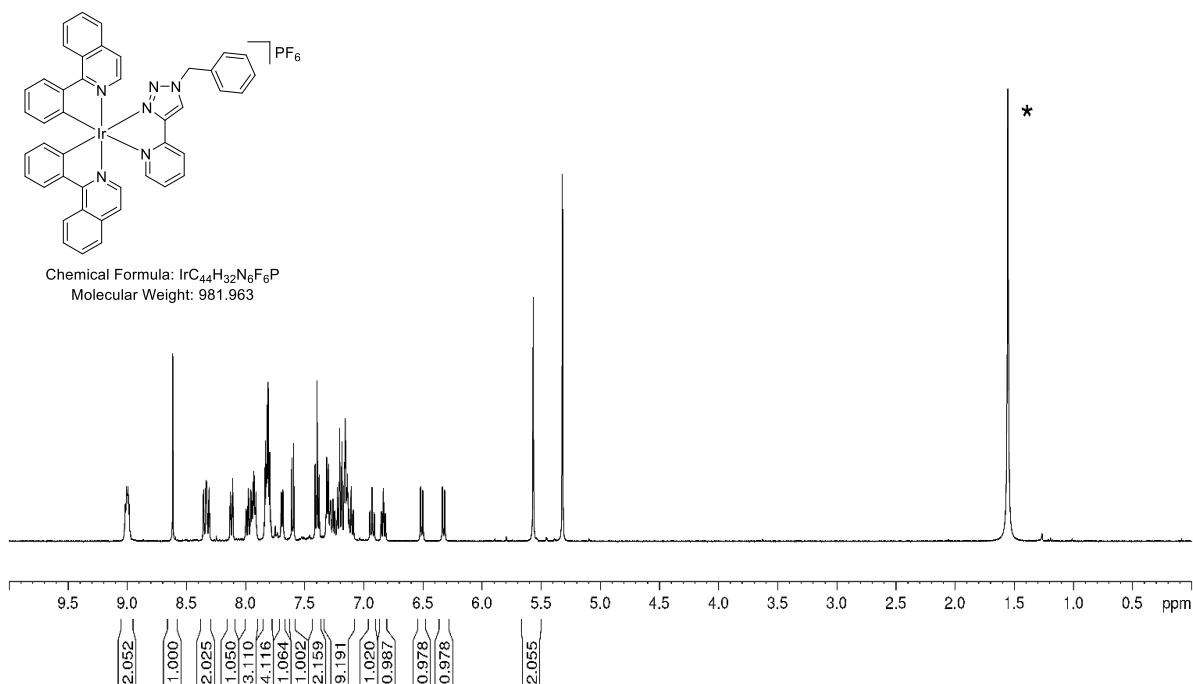
Chemical Formula: IrC$_{44}$H$_{32}$N$_6$F$_6$P
Molecular Weight: 981.963

¹H NMR spectra was consistent with the literature values. ¹H NMR (400 MHz; CD$_2$Cl$_2$): δ 9.00 (m, 2H), 8.62 (s, 1H), 8.33 (m, 2H), 8.12 (d, J = 7.9 Hz, 1H), 7.91-8.00 (m, 3H), 7.84-7.99 (m, 4H), 7.69 (d, J = 5.6 Hz, 1H), 7.60 (d, J = 6.4 Hz, 1H), 7.39 (t, J = 6.9 Hz, 2H), 7.09-7.33 (m, 9H), 6.93 (t, J = 7.4 Hz, 1H), 6.84 (t, J = 7.4 Hz, 1H), 6.51 (d, J = 7.6 Hz, 1H), 6.32 (d, J = 7.6 Hz, 1H), 5.57 (s, 2H).

¹H NMR spectrum of [Ir(ppy)₂(ptb)](PF₆)
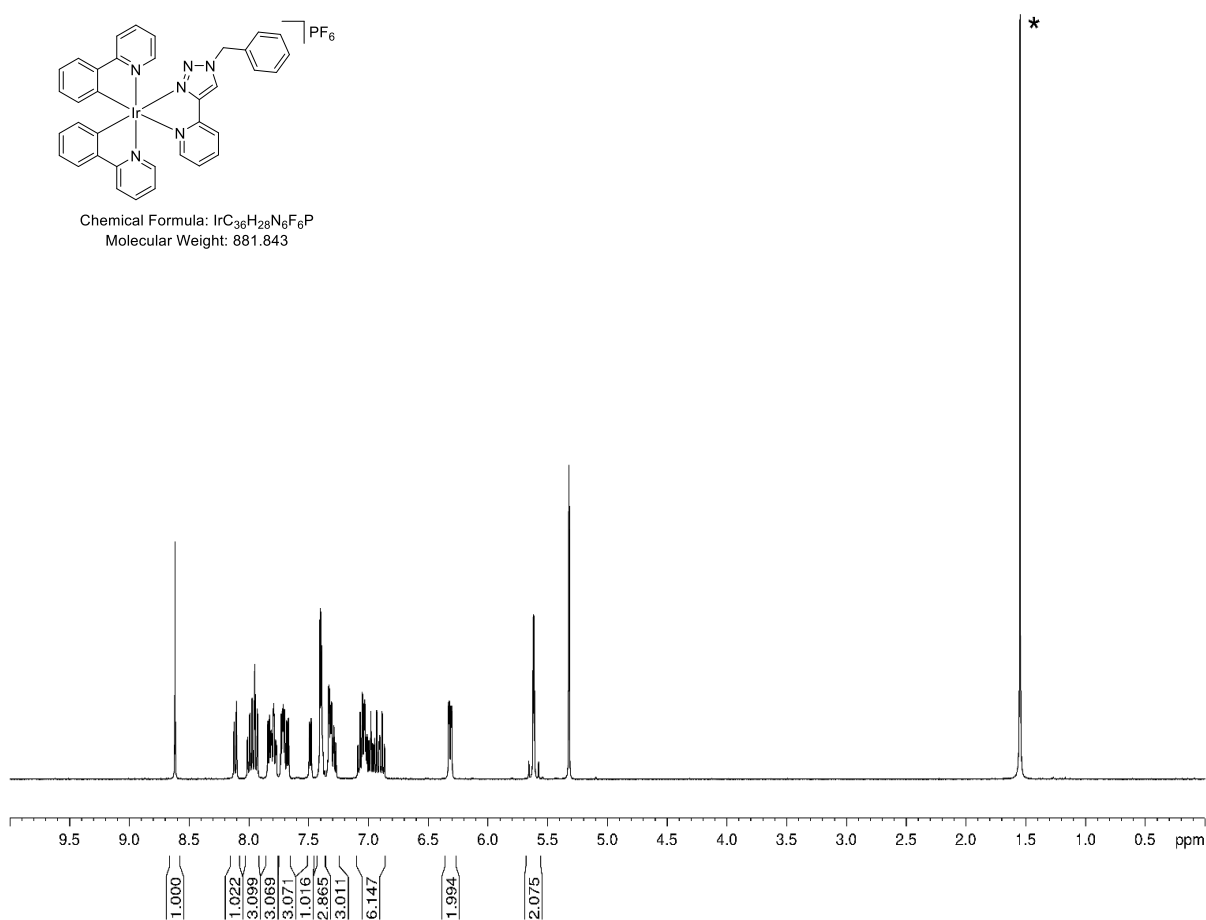
Chemical Formula: IrC₃₆H₂₈N₆F₆P
Molecular Weight: 881.843

¹H NMR (400 MHz; CD₂Cl₂): δ 8.62 (s, 1H), 8.11 (d, *J* = 7.9 Hz, 1H), 7.99 (dt, *J* = 7.9, 1.6 Hz, 1H), 7.95 (t, 8.8 Hz, 2H), 7.76-7.84 (m, 3H), 7.69-7.74 (m, 2H), 7.67 (d, *J* = 5.8 Hz, 1H), 7.49 (d, *J* = 5.8 Hz, 1H), 7.38-7.42 (m, 3H), 7.26-7.34 (m, 3H), 7.00-7.09 (m, 3H), 6.98 (ddd, *J* = 7.5, 5.8, 1.4 Hz, 1H), 6.93 (td, *J* = 7.5, 1.3 Hz, 1H), 6.88 (td, *J* = 7.5, 1.3 Hz, 1H), 6.32 (dd, *J* = 7.7, 0.6 Hz, 1H), 6.31 (dd, *J* = 7.6, 0.8 Hz, 1H), 5.62 (m, 2H).

¹H NMR spectrum of [Ir(df-ppy)₂(ptb)](PF₆)
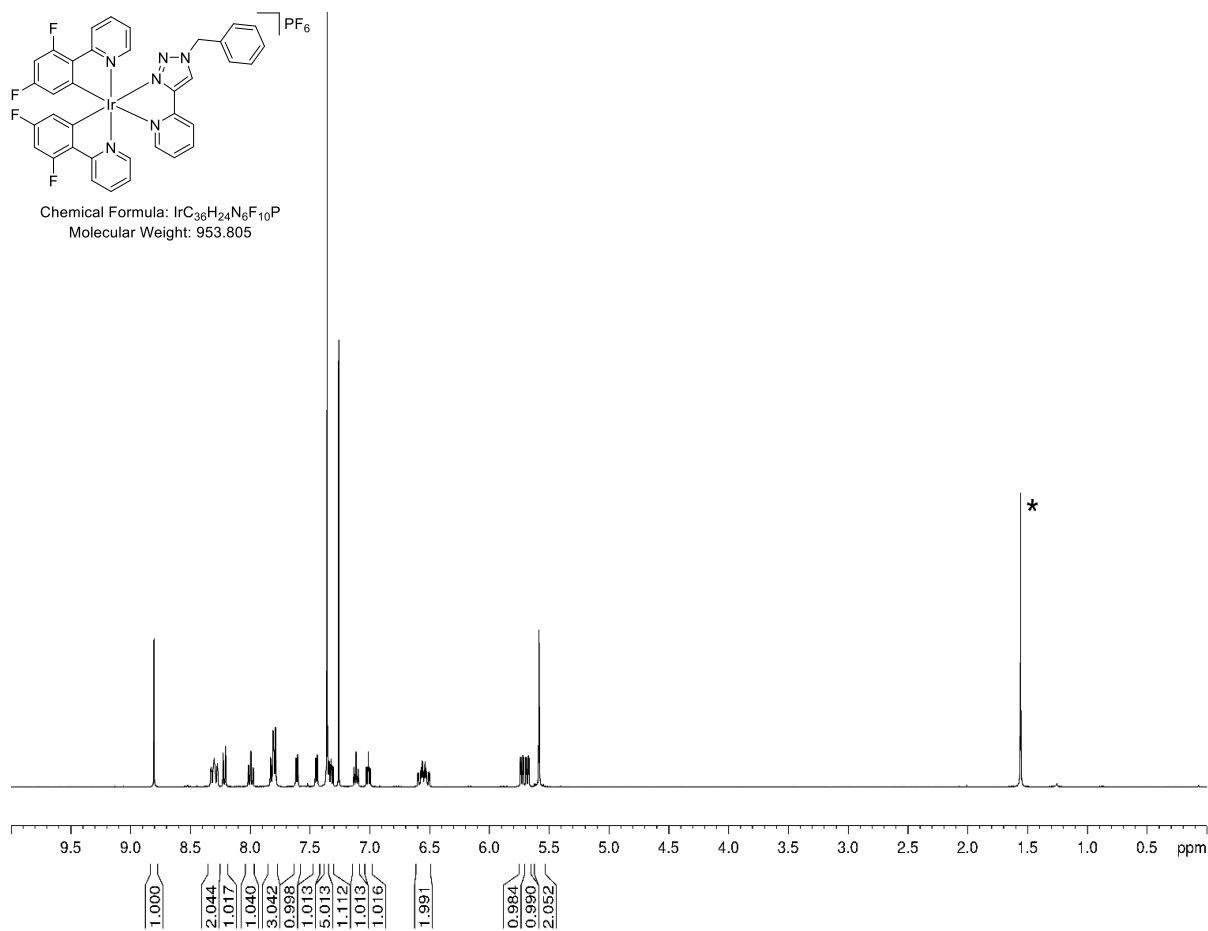
Chemical Formula: IrC$_{36}$H$_{24}$N$_6$F$_{10}$P
Molecular Weight: 953.805

^{1}H NMR (400 MHz; CDCl$_3$): δ 8.80 (s, 1H), 8.30 (t, J = 10.5 Hz, 2H), 8.22 (d, J = 7.9 Hz, 1H), 8.00 (td, J = 7.9, 1.5 Hz, 1H), 7.79-7.83 (m, 3H), 7.61 (d, J = 5.8 Hz, 1H), 7.45 (d, J = 5.8 Hz, 1H), 7.36 (s, 5H), 7.32 (m, 1H), 7.11 (ddd, J = 7.3, 5.9, 1.3 Hz, 1H), 7.01 (ddd, J = 7.3, 5.9, 1.3 Hz, 1H), 6.55 (m, 2H), 5.73 (dd, J = 8.5, 2.5 Hz, 1H), 5.68 (dd, J = 8.5, 2.3 Hz, 1H), 5.58 (s, 2H).

NMR spectra of [Ir(C^N)₂(pt-TEG)]Cl complexes

[Ir(ppy)₂(pt-TEG)]Cl, CDCl₃. Residual solvent marked with an asterisk.
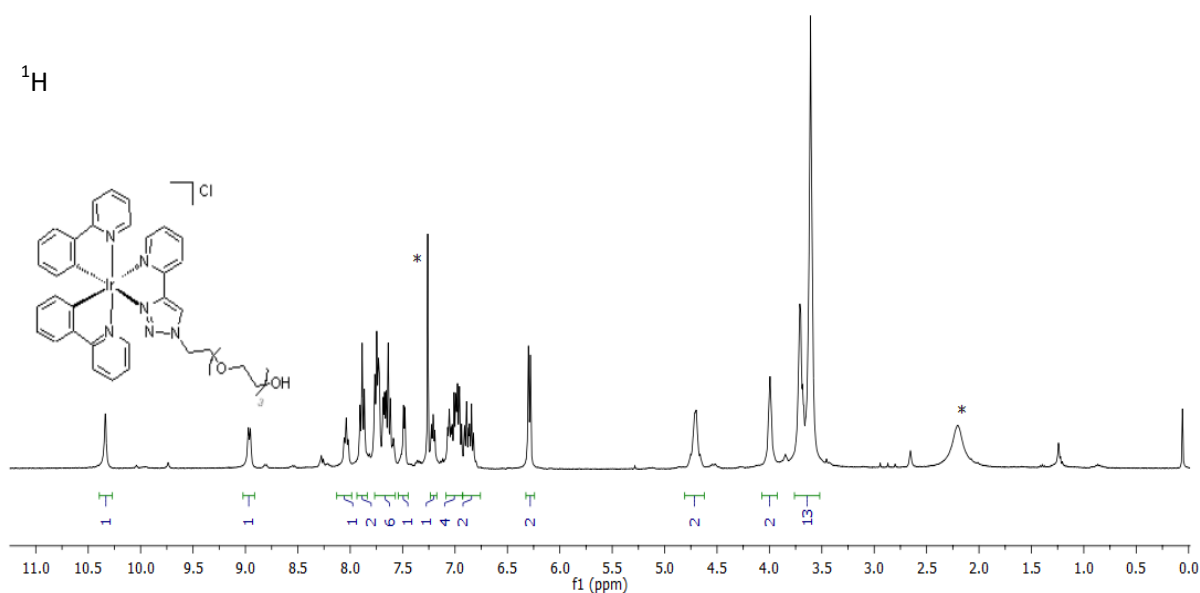
^{1}H NMR (500 MHz; CDCl₃): δ 10.46 (s, 1H), 9.04 (d, J = 8.0 Hz, 1H), 8.04 (td, J = 7.8, 1.5 Hz, 1H), 7.90 (m, 2H), 7.78-7.74 (m, 3H), 7.70 (dd, J = 5.8, 0.7 Hz, 1H), 7.67-7.64 (m, 2H), 7.50 (dd, J = 5.8, 0.7 Hz, 1H), 7.22 (ddd, J = 7.6, 5.6, 1.3 Hz, 1H), 7.07 (ddd, J = 7.3, 5.9, 1.4 Hz, 1H), 7.03 (td, J = 7.5, 1.0 Hz, 1H), 7.00-6.97 (m, 2H), 6.91 (td, J = 7.4, 1.2 Hz, 1H), 6.87 (td, J = 7.4, 1.2 Hz, 1H), 4.77-4.68 (m, 2H), 4.05-3.99 (m, 2H), 3.76-3.66 (m, 4H), 3.68-3.57 (m, 8H).

^{13}C{^{1}H}
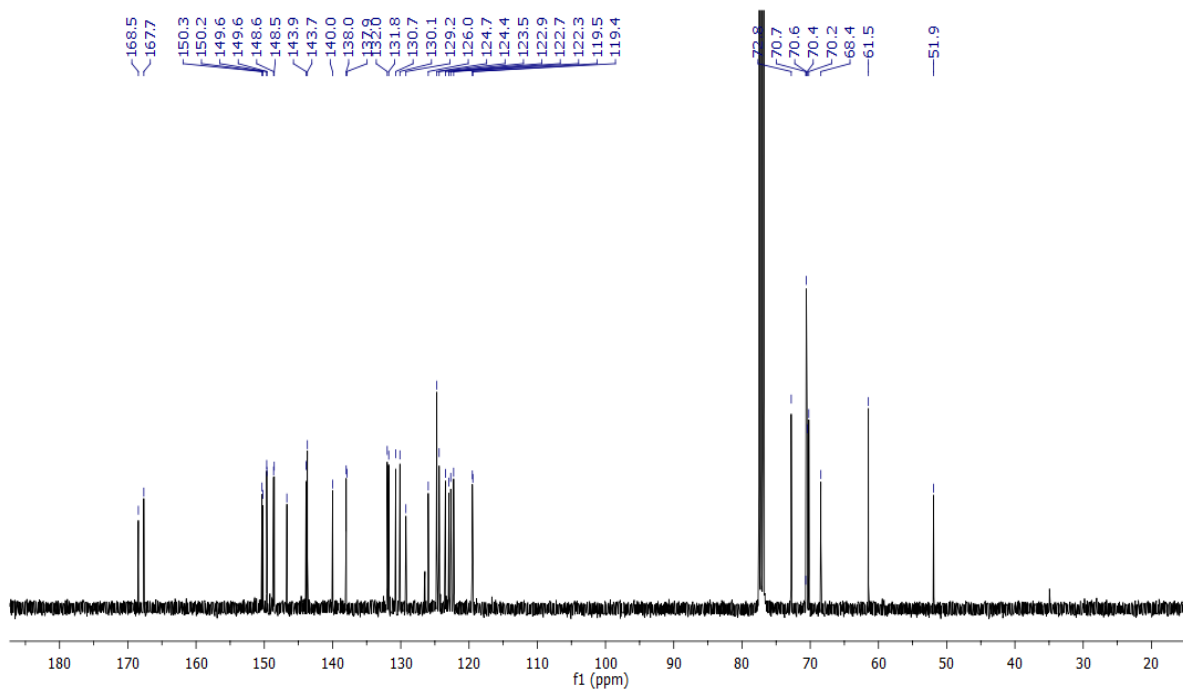
^{13}C NMR (126 MHz; CDCl$_3$): δ 168.4, 167.6, 150.3, 150.1, 149.5, 149.4, 148.5, 148.4, 146.6, 143.8, 143.6, 139.8, 137.8, 137.7, 131.9, 131.7, 130.6, 130, 129.3, 125.8, 124.7, 124.6, 124.2, 123.3, 122.8, 122.6, 122.1, 119.4, 119.3, 72.6, 70.5 (2C), 70.4, 70.1, 68.3, 61.4, 51.8.

[Ir(df-ppy)₂(pt-TEG)]Cl, CDCl₃. Residual solvent marked with an asterisk.

^{1}H

^{1}H NMR (500 MHz; CDCl₃): δ 9.16 (s, 1H), 8.40 (d, J = 8.0 Hz, 1H), 8.28 (t, J = 10.0 Hz, 2H), 8.01 (t, J = 7.8 Hz, 1H), 7.80 (m, 3H), 7.65 (d, J = 5.7 Hz, 1H), 7.50 (d, J = 5.7 Hz, 1H), 7.31 (t, J = 6.6 Hz, 1H), 7.15 (t, J = 6.7 Hz, 1H), 7.05 (t, J = 6.7 Hz, 1H), 6.55 (m, 1H), 6.48 (m, 1H), 5.71 (d, J = 7.7 Hz, 1H), 5.66 (d, J = 8.0 Hz, 1H), 4.69-4.58 (m, 2H), 3.95-3.89 (m, 2H), 2.69 (broad s, 1H).
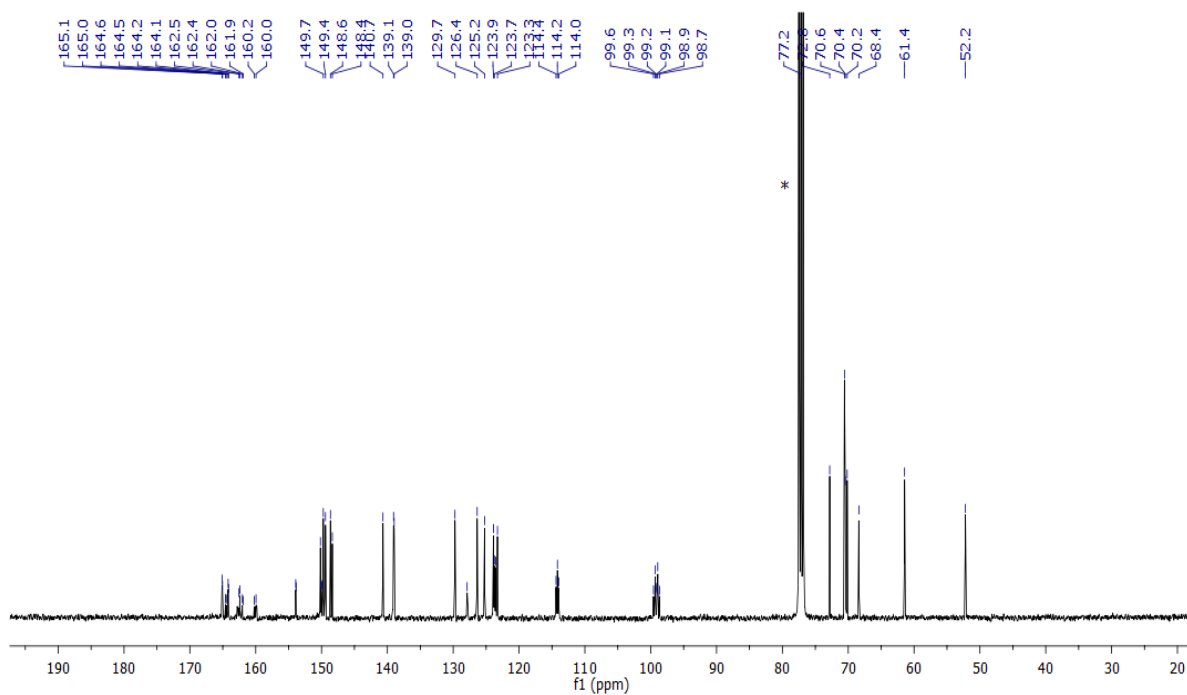
^{13}C NMR (101 MHz; CDCl$_3$): δ 165.1 (m, CF), 164.5 (m, CF), 164.2 (m, CF), 162.6 (m, CF), 162.0 (m), 160.0 (m), 153.9 (d), 150.2, 150.0 (d), 149.7, 149.4, 148.7, 148.4, 140.7, 139.1, 139.0, 129.7, 127.9 (m, 2C), 126.4, 125.2, 123.9, 123.7 (d), 123.5 (d), 123.3, 114.2 (m, 2C), 99.1 (m, 2C), 77.4, 72.8, 70.6, 70.5, 70.2, 68.4, 61.4, 52.2.

^{19}F NMR (376 MHz; CDCl$_3$): δ -106.3 (m, 1F), -107.2 (m, 1F), -109.2 (m, 1F), -110.1 (m, 1F).

[Ir(bt)$_2$(pt-TEG)]Cl, d$_6$-DMSO. Residual solvent marked with an asterisk.
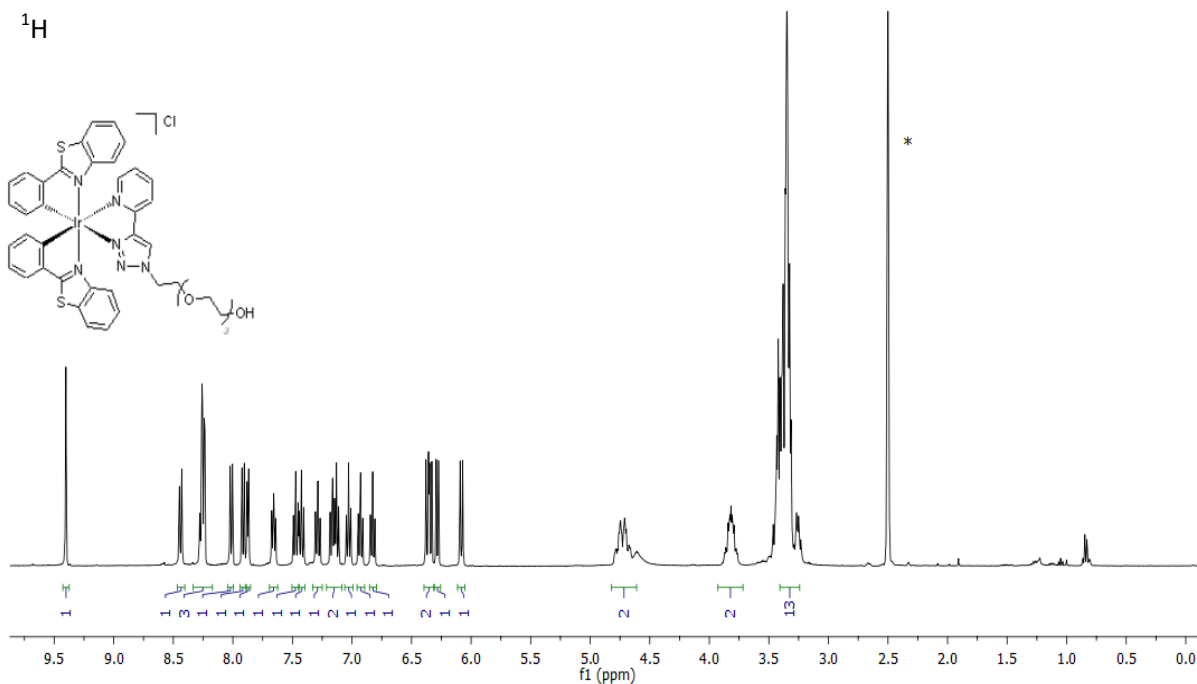
^{1}H NMR (400 MHz; DMSO-d$_6$): δ 9.40 (s, 1H), 8.44 (d, J = 8.0, 1H), 8.25 (m, 3H,), 8.01 (d, J = 7.7 Hz, 1H), 7.91 (d, J = 7.6 Hz, 1H,), 7.87 (d, J = 5.5 Hz, 1H), 7.66 (m, 1H), 7.46 (m, 1H), 7.42 (m, 1H), 7.29 (m, 1H), 7.14 (m, 2H), 7.02 (m, 1H), 6.93 (m, 1H), 6.83 (m, 1H), 6.35 (m, 2H), 6.28 (d, J = 7.7, 1H), 6.08 (d, J = 8.4, 1H), 4.73 (m, 2H), 3.82 (m, 2H), 3.45 (m, 13H).
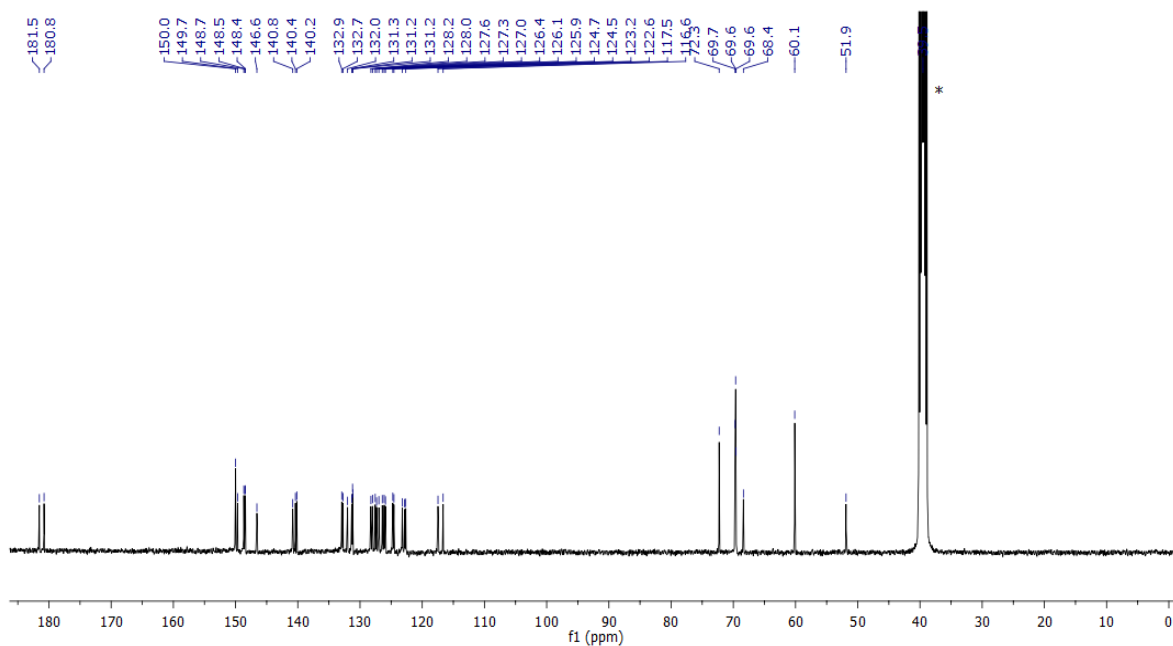
^{13}C{^{1}H} NMR (101 MHz; DMSO-d$_6$): δ 181.5, 180.8, 150.0, 149.7, 148.7, 148.5, 148.4, 146.6, 140.8, 140.4, 140.2, 132.9, 132.8, 132.0, 131.3, 131.2 (2C), 131.2, 128.3, 128.0, 127.6, 127.3, 127.0, 126.4, 126.1, 125.9, 124.7, 124.6, 123.2, 122.8, 122.7, 117.5, 116.6, 72.3, 69.7, 69.6, 69.6, 69.6, 68.4, 60.1, 51.9.

Ir(piq)₂(pt-TEG)]Cl, CDCl₃. Residual solvent marked with an asterisk.
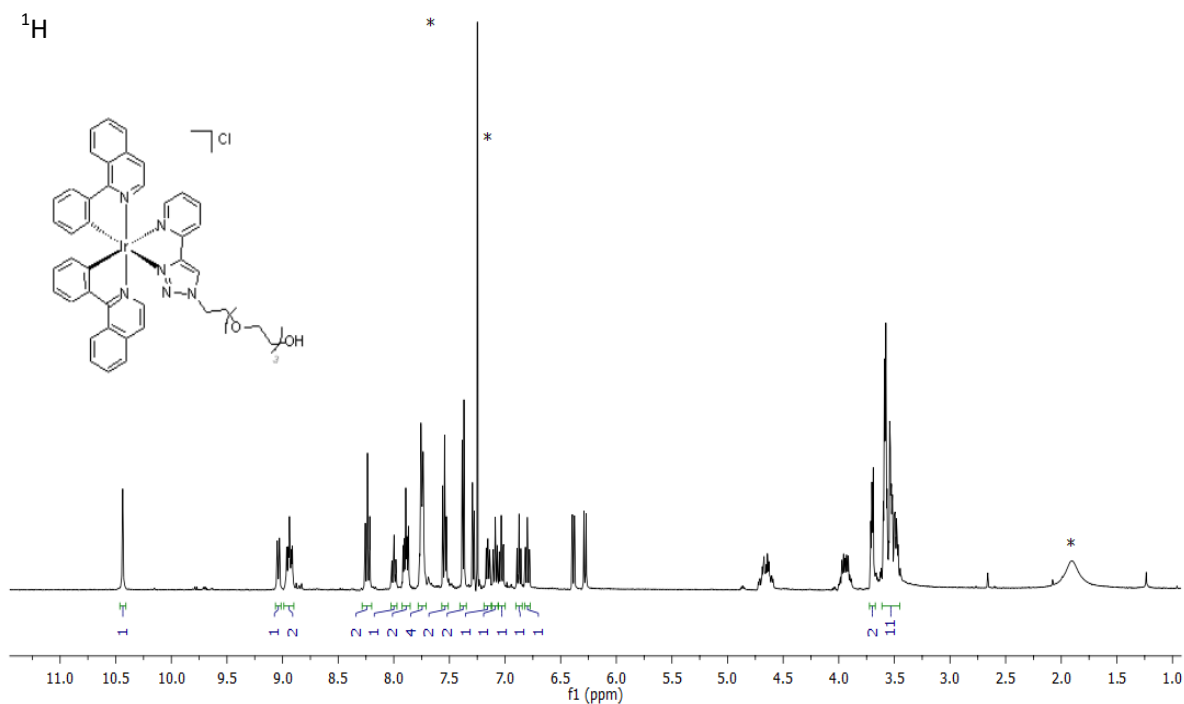
¹H NMR (400 MHz; CDCl₃): δ 10.38 (s, 1H), 9.02 (d, J = 7.9, 1H), 8.95 (ddd, J = 10.5, 6.9, 3.4, 2H), 8.24 (dd, J = 10.4, 5.9, 2H), 8.01 (td, J = 7.8, 1.5, 1H), 7.93-7.87 (m, 2H), 7.79-7.72 (m, 4H), 7.58-7.53 (m, 2H), 7.41-7.37 (m, 2H), 7.32-7.28 (m, 1H), 7.18-7.14 (m, 1H), 7.12-7.08 (m, 1H), 7.06-7.02 (m, 1H), 6.90-6.86 (m, 1H), 6.83-6.79 (m, 1H), 6.39 (dd, J = 7.7, 1.1, 1H), 6.30-6.28 (m, 1H), 4.70-4.61 (m, 2H), 3.94 (ddd, J = 13.0, 6.4, 4.2, 1H), 3.71 (dd, J = 6.0, 3.0, 2H), 3.64-3.45 (m, 11H).
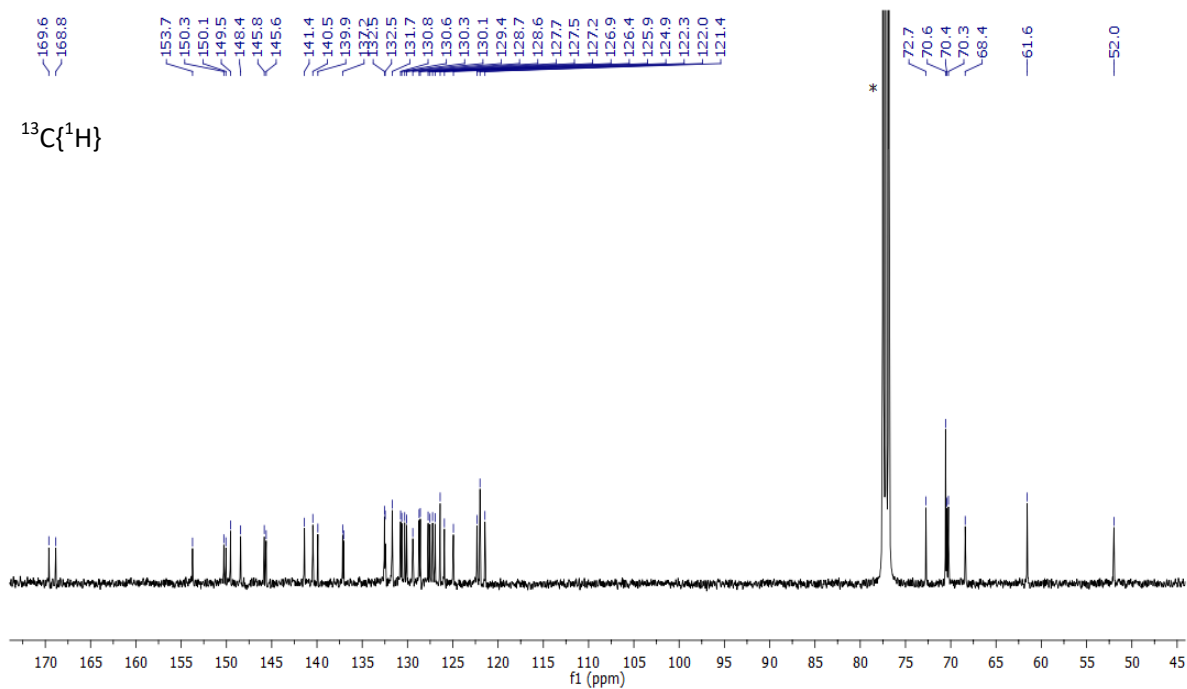
$^{13}C\{^1H\}$

$^{13}C\{^1H\}$ NMR (101 MHz; CDCl$_3$): δ 169.6, 168.8, 153.7, 150.2, 150.1, 149.6, 148.4, 145.8, 145.6, 141.4, 140.5, 139.9, 137.2, 137.1, 132.6, 132.5, 131.7, 131.7, 130.8, 130.6, 130.3, 130.1, 129.3, 128.7, 128.6, 127.7, 127.5, 127.2, 126.9, 126.4, 125.9, 124.9, 122.3, 122.0, 121.0, 121.5, 77.4, 72.8, 70.6, 70.6, 70.4, 70.2, 68.4, 61.5, 52.0.
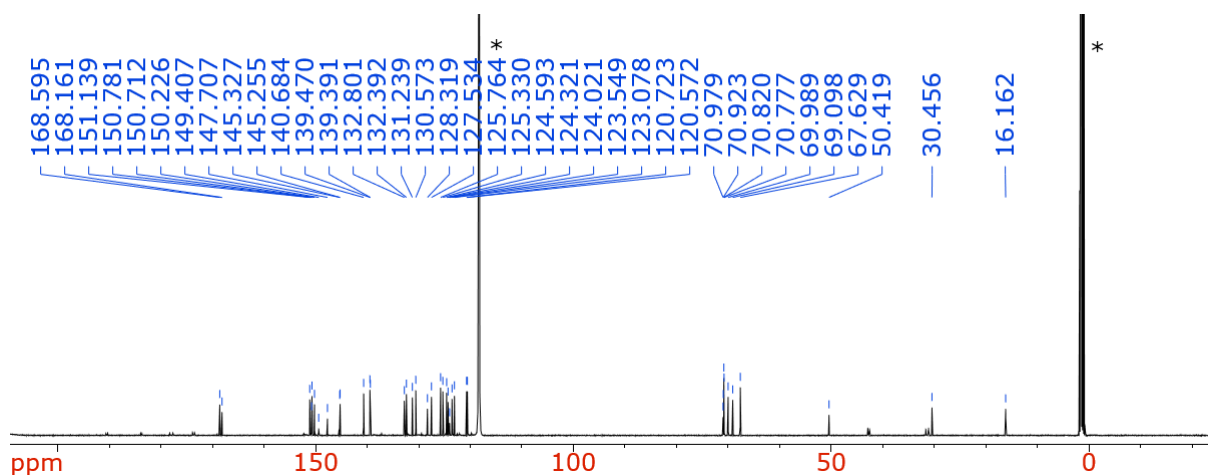
NMR spectra of [Ir(C^N)₂(pt-TOxT-Sq)]Cl ECL labels

[Ir(ppy)₂(pt-TOxT-Sq)]Cl, CD₃CN. Residual solvent marked with an asterisk.
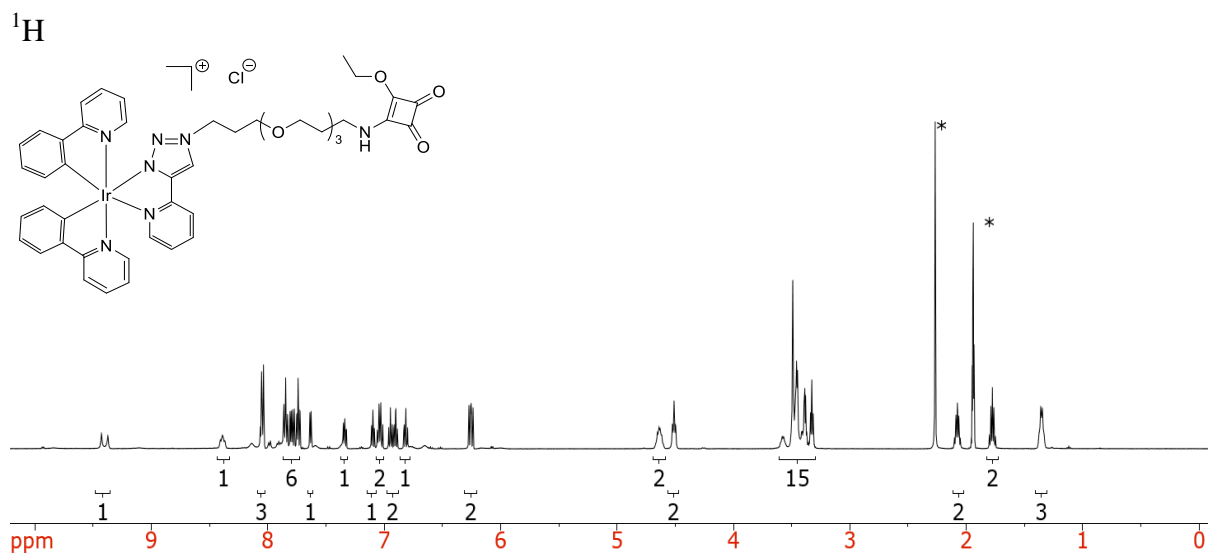
¹H

¹H NMR (500 MHz; CD₃CN): δ 9.40 (m, 1H), 8.41-8.37 (m, 1H), 8.05 (m, 3H), 7.86-7.74 (m, 6H), 7.63 (d, *J*=5.3 Hz, 1H), 7.34 (ddd, *J* =7.4, 5.8, 1.3 Hz, 1H), 7.10 (ddd, *J* = 7.3, 6.0, 1.3, 1H), 7.04 (m, 2H), 6.92 (m, 2H), 6.81 (td, *J* = 7.4, 1.1 Hz, 1H), 6.26 (m, 2H), 4.64 (m, 2H), 4.51 (m, 2H), 3.45 (m, 15H), 2.08 (q, *J* = 6.2, 2H), 1.78 (q, *J* = 6.4, 2H), 1.35 (m, 3H).

$^{13}C\{^1H\}$

$^{13}C\{^1H\}$ NMR (126 MHz; CD$_3$CN): δ 168.6, 168.2, 151.1, 150.8, 150.7, 150.2, 149.4, 147.7, 145.3, 145.3, 140.7, 139.5, 139.4, 132.8, 132.4, 131.2, 130.6, 128.3, 127.5, 125.8, 125.3, 124.6, 124.3, 124.0, 123.5, 123.1, 120.7, 120.6, 71.0, 70.9, 70.8, 70.8, 70 .0, 69.1, 67.6, 50.4, 30.5, 16.2.

[Ir(bt)₂(pt-TOxT-Sq)]Cl, CD₃CN. Residual solvent marked with an asterisk.
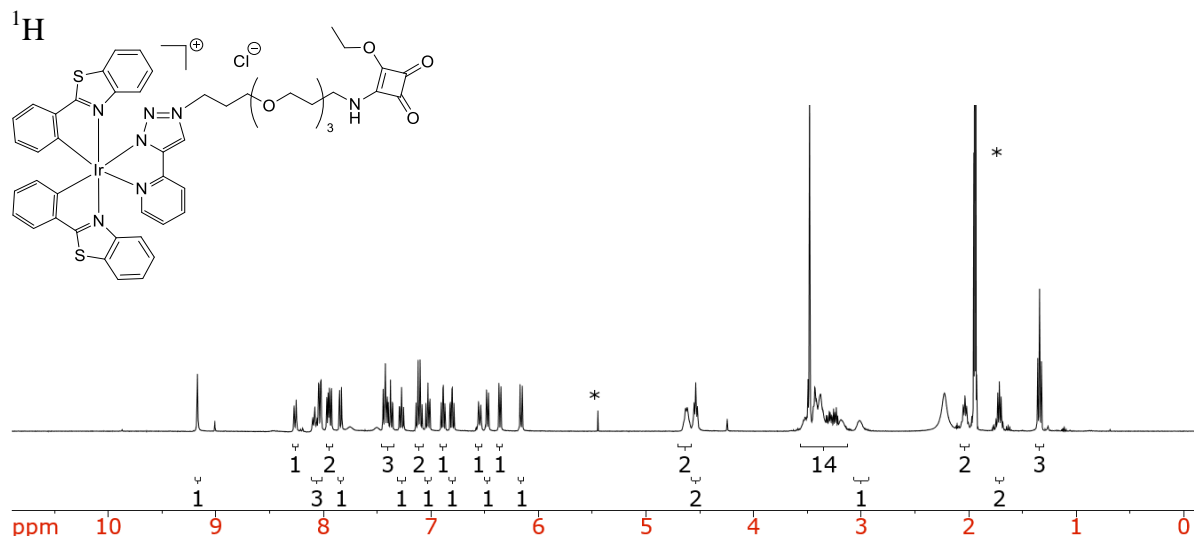
¹H NMR (400 MHz; CD₃CN): δ 9.16 (s, 1H), 8.26 (d, $J = 7.9$ Hz, 1H), 8.06 (m, 3H), 7.95 (m, 2H), 7.84 (m, 1H), 7.40 (m, 3H), 7.27 (m, 1H), 7.11 (m, 2H), 7.03 (td, $J = 7.5, 1.0$ Hz, 1H), 6.89 (td, $J = 7.5, 1.3$ Hz, 1H), 6.80 (td, $J = 7.5, 1.3$ Hz, 1H), 6.55 (d, $J = 8.3$ Hz, 1H), 6.47 (d, $J = 7.6$ Hz, 1H), 6.36 (d, $J = 7.6$ Hz, 1H), 6.16 (d, $J = 8.4$ Hz, 1H), 4.62 (d, $J = 6.3$ Hz, 2H), 4.54 (t, $J = 6.5$ Hz, 2H), 3.37 (m, 14H), 3.02 (s, 1H), 2.03 (q, $J = 6.1$, 2H), 1.71 (q, $J = 6.3$, 2H), 1.34 (t, $J = 14.1$, 3H).

$^{13}C\{^1H\}$
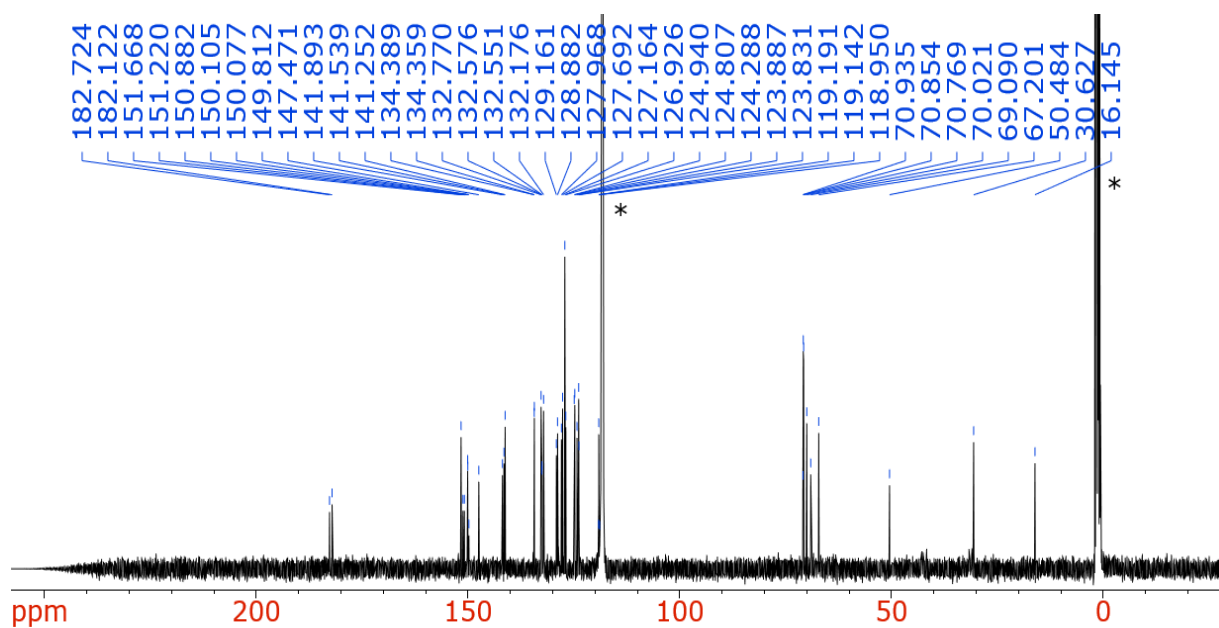
$^{13}C\{^1H\}$ NMR (101 MHz; CD$_3$CN): δ 182.7, 182.1, 151.7, 151.2, 150.9, 150.1, 150.1, 149.8, 147.5, 141.9, 141.5, 141.3, 134.4, 134.4, 132.8, 132.6, 132.6, 132.2, 129.2, 128.9, 128.6, 128.0, 127.7, 127.2, 126.9, 124.9, 124.8, 124.3, 123.9, 123.8, 119.1, 118.3, 70.9, 70.9, 70.8, 70.0, 69.1, 67.2, 50.5, 42.9, 42.6, 31.6, 31.0, 30.6, 18.8, 16.1.

[Ir(piq)₂(pt-TOxT-Sq)]Cl, CD₃CN. Residual solvent marked with an asterisk.
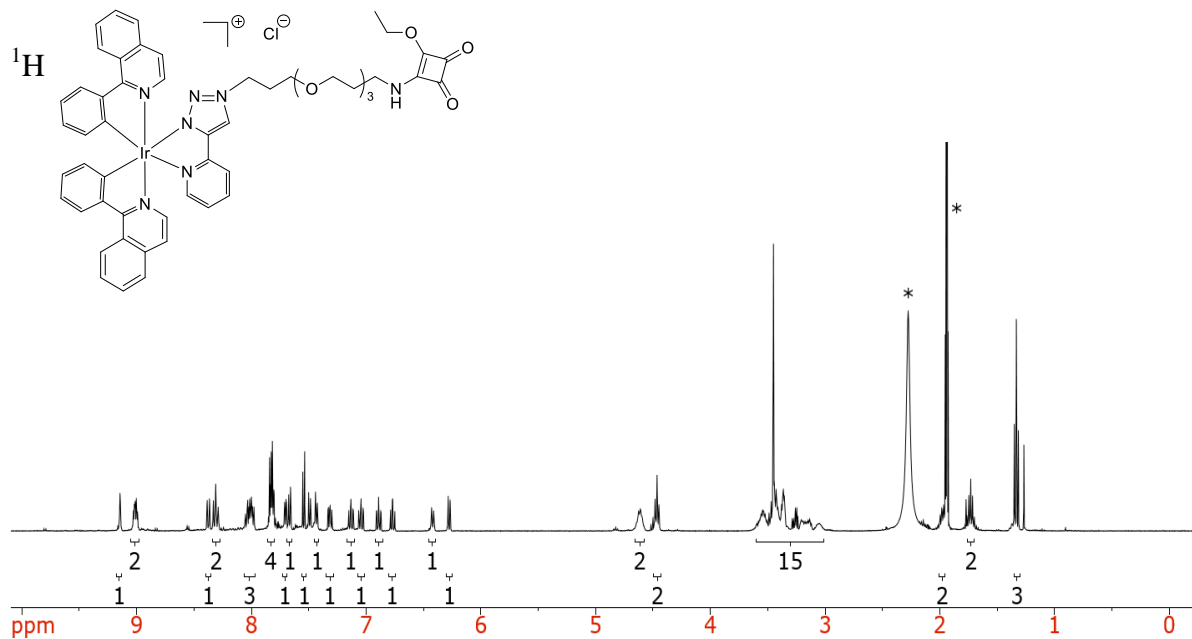

¹H NMR (400 MHz; [CD₃CN]): δ 9.14 (s, 1H), 9.01 (m, 2H), 8.38 (d, *J* = 8.0 Hz, 1H), 8.31 (m, 2H), 8.02 (m, 3H,), 7.83 (m, 4H), 7.70 (m, 1H), 7.67 (d, *J* = 6.4 Hz), 7.54 (d, *J* = 6.4 Hz, 1H), 7.49 (d, *J* = 6.4, 1H), 7.43 (d, *J* = 6.4 Hz, 1H), 7.31 (ddd, *J* = 7.7, 5.6, 1.3 Hz, 1H), 7.13 (ddd, *J* = 8.2, 7.2, 1.2 Hz, 1H), 7.04 (ddd, *J* = 8.2, 7.1, 1.2 Hz, 1H), 6.89 (td, *J* = 7.4, 1.2 Hz, 1H), 6.77 (td, *J* = 7.4, 1.2 Hz, 1H), 6.42 (d, *J* = 7.5 Hz, 1H), 6.28 (dd, *J* = 7.7, 1.1 Hz, 1H), 4.62 (m, 2H), 4.46 (t, *J* = 6.8 Hz, 2H), 3.32 (m, 15H), 1.98 (dd, *J* = 6.5, 5.2 Hz, 2H), 1.73 (q, *J* = 6.4 Hz, 2H), 1.33 (t, *J* = 7.1 Hz, 3H).
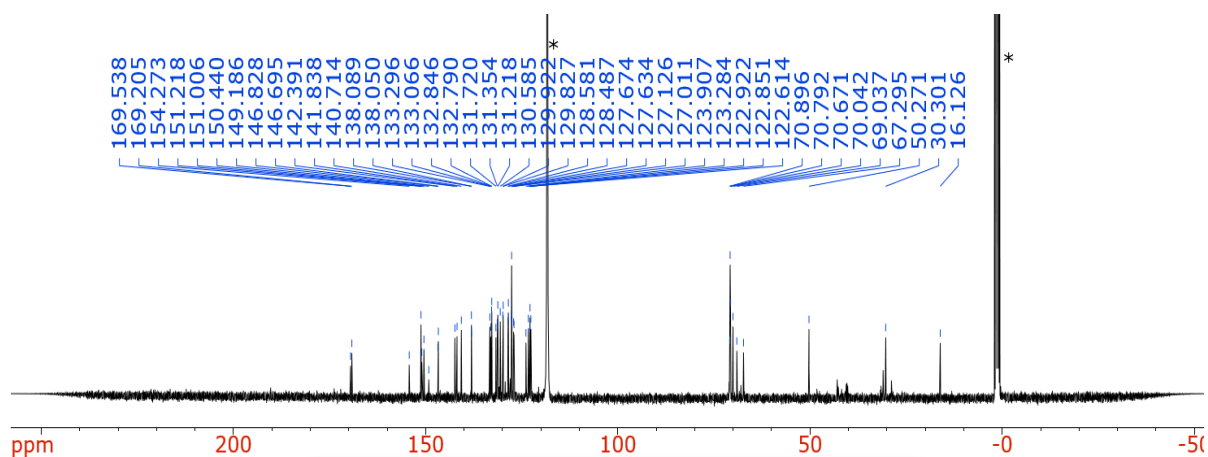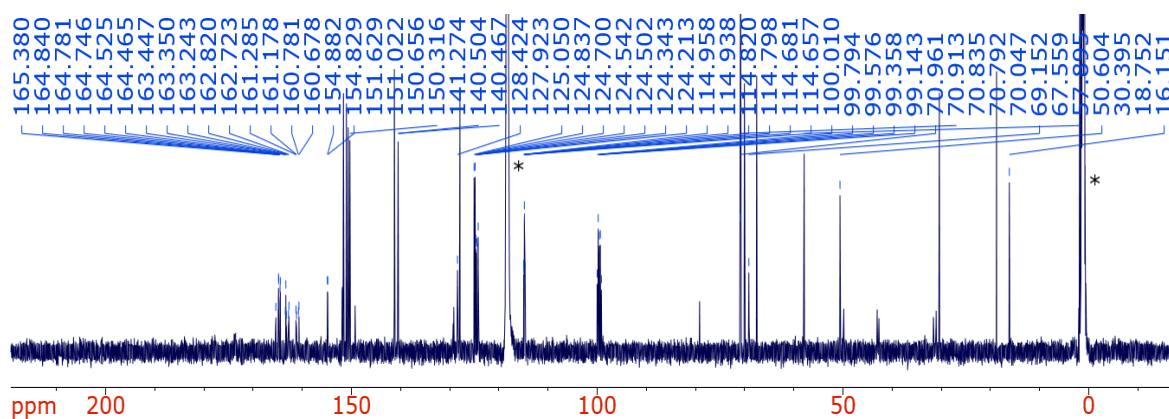
$^{13}C\{^1H\}$

$^{13}C\{^1H\}$ NMR (101 MHz; [CD$_3$CN]): δ 169.5, 169.2, 154.3, 151.2, 151.0, 150.4, 149.2, 146.8, 146.7, 142.4, 141.8, 140.7, 138.1, 138.0, 133.3, 133.1, 132.8, 132.8, 131.7, 131.3, 131.2, 130.6, 129.9, 129.8, 128.6, 128.5, 128.1, 127.7, 127.6, 127.1, 127.0, 123.9, 123.3, 122.9, 122.8, 122.6, 70.9, 70.8, 70.7, 70.0, 69.0, 67.3, 50.3, 30.3, 16.1.

[Ir(df-ppy)₂(pt-TOxT-Sq)]Cl, CD₃CN. Residual solvent marked with an asterisk.
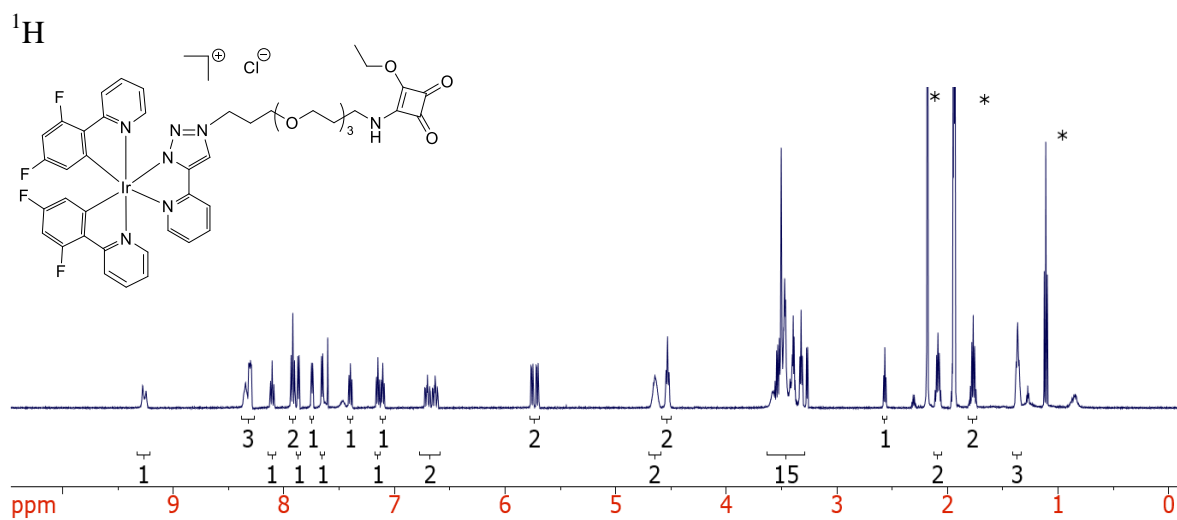
¹H

¹H NMR (500 MHz; CD₃CN): δ 9.50 (m, 1H), 8.44 (m, 1H), 8.30 (m, 2H), 8.10 (m, 1H), 7.89 (m, 3H), 7.76 (m, 1H), 7.66 (m, 1H), 7.39 (m, 1H), 7.13 (m, 2H), 6.66 (m, 2H), 5.73 (ddd, *J* = 24.1, 8.7, 2.3 Hz, 2H), 4.63 (m, 2H), 4.54 (m, 2H), 3.45 (m, 15H), 2.09 (q, *J* = 6.2 Hz, 2H), 1.78 (q, *J* = 6.4 Hz, 2H), 1.36 (m, 3H).

¹³C{¹H}

¹³C{¹H} NMR (126 MHz; CD3CN): δ 164.7 (m, CF), 163.4 (m, CF), 162.8 (m,CF), 161.0 (m, CF), 154.9 (m, CF), 151.9 (m, CF), 151.6, 151.0, 150.7, 150.3, 141.3, 140.5, 140.5, 128.4, 128.0, 125.1, 124.8, 124.7, 124.54, 124.5, 124.3, 124.2, 114.8 (m, CF), 99.6 (m, CF), 71.0, 70.9, 70.8, 70.79, 70.0, 69.2, 67.6, 57.9, 50.6, 30.4, 18.8, 16.2.

¹⁹F
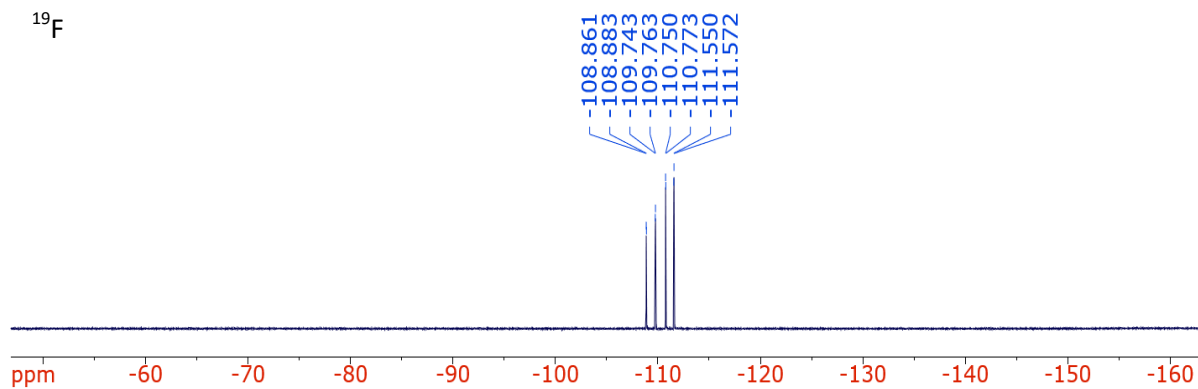
¹⁹F NMR (471 MHz; CD₃CN): δ -106.18 (d, *J* = 10.6, 1F), -107.06 (d, *J* = 9.6, 1F), -108.07 (d, *J* = 10.5, 1F), -108.87 (d, *J* = 10.2, 1F).

References

1. Miao, W.; Choi, J.-P.; Bard, A. J., Electrogenerated chemiluminescence 69: the tris(2,2'-bipyridine)ruthenium(II), $(Ru(bpy)_3^{2+})$/tri-*n*-propylamine (TPrA) system revisited - a new route involving TPrA$^{\bullet +}$ cation radicals. *J. Am. Chem. Soc.* **2002,** *124*, 14478-14485.

2. Connell, T. U.; White, J. M.; Smith, T. A.; Donnelly, P. S., Luminescent iridium(III) cyclometalated complexes with 1,2,3-triazole "Click" ligands. *Inorg. Chem.* **2016,** *55*, 2776-2790.

3. (a) Connell, T. U.; Hayne, D. J.; Ackermann, U.; Tochon-Danguy, H. J.; White, J. M.; Donnelly, P. S., Rhenium and technetium tricarbonyl complexes of 1,4-substituted pyridyl-1,2,3-triazole bidentate 'click' ligands conjugated to a targeting RGD peptide. *J. Labelled Compd. Radiopharm.* **2014,** *57*, 262-269; (b) Doeven, E. H.; Barbante, G. J.; Harsant, A. J.; Donnelly, P. S.; Connell, T. U.; Hogan, C. F.; Francis, P. S., Mobile phone-based electrochemiluminescence sensing exploiting the 'USB On-The-Go' protocol. *Sens. Actuators, B* **2015,** *216*, 608-613.

4. Connell, T. U.; James, J. L.; White, A. R.; Donnelly, P. S., Protein labelling with versatile phosphorescent metal complexes for live cell luminescence imaging. *Chem. - Eur. J.* **2015,** *21*, 14146-14155.

5. (a) Chiu, M.-H.; Wu, H.; Chen, J.-C.; Muthuraman, G.; Zen, J.-M., Disposable screen-printed carbon electrodes for dual electrochemiluminescence/amperometric detection: sequential injection analysis of oxalate. *Electroanalysis* **2007,** *19*, 2301-2306; (b) Delaney, J. L.; Hogan, C. F.; Tian, J.; Shen, W., Electrogenerated chemiluminescence detection in paper-based microfluidic sensors. *Anal. Chem.* **2011,** *83*, 1300-1306; (c) Delaney, J. L.; Doeven, E. H.; Harsant, A. J.; Hogan, C. F., Use of a mobile phone for potentiostatic control with low cost paper-based microfluidic sensors. *Anal. Chim. Acta*

2013, *790*, 56-60; (d) Chen, Y.; Wang, J.; Liu, Z.; Wang, X.; Li, X.; Shan, G., A simple and versatile paper-based electrochemiluminescence biosensing platform for hepatitis B virus surface antigen detection. *Biochem. Eng. J.* **2018,** *129*, 1-6.